Flow Boiling in Vertical Small to Micro Scale Tubes

By

Asseel Majed Rasheed Al Gaheeshi

Supervisor: Professor Tassos G. Karayiannis

Dissertation submitted in partial fulfilment for the degree of
Doctor of Philosophy (PhD) in Chemical Engineering/Industrial Processes

College of Engineering, Design and Physical Sciences
Brunel University London
Uxbridge, UB8 3PH
United Kingdom

June 2018

Abstract

The growing demand for the development of efficient miniature cooling systems has led to stimulating numerous investigations on two-phase flow boiling in small to microscale tubes. Because of the variation in properties of synthetic cooling fluids, this causes an inaccuracy of existing flow boiling prediction models or correlations in the literature to interpolate or extrapolate the two-phase flow boiling heat transfer and pressure drop. The purpose of this investigation was to study experimentally the parametric aspects of flow boiling characteristics inside vertical stainless-steel tubes with four different internal diameters (1.1, 2.01, 2.88 and 4.26 mm). The R245fa (1,1,1,3,3-pentafluoropropane, HFC-245fa) was used as working fluid. The experiments were carried out under a system pressure range of 185 – 310 kPa (which correspond to a saturation temperature range of 31 – 46 °C), mass flux range of 200 – 500 kg/m^{2}s, heat flux range of 3 – 188.5 kW/m^2, vapour quality up to the onset of dryout and 5 K inlet subcooling. Flow pattern visualisations, two-phase pressure drops and saturated flow boiling heat transfer coefficients were presented. The experimental data of R134a employed for comparison is acquired from the previous studies of Huo et al. (2007), Shiferaw et al. (2011) and Mahmoud et al. (2014a). These studies were carried out in the same experimental facility and under the similar operating conditions.

The Two-phase flow regimes inside four tubes were visualised in a borosilicate glass tube located at the heated section outlet to capture the dominant flow patterns which assist to elucidate the heat transfer results. The flow boiling visualisation was recorded by a high-speed camera with experiments of increasing and decreasing heat flux. The four observed flow regimes are identified as bubbly flow, slug flow, churn flow and annular flow. In increasing heat flux experiments, the churn and annular flows were only the dominant patterns in all four tubes. The slug flow was often discerned at lower mass flux except for the tube of 1.1 mm where it was not observed at all. This is contrary to decreasing heat flux experiments where all flow patterns including the bubble flow were observed in all the tubes. This shows a strong impact of hysteresis, which is a result of nucleation sites remained active as the heat flux is reduced. The flow patterns and transition boundaries for R245fa are affected by mass flux, system pressure, and tube diameter. The vapour quality corresponding to flow pattern transition boundary tends to decrease with increasing mass flux and tends to increase with increasing system pressure and decreasing tube diameter. Except for the bubbly-slug boundary, its vapour quality decreases with decreasing tube diameter. The experimental flow pattern maps of R245fa were fairly

predicted with the predictive models developed for mini- and micro-channels by Tibiriçá et al. (2017).

The two-phase pressure drop of R245fa is affected by mass flux, heat flux, system pressure, tube diameter and surface topography. The two-phase pressure drop increases with increasing mass flux and heat flux (vapour quality) and decreases with increasing system pressure and tube diameter. The two-phase pressure drop of the coated tube is higher than that of the uncoated tube. This is attributed to the coated tube having a higher surface roughness compared to the uncoated tube. The comparison between R245fa and R134a shows that the measured two-phase pressure drop of R245fa is dramatically higher than that of R134a. This arises from the difference in physical properties of the two fluids. The experimental data of two-phase pressure drop for 4.26 mm tube were reasonably predicted by Müller-Steinhagen and Heck (1986) correlation. Further, the experimental data of 2.88 mm and 2.01 mm tubes were well predicted by Chisholm (1973a), and Kim and Mudawar (2013), respectively. The experimental data of 1.1 mm tube were not well predicted by any of the selected predictive methods.

The local heat transfer coefficient of all tubes increases with increasing heat flux for low and intermediate vapour qualities. After this vapour qualities, the heat flux effect diminishes. Then, the local heat transfer coefficient increased slightly with vapour quality, especially for higher heat flux near the outlet of the tube. However, the dryout inception in the 1.1 mm tube occurs after the intermediate vapour quality value and expands along the high vapour quality region. The behaviour of the local heat transfer coefficients of 1.1 and 2.88 mm tube is slightly dependent on the mass flux and vapour quality. Contrarily, there is insignificant effect of mass flux along 2.01 and 4.26 mm tube. This gives an indication of the contribution of nucleate boiling in the heat transfer process at lower and medium heat fluxes and nucleate boiling plus convective evaporation at higher heat fluxes near the tube outlet. Further, the local heat transfer coefficient increases as the system pressure increases. The tube diameter has a strong influence on the enhancement of local heat transfer coefficient. The enhancement in average heat transfer coefficient approaches 83% when the tube diameter is reduced from 4.26 to 1.1 mm. The trend of the local heat transfer coefficient of R134a was almost similar to that of R245fa with the exception of local dryout. The average heat transfer coefficient of R134a is about 106-151% larger than that of R245fa for the operational range studied. The dominant heat transfer mechanism is also represented by nucleate boiling for both fluids, particularly for 4.26 mm tube tested in this study. Also, the average heat transfer coefficient was enhanced by 33% when the inner tube surface coated with a copper coating. Finally, the correlation of Fang et al. (2017) predicted all experimental data for the four tubes with fair and similar accuracy.

Declaration

This research is the original work of the author except where otherwise specified, or where acknowledgements are made by references. This research was conducted at the College of Engineering, Design and Physical Sciences, Brunel University London, under the supervision of Prof. T. G. Karayiannis and Dr. J. Xia.

The work has not been submitted for another degree or award to any other institution.

Acknowledgements

Firstly, I would like to express my appreciation and gratefulness to the Ministry of Higher Education and Scientific Research, University of Kerbala and Iraqi Cultural Attaché-London for sponsorship and funding my PhD study and managing the student affairs.

I would like to thank my supervisor, Professor Tassos G. Karayiannis for his guidance during the PhD period and valuable assistance over the last three years, you have given me this wonderful opportunity and I am so deeply grateful that you took a chance on me. Mere words cannot express my awe for you, thank you very much for always supporting me.

To my parents and my family (Roaa, Zahraa and Yousif), I would like to thank you for being beside me as a source of care, love, encouragement and motivation which fill me with patience and commitment during this period. There are no any proper words to express my gratitude. They also constantly prayed for me. They are one in a world for me. I would also like to thank my lovely wife deeply for her patience and encouragement all the time. Without her support, this work would not have been possible.

I am so thankful to my second supervisor Dr. J. Xia. for his support and encouragement. I would also like to thank Dr. M.M. Mahmoud for teaching and offering me his knowledge and useful advice about the experimental facility helped me to finish my experiments. I am grateful to the technicians Mr. Costas Xanthos and Mr. E. Wyse for helping me with my experiments and keeping me company in the laboratory.

Finally, I am extremely thankful for the amazing support and friendship of all my friends especially Claire king and Dr. Jurriath Azmathi Mumith.

Contents

List of Figures

List of Tables

Nomenclature

Latin	Description	SI unit
B	coefficient	(-)
Bd	Bond number, $\frac{g\Delta\rho D^2}{\sigma}$	(-)
Bo	Boiling number, $\frac{q}{Gh_{lv}}$	(-)
B_X	systematic error	(-)
C	Chisholm parameter	(-)
Ca	Capillary number, $\frac{\mu U_b}{\sigma}$	(-)
Co	Confinement number, $\frac{\sqrt{\sigma/g\Delta\rho}}{D}$	(-)
C_o	distribution parameter	(-)
Cov	Convection number, $\left(\frac{1-x}{x}\right)^{0.8}\left(\frac{\rho_v}{\rho_l}\right)^{0.5}$	(-)
Cp	specific heat capacity	(J/kgK)
D	diameter	(m)
e	surface roughness	(m)
E	enhancement factor	(-)
$Eö$	Eötvös number, $\frac{g\Delta\rho D^2}{\sigma}$	(-)
f	Fanning friction factor	(-)
F	multiplier factor	(-)
Fa	Fang number, $\frac{\Delta\rho\,\sigma}{G^2 D}$	(-)
F_{fl}	fluid dependent parameter	(-)
Fr	Froude number, $\frac{G^2}{gD\rho^2}$	(-)
g	gravitational acceleration	(m/s)
G	mass flux	(kg/m^{2}s)
Gz	Graetz number, $\frac{Re\,Pr}{L/D}$	(-)
h	specific enthalpy	(J/kg)
h_{lv}	latent heat of vaporization	(J/kg)

I	DC electrical current	(A)
J	superficial velocity	(m/s)
k	thermal conductivity	(W/mK)
$\overline{K}$	thermal loss coefficient	(W/K)
L	length	(m)
La	Laplace constant, $\sqrt{\sigma/g\Delta\rho}$	(-)
L_T	the distance between the first and last thermocouples	(m)
m	mass flow rate	(kg/h)
$\dot{m}$	mass flow rate	(kg/s)
MAE	mean absolute error	(-)
MW	molecular weight	(kg/mole)
n	exponent in Blasius' equation, 0.25	(-)
N	number of samples	(-)
N_a	density of active nucleation site	(-)
Nu	Nusselt number, $\frac{\alpha D}{k}$	(-)
P	pressure	(Pa)
P	perimeter of channel	(m)
Pr	Prandtl number, $\frac{Cp\mu}{k}$	(-)
q	heat flux	(W/m^2)
Q	heat transfer rate	(W)
$\dot{q}$	volumetric heat flux	(W/m^3)
r	radius	(m)
R	result	(-)
R_a	average roughness value	(m)
Re	Reynolds number, $\frac{GD}{\mu}$	(-)
R_p	maximum profile peak height of roughness	(m)
R_q	root mean square roughness value	(m)
R_v	maximum valley depth of roughness	(m)
S	suppression factor	(-)
S_{Bx}	standard deviation of the systematic error	(-)
Su	Suratman number, $\frac{\rho\sigma D}{\mu^2}$	(-)
S_X	standard deviation	(-)
T	temperature	(K)

$t_{95\%}$	95% confidence limit	(-)
U	velocity	(m/s)
U	overall uncertainty	(-)
u_c	combined uncertainty (systematic and random)	(-)
u_{random}	random error	(-)
V	DC electrical voltage	(V)
W	weight	(kg)
We	Weber number, $\frac{G^2 D}{\sigma \rho}$	(-)
x	vapour quality	(-)
X	Lockhart-Martinelli parameter, $\sqrt{\frac{(dP/dz)_l}{(dP/dz)_v}}$	(-)
$\bar{X}$	mean value	(-)
X	measured variable	(-)
z	axial distance	(m)

Greek letters

θ	angle	(degree)
ρ	density	(kg/m^3)
Δ	difference	(-)
α	heat transfer coefficient	(W/m^{2}K)
v	kinematic viscosity	(m^2/s)
β	percentage of data within ±30%	(-)
Γ	physical property coefficient, $\sqrt{\frac{(dP/dz)_{lo}}{(dP/dz)_{vo}}}$	(-)
v	specific volume	(m^3/kg)
σ	surface tension	(N/m)
ϕ	two-phase frictional multiplier	(-)
ψ	two-phase to single-phase heat transfer coefficient ratio	(-)
μ	viscosity	(Pa s)
ϵ	void fraction	(-)

Subscripts

A	annular
av	average
b	bubble

BS	bubble-slug
c	cavity
c	critical
CA	churn-annular
cb	convective boiling
CB	coalescing bubble
e	exit
E	entry
exp	experimental
f	fluid
F	wetted
fr	frictional
FR	related to Froude number
g	gas
grav	gravitational
h	heated
h	hydraulic
H	homogeneous
h,fb	hydrodynamically fully developed
I	intermittent
IB	isolated bubble
in	inlet
inner	inner
ins	insulation
l	liquid
lo	liquid only
loss	loss
lv	difference between liquid and vapour
m	mean
mom	momentum
nb	nucleate boiling
out	outlet
outer	outer
pre	predicted
r	reduced

sat	saturation
SC	slug-churn
sp	single-phase
ss	stainless steel
sub	subcooling
total	total
tp	two-phase
tt	turbulent liquid – turbulent vapor
tv	turbulent liquid – laminar vapor
v	vapour
vo	vapour only
vt	laminar liquid – turbulent vapor
vv	laminar liquid – laminar vapor
w	wall

Chapter 1

Introduction

1.1 Research Background

Flow boiling is the phenomenon of heat transfer during the fluid phase change from liquid to vapour inside the heated channel. The importance of this phenomenon in many industrial applications is well known and very reliable. This is in fact due to the superior capability of flow boiling cooling systems which encounter extremely high heat fluxes under relatively small temperature differences. It is also quite well documented in a considerable volume of literature. During the 19th and early 20th centuries, wide investigations have been dedicated to study, theoretically and empirically, the flow boiling phenomenon. These investigations have been an integral part of early developments in rocket motors, boilers, distillation, petrochemical processes, high-field electromagnets, automobile radiators, modern steam power plants, nuclear reactor channels, refrigeration systems and air-conditioning equipment. In recent years, these investigations and other studies concerning the flow boiling field have received great attention owing to the increased demands for obtaining a more economical and safety design and optimal operating conditions. Despite the rapid increase in the volume of literature on the subject of flow boiling, there is still a small part that deals with heat transfer in the upward flow through vertical channels.

To design cooling systems having optimum performance, it is very important to understand and analyse the local flow boiling conditions. While a coolant flows in a uniformly heated channel, the heat transfer occurs basically via single-phase forced convection. The temperature of bulk coolant then reaches a level less than the saturation temperature to a certain extent, leading to the probable occurrence of subcooled boiling near the channel wall. The bulk coolant temperature afterwards reaches up to the saturation temperature resulting in the incipience of saturated flow boiling phenomenon

(i.e. change phase from liquid to vapour). The latter forms a sequence of flow patterns within the flow field, where the annular flow pattern is characterized by the vapour phase in the tube core and the thin liquid film around the circumference of the channel wall. Because of these conversions, the temperature of bulk coolant reduces constantly and becomes uniform along the two-phase flow boiling region of the channel. Within this region, there is a simultaneous occurrence of several complex mechanisms. The heat transfer mechanism from the channel wall into the two-phase coolant flow and its main effect on the vapour phase formation are not conclusively known. This is due to the topographical differences of the inner surfaces of the channel wall affecting the determination of evaporation mechanism. According to many experimental investigations in the open literature, it is well-known that the vaporization mechanism in flow boiling region represents either only the nucleate boiling or only the convective boiling or both of them, or the thermal equilibrium mechanism at the interface between the vapour and liquid phase, (Tibiriçá and Ribatski, 2010; Thome and Consolini, 2010; Charnay et al., 2014b; Karayiannis and Mahmoud, 2017).

It has been recognized since 1987 that the Montreal Protocol was internationally designed to protect the stratospheric ozone layer from chlorine- and bromine-containing substances. These substances deplete the ozone layer resulting in increased ultraviolet (UV) radiation on the Earth's surface and climate change at the southern high latitudes. From among these substances, chlorofluorocarbons (CFCs) are the most refrigerants used in domestic appliances. However, they cause a severe depletion of the stratospheric ozone layer due to the presence of chlorine in their chemical composition (Boucher, 2010). Furthermore, there is an evidence from the measurements of Potential Ozone Depletion (POD) set by the Environmental Protection Agency (EPA). This agency indicated that in November 2014, global levels of ozone standard ratcheted down from 75 parts per billion to between 65 and 70 parts per billion (Hand, 2015). Therefore, scientific investigations have been aimed to replace chlorofluorocarbons with many alternative refrigerants after comparing their chemical stability, safety, and thermodynamic properties. The majority of researchers concentrate on hydrofluorocarbons (HFCs), especially HFC-134a (R134a) and HFC-245fa (R245fa) as an alternative refrigerant. Since R245fa was considered as an environmentally friendly refrigerant with non-ozone depleting, the two-phase flow boiling of R245fa refrigerant has attracted much attention by some researchers. Although

there have been many investigations on the flow boiling in the small-sized channels, the flow boiling characteristics still need to be better clarified. This is due to the roughness of the channel wall surface and its effect on the heat transfer mechanism in the flow boiling process has not been considered. The entirely different parametric trends of heat transfer coefficient against heat flux, mass flux and vapour quality have been stated in the literature.

1.2 Research Motivation

The rapid developments in the performance and recent miniaturisation trend for electronic devices, laser systems, micro-reactors, have resulted in high levels of heat flux. This necessitates conducting a research in innovative cooling systems. For instance, the miniature electronics have recently provided higher processing speeds which have generally contributed to unusual increases in power consumption. The side effects resulting from the operating of these miniature devices generate a high heat flux that can be avoided only by immediate cooling. If the thermal effects in these electronics are not managed well, this will negatively affect their performance. Therefore, the appropriate thermal management is absolutely necessary to lengthen the duration of performance of small devices. This issue has made an increasing need for researchers to investigate and find proper solutions (Kalani, 2016). Among these researchers who tried to illustrate the growing requirement for solutions, the BCC Research group (2016) has assessed that the market of thermal management in different industries involving automobile, medical, electronics, aerospace, defence and chemical industries. It will grow from $10.7 billion in 2015 to nearly $14.7 billion by 2021 (McWilliams, 2016).

The advanced growth in the market of thermal management systems is mostly due to technological developments in industries which are mentioned above. These developments create several challenges, involving miniaturisation in heat exchangers, decrease in manufacturing cost, constraints of reliability and ultra-performance in miniature heat exchangers, enhancing cooling systems by materials and technology and ultimately harsh conditions (Kalani, 2016). The normal cooling techniques such as air cooling and single-phase cooling have been incapable of overcoming these emerging

challenges, in particular when waste heat flux exceeds the 10 MW/m^2 as reported by Faulkner et al. (2003). All these factors combine to increase the need for advanced cooling technologies to meet current and future needs.

Among the assorted thermal management methods, air cooling (cooling fans) has been favoured for an extensive range of industrial applications on account of low cost, high reliability and air availability. Although the air has been used for decades, it is unable to surmount the new evolutions in the systems of high heat flux. Therefore, the popularity of single-phase liquid cooling systems has begun to increase. The use of liquid cooling techniques is anticipated to meet the thermal management requirements of most high heat flux systems because of the distinguished thermal properties of cooling liquids compared to air (Kalani, 2016). They are already widely utilized in the industry and comprehensive investigations are being carried out to improve their thermal performance (Rosa et al., 2009). Recently, single-phase direct liquid cooling has exhibited superior performance to dissipate a high heat flux. It could be argued that the positive results in improving heat dissipation rates were attributed to the innovative design of heat exchangers and the use of liquid coolants that have high dielectric strength, high stability and to be non-flammable. However, there are some disadvantages in the use of single-phase liquid cooling. One of these drawbacks is that the increase in surface temperature along the field of coolant flow because of heat dissipation leads to irregular cooling along the system. Thus, the temperature of hot surface rises specifically into the downstream section of the system. On the other hand, the increase in bulk coolant temperature necessitates pumping a high flow rate of the coolant to simultaneously maintain a uniform temperature of the bulk coolant and a low temperature of the hot surface. This, in turn, requires a higher pumping power as well as increasing the size of cooling liquid inventory. The high flow rate of coolant causes an increase in the pressure drop inside the system. This also demands the choice of a higher capacity pump, which increases manufacturing energy and cost consumption. Furthermore, higher pressure drops cause undesirable variations in the coolant properties resulting in an unstable flow. These factors have motivated many researchers and engineers to study the fundamental principles of flow boiling phenomenon and also to take advantage of this phenomenon in industrial applications (Kalani, 2016).

Two-phase flow boiling technique is deemed to be better than single-phase flow in providing greater cooling. Figure 1.1 shows that the flow boiling system gives greater thermal performance among all the cooling methods. The reason for this is in the fact that the high latent heat of coolant provides a higher heat dissipation rate owing to the phase change from liquid to vapour (Tullius et al., 2011). This heat dissipation rate is estimated to be about three orders of magnitude greater than that of a single-phase flow. Moreover, there are other benefits of flow boiling such as high-performance in heat transfer, uniform temperature medium, a minor increase in surface temperature and low coolant inventory (Kalani, 2016). Therefore, flow boiling process is a significant means of heat transfer in thermal applications represented by petrochemical processing, micro-chemical and bioreactors, pharmaceuticals, and power generation. The flow boiling phenomenon can be described as evaporation of fluid flowing in a heated channel. Fluid flow in the channel is based on natural convection (Thermosiphon circulation) or the use of a mechanical pump. Researchers have widely studied this phenomenon for use in miniaturizing high-performance heat exchangers.

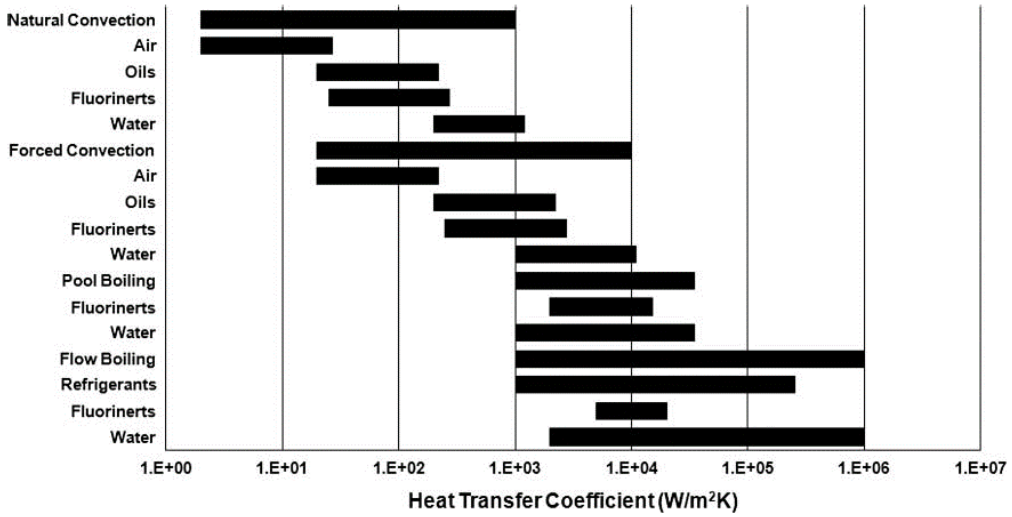

Figure 1.1 Performance of cooling techniques, (Tullius et al., 2011).

In order to reduce energy consumption and CO_2 emissions due to current environmental issues, the thermal and cooling technologies need to be developed. Also, the cooling fluid selected has to be environmentally friendly and have sound thermal properties. The test fluid is refrigerant R245fa, which is deemed as one of motives for the current experimental work in relatively low-pressure cooling systems. R245fa is named

chemically ‘1,1,1,3,3-pentafluoropropane’ and its molecular formula is $CF_3CH_2CHF_2$. Despite that R245fa does not destroy ozone layer (its Ozone Depletion Potential (ODP) is zero because it does not include chlorine), it has a 7.6-year Atmosphere Life Time (ALT) and is therefore considered “environmentally friendly”. However, a global warming potential (GWP) for R245fa is 950-1020 kgeq.CO_2/kg. This refrigerant has a high degree of thermal and hydrolytic stability, is non-flammable, has a favourable toxicological profile and a high critical point (T_c = 154.05 °C and P_c = 3640 kPa), as reported by (Charnay et al., 2015b). As a result, it will boil at a relatively high temperature. Besides, according to the exergy efficiency and thermal efficiency and considering environmental impacts and safety levels, this refrigerant R245fa was defined by previous studies of Zhang et al. (2011a), Wang et al. (2011) and Charnay et al. (2015b) as the most suitable operating fluids for Organic Rankine Cycle (ORC, used in an engine waste heat recovery application).

As a matter of fact, the currently existing flow boiling heat transfer and pressure drop correlations are not validated for this refrigerant or for different fluids at similar reduced pressure. In addition, the literature analysis exhibits that there is a gap in knowledge and understanding of the two-phase flow boiling heat transfer for the new synthetic refrigerants at temperatures ranging between -20 °C and 40 °C corresponding to the applications in the commercial refrigeration (-20 – 0 °C), air-conditioning industry (0 – 10 °C), heat pump (10 – 20 °C), and electronic component cooling (20 – 40 °C) (Charnay et al., 2015a). Notice that for this study, the saturation temperature ranged from 31 to 46 °C corresponding to operating pressure from 185 to 310 kPa, respectively. When the saturation temperature increases or decreases, the thermal-physical properties of these synthetic refrigerants vary. This variation in properties leads to a change in the vapour and liquid velocity and also the predominance of surface tension or gravitational forces. This, in turn, affects the liquid-vapour interactions, and consequently the flow patterns. Therefore, the reliability of existing flow boiling prediction models or correlations in the literature is not ensured to interpolate or extrapolate the two-phase flow boiling heat transfer and pressure drop.

An accurate prediction of heat transfer coefficients and pressure drops is hence the first step to optimize the design of cooling systems as well as keeping pace with the rapid developments in the performance and recent miniaturisation for electronic systems. This can be achieved with flow boiling in microtubes and single/multi microchannels, which achieve high surface area to volume ratio and consequently high heat transfer rates (Mahmoud et al., 2014b). Several fundamental issues in flow boiling at the small to microscale are being investigated in both single and multichannels including tubular geometries, the latter offering better-defined flow parameters to help elucidate the thermo-physical phenomena. In addition, understanding and estimating two-phase flow heat transfer rates in small to microscale tubes is very important for the design of small-scale shell and tube heat exchangers (Karayiannis and Mahmoud, 2017).

1.3 Research Objectives

This study is a part of a long-term investigation at Brunel University London to help elucidate the prevailing fundamental phenomena and conclude on correlations predicting flow pattern transition boundaries, heat transfer rates and pressure drop. In particular, the objectives of the study in vertical tubes using R245fa are:

- Study the effect of tube diameter on flow patterns, pressure drop and heat transfer rate.
- Study the effect of heat flux, mass flux, vapour quality and system pressure on flow patterns, pressure drop and heat transfer rate.
- Study the effect of fluid properties including R134a and R245fa on pressure drop and heat transfer rate.
- Study the effect of surface microstructure (coating) on pressure drop and heat transfer rate.
- Evaluate the predictive methods available in the literature for flow pattern maps, pressure drop, and heat transfer coefficient.

1.4 Dissertation Structure

The dissertation structure includes seven chapters; Chapter 1 provides a brief introduction to flow boiling background, flow boiling applications, safety and alternative refrigerants and relevant flow boiling theory. The motivation for the experimental investigation is presented, followed by the research objective of the current study. Chapter

2 reviews the work done by various authors in the field of flow boiling during small diameter tubes and the experimental studies involving two-phase flow patterns, pressure drop and heat transfer. It provides details on the parametric influences which affected the performance of flow boiling in small channels. Also, the predictive methods of flow pattern transitions, two-phase pressure drop and two-phase heat transfer coefficient are briefly presented. Chapter 3 describes facility setup, test sections, measurement instrumentation and experimental methodology, in details. The single-phase validation, data reduction and uncertainty analysis are also presented. Chapter 4 presents the flow boiling visualisations with a focus on studying basic principles of flow patterns and transition boundaries with the effects of different parameters. The observed flow patterns are also compared to other flow pattern maps presented in the literature. Chapter 5 presents the characteristics of flow boiling pressure drop in small diameter tubes. The parametric influences on the two-phase pressure drop are also shown and discussed. Homogeneous and separated flow models are assessed by comparison with the experimental data. Chapter 6 presents the flow boiling heat transfer characteristics in small diameter tubes with a focus on the parametric effects on the local two-phase heat transfer coefficient. The applicability of existing correlations in the literature are assessed by comparison with the experimental data. Finally, Chapter 7 presents the conclusions drawn from this study and the few recommendations for future work on this topic.

Chapter 2

Small Channel Two-Phase Flow Literature Review

2.1 Introduction

The flow boiling phenomenon in small channels is one of the most effective and promising techniques for cooling high heat flux systems. The knowledge of the basic principles of this phenomenon plays a vital role in the development of the design of high-performance miniature heat exchangers. In this chapter, a state-of-the-art review of the flow boiling characteristics related to two-phase flow patterns, pressure drop and heat transfer coefficient is presented. The channel size is among the most important parameters to enhance the values of heat transfer coefficient and has also a considerable influence on two-phase flow patterns and pressure drop. Therefore, some pioneering investigations that employed small sized channels are included in this chapter. The definition of a small channel is first reviewed. The two-phase flow patterns in tubular channels and the predictive criteria of flow pattern transitions are then presented and discussed. The third section of this chapter is a review on experimental research of two-phase pressure drop in small channels. The fourth section of this chapter shows a review of experimental research of flow boiling heat transfer coefficient in small channels.

2.2 Definition of a small channel

The transition criterion from macro to microchannels is still not defined, despite progress in many studies on single-phase and two-phase flow. In fact, this issue depends on some factors such as thermal or hydrodynamic behaviour, channel geometry, thermophysical fluid properties, flow conditions and operating conditions. Therefore, there are several different classification criteria available in the literature to separate the microchannel from the conventional channel. Some researchers described the transition criterion between macro and micro-passages for two-phase flow and heat transfer based

on the engineering applications and geometrical approach, as shown in Table 2.1. Shah (1986) classified a compact heat exchanger as an exchanger with a surface area density ratio greater than 700 m^2/m^3 which corresponded to a hydraulic diameter lower than 6 mm. Accordingly, the value of 6 mm was identified as the threshold diameter for macro/micro transition. Mehendale et al. (2000) defined various heat exchanger types in terms of the hydraulic diameter. They proposed the hydraulic diameters greater than 6 mm as conventional channels, a range of 1 – 6 mm as compact heat exchangers, a range of 100 μm –1 mm as mesoscale channels and a range of 1 – 100 μm as microchannels. Kandlikar (2002) also recommended the ranges of hydraulic diameters to classify different channels for single-phase and two-phase flows without being based on any physical laws, but they depended on engineering practice and different studies in the literature. They defined the hydraulic diameters greater than 3 mm as conventional channels, 3 mm $\geq D_h >$ 200 μm as minichannels, and 200 μm $\geq D_h >$ 10 μm as microchannels. According to this definition, the distinction between macro and microchannels is 3 mm.

Table 2.1 Summary of heat exchanger classification.

Author(s)	Class of heat exchanger	Hydraulic diameter range
Shah (1986)	Conventional	$D_h > 6$ mm
	Micro	$D_h \leq 6$ mm
Mehendale et al. (2000)	Conventional	$D_h > 6$ mm
	Compact	1 mm $\leq D_h < 6$ mm
	Macro or mini	100 μm $\leq D_h < 1$ mm
	Micro	1 μm $\leq D_h <$ 100 μm
Kandlikar (2002)	Conventional	$D_h > 3$ mm
	Macro or mini	200 μm $\leq D_h < 3$ mm
	Micro	10 μm $\leq D_h <$ 200 μm

Other researchers defined the macro/micro transition criteria based on bubble confinement, dominant surface tension and gravitational forces where these criteria were characterized in terms of dimensionless numbers, as summarized in Table 2.2. Since the Laplace constant $La = \sqrt{\sigma/g\Delta\rho}$ represents the effects of surface tension and gravity, some researchers adopted the Laplace constant to distinguish the macro/micro transition criteria. Suo and Griffith (1964) proposed the transition criterion as $La/D \geq 3.3$ while Triplett et al. (1999) defined flow channels with hydraulic diameters equivalent to or

smaller than the Laplace constant. Kew and Cornwell (1997) suggested using the Confinement number with a value of 0.5 as a criterion to define the threshold diameter for macro/micro transition. Confinement number actually depends on the definition of the Laplace constant, as $Co = \sqrt{\sigma/g\Delta\rho}/D_h$. According to this definition, when the Confinement number is less than 0.5, the channel is considered as micro scale channel. Ong and Thome (2011a) experimentally studied two-phase flow patterns for R134a, R236fa and R245fa in small tubes of 1.03, 2.20 and 3.04 mm. According to their flow visualisations and film thickness measurements, they observed that the gravitational effect was more prevalent when the Confinement number was smaller than 0.34, otherwise, it was suppressed when the Confinement number was greater than 1. Eötvös number ($E\ddot{o} = g\Delta\rho D^2/\sigma$) was also employed for defining the relative significance of gravity and surface tension by Brauner and Maron (1992). The authors proposed a criterion in terms of Eötvös number based on a linear stability analysis of stratified flow taking into account the significance of surface tension in overcoming gravity given as $(2\pi)^2/E\ddot{o} > 1$. Ullmann and Brauner (2007) also employed Eötvös number as macro/micro transitional criterion on the basis of flow pattern maps. They suggested $E\ddot{o} \leq 1.6$ as micro scale channels. Cheng and Wu (2006) presented channel classifications based on Bond number $Bd = g\Delta\rho D^2/\sigma$, namely; Bd < 0.05 as micro-channel, 0.05 < Bd < 3 as mini-channel and Bd > 3 as macro-channel. Harirchian and Garimella (2010) suggested another micro to macro-transitional criterion based on a Convective confinement number. The authors defined the Convective confinement number as $Bd^{0.5} \times Re = 160$. In this criterion, the authors attempted to relate the mass flux and viscosity together with surface tension and gravity as well as their influences on flow confinement in a micro channel. However, this distinction does not highlight the flow behaviour and thus requires further validation with the experimental data. Other new transition criteria have also been suggested by Tibiriçá and Ribatski (2015). They conducted analyses of flow pattern data to identify main phenomenological differences between macro and micro scale phenomena. According to these analyses, the authors proposed two phenomenological macro/micro transitional criteria ($D_h = \sqrt{8\,\sigma\cos\theta\,/g\Delta\rho}$ and $D_h = \sqrt{\sigma/20\;g\Delta\rho}$) on the basis of the existence of stratified flow and the degree of uniformity of the liquid film along the tube perimeter during annular flow, respectively.

Table 2.2 Summary of the macro to micro scale transition criteria.

Author(s)	Channel class	Criterion
Suo and Griffith (1964)	Micro	$La/D \geq 3.3$
Triplett et al. (1999)	Micro	$La/D \geq 1$
Kew and Cornwell (1997)	Micro	Co > 0.5
Ong and Thome (2011a)	Macro	Co < 0.34
	Micro	Co > 1
Brauner and Maron (1992)	Micro	$(2\pi)^2/E\ddot{o} > 1$
Ullmann and Brauner (2007)	Micro	$E\ddot{o} \leq 1.6$
Cheng and Wu (2006)	Macro	$Bd > 3$
	Mini	$0.05 < Bd < 3$
	Micro	$Bd < 0.05$
Harirchian and Garimella (2010)	Micro	$Bd^{0.5} \times Re_l \leq 160$
Tibiriçá and Ribatski (2015)	Micro	$\sqrt{8\,\sigma \cos\theta\,/g\Delta\rho}/D \geq 1$
	Micro	$\sqrt{\sigma/20\;g\Delta\rho}/D \geq 1$

However, it is concluded that the available dimensionless numbers in literature such as Confinement number have been given different assessments based on individual experimental data. This is because of the lack of a well-established theory, which depends on thermophysical fluid properties and operating parameters, to know the threshold boundaries between macro and microscale channels. In this study, the definition of Kew and Cornwell (1997) is used to determine the micro-channel.

2.3 Two-phase flow patterns

In the two-phase flow through a vertical channel, the liquid and vapour phases are distributed in the flow channel with the various flow structures. These identified distributions of both phases are termed 'two-phase flow patterns'. The effect of geometrical or physical characteristics of two-phase flows on flow pattern structures can be investigated visually. The visual observation is a method of flow regime recognition which relies on the use of high-speed camera and image processing techniques. Flow patterns are a very important feature for any two-phase flow issues. The conduct of vapour–liquid flow includes many of the fundamental relations, which are required for solving two-phase conservation equations. The particular characteristics of flow patterns are an important aspect of the predictions of heat transfer coefficient and pressure drop. Therefore, the description and prediction of flow patterns are an important aspect of essential modelling of the boiling process. Recently, the predictive models of heat transfer

coefficient for flow boiling in the narrow channel relies on local flow pattern and its type in local flow circumstances. The recognised flow pattern requires dependable maps that are typically used to identify the type of flow pattern and to predict the transition boundaries between the flow patterns.

The two-phase flow patterns of flow boiling in a vertical upflow tube can be described in Figure 2.1 as a conceptual diagram of what may occur in this case. This phenomenon can be illustrated by considering the case of increasing heat flux in successive equal steps. A working fluid boils when it flows through a vertical evaporator tube and the various two-phase flow patterns arise. They develop from single-phase fluid flow, through bubbly flow, slug flow, churn flow and annular flow. The vapour is initially formed by active nucleation sites at tube wall. At low heat fluxes, the onset of nucleate boiling may be delayed past the point at which the vapour quality equals to zero. The liquid can be much superheated before any vapour is generated with low heat fluxes. However, at higher heat fluxes, nucleation inception takes place upstream of the saturation position (zero vapour quality). The subcooled boiling is distinguished here by a subcooled liquid core with vapour bubbles tending to stay near to the tube wall until the saturation condition is approached. As the fluid continues up the channel, vapour generation is significantly increased at the active nucleation sites and also by evaporation from the liquid-vapour interfaces. The vapour bubbles are dispersed in the form of discrete bubbles in the continuous liquid phase. With increasing vapour quality along the tube, the proximity of these bubbles allows the occurrence of collision and coalescence between vapour bubbles. This then leads to the formation of large vapour bubbles that characterise the slug flow. The dimension of slug bubbles is similar to the tube diameter. Moreover, the deformity of the liquid film surrounding slug bubbles because of further evaporation results in the formation of churn flow. The efficiency of the evaporation process becomes greater as the thermodynamic vapour quality increases along the evaporator tube due to the thinning of the liquid film. This process eventually comes to be very efficient to prevent the occurrence of vapour nucleation at the tube wall. Therefore, the nucleation mechanism is suppressed and typical nucleate boiling moves to the entrance region of the evaporator tube. In the annular flow pattern, the flow is defined by the liquid in the annular film on tube perimeter as well as the vapour in the tube centre. The thickness of the liquid film is then reduced by the evaporation process and by the

entrainment process and the wall at the end tube becomes dry. This phenomenon is known as "critical heat flux" or "dryout" and is accompanied by a significant increase in the wall temperature. The dryout phenomenon is propagated downstream if the heat flux is further increased. Characteristically, the overheating in this dryout region results from the formation of a thin vapour film on the tube wall with a continuum of entrained liquid droplets in the core. This regime type is termed as “mist flow” (Hewitt and Hall-Taylor, 1970). In this work, the range of measured CHF for the 1.1 mm tube is between 52 and 136 kW/m^2.

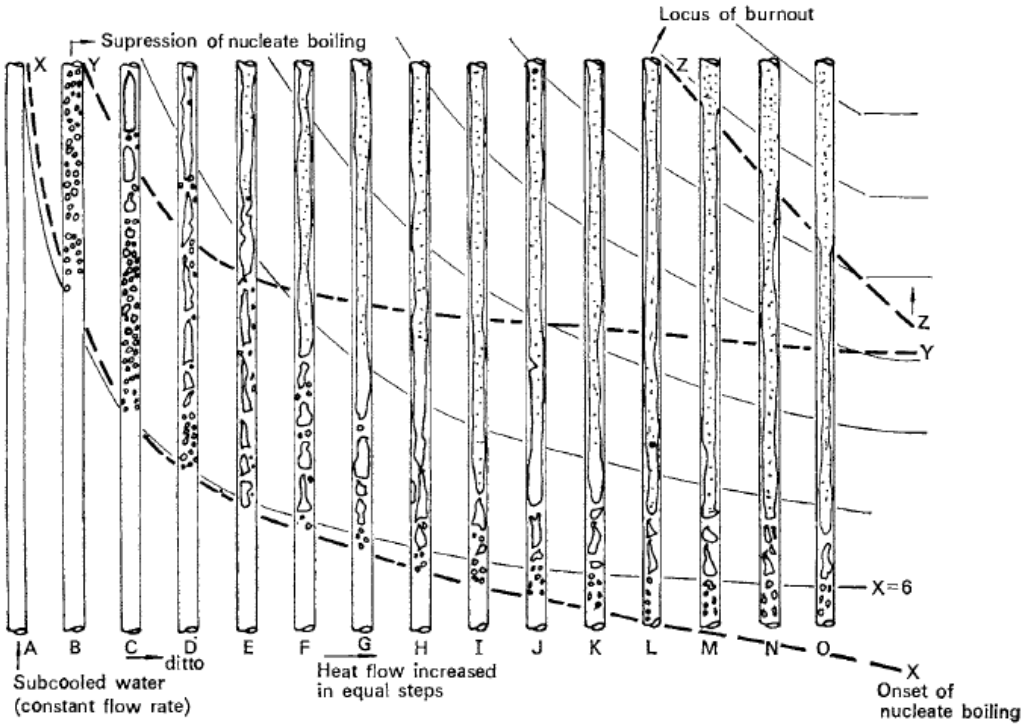

Figure 2.1 Flow regimes in a vertical evaporator tube from Hewitt and Hall-Taylor (1970).

2.4 Key Factors influencing flow patterns

The fundamental understanding of morphological interactions between the liquid and gas phases during two-phase flow in small diameter tubes is emerging as a topic of current intensive research interest. The two-phase flow investigations can be categorised into three groups, namely; adiabatic liquid-gas flow, adiabatic liquid-vapour flow and diabatic liquid-vapour flow (flow boiling) groups Zhang et al. (2010; 2012). Adiabatic liquid-gas flow and flow boiling occupy most of the experimentally academic research

along last decades. The scientists and researchers investigated the influence of geometrical or physical characteristics of two-phase flows on flow pattern structures visually. Also, there are many theoretical and empirical studies on two-phase flow patterns in horizontal and vertical channels so far, although most of them focus on the effect of channel size with different working fluids such as air-water and refrigerants. They rarely give precise criteria of the transition boundaries between flow patterns Zhu et al. (2017a). These studies can be divided into macroscale and microscale channels based on the criterion of Kandlikar (2002) utilising the threshold value of 3 mm. The surface tension forces play an essential role when shrinking the dimensions of channels. Preliminary studies pointed out that the effect of surface tension alters the flow patterns to some extent, such as the absence of stratified flow denoting a slight impact gravitational force. However, it is deemed that the basic features of two-phase flow are still preserved, with the prevailing force of surface tension in the flow field (Kandlikar and Grande, 2003). Therefore, many recommendations in literature were dedicated by the researchers to this issue in small/micro channels through experimental investigations so far (Wei et al., 2017).

2.4.1 Effect of channel size

The influence of channel size on flow patterns and their transition boundaries was studied through several experimental investigations regarding adiabatic and diabatic two-phase flow in vertical and horizontal channels. Coleman and Garimella (1999) conducted adiabatic two-phase flow test to investigate the effect of diameter on the flow pattern transition boundaries in tubes with diameter range 1.3 – 5.5 mm. They reported that the flow mechanisms in mini diameter tubes are different from conventional tubes because of the interaction of surface tension, shear (inertia) and gravitational forces. They compared their experimental data with flow pattern transition models from literature and found some deviations. Therefore, they concluded that the reduction of tube diameter affects the magnitude of these forces resulting in transition boundaries between flow patterns moving to higher superficial gas and liquid velocity. Chung and Kawaji (2004) investigated channel diameter effect on two-phase flow patterns. They conducted adiabatic tests with a mixture of nitrogen gas and water in horizontal channel diameter of 0.53 – 0.05 mm. The authors observed that the absence of churn flow in 0.1 mm and 0.05

mm and also slug flow was the prevailing flow regime. Pehlivan et al. (2006) studied the diameter influence on flow regime transitions in tubes with diameter range 0.8 – 3 mm. They also found the microchannel size having a strong effect on flow pattern transitions. Their flow pattern results revealed that the stratified flow becomes invisible in any microchannel experiment. This is because of the dominance of surface tension effects in the microchannel in contrast with the macrochannels. They classified the flow patterns into surface tension- and inertia-predominated regions. Fukano and Kariyasaki (1993) and Ide et al. (2007) studied the effect of tube diameter on adiabatic two-phase flow in small tubes having inner diameter range 1 – 9 mm. They noticed that the peripheral distribution of the liquid film thickness becomes more uniform with the reduced channel size resulting in an axisymmetric flow pattern due to the effects of surface tension. Venkatesan et al. (2010) investigated the effect of tube diameter on the gas-liquid flow regimes during small-diameter channels with range 0.6 – 3.4 mm internal diameter. They found that due to the effect of diameter, the stratified and wavy-annular flows were not observed in tube diameter less than 2 mm with the occurrence of move in flow pattern transitions. The authors reported that the reduced channel diameter leads to the absence of buoyancy forces due to predominate of surface tension forces and thus the increase in acceleration of gas phase (higher superficial gas velocity). It seems that all those factors affect the coalescence mechanisms between successive bubbles. Zhang et al. (2011b) experimentally investigated the effect of channel diameter on two-phase flow regimes during horizontal microchannel with a diameter range of 0.302 – 0.916 mm. They stated that, by decreasing tube diameter, the bubbly to slug transition tended to lower vapour and liquid superficial velocities while slug to churn and churn to annular transitions shifted into higher vapour and liquid superficial velocities. The authors interpreted this phenomenon based on the dominance of surface tension force with reducing tube diameter. Saljoshi and Autee (2017) performed adiabatic two-phase flow in 1.1 – 3 mm tubes to investigate the effects of the channel size on flow patterns. They observed that the reduced tube diameter leads to shifting the bubbly-slug transition towards the lower liquid and gas superficial velocities. They reported that reduced tube diameter causes an increase in the surface tension force and a decrease in the gravitational force. However, the annular flow shifts to higher superficial gas velocities when the channel size reduces. They illustrated that the thickness of the liquid film becomes thinner in a smaller diameter and thus increased shear stress between liquid and tube wall.

Regarding the experimental data obtained from the diabatic two-phase flow, Chen et al. (2006) studied flow boiling of R134 inside small-diameter tubes with an inner diameter of 1.1 – 4.26 mm. They observed the seven typical flow patterns that include the dispersed bubble, bubbly, confined bubble, slug, churn, annular and mist flow (see Figure 2.2). The mist flow was observed only in 4.26 mm tube while the annular-mist flow was observed in 2.01, 2.88, and 4.26 mm tubes. The confined bubble flow was observed only in 1.1 mm tube. The chaotic behaviour of churn flow also diminishes when channel diameter is reduced.

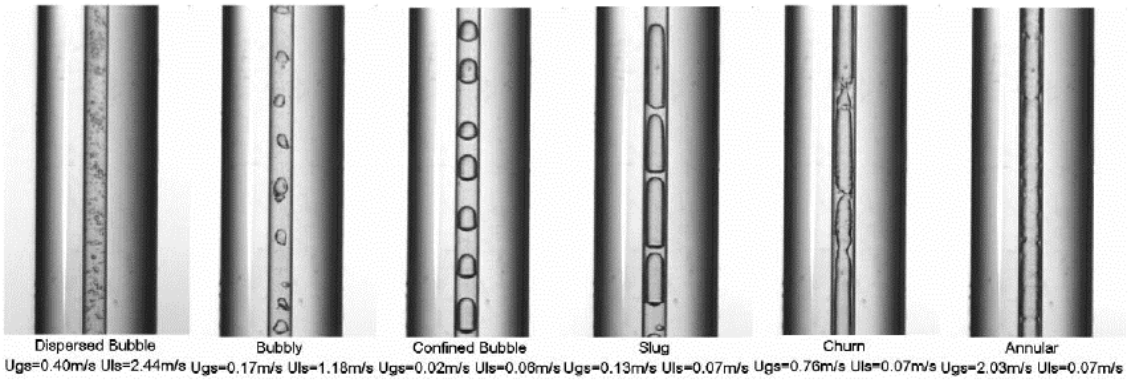

(a)

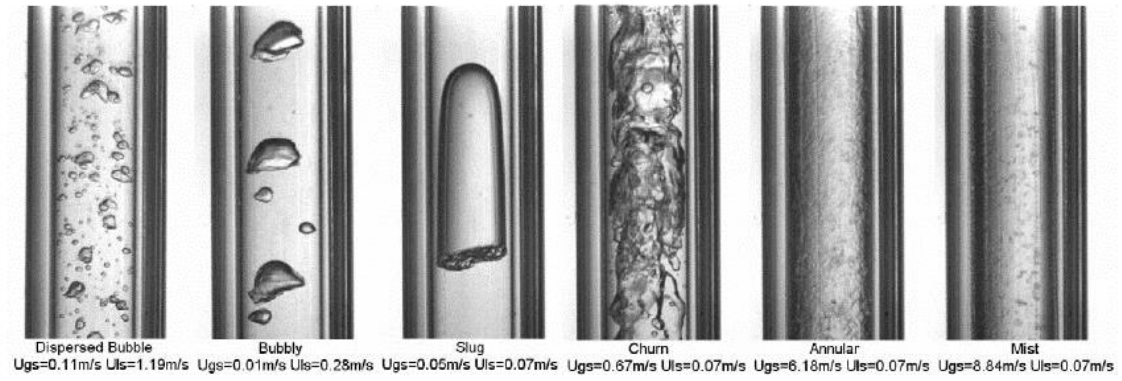

(b)

Figure 2.2 Flow patterns of R134a observed by Chen et al. (2006) at 10 bar in: (a) 1.1 and (b) 4.26 mm tube.

Figure 2.3 shows the effect of diameter on transition boundaries of flow regimes. They found that the transition boundaries for the slug to churn and churn to annular, strongly depends on the tube diameter and they shifted to higher superficial vapour velocities. The dispersed bubble-bubbly transition also moved to higher superficial liquid velocities. In contrast, transition regions of bubbly-churn and bubbly-slug are only slightly influenced by the decrease in diameter size. Also, they noted that with the

reduction of tube diameter, the surface tension became the prevailing force in the flow field at all test pressures and lower fluid velocities.

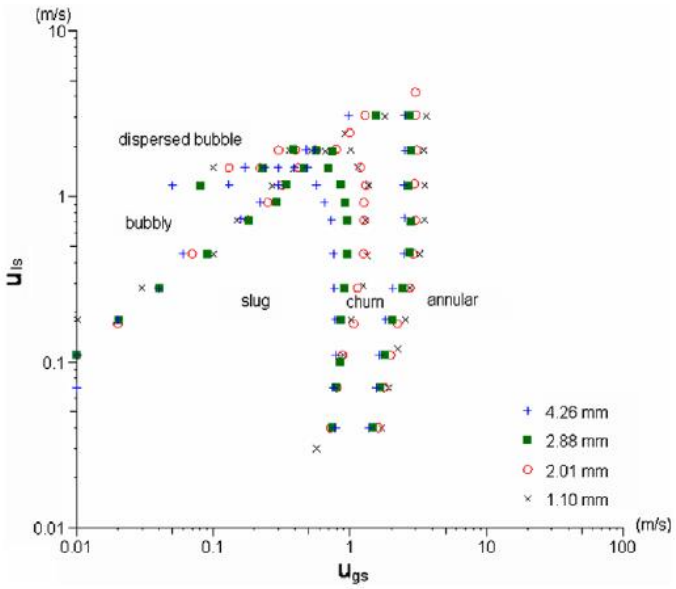

Figure 2.3 Effect of diameter on transition boundaries for R134a at 600 kPa, (Chen et al., 2006).

Zhang and Fu (2009) studied the influences of channel size on the flow regime map. They conducted two-phase flow boiling of N_2 in vertical tubes with 0.531–1.042 mm inner diameter. They found that the slug-churn and churn-annular flow transitions shift to lower superficial vapour velocity, while the bubbly-slug flow transition moves to higher superficial vapour velocity. The authors have drawn attention to the decreased channel size leading to suppression of gravitational forces with the dominance of surface tension forces and inertial forces. They considered that these major factors affect flow pattern transitions. Yang and Shieh (2001) introduced the experimental investigation to study effects of channel size on two-phase flow patterns inside 1 – 3 mm diameter tubes. They found that a change of channel size leading to the slug-annular transition boundary of R134a flow shifts towards a lower vapour superficial velocity. They concluded from these variations in transitions, three important parameters namely; surface tension force, buoyancy force and turbulent fluctuations. These have a strong impact on the determination of flow pattern transition in small channels. Particularly, surface tension force reduces the system's interfacial area causing the bubbles to keep the circular shape and the liquid holdup also retains between the tube walls. These situations, in turn, delay

the slug-annular transition for air-water flow. Pamitran et al. (2010) investigated the effect of channel diameter on the flow pattern boundaries through tube diameter range 0.5 – 3 mm. They found that the decreasing diameter leads to shifting the annular transition to lower vapour qualities. Tibiriçá et al. (2012) performed a study of channel size effect on flow patterns for 1 and 2.2 mm tubes. The authors reported that the transition from churn to annular flow is shifted to low vapour quality as a tube diameter is reduced from 2.2 to 1 mm. Ali et al. (2013) presented visualisation results of R134a flow patterns in 0.781 mm tube and utilized the experimental results of Martín-Callizo et al. (2010) for 1.33 mm tube to study the influence of channel size on flow regimes neglecting flow orientation effect. They reported that the reduction in tube sizes leads to move the bubbly-slug transition boundary to lower values of vapour quality due to confinement influences. In contrast, the slug-annular transition boundary moves to higher values of vapour quality on account of the surface tension effect in microtubes. Sempértegui-Tapia et al. (2013) investigated the effect of channel size on flow patterns during flow boiling in tube diameter of 1.1 – 2.32 mm. They found that the vapour quality corresponding to churn-annular flow transition decreases when tube diameter reduces. However, the transition of elongated bubble-churn shifted into low vapour qualities with increasing tube diameter from 1.1 to 2.32 mm. They reported that the changes in flow pattern boundaries resulted from increased surface tension effects and reduced turbulence effects with decreasing channel diameter. Tibiriçá and Ribatski (2014) performed experiments for flow boiling in 0.4, 1 and 2 mm tubes. They found that the decrease of tube size less than 2 mm for R245fa causes the absence of stratified flow. The authors attributed this to the strong effect of surface tension force which overcomes the gravitational force. Zhu et al. (2017a) investigated the flow patterns of R32 through boiling in 1 and 2 mm tubes. They noticed that expansion in the annular flow and mist flow regions occurs when the tube diameter reduces. In contrast, the slug flow region decreases with decreasing tube diameter.

There is a contradictory standpoint in the effect of channel size on flow patterns. Revellin and Thome (2007a) carried out flow boiling experiment to study diabatic flow patterns in microchannels with 0.5 mm and 0.8 mm tube diameter. The authors did not notice any effect of channel diameter on flow patterns. Liu and Wang (2008) experimentally studied flow patterns of air-water flow in vertical channels with diameter range 1.47 – 3.04 mm. They noticed that the diameter effect on the flow patterns is not

remarkable. They thought that the two-phase flow patterns are dependent on gas and liquid velocities. The researchers did not give any explanation for no effect of the channel size on the flow pattern.

Finally, the deduction is that there are discrepancies in the reported two-phase flow patterns and the effect of channel size. Some researchers agreed that the decreasing channel size leads to main changes in two-phase flow patterns and their transition boundaries such as the absence of some flow regimes or the presence of new features, while others did not observe any effect of channel size on flow patterns such as Liu and Liu and Wang (2008) and Revellin and Thome (2007a)**.** When the tube diameter reduces to microchannel size, surface tension effects overcome gravity and buoyancy effects and thus some flow regimes become absent (such as stratified and wavy-annular flows) or their transition boundaries shift. Some researchers found that the bubbly-slug flow transition shifted into lower vapour and liquid superficial velocities, while the slug-churn and churn-annular flow transitions moved to higher superficial vapour velocities. Therefore, the flow patterns in microchannels may differ from that in conventional channels. In this work, the effect of four diameter tubes on flow regimes were studied, including 1.1 mm, 2.01 mm, 2.88 mm, 4.26 mm inner diameter tubes. The decreasing diameter tube from 4.26 mm to 1.1 mm resulted in main changes in two-phase flow patterns and their transition boundaries such as the absence of slug flow and shifting the churn-annular transition to higher superficial vapour velocity.

2.4.2 Effect of pressure and fluid properties

The two-phase flow in small channels is likely to be strongly dependent on the viscosity, density and surface tension. These properties vary from fluid to another with taking into account the influence of saturation temperature corresponding to operating pressure. They also cause significant changes in the two-phase flow patterns between conventional channels and small channels. There were several experimental studies of two-phase flow in vertical and horizontal channels confirming the effect of fluid properties on flow patterns and their transition boundaries.

Among these studies concerning flow patterns in vertical channels, Furukawa and Fukano (2001) investigated the viscosity influence on transitions between flow patterns in 19.2 mm vertical tube isothermally. Water and aqueous glycerol solutions, kinematic viscosities range of $1\times10^{-6} - 14.7\times10^{-6}$ m^2/s were employed as working fluids. They found that increasing liquid viscosity moves the bubbly-slug transition boundary to lower gas superficial velocities and the annular transition to regions of higher gas superficial velocities. It is perceived that the liquid film in both slug and annular flows affect the change in liquid viscosity. Zhang et al. (2011b) experimentally investigated the effect of physical fluid properties on two-phase flow regimes in a horizontal microchannel. They noticed that with increasing liquid viscosity, the transitions of the slug to churn and churn to slug-annular flow occurs at higher vapour and liquid superficial velocities. However, with decreasing surface tension and fixed channel diameter, the bubbly to slug transition occurs early. The same thing also happens with transitions from slug to churn and to slug-annular. The authors attributed this case to the contraction of a region dominated by surface tension forces. Martín-Callizo et al. (2010) studied the effect of saturation temperature on R134a flow patterns in a microtube. They found that an increase in the saturation temperature has a strong influence on shifting the transition boundaries of flow regimes towards high vapour qualities. They attributed the shift of flow pattern transitions to the effect of saturation temperature on liquid-vapour density ratio. Namely, the density ratio decreases with increasing saturation temperature. Thus, the smaller bubbles are formed. The authors also reported that the occurrence of coalescence between smaller bubbles naturally needs more energy. Yang and Shieh (2001) presented the experimental investigation to study effects of fluid properties on two-phase flow patterns for R134a and air-water inside small diameter tubes with the diameter range of 1.0 – 3.0 mm. The variance in properties of working fluids drew the authors' attention that the transition from bubbly to intermittent (plug-slug) flow for air-water takes place earlier than that for fluid R134a in the same tube and conditions. They indicated to the variations in flow patterns transitions between air-water and R143a because R134a has a lower surface tension value than air-water.

The flow patterns of different working fluids were experimentally investigated by Arcanjo et al. (2010) to study bubble characteristics for flow boiling in a single horizontal mini tube. The authors took into account the effect of the fluid properties on transition

boundaries of flow patterns. Therefore, they tested the influence of working fluids and different saturation temperatures on bubble characteristics. They found that the measured bubble velocity increases with decreasing saturation temperature. They also observed that the measured velocity of the elongated bubble of R245fa is higher than that of R134a at the same operating conditions. Meanwhile, the slug-churn and churn-annular flow transitions move towards higher vapour qualities for higher saturation temperature and R134a. The authors thought that the superficial vapour velocity increases with decreasing vapour density, resulting in increased inertial forces to break up liquid bridges existing in the intermittent flow. This is due to the vapour density increases with increasing saturation temperature and its value is lower for the R245fa than for the R134a. Tibiriçá et al. (2012) performed flow boiling experiments for R134a and R1234ze(E) in 1 and 2.2 mm tubes to investigate the fluid effect on flow patterns. They noticed that the flow pattern transitions for both fluids in the same flow conditions are similar. This implies that R1234ze(E) has similar properties to R134a, i.e. it is considered as an alternative fluid to the R134a. Ali et al. (2013) investigated the effect of pressure on flow patterns for R134a in a microtube. They represented their results on the flow regime maps, which were identified in terms of gas-liquid superficial velocities. These maps showed the transition lines for Slug-Semi-annular and Semi-annular-Annular are moved towards lower vapour velocities as reported. The authors elucidated that the pressure affects the fluid properties. In other words, the liquid and vapour density ratio became higher when the pressure decreased leading to higher vapour velocity and consequently the shift of flow pattern transitions to low vapour quality and low vapour velocities. Sempértegui-Tapia et al. (2013) studied the effect of two fluids and saturation temperatures on two-phase flow patterns during flow boiling in horizontal tubes. They noticed that the flow pattern transitions for R245fa take place at lower vapour quality earlier than these for R134a under the same operating conditions. Moreover, an increase in saturation temperature leads to the vapour quality transition of churn-annular increased for the same tube and fluid. These cases have been explained by the authors as follows: the vapour specific volume of R245fa is larger than that of R134a and also the specific volume of vapour decreases with increasing saturation temperature. Charnay et al. (2014a) carried out flow visualisations in a 3 mm internal diameter tube to study the effects of high saturation temperature on flow patterns transitions. They reported that dryout and mist flows were not observed at the saturation temperature of 60 °C. On the contrary, they

were observed and expanded to low vapour quality when the saturation temperature was increased to more than 60 °C. The range of annular flow became narrow when the saturation temperature increased. The authors interpreted this case based on decreasing surface tension with increased saturation temperature. Therefore, the liquid film moved towards high vapour velocity core. Zhu et al. (2017a) investigated the effect of pressure on flow patterns of R32 in 1 and 2 mm diameter tube. They observed that the increase in saturation temperatures corresponding to operating pressures leads to larger slug and mist flow region, and smaller annular flow region. Moreover, the slug-churn and the churn-annular transitions shift to higher vapour qualities. Also, the annular-dryout and dryout-mist transitions shift to lower vapour qualities. The authors mentioned that the decreasing liquid-vapour density ratio with increasing saturation temperature is harder to generate continuous vapour in the tube core. However, the surface tension decreases when saturation temperature increases. This leads to the difficulty of forming a liquid-vapour interface. The surface tension plays a prevailing role in the formation of a liquid film on the channel wall at high vapour qualities. As the surface tension decreases, the liquid film on the channel wall is more likely to break and consequently lead to an early occurrence of dryout.

Even though various experimental data have been reported on two-phase flow patterns in macro, mini and microchannels, a conclusion can be drawn from the above; the flow patterns and their transition boundaries are affected by fluid properties and saturation temperature corresponding to system pressure. Thus, the liquid-vapour density ratio affects vapour velocity, while liquid viscosity and surface tension play a significant role in effect on bubble characteristics and the thickness of the liquid film on the tube wall. Generally, the increased pressure and the fluid having higher reduced pressure move the bubbly-slug transition boundary to lower superficial vapour velocities and the transitions of the slug-churn and churn-annular flow to regions of higher superficial vapour velocities. The experimental data for three low pressures were used in the present work to study their effects on flow regimes, including those for 185, 245 and 310 kPa.

2.4.3 Effect of flow orientation

The two-phase flow in the small channel is probably affected by flow orientation due to the effect of gravitational forces. Therefore, the influence of flow orientation on flow patterns and their transitions has been associated with the effect of channel size, surface tension and gravity. The influence of flow orientation (vertical or horizontal direction) on flow patterns was studied through experimental investigations for adiabatic and diabatic two-phase flow in small channels.

Barnea et al. (1983) performed experiments of adiabatic two-phase flow in five small diameter tubes, 4 – 12.3 mm, with horizontal and vertical upward orientation flow. They observed the stronger effect of surface tension on the transition boundary of stratified-slug flow. They accentuated this case with decreasing channel diameter. The experiments of gas-liquid flow inside vertical and horizontal glass tubes with 1 and 1.5 mm inner diameter were conducted by Chen et al. (2002). They also noticed that the flow patterns for both vertical and horizontal flows are quite similar, with the same gas and liquid superficial velocities. They indicated that the surface tension force prevails in microtubes. The investigation of two-phase flow in four tubes of inner diameter 1, 2.4, 4.9 and 9 mm with different orientations (horizontal flow and vertical up-and down-ward flow) was carried out by Fukano and Kariyasaki (1993) and Ide et al. (2007). They found that the orientation of the tube does not affect the flow patterns and their transition boundaries in mini diameter tubes (< 4.9 mm). The authors explained that the surface tension force has a much strong impact on the flow pattern than the gravitational force for a two-phase flow in microchannels. Saisorn et al. (2013) investigated the influences of flow orientation and system pressure on flow patterns in 1.75 mm tube. The authors found that the channel direction had an insignificant effect on the flow regime at a system pressure of 8 bar. However, with increasing pressure, the flow regime transitions for vertical upward flow differ from those for horizontal flow, as shown in Figure 2.4. The authors adopted the proposed clarification of Kandlikar (2010) which included five major forces having a significant impact on the flow boiling process. These forces included surface tension, inertia, gravitational, viscous and evaporation momentum forces. The interaction of these forces with the relative change in system pressure yielded the variations in transitions of flow pattern for both directions. This means that the surface tension force and evaporation

momentum force have been reduced by increasing system pressure. This, in turn, leads to a gravitational force becoming more influential on the vertical upward flow, resulting in the flow pattern transition for the vertical flow being different from that of horizontal flow. Ali et al. (2013) utilized the experimental results of Martín-Callizo et al. (2010) to study the influence of flow orientation on flow regimes. It is noted that the churn flow was not observed in the horizontal microtube. They considered that the effect of surface tension forces in microtubes caused the absence of some flow patterns. Mehta and Banerjee (2014) presented an experimental study on the influence of flow orientation (horizontal flow and vertical up-and down-ward flow) on isothermal two-phase flow patterns in a 2.1 mm tube. They observed that at low gas and liquid flow rate, the slug flow converts to annular flow when the flow orientation changes from horizontal to vertical down flow. The authors also found that the slug length increases when changing the flow orientation to upward flow. They attributed this phenomenon to the dominance of gravitational effect over surface tension effect. However, with increasing liquid flow rate and keeping low gas flow rate, the flow orientation from horizontal to vertical upward flow has a slight effect on flow patterns. Mohseni and Akhavan-Behabadi (2014) investigated the effect of different channel inclinations on flow patterns for R134a in 8.9 mm diameter tube. They observed that the different tube inclinations in a range of −90° to +90° affects the distributions of vapour and liquid phases. They attributed these variations in flow patterns to effects of gravitational, inertia and buoyancy force on two-phase flow.

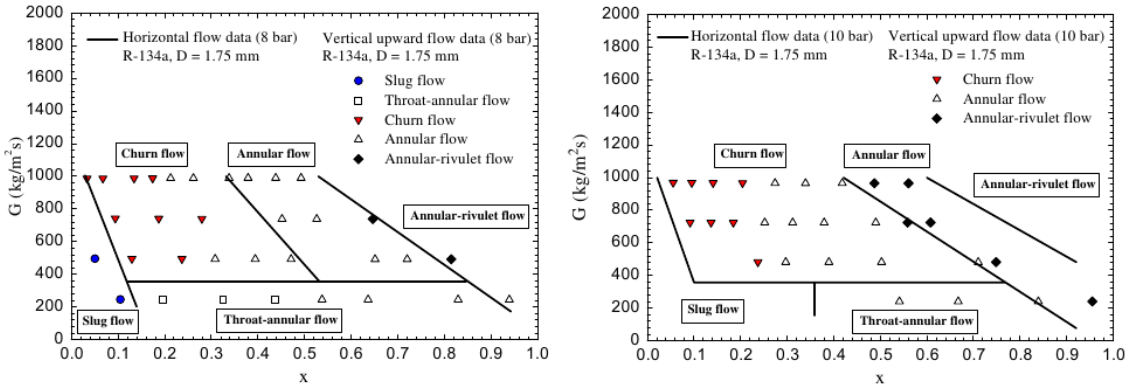

(a) (b)

Figure 2.4 Effect of channel orientation on flow patterns for R134a in 1.75 mm tube at: (a) a pressure of 8 bar and (b) a pressure of 10 bar from Saisorn et al. (2013).

It can be inferred from the above, when tube diameter decreases to smaller than 4 mm, the effect of channel orientation diminishes and the surface tension becomes the dominant force over gravitational force in the flow field. This, in turn, influences the distributions of vapour and liquid phase in small-diameter channels. Therefore, the observed flow patterns in the horizontal channel are not noticeable in the vertical channel, such as the stratified flow regime. In this work, the vertical orientation was chosen because there is still a small part of the literature that deals with two-phase flow patterns through vertical small channels.

2.4.4 Effect of mass flux

The mass flux has a strong impact on the variations in two-phase flow patterns because it affects the behaviour of the departure bubbles and the mechanism of coalescence between bubbles. It was also considered by most researchers as a basic factor with vapour quality in the representation of their experimental data on the flow pattern maps.

One of these researchers, Ali et al. (2013) presented visualisation results of R134a which were obtained for flow boiling in 0.781 mm horizontal tube. The results revealed that mist flow pattern occurs at low mass flux while wavy-annular flow is observed at high mass flux. They also studied the characteristics of bubble flow, and they found that the increase in the mass and heat fluxes leads to increasing bubble frequency and consequently bubble coalescence rate. As a result of this, the transition to annular flow occurs early. Pamitran et al. (2010) found that smaller tube diameter and higher mass flux lead to shifting the annular transition to lower vapour qualities. Arcanjo et al. (2010) studied bubble characteristics and flow regimes for flow boiling in a single horizontal mini tube with inner diameter of 2.32 mm. The authors took account of the effect of mass flux on transition boundaries of flow patterns. Therefore, they tested its influence on bubble characteristics. They found that the measured bubble velocity increases with increasing mass flux and vapour quality and decreasing saturation temperature. Tibiriçá and Ribatski (2014) confirmed that the bubble frequency increases with increasing mass flux. This affects the coalescence mechanism and thus leads to the shift of flow regime transitions or the absence of some flow patterns such as stratified flow. Charnay et al.

(2014a) conducted flow visualisations during R245fa flow boiling in 3 mm internal diameter tube. They reported that the intermittent flow (bubbly flow, bubbly-slug flow and slug flow) range reduced with increasing mass flux due to increasing coalescence rate between bubbles. This, in turn, accelerated the occurrence of annular flow. Zhu et al. (2017a) investigated the flow patterns of R32 through boiling in 1 and 2 mm inner diameter tubes. They observed that the mass flux has a significant impact on slug, annular and mist flows. Namely, the slug and annular flow ranges reduce and the mist flow range in flow regime map expands with increasing mass fluxes.

It can be concluded from the above that all researchers agreed that the mass flux has a significant effect on bubble characteristics and consequently on the distributions of the phases in small channels. That is, increased mass flux leads to increasing bubble velocity, bubble frequency and consequently bubble coalescence rate. This, in turn, results in the absence of some flow patterns such as stratified flow and the shift of flow pattern boundaries to the lower vapour qualities such as the early occurrence of annular flow. The changes of mass flux for vertical tubes and their effects on flow regimes were experimentally studied in this work with the range of 200 – 500 kg/m^{2}s.

2.5 Flow Pattern Maps

The flow pattern map is employed to determine the transition boundaries between flow regimes in the channel. The identification and prediction of flow patterns have a significant role in the development of the flow boiling process. Particularly, it assists in the development of predictive models for heat transfer coefficient and pressure drop in mini/micro-channels. Also, it provides an insight into the heat transfer mechanisms in a channel. Therefore, there are many studies that have specialised in investigating the flow pattern maps such as Alexeyev et al. (1991), Kattan et al. (1998), Coleman and Garimella (1999), Chen et al. (2006) and Revellin and Thome (2007a). The researchers took into account the effective parameters which affect the applicability of flow pattern map in flow boiling fields such as fluid properties, channel size, channel orientation and operating conditions. The studies of two-phase flow patterns were categorised into two groups (theoretical and visual) Charnay et al. (2013). In a theoretical study, the researchers tried to organise relations based on physical characteristics of flow such as

viscosity, surface tension, density and void fraction. For example, Taitel et al. (1980), Mishima and Ishii (1984), and McQuillan and Whalley (1985) established such relations for transitions of two-phase flow patterns in vertical upward tubes, which are recently the basis of comparison for many studies. In a visual study, the researchers tried to collect experimental observation data by using a high-speed camera and then organise based on operating parameters such as pressure, mass flux, vapour quality, geometrical characteristics and gas and liquid velocity.

Several studies available in the literature over the past decades have provided significant knowledge for two-phase flow maps in regard to the flow in conventional channels. These studies are primarily the start point for the transition to small channels. The details of conventional channel studies regarding observed flow regimes, working fluids and channel size are listed in Table 2.3. An early study of two-phase vertical flow in the conventional channel was conducted by Hewitt and Roberts (1969). They suggested a two-phase flow map for vertical upward flow as shown in Figure 2.5; the mass flux to density ratios of liquid and gas coordinated the values of the ordinate and abscissa, respectively. The flow patterns are predicted at the intersection of these two values on the map.

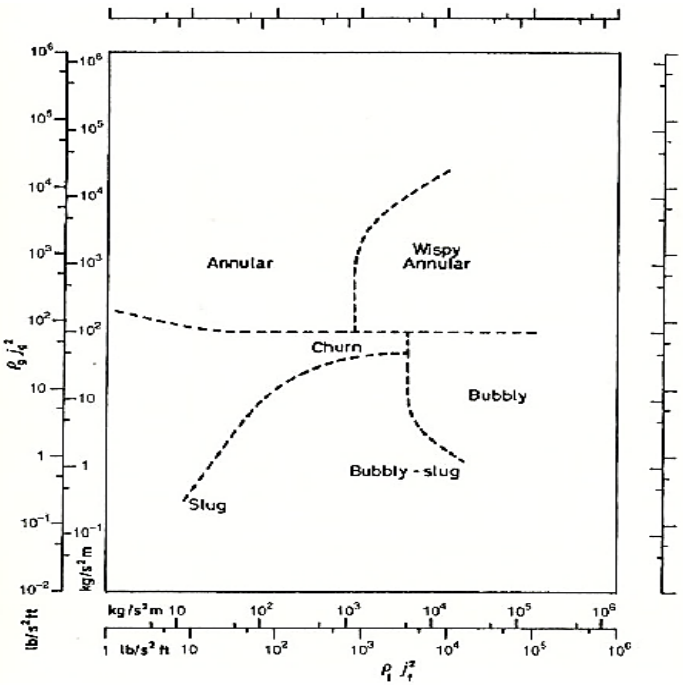

Figure 2.5 Two-phase flow pattern map of Hewitt and Roberts (1969) for vertical tubes cited from (Thome, 2007).

Taitel et al. (1980) developed theoretical models for predicting the transition boundaries of flow regimes during stable gas-liquid flow in vertical channels. They incorporated the effect of channel size and fluid properties in their models based on physical mechanisms proposed for each flow pattern transition.

Table 2.3 Summary of flow patterns covered in the existing flow pattern maps for conventional channels.

Author(s)	Fluids	D_h (mm)	Orientation	Flow patterns
Hewitt and Roberts (1969)	Air-water	31.75	Vertical	Bubbly Bubbly-Slug Slug Churn Wispy-Annular Annular
Taitel and Dukler (1976)	Air-water Crude oil- natural gas	12.5–300	Horizontal	Stratified-Smooth Stratified-Wavy Dispersed bubble Intermittent Annular-Dispersed
Taitel et al. (1980)	Air-water Crude oil- natural gas	25–50	Vertical	Dispersed bubble Slug Churn Annular
Barnea et al. (1983)	Air-water	4–12.3	Horizontal Vertical	Stratified Dispersed bubble Intermittent Annular
Mishima and Ishii (1984)	Air-water	-	vertical	Bubbly Slug Churn Annular
Kattan et al. (1998)	R134a R123 R404a R404a R502	12	Horizontal	Intermittent Annular Mist Stratified-Wavy
Thome and El Hajal (2003)	R134a	12–14	Horizontal	Model only for Intermittent Stratified –Wavy Stratified Annular Mist

Figure 2.6 shows the theoretically predicted transitions for air-water upward flow in 50 mm inner diameter tube. The map is presented in terms of gas and liquid superficial

velocities. Mishima and Ishii (1984) developed theoretically the gas-liquid flow regime transition criteria for vertical upward conventional tubes based on the one-dimensional drift-flux model of Ishii (1977). The regime criteria presented satisfactory agreements with air-water and steam-water data as well as their applicability to boiling flow.

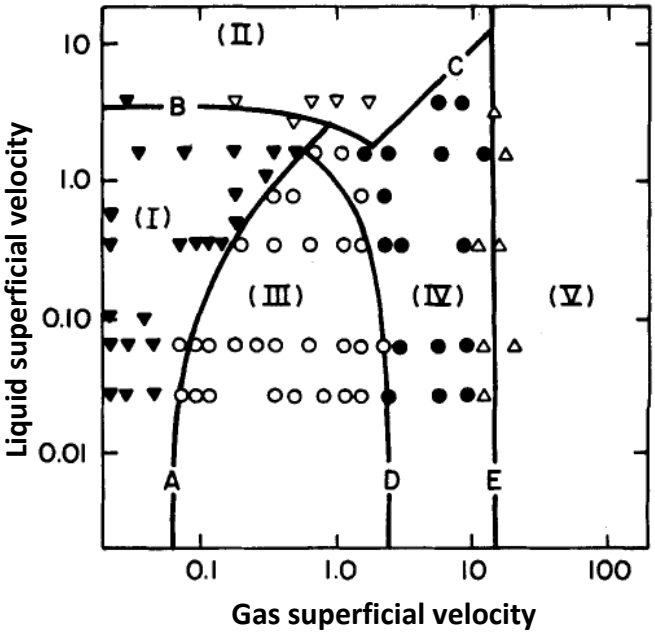

Figure 2.6 The flow pattern map of Taitel et al. (1980) for air-water flow in 50 mm vertical tube; I is bubbly flow; II is dispersed bubble flow; III is slug flow; IV is churn flow; V is annular flow.

Figure 2.7 depicts the transition criteria for bubbly-slug, slug-churn, and churn-annular transition boundaries. The transition line of annular-annular/mist depended on the criterion for larger tubes. Another theoretical study of two-phase flow adopting the transition flow pattern equations for Taitel et al. (1980) and Mishima and Ishii (1984) has succeeded in improving the predictions of flow patterns and transition boundaries. This study was conducted by McQuillan and Whalley (1985) to predict the gas-liquid flow patterns and transitions for upward flow in a vertical tube. Furthermore, they modelled the transition boundary between plug flow and churn flow under the flooding theory (flow reversal of the falling liquid film in a counter-current two-phase flow system). In this transition flow pattern model, they assumed that the plug flow stability is limited by the flooding of the falling liquid film. They combined this model with other models of flow pattern transitions to form theoretical flow regime map as shown in Figure 2.8.

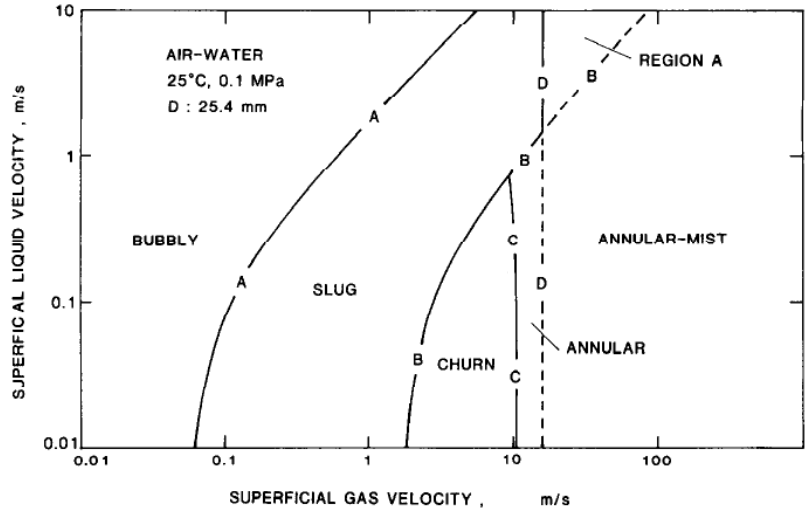

Figure 2.7 Flow patterns map was developed by Mishima and Ishii (1984).

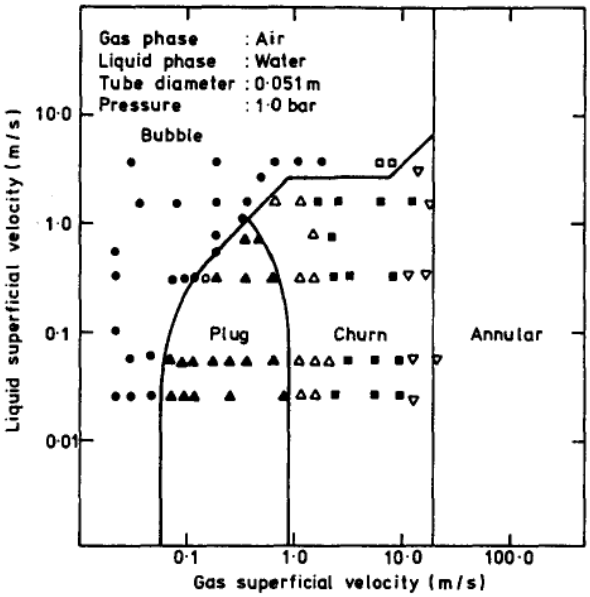

Figure 2.8 Flow patterns map was developed by Mishima and Ishii (1984).

Taitel and Dukler (1976) developed a theoretical model to predict the transition boundaries physically between flow pattern regimes for gas-liquid two-phase flows in conventional horizontal or inclined tubes. This model is based on the relation between channel size, inclination, gas and liquid mass flow rate and fluid properties. It is observed that fluid properties and channel size have a significant effect on the displacement of transition boundaries of two-phase flow patterns for the circular tube as shown in Figure 2.9. However, their model does not consider the surface tension effect.

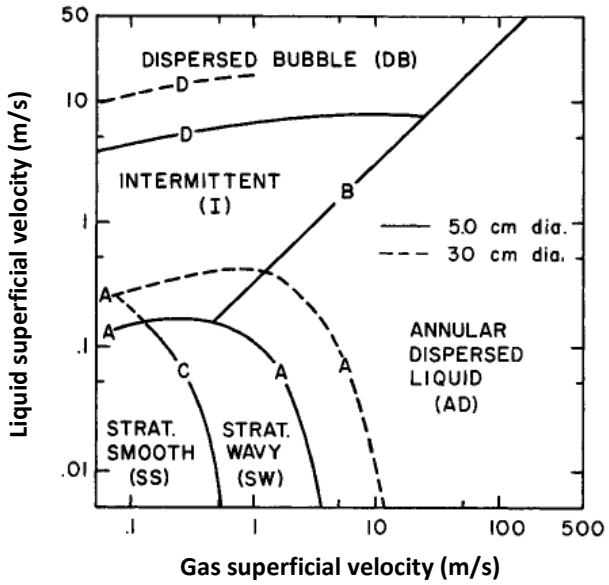

(a)

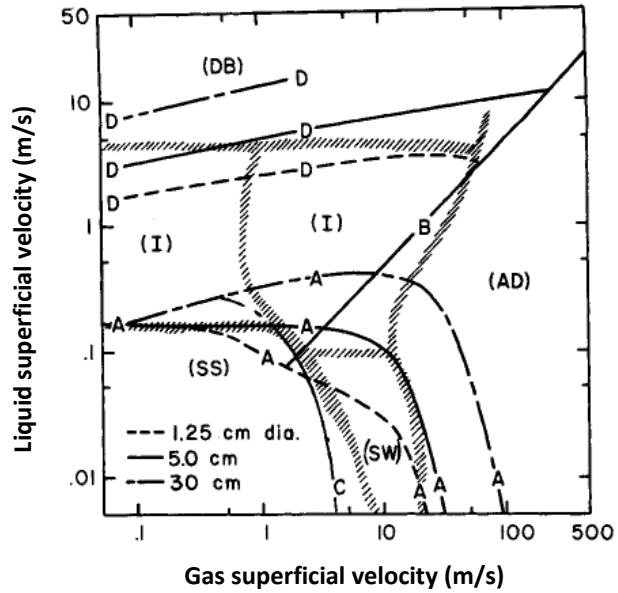

(b)

Figure 2.9 the channel size effect on transition boundaries in the horizontal channel: (a) fluid properties effect and (b) channel size effect, (Taitel and Dukler, 1976).

Barnea et al. (1983) performed experiments for adiabatic two-phase flow in five small diameter tubes 4-12.3 mm with horizontal and vertical upward orientation flow at 25°C and atmospheric pressure using air-water as a working fluid. They observed the stronger effect of channel geometry on the transition lines of flow regimes. They also establish that surface tension has a great influence on flow patterns only in mini diameter tubes. Therefore, they detected that the transition model for conventional diameters could not predict transition boundaries in mini tubes because it does not take into account the

effect of surface tension like Taitel and Dukler (1976) and Taitel et al. (1980) models, as shown in Figure 2.10. Thus, they suggested improvements to these models that consider the typical influence of surface tension in mini diameter tubes.

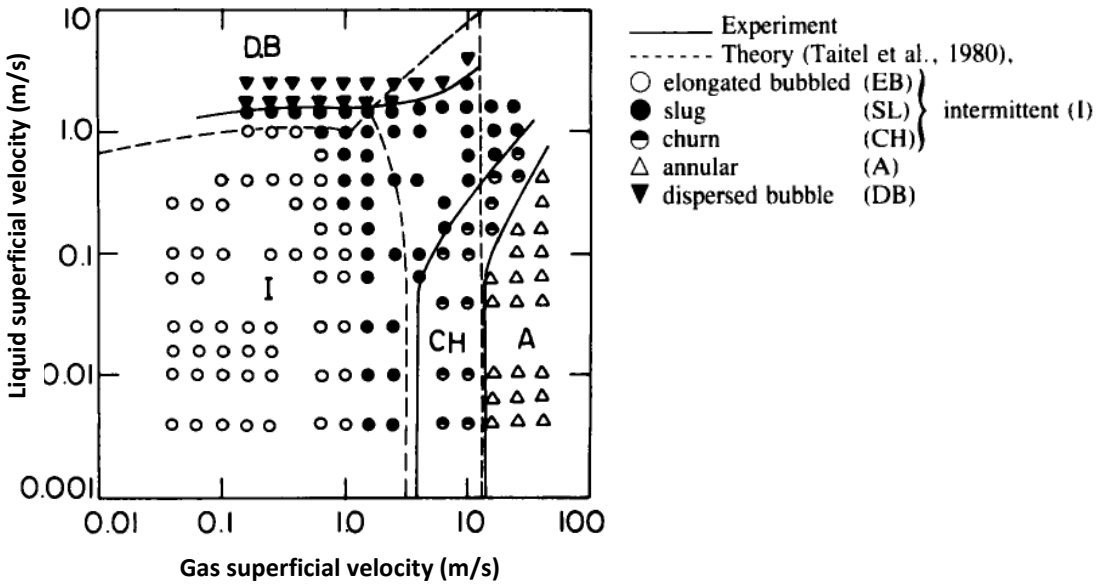

Figure 2.10 Flow patterns map for air-water flow in an upward vertical tube of 4 mm at 0.1 MPa and 25°C, (Barnea et al., 1983).

In order to understand the flow pattern transitions through flow boiling, it would be necessary to take into account the heat flux effect on flow patterns. Therefore, the study of Kattan et al. (1998) made a major contribution to developing a flow pattern map based on experimental data. It qualified to be applicable to both diabatic and adiabatic conditions. The map was presented in terms of mass velocities and exit vapour qualities. Thome and El Hajal (2003) modified the flow pattern map model of Kattan et al. (1998) which was utilized to predict the transition boundaries of flow patterns for evaporation in horizontal small-diameter tubes. The authors proposed a model for predicting the void fraction by using drift flux model of Rouhani and Axelsson (1970). The proposed map considering the effects of fluids and channel size was shown in Figure 2.11. The map was also valid for conventional channels under adiabatic flow conditions. However, it did not have validation to be applicable to microchannels. The authors used the suggested model of Kattan et al. (1998) with a fixed value of Lockhart and Martinelli (1949) parameter (X_{tt}=0.34) to determine the transition boundary between intermittent (plug and slug flow) flow and annular flow.

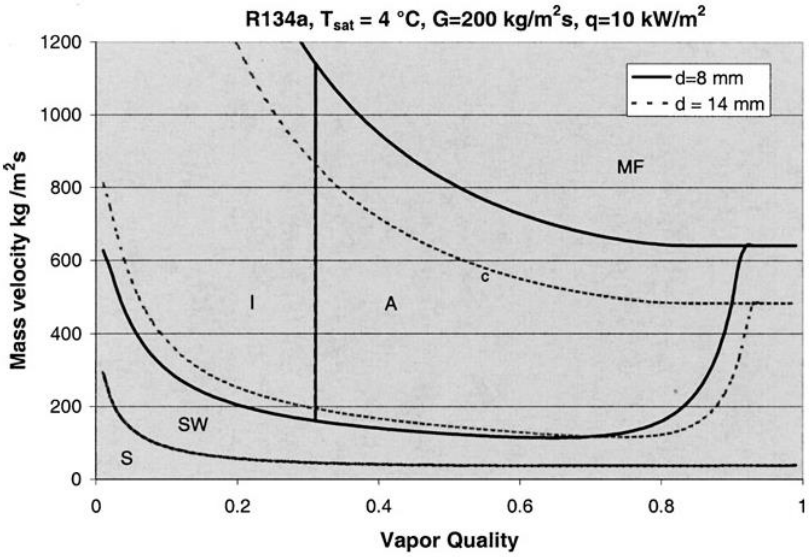

(a)

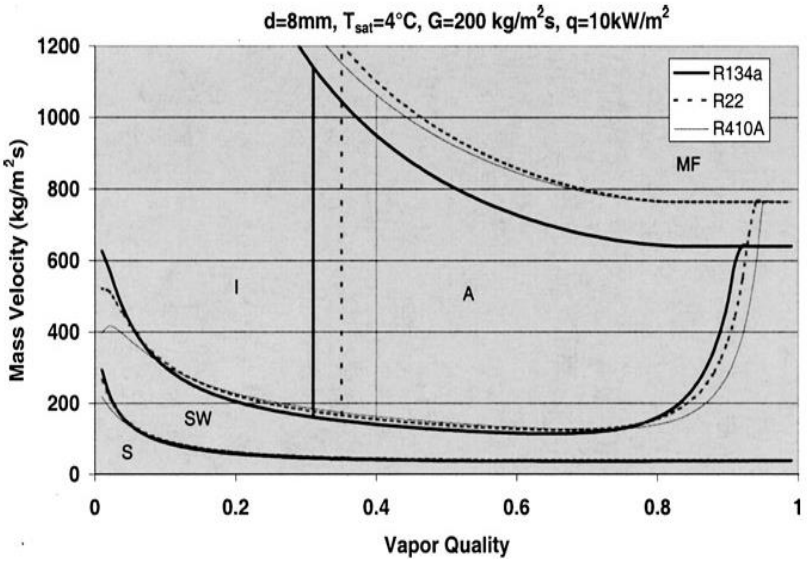

(b)

Figure 2.11 Flow pattern map was proposed by Thome and El Hajal (2003) for horizontal channels considering the effects of (a) channel size and (b) working fluids.

The greater part of the literature on flow patterns and transition boundaries is concerned with mini and microchannels as listed in Table 2.4. Experimental and analytical study of adiabatic two-phase flow in horizontal microtubes was carried out by Suo and Griffith (1964). They researched the effect of different working fluids and diameter tube on flow patterns. In particular, the authors focused on liquid-gas density ratio and liquid film around a long bubble. Therefore, they have made a reasonable model for the density and the liquid film thickness around a gas bubble. They also suggested the restrictions to define transition lines based on analytical work and experimental data considering the effect of fluid properties. The authors have reached to conditions of

$(\rho_l/\rho_g) \gg 1$, $(\mu_l/\mu_g) < 25$ and $(g\rho_g D^2/4\,\sigma) < 0.22$ at which slug flow occurred in two-phase flow. They also noticed that the gas flow corresponds to the long bubble and they pointed out the dominance of surface tension force over the gravitational force. Alexeyev et al. (1991) performed experiments to investigate flow patterns in the round and rectangular channel. The authors developed a map of two-phase flow pattern according to vapour and liquid superficial velocities using previous data from literature and obtained data. They found that the slug flow did not appear in their tests. They explained the effect of geometrical or hydrodynamic factor through associating the position of the flow pattern transition with the instability of vapour-liquid interface. Moreover, they detected that as the system pressure changed, the flow pattern transition boundaries of helium changed. The transition lines differ not only in changing pressure but also in the use of different fluids. The authors concluded that this is due to changes in fluid properties.

The influences of geometrical shape and channel size on flow patterns were studied by Coleman and Garimella (1999). The two-phase flow tests were conducted in circular and rectangular horizontal channels. They presented flow pattern map for adiabatic two-phase flow, and its boundaries were identified in terms of gas and liquid superficial velocities. The authors noticed that as the tube size was reduced to less than 10 mm, the surface tension force had a stronger impact on flow regimes and their transition boundaries. Furthermore, the region of the intermittent flow regime (elongated bubble and slug) was enlarged, and the stratified flow was suppressed. Akbar et al. (2003) proposed the flow pattern map based on collected gas-liquid data from the literature. They divided it into four zones, namely as surface tension-dominated zone (bubbly, plug and slug flows), inertia-dominated zone I (annular flows), inertia-dominated zone II (dispersed bubble) and transition zone, as depicted in Figure 2.12. These transition boundaries fitted to data for flow in microtubes with $D \leq 1$ mm. They inferred that the orientation of tube did not have any influence at this size of the tube.

Table 2.4 Summary of flow patterns covered in the existing flow pattern maps for mini/microchannels.

Author(s)	Fluids	D_h (mm)	Orientation	Observed flow patterns
Suo and Griffith (1964)	Air-water N_2-water N_2-heptane He-heptane	0.514–0.795	Horizontal	Slug Bubbly-slug Annular
Alexeyev et al. (1991)	He	1	Horizontal	Bubbly Stratified Intermittent Annular-dispersed Mist
Coleman and Garimella (1999)	Air-water	1.3–5.5	Horizontal	Intermittent
Garimella et al. (2002)	R134a	0.5–4.91	Horizontal	Intermittent
Akbar et al. (2003)	Air-water	< 1	Horizontal	Bubbly Plug Slug Dispersed bubble Transition Annular
Hassan et al. (2005)	Air-water N_2-water	0.1–1	Horizontal Vertical	Bubbly Intermittent Churn Annular
Cheng et al. (2006)	CO_2	0.8–10	Horizontal	Slug Intermittent Stratified Stratified-wavy Dryout Mist
Revellin and Thome (2007a)	R245fa R134a	0.509–0.79	Horizontal	Isolated bubble Coalescing bubble Annular Post dryout
Harirchian and Garimella (2010)	FC27	-	Horizontal	Confined slug Churn-confined-annular Bubbly Churn-wispy-annular Churn-annular
Ong and Thome (2011a)	R134a R236fa R245fa	0.5–3.04	Horizontal	Isolated bubble Coalescing bubble Wavy-annular Smooth-annular
Charnay et al. (2013)	R245fa	3	Horizontal	Bubbly Bubbly-slug Slug Annular
Mahmoud and Karayiannis (2016)	R245fa	1.1	Vertical	Bubbly Slug Churn Annular

Zhu et al. (2017a)	R32	1–2	Horizontal	Slug Churn Annular Dryout Mist Stratified
Tibiriçá et al. (2017)	R134a R1234ze(E) R236fa R245fa Air-water	0.25–5.5	Horizontal	Bubbly Slug Churn Annular Dryout

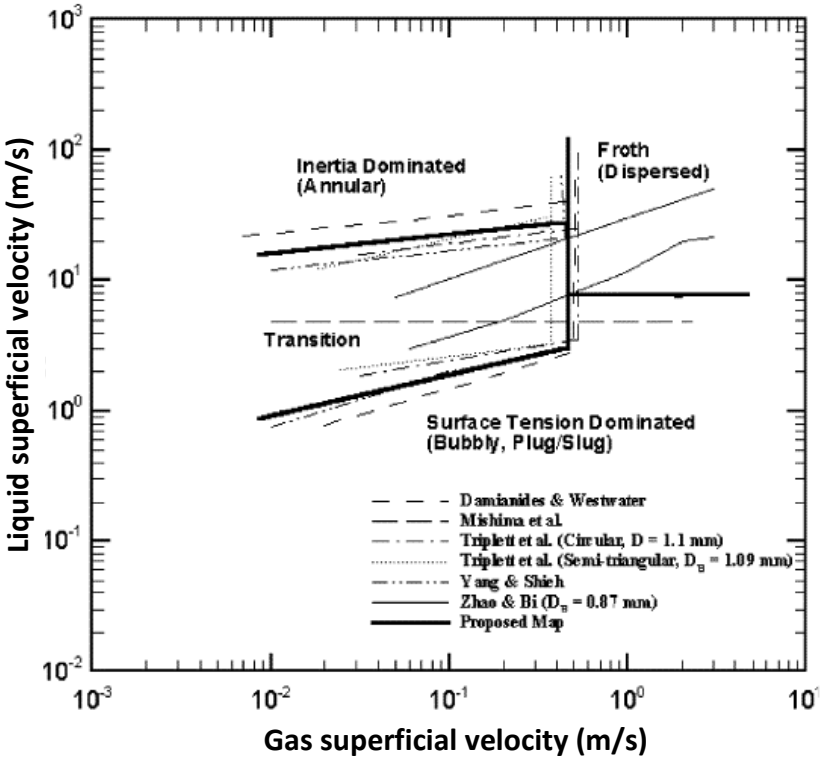

Figure 2.12 Flow regime transition lines for circular channels $D \leq 1$ mm were proposed by Akbar et al. (2003).

In a follow-up research, Hassan et al. (2005) present two universal flow pattern maps for adiabatic two-phase flow in horizontal and vertical microtubes as shown in Figure 2.13. The maps were presented in terms of gas and liquid superficial velocities. The authors found that surface tension has a significant influence for microchannels and it affects two-phase flow patterns and transition boundaries. They suggested two principal regions of flow regimes based on the dominance of force-type. The first one is considerably affected by surface tension forces which involves bubbly flow, slug flow and confined flow. The second one is strongly affected by inertia forces which includes

only dispersed flow and annular flow. The authors relied on collected two-phase flow database from the literature and their experimental data to propose two flow regime maps for horizontal and vertical microchannels as seen in Figure 2.13. They also reported that the proposed flow regime map required further efforts to acquire large experimental databases, especially for tube size less than 0.5 mm. Moreover, they recommended that the heat flux could be considered in the implementation of flow regime maps due to its significant influences on the flow regimes and transition boundaries.

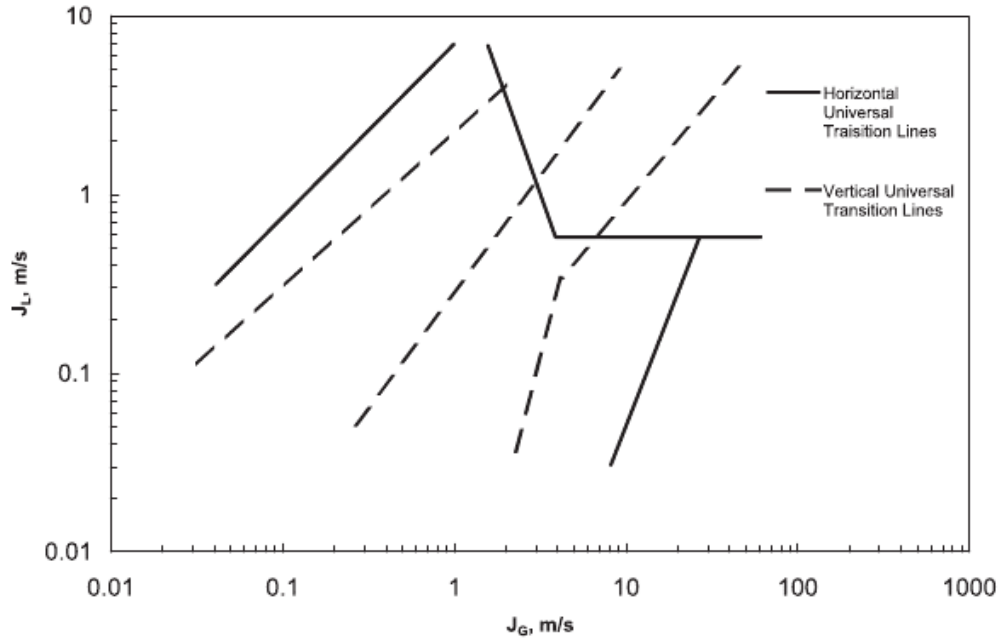

Figure 2.13 Universal flow pattern maps were modified by Hassan et al. (2005) for horizontal and vertical flow in tube diameter of 1 mm.

After the recommendation of Hassan et al. (2005) for considering the effect of heat fluxes, several studies have emerged to develop and update the flow pattern map in addition to investigating the relation between flow regime map and heat transfer mechanisms. Cheng et al. (2006) employed experimental flow boiling data of CO_2 in a horizontal channel to modify the flow pattern map of Wojtan et al. (2005). They relied on heat transfer mechanisms in different two-phase flow patterns to propose new criteria for transition boundaries, especially the intermittent-annular transition and annular-dryout transition. In a major study of two-phase flow patterns, Revellin and Thome (2007a) performed flow boiling experiments to study diabatic flow patterns in horizontal microchannels. They utilized special optical technique (laser instrumentation) to determine the bubble frequency (bubble statistics) and identify flow patterns in the micro-

evaporator. It is apparent from the use of this technique that the bubble coalescence mechanism affects flow regime transitions in addition to the effect of heat flux. Furthermore, the authors proposed a new flow regime map involving four regimes, namely; an isolated bubble regime, a coalescing bubble regime, an annular flow regime and a post dryout regime. The models of transition boundaries from isolated bubble flow (IB) to coalescing bubble flow (CB) and CB to annular flow (A) are given by:

$$x_{IB/CB} = 0.763\left(\frac{Re_l Bo}{We_v}\right)^{0.41} \tag{2.1}$$

$$x_{CB/A} = 0.00014 Re_l^{1.47} We_l^{-1.23} \tag{2.2}$$

The map was presented in terms of mass flux and exit vapour quality as shown in Figure 2.14. The isolated bubble regime represents both, bubbly and slug flows where the bubble coalescence rate is much smaller than bubble generation rate while the coalescing bubble regime is distinguished by bubble generation rate that is much smaller than bubble coalescence rate. The authors also advised to consider the effect of the flow instability on the flow regime transitions through the occurrence of backflow in microchannels. Therefore, the development of typical flow pattern maps requires more effort if they are to include this phenomenon.

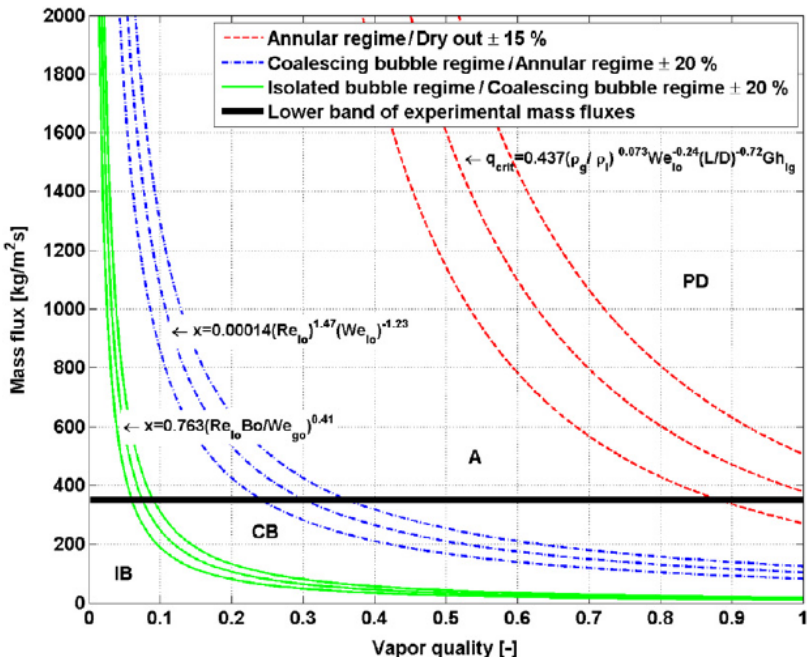

Figure 2.14 Diabatic coalescing bubble map for evaporating flow in circular uniformly heated microchannels: R134a, D = 0.5 mm, L = 70 mm, T_{sat} = 30 °C, q = 50 kW/m^2 and ΔT_{sub} = 0 °C, (Revellin and Thome, 2007a).

Cheng et al. (2008a) updated the experimental database of CO_2 involving a much wider range of channel size 0.6-10 mm inner diameter tubes. The transitions from annular to dryout and from dryout to mist regimes have been updated in their new flow pattern map. They also divided the stratified-wavy regime into three zones, namely slug, slug/stratified-wavy and stratified-wavy zones. They noticed that the bubbly regime takes place at low vapour quality and high mass fluxes. Ong and Thome (2011a) investigated the influences of channel confinement on flow patterns during flow boiling in horizontal small diameter tubes. They identified the flow regime map in terms of mass flux and vapour quality and also proposed new criteria for flow regime transition boundaries. The authors considered the effects of channel size, fluid properties and working conditions. They observed that the surface tension overcomes gravitational force leading to suppression of gravitational force. Harirchian and Garimella (2010) also studied the effect of confinement on flow patterns and their transitions physically during flow boiling in microchannels. Additionally, they utilized a wide range of experimental data to propose a dimensionless criterion for confinement in microscale channels which has named Convective confinement number ($Bo^{0.5}Re$ =160). This dimensionless criterion involved the effects of mass flux, fluid properties and channel size in addition to determining the transition between unconfined and confined flow. Based on this criterion and 390 visualised flow data of FC77 flow boiling, the authors developed a flow regime map identifying $Bo^{0.5}Re$ and $Bl\ Re$ as abscissa and ordinate, respectively. The diagonal transition line (Bl=0.017($Bo^{0.4}Re^{-0.3}$)) as shown in Figure 2.15 represents the transition boundary from intermittent to non-intermittent flow where here Bo is Bond number ($Bo = g\Delta\rho D^2/\sigma$) and Bl is Boiling number ($Bl = q/Gh_{lv}$).

Recently, most researchers have been concerned primarily with the important role of transition boundary from intermittent (plug and slug) to annular flow pattern, which controls the heat transfer mechanisms of flow boiling in small-diameter tubes. Charnay et al. (2013) used the optical measurement technique to study flow regimes of R245fa flow boiling in horizontal small diameter tubes. They noticed that the intermittent-annular transition boundary depends on heat flux. They also measured the characteristics of the bubble generated in mini-evaporator. The results showed that the flow pattern changes at the peak of bubble frequency. Furthermore, the authors reported some coincided between

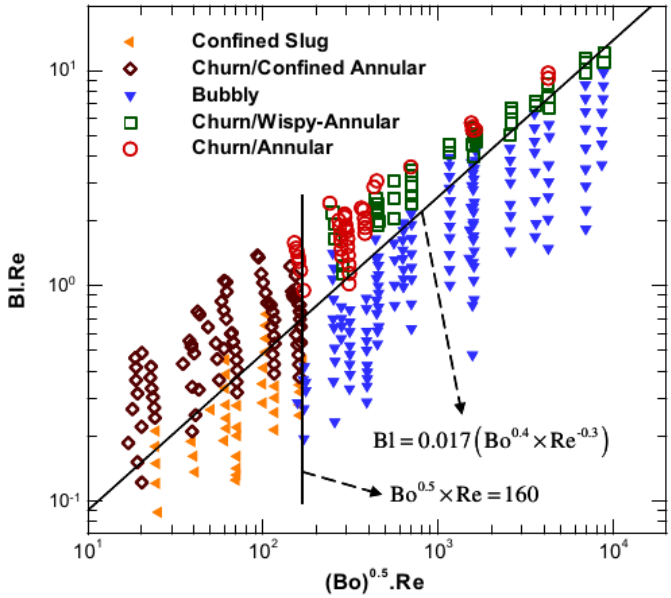

Figure 2.15 The flow regime map for FC77, developed by Harirchian and Garimella (2010).

predominant heat transfer mechanism and intermittent-annular transition. In other words, they detected that the transition from nucleation to convection mechanism corresponds to transition from intermittent to annular flow regime. Mahmoud and Karayiannis (2016) evaluated existing models and correlations of flow pattern maps in order to predict the flow patterns of fluid R245fa in 1.1 mm tube. They found that the current flow regime maps cannot predict the transition boundaries of R245fa flow pattern except for the model of Chen (2006). However, the transition line between the bubble and slug flow pattern for R245fa cannot be predicted in the map of Chen (2006). Therefore, the authors suggested theoretically a new modified model of this bubbly-slug transition based on force balance on the spherical bubble in the flow field. Figure 2.16 demonstrates the shift of bubbly-slug transition line towards lower liquid superficial velocities. The authors attributed this case to the effects of inertia and surface forces on bubble size, especially at low liquid velocity.

More recently, Zhu et al. (2017a) studied the flow patterns of R32 during flow boiling in horizontal mini-scale channels by using an optical measurement method. They identified the observed flow patterns on the flow regime map considering mass flux and exit vapour quality as coordinates. The observed flow regimes were compared with the

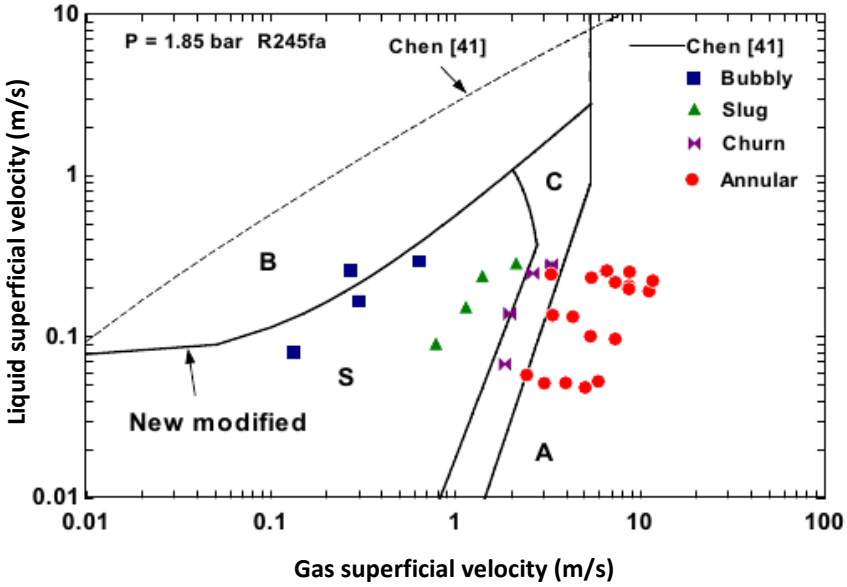

Figure 2.16 the flow pattern map of Chen (2006) was modified by Mahmoud and Karayiannis (2016).

flow pattern maps of Wojtan et al. (2005) and Cheng et al. (2008a). They found that these two maps could not predict all flow pattern data of R32 just about 50.2% and 55.7% of data, respectively. Therefore, they established a new flow pattern map using the *Bo* number. The authors employed the existing models intending for other working conditions and made the best fit with experimental data to obtain typical coefficients in their new models. Their new flow pattern map established a good agreement with the experimental data of R32. Tibiriçá et al. (2017) developed a complete set of optimised correlations for the prediction of flow pattern transition in horizontal microchannels under adiabatic and diabatic flow conditions. The dimensionless parameters in these transition correlations were linearized and analytically inversed. These proposed dimensionless parameters involved the effects of channel size, different fluids and thermophysical fluid properties. The authors coordinated the flow pattern transitions in the flow map in terms of mass flux and exit vapour quality. Their map included transitions of the bubble-slug (BS), slug to churn (SC), churn to annular (CA) and eventually dryout incipience (D). They proposed these transition correlations based on 395 data points and the liquid to vapour density ratio (ρ_l/ρ_v) was found in all transition correlations revealing an effective role of density ratio in flow pattern transitions.

In summary, most studies have presented several flow regimes which were observed in vertical and horizontal channels. The dispersed bubble flow, bubbly flow, intermittent (slug and churn) flow and annular flow can be regarded as the essential flow patterns identified in both vertical and horizontal flow within the range of mini and microchannels. Limited flow pattern maps are available in the literature for flow boiling in vertical upward small-scale channels and a universal flow pattern map is required. The discrepancies between the flow pattern data of researchers, their comparison with existing flow regime maps and the effect of the different parameter on flow patterns revealed that no theoretical models effectively predict the flow regime transition boundaries in the mini and micro-scale channels. Although studies have been conducted on the flow regime maps of the conventional channel, most of these flow maps were not systematically applicable to predict flow patterns and their transition boundaries for flow in mini and microchannels. The influence of flow orientations was insignificant in small-scale channels due to the dominance of surface tension. What is more, the prediction of the flow patterns and their transition boundaries encounter many challenges because of the instability of flow boiling in small-scale channels. This instability arises from the effects of surface tension, inertial, viscous, shear forces on bubble frequency and bubble coalescence mechanism. This work considered as an attempting to develop or find the recommended flow pattern map for flow boiling in vertical small tubes using R245fa as working fluid.

2.6 Two-phase pressure drop

Further miniaturisation and enhancement of cooling systems are achieved through employing flow boiling heat transfer in mini and microchannels due to their great surface area to volume ratio. However, the associated significant two-phase pressure drop penalty of mini and microchannels impede their development in many practical applications. With decreasing channel dimension, the surface tension effect and inertia force became known to dominate in the flow channel. Therefore, the increase of friction forces leads substantially to increased pressure drop in small-scale channels. Additionally, the flow boiling pressure drop in small channels determines the system pumping power, which is considered as a crucial parameter for the design of two-phase cooling systems Wu and Sundén (2014). Consequently, it is a necessity to systematically and comprehensively

study the two-phase flow pressure drop in mini and microscale tubes, and develop a sound prediction correlation. In this work, we look into the pressure drop in small tubes with coating and upward flow in the vertical orientation.

2.7 Key Factors influencing pressure drop

Two-phase flow pattern characteristics are significant for understanding the flow boiling process were reviewed in the former sections. Another major parameter having an important effect on the process is a two-phase pressure drop. In this section, the flow boiling studies focusing on two-phase pressure drop characteristics in small-diameter channels are presented. Table 2.5 summarizes the experimental two-phase flow pressure drop studies for mini- and microchannels. Among pressure drop characteristics in two-phase is the effect of vapour quality which is considered the influential parameter. Generally, the two-phase pressure drop increases with vapour quality as mentioned in the literature. There are other parameters having a strong effect on two-phase pressure drop as follows.

2.7.1 Effect of channel size

The channel size has a considerable influence on the flow boiling process as shown in the past literature. In particular, its effect on pressure drop, which then requires an appropriate pump to circulate the cooling fluid. The effect of channel diameter on two-phase pressure drop in small channels was reported by various investigators. Hwang and Kim (2006) carried out the study about the pressure drop of the two-phase flow in the microchannels with the diameter from 0.244 to 0.792 mm. They noticed that the two-phase flow pressure drop increased with decreasing tube diameter. Also, the influence of channel diameter on the two-phase frictional pressure drop of R245fa and R134a flowing in 0.97 and 0.509 mm inner tube diameters was studied by Revellin and Thome (2007b). They stated that the channel diameter plays an important role in increasing two-phase pressure drop. Quibén and Thome (2007) compared the two-phase frictional pressure drops for the two tested tube diameters (8 and 13.8 mm) at a set of identical test conditions. The comparison revealed that a larger two-phase pressure gradient is a presence in smaller diameter tube. Jang et al. (2008) carried out flow boiling experiments

Table 2.5 Summary of experimental two-phase flow pressure drop studies for mini- and micro-channels.

Author(s)	Fluid	Diameter, mm	Orientation	Conditions
Yan and Lin (1998)	R134a	2	Horizontal	T_{sat} = 5-31 °C G = 100–800 kg/m^{2}s q = 5–20 kW/m^2 x = 0.1–0.9
Tran et al. (2000)	R134a R12 R113	2.46-3.38	Horizontal	P = 138-856 kPa G = 33–832 kg/m^{2}s q = 2.2–129 kW/m^2 x = 0.02–0.95
Hwang and Kim (2006)	R134a	0.244-0.792	Horizontal	P = 138-856 kPa G = 140–950 kg/m^{2}s x = 0.08–0.95
Revellin and Thome (2007b).	R134a R245fa	0.509 0.79	Horizontal	P = 210-890 kPa G = 210–2094 kg/m^{2}s q = 3.1–415 kW/m^2 x = 0–0.95
Quibén and Thome (2007)	R134a R22 R410A	8 13.8	Horizontal	T_{sat} = 5 °C G = 70–700 kg/m^{2}s q = 6–57.5 kW/m^2 x = 0–1
Jang et al. (2008)	FC72	2 4	Horizontal	T_{sat} = 45-75 °C G = 132.7– 663.1kg/m^{2}s x = 0.01–0.7
Owhaib et al. (2008)	R134a	0.826-1.7	Vertical	T_{sat} = 34 °C G = 100–400 kg/m^{2}s q = 10-30 kW/m^2 x = 0–0.6
Quibén et al. (2009)	R22 R410a	5.3-8.6	Horizontal	T_{sat} = 5 °C G = 150–500 kg/m^{2}s q = 6-40 kW/m^2 x = 0.05–0.95
Choi et al. (2009)	Propane	1.5 3	Horizontal	T_{sat} = 0–10 °C G = 50–400 kg/m^{2}s q = 5-20 kW/m^2 x = 0–1
Pamitran et al. (2010)	R22 R134a R410a R290 R744	0.5-3	Horizontal	T_{sat} = 0–15 °C G = 50–600 kg/m^{2}s q = 5-40 kW/m^2 x = 0–1
Ali et al. (2011)	R134a R245fa	0.781	Horizontal	T_{sat} = 25–40 °C G = 100–650 kg/m^{2}s q = 6-41 kW/m^2 x = 0.1–0.86
Tibiriçá and Ribatski (2011)	R245fa	2.32	Horizontal	T_{sat} = 31–41 °C G = 100–700 kg/m^{2}s q = 0-55 kW/m^2 x = 0.1–0.99
Tibiriçá et al. (2011)	R134a	2.32	Horizontal	T_{sat} = 31 °C G = 100–600 kg/m^{2}s q = 10-55 kW/m^2 x = 0.2–0.99
Maqbool et al. (2012b)	Ammonia	1.7 1.224	Vertical	T_{sat} = 23-43 °C G = 100–500 kg/m^{2}s q = 15-355 kW/m^2

				x = 0–1.1
Maqbool et al. (2013)	Propane	1.7	Vertical	*T_{sat} = 23-43 °C* *G = 100–500 kg/m²s* *q = 5-280 kW/m²* *x = 0–1.1*
Grauso et al. (2013)	R1234ze(E) R134a	6	Horizontal	*T_{sat} = -2.9-12.1 °C* *G = 146–520 kg/m²s* *q = 5-20.4 kW/m²* *x = 0–1*
Mahmoud et al. (2014a)	R134a	0.52-1.1	Vertical	*P = 600-1000 kPa* *G = 200–500 kg/m²s* *q = 1-140 kW/m²* *x = 0–1*
Pike-Wilson and Karayiannis (2014)	R245fa	1.1	Vertical	*P = 180 kPa* *G = 100–400 kg/m²s* *q = 10–60 kW/m²* *x = 0–0.95*
Anwar et al. (2015b)	R1234yf R134a	1.6	Vertical	*T_{sat} = 27-32 °C* *G = 100–500 kg/m²s* *q = 5–130 kW/m²* *x = 0–0.95*
Charnay et al. (2015a)	R245fa	3	Horizontal	*T_{sat} = 60-120 °C* *G = 100–1500 kg/m²s* *q = 5–130 kW/m²* *x = 0–1*
Longo et al. (2016a)	R32 R410a	4	Horizontal	*T_{sat} = 5-20 °C* *G = 196.1–821.3 kg/m²s* *q = 11.7–51.6 kW/m²* *x = 0.06–0.9*
Longo et al. (2016b)	R1234ze(E) R134a	4	Horizontal	*T_{sat} = 10-20 °C* *G = 196.2–610.4 kg/m²s* *q = 10.1–30.6 kW/m²* *x = 0.08–0.97*
Xu et al. (2016a)	R134a	1.002-4.065	Horizontal	*P = 578-820 kPa* *G = 185–935 kg/m²s* *q = 18–35.5 kW/m²* *x = 0.03–1*
Hardik and Prabhu (2016)	Water	5.5-12	Horizontal	*P = 100-300 kPa* *G = 100–1200 kg/m²s* *q = 400–1800 kW/m²* *x = 0.18–0.65*
Chen et al. (2017)	N_2	2.92 3.96	Horizontal	*P = 170-350 kPa* *G = 140–330 kg/m²s* *q = 0.5–69.4 kW/m²* *x = 0.09–0.62*
Zhu et al. (2017b)	R32	1 2	Horizontal	*T_{sat} = 10-20 °C* *G = 50–600 kg/m²s* *q = 10–30 kW/m²* *x = 0–1*
Huang and Thome (2017)	R1233zd(E) R245fa R236fa	0.1	Horizontal	*T_{sat} = 31.5-40 °C* *G = 500–2750 kg/m²s* *q = 20–64 W/cm²* *x = 0.034–0.51*
Sempértegui-Tapia and Ribatski (2017b)	R134a R1234ze(E) R1234yf R600a	0.634-1.1	Horizontal	*T_{sat} = 31-41 °C* *G = 100–1600 kg/m²s* *x = 0.05–0.95*

Yang et al. (2018b)	R1234ze(E) R600a	6	Horizontal	*P = 215-415 kPa* *G = 130–258 kg/m^{2}s* *q = 10.6–74.8 kW/m^2* *x = 0–0.95*
Saisorn et al. (2018)	R134a	1	Horizontal Vertical	*P = 800 kPa* *G = 250–820 kg/m^{2}s* *q = 1–60 kW/m^2* *x = 0.01–1*

of FC72 flow in tube diameter range of 2 – 4 mm in order to study the diameter influence on two-phase pressure drop. They inferred that the small channel (2 mm) creates nearly 100.1% higher pressure drop than the big channel (4 mm). They depended on Stokes' equation to demonstrate the effect of channel diameter. This equation includes the influence of channel diameter on the fluid viscosity. In other words, the bubble velocity decreased with decreasing the channel diameter keeps constant fluid viscosity at a fixed diameter of the departed bubble. Thus, the flow resistance of the bubble increases with decreasing channel diameter owing to the increased wall effects (confinement). The effective viscosity that included wall effects of the fluid in the small channel affects consequently pressure drop in two-phase flow. However, Owhaib et al. (2008) observed that the two-phase pressure drop appears roughly independent of the tube diameter. They attributed this case to the key influence of the flow pattern on the pressure drop. Quibén et al. (2009) pointed out to the increased frictional pressure drop with decreasing channel size based on the confinement effect. Pamitran et al. (2010) investigated the tube diameter influence on two-phase pressure drop in flow boiling of five refrigerants in small diameter tube with a range of 0.5 – 3 mm. They reported that the small diameter tube has a strong effect on increasing two-phase flow pressure drop. The authors illustrated that the increase in pressure drop with reducing channel size is because of higher friction factor resulting from higher wall shear stress. In addition, Maqbool et al. (2012b) found, from their experimental results on flow boiling pressure drop of vertical tubes with 1.7 and 1.224 mm inner diameter, that the pressure drop increased with decreasing channel diameter. They pointed out that the reduced channel diameter brings on an increase in wall shear stress due to higher velocity gradient of the two-phase mixture in the channel, thus increasing two-phase pressure drop. Similar findings were attained by the experimental study of Mahmoud et al. (2014a) for flow boiling of R134a in 0.52 and 1.1 mm tubes. They attributed this to the large velocity gradient in the thin liquid film close to tube wall leading to significant increase in the wall shear stress and subsequently the

frictional pressure drop. Xu et al. (2016a) presented an experimental investigation to seek out the effect of channel size. They found that based on the experimental results R134a boiling in tube diameter range 1.002 – 4.065 mm, the frictional pressure drop in the small tube is higher than that of big ones at the same test condition. Similar empirical findings were obtained by Hardik and Prabhu (2016) when they carried out the flow boiling test for water in 5.5 – 12 mm diameter tubes. Recently, Chen et al. (2017) performed an investigation on the effect of channel diameter on two-phase flow pressure drop for Nitrogen in small tubes with an inner diameter range of 2.92 – 3.96 mm. They obtained same experimental results as mentioned above, and concluded a similar explanation of channel effect on pressure drop (high wall shear stress and high flow velocity with reducing tube diameter). Zhu et al. (2017b) used R32 refrigerant to test the influence of mini-tubes on pressure drop in two-phase flow. They also found that the decreasing the tube diameter from 2 to 1 mm resulted in an increase of the frictional pressure gradient.

It can be concluded from the above that the channel size is an influential parameter in the flow boiling process, especially, for its effect on two-phase pressure drop. The majority of researchers have reached agreement on increasing two-phase pressure drop with decreasing channel size except Owhaib et al. (2008). Owhaib et al. (2008) thought that the influence of flow pattern overcomes the influence of channel size on two-phase pressure drop (i.e. the channel size has an insignificant effect on pressure drop). Moreover, the reason for increasing pressure drop with decreasing channel size attributes to increasing wall shear stress and flow velocity in the flow channel. Furthermore, due to the confinement effect, which increases the resistance to bubbles with fixed bubble diameter in a flow field resulting in an increase of pressure drop. The effect of four diameter tubes on the two-phase pressure drop for R245fa were studied in the present work, including 1.1 mm, 2.01 mm, 2.88 mm, 4.26 mm inner diameter tubes. The decrease of diameter tube causes an increase in the pressure drop inside the flow boiling system. This demands the choice of a higher capacity pump, which increases higher power consumption.

2.7.2 Effect of pressure and fluid properties

The two-phase flow pressure drop in small channels depends considerably on the viscosity and density of both phases. Knowing that these properties vary from one fluid to another and are also influenced by pressure. They also significantly affect the distribution of both phases in the flow path and consequently two-phase flow velocity. There were several experimental studies of two-phase flow in macro and microchannels verifying the effect of physical fluid properties and operating pressure on two-phase flow pressure drop. Yan and Lin (1998) observed that the measurements of R134a frictional pressure drop in 2 mm horizontal tube decrease with increasing saturation temperature from 5 to 31 °C. Tran et al. (2000) presented measurements of flow boiling pressure drop across mini channels with three refrigerants (R12, R113, and R134a) and saturation pressure range of 138 – 856 kPa. They observed an increase in pressure drop when the saturation pressure decreased for all three refrigerants. They also investigated the performance of refrigerants in terms of two-phase pressure drop as well as the impact of the fluid properties on the two-phase pressure drop. They observed that the pressure drop of R134a is nearly 31% higher than R12 at the same test conditions. They considered the liquid-vapour density ratio as a key parameter which was changed by saturation pressure and fluid type and thus affecting pressure drop. Similar experimental findings were reported by Quibén and Thome (2007) when they carried out the comparison study for three fluids (R134a, R12, and R410a). R134a showed higher two-phase frictional pressure drop compared to the other fluids. Revellin and Thome (2007b) performed the flow boiling tests for R245fa and R134a in a microchannel with an inner diameter range of 0.507 and 0.79 mm. They observed that the two-phase frictional pressure drop is lower as the saturation temperature is higher. They stated that the elevation of saturation temperature results in increased vapour density, decreased vapour velocity and by consequence decreasing the two-phase frictional pressure drop. They also found that the frictional pressure drop of R245fa is significantly higher than that of R134a because they concluded the vapour density of R134a is three times the vapour density of R245fa at the test conditions. This results in the vapour velocity for R245fa being higher than for R134a and thus higher pressure drop for R245fa. Pamitran et al. (2010) studied the effects of pressure and fluid type on the flow boiling pressure drop in mini and microchannels. The results exhibited that the two-phase pressure gradient increased with decreasing saturation pressure. To explain their results, the authors depended on the effect of physical properties

of fluid on two-phase pressure drop at different pressures. That is, the vapour density and vapour viscosity decreases and liquid density and liquid viscosity increases with low saturation pressure. This leads respectively to higher vapour velocity and lower liquid velocity and consequently high-pressure gradient. The results exhibited that the order of the two-phase pressure gradients from the highest to the lowest were R134a, R22, R290, R410a, and R744, i.e. the R744 had the lowest two-phase pressure gradient. Their explanation was also based on the effect of physical properties of the fluid such as density ratio, viscosity ratio, surface tension and pressure, i.e. the fluid with higher two-phase pressure gradients had higher liquid-vapour density ratio, liquid-vapour viscosity ratio, surface tension, and lower saturation pressure.

Ali et al. (2011) conducted an investigation to study the influence of system pressure on two-phase pressure drop for R134a and R245fa flowing in a 0.781 mm tube. They noticed that the system pressure has a strong effect on pressure drop for the R134a, but this effect is not observed in the pressure drop of R245fa. However, they did not provide any interpretation of this behaviour of R245fa. For R134a, they explained the decrease of pressure drop with increasing system pressure based on physical properties of the fluid, where vapour density increased with system pressure resulting in lower vapour velocity. Moreover, they found a higher pressure drop for R245fa as compared to R134a at the same conditions. This is due to the liquid density and liquid viscosity being higher for R245fa than R134a at the same saturation temperature, which leads to higher vapour velocity and by consequence increases vapour shear at the liquid-vapour interface. Tibiriçá and Ribatski (2011) studied the influence of saturation pressure on the two-phase pressure drop of R245fa in a 2.32 mm tubes. They noted that the frictional pressure drop decreases as the saturation temperature increases from 31 °C to 41 °C. Maqbool et al. (2012b) mentioned that the pressure drop increases with decreasing pressure based on flow boiling of ammonia in 1.7 and 1.224 mm vertical tubes. They explained that the vapour velocity and the liquid viscosity decrease with saturation pressure which give rise to lower pressure drop. The decrease in vapour velocity is also due to higher vapour density. Maqbool et al. (2013) reported that the two-phase frictional pressure drop of propane at certain mass flux and vapour quality is lower for higher saturation temperature. They gave the similar interpretation which is provided in their earlier Maqbool et al. (2012b) study in effect pressure on two-phase pressure drop. Grauso et al. (2013) carried

out experimental tests to study the influences of the saturation temperature and fluid on two-phase pressure gradients for R1234ze(E) and R134a flowing in a 6 mm tube. They drew a conclusion from experimental results that the drop of two-phase pressure gradient for both refrigerants occurs as a result of the increased saturation temperature. They attributed this behaviour to the decreasing liquid viscosity and increasing liquid density with increasing saturation temperature. In addition, the frictional pressure gradients for both refrigerants were identical at a fixed saturation temperature as a consequence of similar liquid and vapour viscosities of both the refrigerants as well as the vapour-liquid density ratios. Mahmoud et al. (2014a) found the same results for R134a fluid flowing in 0.52 and 1.1 mm vertical tubes. The two-phase pressure drop increased when system pressure decreased. They explained their findings on the basis of pressure influencing the fluid properties, i.e. the low liquid density and high vapour density with high system pressure. This causes a decrease in the vapour superficial velocity and thus a decrease in the acceleration component of pressure drop. Moreover, the high system pressure causes a reduction in liquid and vapour viscosities leading to a decrease in the frictional component of pressure drop. Anwar et al. (2015b) conducted flow boiling experiments for R1234yf and R134a using a vertical tube with inner diameter of 1.6 mm. The authors observed that the saturation temperature has a strong influence on the two-phase frictional pressure drops for R1234yf and R134a. Also, R134a displayed high frictional pressure drop compared to R1234yf, where frictional pressure drop of R1234yf was about 30% less than R134a.They presented a similar explanation which was mentioned in previous studies, i.e. Tran et al. (2000) and Quibén and Thome (2007). Charnay et al. (2015a) performed an investigation on the effect of the saturation temperature on the frictional pressure drop of R245fa in 3 mm tube at high and different saturation temperatures. Their findings exhibited the decrease of frictional pressure drop when the saturation temperature was increased. They reported that this is due to an increase in the vapour density, a decrease in the slip ratio (gas-liquid velocity ratio), and a decrease in the vapour velocity when the saturation temperature increases, which leads to decreasing frictional pressure drop.

Longo et al. (2016a) and Longo et al. (2016b) conducted the comparative analysis of R32, R410a, R1234ze(E) and R134a during flow boiling inside a 4 mm tube at three different saturation temperatures. Saturation temperature has a remarkable impact on the

frictional pressure drop for all refrigerants. Under the same operating conditions, the R32 exhibited a frictional pressure drop of about 22 – 36 % higher than that of R410a whereas R1234ze(E) exhibited a slightly higher frictional pressure drop than R134a about (10 – 25 %). Huang and Thome (2017) described the effect of the saturation temperature on the two-phase pressure drops for two fluids (R245fa and R236fa) in multichannel. The pressure drop decreased slightly with the increase in the saturation temperature. The authors attributed this trend to the decrease in the shear stress at the two interfaces of vapour-liquid and liquid-wall. That is, the wall shear stress decreased because the liquid viscosity decreased at higher saturation temperatures. Also, the decrease of shear stress at the liquid-vapour interface occurred as a result of the reduction in the slip ratio (owing to the decreasing liquid to vapour density ratio) as the saturation temperature increases. On the other hand, the influence of fluids on the two-phase pressure drop, the authors found that the results of R1233zd(E) coincided with R245fa because of their similar properties at the same saturation temperature. The pressure drop of R236fa was lower than the others. They reported that this phenomenon was due to the smaller liquid-vapour density ratio and liquid viscosity of R236fa compared to R1233zd(E) and R245fa and as explained above, this resulted in a low-pressure drop. Sempértegui-Tapia and Ribatski (2017b) observed that the flow boiling pressure drop gradient for R600a is higher compared to R1234ze(E), R1234yf and R134a. They explained this behaviour by the specific vapour volume for R600a being higher than for the other fluids and consequently higher superficial velocity of the two-phase mixture for R600a. This implies increasing pressure drop gradients with a superficial velocity of both phases. They noticed that the increase in saturation temperature corresponding to the operating pressure has a strong impact on frictional pressure drop gradient leading to its decrease. Yang et al. (2018b) presented a study on the effect of pressure and fluid type on two-phase pressure drop through flow boiling in a 6 mm tube. They found that the frictional pressure drop decreases with increased saturation pressure. Also, under the same operating conditions, the results revealed that frictional pressure drop of R600a is larger than R1234ze(E). The authors thought that the physical fluid properties play an important role in influencing pressure drop when the saturation pressure or fluid type is changed. That is, the higher pressure, higher vapour viscosity and vapour density lead to lower vapour velocity and consequently lower pressure drop. In addition, the liquid or vapour density of R1234ze(E)

is larger than R600a under the same pressure. Therefore, the velocity of R600a is larger than R1234ze(E) which brings about a higher pressure drop.

As previously discussed above, it can be concluded from these studies that the working fluids and saturation temperature corresponding to the operational pressure have a strong impact on flow boiling pressure drop in small and microchannels. This is because of the working fluid having higher reduced pressure and increased saturation temperature give rise to increasing vapour density and decreasing liquid viscosity. The increased vapour density leads to decreasing vapour velocity and consequently decreasing acceleration pressure drop. Also, the decreased liquid viscosity results in decreasing frictional pressure drop which leads finally to decreasing total pressure drop in two-phase flow. The experimental data for three low pressures were used in this work to study their effects on flow boiling pressure drop, including those for 185, 245 and 310 kPa.

2.7.3 Effect of mass flux

The role of mass flux on two-phase flow pressure drop has received increased attention as one of the influential parameters in flow boiling. There are several experimental studies in the literature that have dealt with the importance of the effect of mass flux on pressure drop in two-phase flow. Hwang and Kim (2006) carried out flow boiling tests of R134a in micro-tubes with a range of 0.244 – 0.792 mm. They reported that the influence of mass flux on the pressure drop gradient in two-phase flow is highly significant because the friction force of fluid flow against tube wall arises from increased mass flux. In addition, the change in mean velocity in the flow channel depends directly on increasing mass flux and vapour quality. Quibén and Thome (2007) reported similar experimental findings for R22 and R410a in 8 and 13.8 mm tubes. Owhaib et al. (2008) found that with an increase in the mass flux of R134a in mini tubes, the exit vapour quality decreases and simultaneously the two-phase frictional pressure drop increases with a remarkably linear slope. Pamitran et al. (2010) performed an experimental study to investigate the effect of mass flux on flow boiling pressure drop of refrigerants in mini and micro channels. The results showed that the two-phase pressure drop increases with mass flux. They reported that the conditions of flow pattern (such as wavy stratified flow) and the potential for turbulent flow in higher mass flux may cause a higher pressure drop.

Furthermore, the increase in mass flux leads to increasing frictional and acceleration pressure drop due to higher flow velocity in the flow field. The same observations were obtained by Tibiriçá et al. (2011) for flow boiling of R134a in a 2.32 mm tube. Also, Maqbool et al. (2012b) studied the effect mass flux on two-phase pressure drop for ammonia flowing in 1.7 and 1.224 mm tubes. Their experimental results demonstrated that the two-phase pressure drop increases with increasing mass flux. Grauso et al. (2013) conducted flow boiling tests for R1234ze(E) and R134a flowing 6 mm tube. They found that an increase in mass flux results in a significant increase of the two-phase frictional pressure gradients of both the refrigerants. The authors explained this phenomenon based on physical fluid properties, i.e. both refrigerants have low reduced pressure, low liquid-vapour density ratio. Thus, these properties result in a strong variation of the two-phase density, which leads to a considerable dependence on mass flux. Maqbool et al. (2013) conducted an experimental study on the effect of mass flux on flow boiling pressure drop of propane in a 1.7 mm tube. They reasoned out that increasing frictional pressure drop with mass flux is due to increasing flow velocity with the increase of mass flux and vapour quality. Mahmoud et al. (2014a) carried out flow boiling experiments on two-phase flow pressure drop of R134a in microtubes of 0.52 and 1.1 mm inner diameter. Their experimental data demonstrated that the pressure drop increases with mass flux. They thought that the pressure drop depends on mass flux and vapour quality based on the momentum equation. That is, the mass flux has a strong effect on the frictional and acceleration components. Pike-Wilson and Karayiannis (2014) observed the same results with R245fa flow in different metallic tubes of 1.1 mm inner diameter. The influence of mass flux on two-phase pressure drop was small in the brass tube compared with stainless steel and copper tubes because the brass tube has a higher surface roughness comparing to surface roughness of the stainless steel and copper tube. Charnay et al. (2015a) studied the effect of mass flux on frictional pressure drop for R245fa boiling in a 3 mm tube. They found that the increase in mass flux causes an increasing two-phase frictional pressure drop at two different high saturation temperatures (80 and 100 °C). They report that the increase in mass flux leads to higher flow inertia and higher flow velocity. This results in increasing the frictional pressure drop.

Longo et al. (2016b), Longo et al. (2016a), and Xu et al. (2016a) reported that the mass flux has a remarkable influence on the frictional pressure drop. However, they did

not give any interpretation of their results. The empirical results of Chen et al. (2017) for liquid nitrogen in mini channels showed that the increasing mass flux causes an increase in frictional pressure drop. They illustrated that the two-phase mean velocity of fluid flow increases with mass flux. This results in increasing the friction force between the fluid and tube wall. Sempértegui-Tapia and Ribatski (2017b) concluded that the two-phase flow pressure drop gradient increases with mass flux regardless of channel geometry. Yang et al. (2017) presented a study of mass flux effect on the frictional pressure drop for R600a flow boiling in 6 mm tube. The experimental results displayed that the frictional pressure gradient in two-phase flow increases with increasing mass flux as well as the influence of mass flux become weak as the pressure increases. They mentioned that the increase of mass flux causes the higher flow velocity and subsequently higher friction force which results in higher frictional pressure gradient. However, when the test pressure increases, the vapour density increases leading to lower vapour velocity and hence the effect of mass flux turns into small. Saisorn et al. (2018) studied experimentally the effect of mass flux on flow boiling pressure drop in 1 mm tube. Their results illustrated that the pressure drop increases with increasing mass flux. They reported that the increased mass flux results in the enhancement of shear forces at the tube wall as well as at the liquid-vapour interface. Yang et al. (2018b) noticed that the effect of mass flux on pressure drop becomes significant in high vapour quality due to the change of flow pattern to slug flow and then annular flow. As a result, the formation of vapour in tube core and a liquid film on tube wall causes higher vapour velocity and thus increasing frictional pressure drop.

In summary, these studies indicated that the mass flux has a strong impact on two-phase flow pressure drop and all the researchers agreed on this fact. Moreover, the mass flux is considered to be an influential factor in increasing friction force between fluid flow and channel wall in addition to its significant effect with vapour quality on acceleration pressure drop due to the higher velocity of liquid-vapour mixture in the flow field. In this work, the changes of mass flux for vertical tubes and their effects on flow boiling pressure drop were empirically studied with the range of 200 – 500 kg/m^{2}s.

2.7.4 Effect of heat flux

The influence of heat flux is one of the crucial parameters studied for the comprehensive understanding of two-phase flow boiling phenomena. There are several studies in the literature which focused on the effect of heat flux on two-phase drop pressure. Yan and Lin (1998) observed that friction pressure drop increases with heat flux for R245fa flowing in a 2 mm tube. However, Quibén and Thome (2007) found that the influence of the heat flux on the two-phase frictional pressure drop is negligible, excluding vapour qualities near and after the dryout inception. They related this phenomenon to the damping out of interfacial waves when the annular film thins. Similar findings were reported by Quibén et al. (2009). Choi et al. (2009) found that the pressure drop of propane in mini tubes increases with increasing heat flux. They presumed that higher vaporization results from increasing heat flux leading to increase in vapour quality and flow velocity. This thus causes an increase in pressure drop. The same conclusion was also found by Maqbool et al. (2013). Pamitran et al. (2010) noticed that the heat flux has a significant effect on two-phase pressure gradient. They illustrated that the vaporization in the flow channel as a result of increasing heat flux causes an increase in the formation of bubbles and slugs. This increases the vapour quality, vapour void and flow velocity leading to a higher pressure drop and varying the flow momentum along the channel. Tibiriçá and Ribatski (2011) conducted an experimental investigation to study the effect heat flux on the two-phase pressure drop of R245fa in 2.32 mm horizontal tube. The vapour quality reported was the average value over the two-phase length. They found that the frictional pressure drop is independent of heat flux effect. They attributed an increase in two-phase pressure drop to increasing acceleration pressure with the variation of vapour quality as well as saturation temperature gradient along the test section. Ali et al. (2011) also reported similar results based on their experimental data of refrigerants R134a and R245fa. Pike-Wilson and Karayiannis (2014) studied the effect of heat flux on two-phase pressure drop for R245fa flowing in three different metallic tubes with 1.1 mm tube diameter. They found that two-phase pressure drop in the brass tube increases steeply with increasing heat flux due to the effect of the surface structure of the tube walls. Mahmoud et al. (2014a) clarified that the increasing two-phase pressure drop with heat flux is due to the contribution of the acceleration pressure drop, which increases with increasing vapour quality. Moreover, the experimental study of Chen et al. (2017) showed that the two-phase frictional pressure drop of N_2 flowing in minichannel increases

with increasing heat flux. The authors reported that the increasing heat flux brings about an increase in the number of bubbles near the channel walls and thus cause more disturbance close to the tube surface. Accordingly, the pressure drop increases with the increasing heat flux. Zhu et al. (2017b) studied the effect of heat flux on the frictional pressure drop of R32 in the mini channel with a range of 1 – 2 mm inner diameter. They observed that the frictional pressure drop increases with increasing heat flux. Saisorn et al. (2018) investigated the effect heat flux on two-phase flow pressure drop. They found from their flow boiling results in 1 mm tube that the pressure drop tends to increase with heat flux. The authors illustrated that the vapour velocity can be enhanced with the increment of heat flux through the phase-change process, leading to the increased pressure drop. There is a contradictory view of the effect of heat flux on the two-phase pressure drop. Xu et al. (2016a) found that the influence of heat flux on the two-phase frictional pressure drop of the R134a is negligible for all the 3 tubes (1.002, 2.168 and 4.065) of their study. Longo et al. (2016a) and Longo et al. (2016b) also deduced that the heat flux has a weak or no effect on two-phase frictional pressure drops. The researchers did not give any justification for no effect of the heat flux on the two-phase pressure drop.

In summary, it has been shown from this review that there were remarkable discrepancies between experimental findings on the effect of heat flux on pressure drop from different researchers. Some of them found its influence to be insignificant, while others agreed that the heat flux has an influential role in increasing vapour quality, thereby increasing two-phase pressure drop. In this work, the changes of heat flux for vertical tubes and their effects on flow boiling pressure drop were experimentally investigated with the range of 3 – 188 kW/m^2.

2.8 Two-phase pressure drop correlations

The two-phase pressure drop in the channel is attributable to the variation of potential and kinetic energy of the two-phase gas-liquid mixture flowing across a narrow passage. The pressure drop generally results from fluid friction on the wall surfaces of the flow channel. Therefore, the total two-phase pressure drop is represented by the sum of three components, namely; the frictional pressure drop, the acceleration pressure drop

(momentum) and the gravitational pressure drop (static or elevation head). The acceleration and gravitational components can be directly estimated if the vapour void fraction is known. The most significant and problematic components are the frictional pressure drop, which is expressed as a function of the two-phase friction factor. The two-phase frictional pressure drop resulting from the shear stress is determined by either homogeneous equilibrium flow model (predicting two-phase friction factor) or separated flow model (predicting two-phase friction multiplier).

The homogeneous equilibrium flow model postulates the liquid and vapour phase motion along the channel having an identical velocity (slip ratio = 1). This model is generally suitable for bubbly flow or slug flow, where the vapour quality is low. It depends on more complex physically-based models such as two-phase density and two-phase viscosity to predict the frictional pressure drop component. For instance, the two-phase viscosity is determined on the basis of a specific mixing law between the properties of liquid and vapour phase according to various models. Table 2.6 presents some well-known models that describe two-phase flow viscosity.

The separated flow model assumes an interface between the liquid phase and vapour phase with moving individually along the channel. This model is appropriate for annular flow with the vapour phase moving in the channel core and thin liquid film between the vapour centre and the channel wall. It depends on empirically simplified models containing parameters, which are assessed from experimental data. The two-phase frictional pressure drop is calculated by multiplying the two-phase friction multiplier with the pressure drop of either the liquid phase or the vapour phase. The two-phase friction multiplier is classified into two well-defined models: ϕ_l^2 based model and ϕ_{lo}^2based model. The ϕ_l^2 based model is recognized as the ratio of the two-phase friction pressure drop to the friction pressure drop of liquid phase flowing alone, while the ϕ_{lo}^2 based model is recognized as the ratio of the two-phase friction pressure drop to the friction pressure drop of the total liquid-vapour mixture flowing as liquid only.

In the literature, the extensive experimental studies of two-phase flow pressure drop in mini and micro-scale tubes have been conducted and thus several models have been

Table 2.6 Summary of previous two-phase flow viscosity model for Homogeneous Equilibrium flow.

Reference	Correlation
McAdams et al. (1942)	$\frac{1}{\mu_{tp}} = \frac{x}{\mu_v} + \frac{1-x}{\mu_l}$
Akers et al. (1958)	$\mu_{tp} = \frac{\mu_l}{\left[(1-x) + x\sqrt{\frac{v_v}{v_l}}\right]}$
Cicchitti et al. (1960)	$\mu_{tp} = x\mu_v + (1-x)\mu_l$
Dukler et al. (1964)	$\mu_{tp} = \frac{xv_v\mu_v + (1-x)v_l\mu_l}{xv_v + (1-x)v_l}$
Beattie and Whalley (1982)	$\mu_{tp} = \epsilon\mu_v + (1-\epsilon)(1+2.5\epsilon)\mu_l$ $\epsilon = \frac{xv_v}{v_l + xv_{lv}}$
Lin et al. (1991)	$\mu_{tp} = \frac{\mu_l\mu_v}{\mu_v + x^{1.4}(\mu_l - \mu_v)}$
Fourar and Bories (1995)	$\mu_{tp} = \rho_{tp}\left(\sqrt{x\mu_v v_v} + \sqrt{(1-x)v_l\mu_l}\right)^2$ $\rho_{tp} = (xv_v + (1-x)v_l)^{-1}$

proposed for two-phase friction multiplier. A general model for predicting two-phase pressure drop of isothermal gas-liquid flow in conventional tubes was presented by Lockhart and Martinelli (1949). They assumed that each phase flows separately bringing about the presence of four types of two-phase flow mechanisms during the simultaneous liquid-gas flow in the horizontal channel. These mechanisms might occur on the basis of whether each phase flowed as a turbulent flow or a viscous flow. Based on the data analysis of the frictional pressure drop, they postulated that firstly, the static pressure drop for the liquid phase must be equal to that of the gas phase regardless of the flow pattern. Secondly, the gas phase volume plus the liquid phase volume have to equal the total tube volume. The authors correlated the frictional pressure drop in two-phase flow with that of single-phase alone as a function of a square root of the multiplier (ϕ), which can be expressed by

$$\left(\frac{dP}{dz}\right)_{tp} = \phi_l^2 \left(\frac{dP}{dz}\right)_l \tag{2.1}$$

where $(d/dz)_l$ is the single-phase liquid pressure gradient. Chisholm (1967) fitted the Lockhart-Martinelli's parameters (two-phase frictional multiplier ϕ_l^2 and Lockhart-Martinelli parameter *X*) by means of relationship as follows:

$$\phi_l^2 = 1 + \frac{C}{X} + \frac{1}{X^2} \tag{2.2}$$

where C is a value based on nature of laminar or turbulent flow in both gas and liquid phases. The values of the C parameter proposed by Chisholm (1967) for the macro-scale flow was given as 5 for laminar-laminar flow, 10 for turbulent-laminar flow, 12 for laminar-turbulent flow and 20 for turbulent-turbulent flow. The Lockhart-Martinelli parameter (*X*) takes viscous and inertial forces of both phases into account and is expressed by

$$X^2 = \frac{(dP/dz)_l}{(dP/dz)_g} \tag{2.3}$$

where $(dP/dz)_g$ is the single-phase gas pressure gradient. It seems that the presence of the C parameter in the Lockhart and Martinelli (1949) models was likely to play an influential role in the characteristics of the two-phase flow pressure drop. Interestingly, this parameter represents the level of interactions between vapour and liquid phase. There are several factors affecting the C value such as channel diameter, saturation pressure, fluid properties, mass flux and vapour quality. Therefore, the researchers proposed different models to predict C for small-scale flow. Table 2.7 summarizes the predictive models and correlations recently proposed by several investigators on the basis of the main parameters acquired from the consolidated database. Mishima and Hibiki (1996) modified the parameter of Chisholm (1967) to better match their data under the turbulent-turbulent flow condition for capillary tubes with an inner diameter range of 1 – 4 mm. They tried to remove the dependence of Chisholm's parameter *C* on Reynolds number and superficial velocity and used only the value of turbulent-turbulent flow in addition to the effect of channel hydraulic diameter. Qu and Mudawar (2003) incorporated the influences of both channel size and mass flux to improve the predictive performance of the Chisholm's parameter in two-phase multipliers model of Mishima and Hibiki (1996) for mini and micro-channels. English and Kandlikar (2006) also developed the model of Mishima and Hibiki (1996) to extend the dependence of the *C* parameter on the hydraulic diameter for laminar–laminar flow in minichannel by substituting the Chisholm value for

Table 2.7 Summary of predictive models for *C* parameters proposed by several studies.

Author(s)	Model	Conditions
Chisholm (1967)	$C = \begin{cases} 5, & Re_l < 1000\ Re_g < 1000 \\ 10, & Re_l > 2000\ Re_g < 1000 \\ 12, & Re_l < 1000\ Re_g > 2000 \\ 20, & Re_l > 2000\ Re_g > 2000 \end{cases}$	*D: 1.49 – 25.83 mm* *Fluid: Air-Benzene, Air-Kerosene, Air-Water, Air-various oils*
Mishima and Hibiki (1996)	$C = 21(1 - e^{-319D})$	*D: 1.05 – 4.08 mm* *J_g: 0.02 – 50 m/s* *J_l: 0.002 – 8 m/s* *Fluid: Air-water*
Qu and Mudawar (2003)	$C = 21(1 - e^{-319})(0.00418G + 0.0613)$	*D: 0.35 mm* *G: 134.9– 400.1 kg/m^{2}s* *Fluid: Water*
Hwang and Kim (2006)	$C = 0.227 Re_{lo}^{0.452} X^{-0.32}$	*D: 0.244 – 0.792 mm* *G: 140 – 950 kg/m^{2}s* *x: 0.08 – 0.95* *Fluid: R134a*
English and Kandlikar (2006)	$C = 5(1 - e^{-319D})$	*D: 1 mm* *J_g: 3.19 – 10.06 m/s* *J_l: 0.0005 – 0.022 m/s* *Fluid: Air-Water*
Sun and Mishima (2009)	For laminar flow (Re_l < 2000 and Re_v < 2000): $C = 26\left(1 + \frac{Re_l}{1000}\right)\left[1 - e^{\left(\frac{-0.153}{0.8+0.27Co}\right)}\right]$ For turbulent flow (Re_l > 2000 and Re_v > 2000): $C = 1.79\left(\frac{Re_v}{Re_l}\right)^{0.4}\left(\frac{1-x}{x}\right)^{0.5}$	*2092 data points* *D: 0.506 – 12 mm* *G: 50 – 2000 kg/m^{2}s* *Fluid: R123, R134a, R22, R236ea, R245fa, R404a, R407C, R410a, R507, CO_2, air-Water*
Li and Wu (2010a)	$C = \begin{cases} 11.9Bd^{0.45}, & Bd \le 1.5 \\ 109.4(BdRe_l^{0.5})^{-0.56}, & 1.5 < Bd \le 11 \end{cases}$	*769 data points* *D: 0.148 – 3.25 mm* *G: 198 – 2000 kg/m^{2}s* *x: 0 – 1* *Fluid: R134a, R245fa, R236ea, R410a, Ammonia, Propane, R22, R12, R404a, N_2, R422d, R32*
Zhang et al. (2010)	$C = 21\left(1 - e^{-0.358/Co}\right)$	*2201 data points* *D: 0.014 – 6.25 mm* *Fluid: Air, water, N_2, ethanol, oil, Ammonia, R22, R404a, R236ea, R410a, R12, R113, R134a*
Lee et al. (2010)	$C = 121.6(1 - e^{-22.7Bd})x^{1.85}$	*484 data points* *D: 0.35 – 2.46 mm*

		G: 20.3 – 2267 kg/m²s *x: 0 – 0.98* *Fluid: Water, N-pentane, Ammonia, CO_2, R410a, R134a, R12*
Kim and Mudawar (2012)	$C = \begin{cases} 3.5 \times 10^{-5} Re_{lo}^{0.44} Su_{vo}^{0.5} \left(\frac{\rho_l}{\rho_v}\right)^{0.48}, & (ll) \\ 0.0015 Re_{lo}^{0.59} Su_{vo}^{0.19} \left(\frac{\rho_l}{\rho_v}\right)^{0.36}, & (lt) \\ 8.7 \times 10^{-4} Re_{lo}^{0.17} Su_{vo}^{0.5} \left(\frac{\rho_l}{\rho_v}\right)^{0.14}, & (tl) \\ 0.39 Re_{lo}^{0.03} Su_{vo}^{0.1} \left(\frac{\rho_l}{\rho_v}\right)^{0.35}, & (tt) \end{cases}$	*7115 data points* *D: 0.0695 – 6.22 mm* *G: 4 – 8528 kg/m²s* *x: 0 – 1* *Fluid: R134a, R12, N_2-water, N_2-ethanol, R410a, R407a, R22, R404a, CO_2, Ammonia, R245fa, R236ea, Propane, Methane, CO_2-water, Air-water*
Kim and Mudawar (2013)	$C = \begin{cases} C^* \left[1 + 60 We_{lo}^{0.32} \left(Bo \frac{P_H}{P_F}\right)^{0.78}\right], & Re_l \geq 2000 \\ C^* \left[1 + 530 We_{lo}^{0.52} \left(Bo \frac{P_H}{P_F}\right)^{1.09}\right], & Re_l < 2000 \end{cases}$ $C^* = \begin{cases} 3.5 \times 10^{-5} Re_{lo}^{0.44} Su_{vo}^{0.5} \left(\frac{\rho_l}{\rho_v}\right)^{0.48}, & (ll) \\ 0.0015 Re_{lo}^{0.59} Su_{vo}^{0.19} \left(\frac{\rho_l}{\rho_v}\right)^{0.36}, & (lt) \\ 8.7 \times 10^{-4} Re_{lo}^{0.17} Su_{vo}^{0.5} \left(\frac{\rho_l}{\rho_v}\right)^{0.14}, & (tl) \\ 0.39 Re_{lo}^{0.03} Su_{vo}^{0.1} \left(\frac{\rho_l}{\rho_v}\right)^{0.35}, & (tt) \end{cases}$	*2378 data points* *D: 0.349 – 5.35 mm* *G: 33 – 2738 kg/m²s* *x: 0 – 1* *Fluid: R134a, R12, R410a, R22, CO_2, Ammonia, R245fa, FC72, Water*
Huang and Thome (2017)	$C = \begin{cases} 0.0037 Re_v^{1.70} Re_{lo}^{-0.83}, & Re_l \leq 2000, Re_v \leq 2000 \\ 0.9 Re_v^{0.034} Re_{lo}^{0.20}, & Re_l \leq 2000, Re_v > 2000 \end{cases}$	*184 data points* *D: 0.1 mm* *G: 1250 – 2750 kg/m²s* *x: 0.034 – 0.51* *Fluid: R1233zd(E), R245fa, R236fa*

laminar-laminar flow (5) instead of their constant (21). Hwang and Kim (2006) found that the channel size, surface tension and Reynolds number have a significant effect on the two-phase flow frictional pressure drop in microtubes. Therefore, they developed the Chisholm's parameter with using the liquid-only Reynolds number, Martinelli parameter, and the Confinement number. Sun and Mishima (2009) found that the Chisholm's parameter *C* is affected by the liquid Reynolds number and Laplace number in laminar flow region while in turbulent flow region, it is significantly affected by the ratio of gas Reynolds number to liquid Reynolds number. Based on the results of statistical analysis,

they proposed two models to modify the Chisholm's parameter, one for laminar flow and another for turbulent flow.

Zhang et al. (2010) analysed the experimental data of mini and microchannels which collected from the literature. They found that the Laplace constant is a major parameter in modifying the Mishima and Hibiki (1996) model. Thus, they replaced the hydraulic diameter with the non-dimensional Laplace constant to correlate the Chisholm parameter. Lee et al. (2010) revealed the influential role of the Bond number, which related the capillary parameter (nominal bubble dimension) with the channel size. They proposed a modification in the Chisholm parameter by using both the Bond number and the exit vapour quality resulting in an improved correlation of two-phase pressure drop for a wide range of working fluids, channel size and operational conditions. Li and Wu (2010a) modified the Chisholm's parameter of two-phase multipliers to develop their correlation of adiabatic two-phase pressure drop across mini and microchannels based on 769 experimental data points. They found that the Bond number and the liquid Reynolds number are the influential parameters. Further, they categorized the data on the basis of Bond number in three ranges, namely region of dominant surface tension ($Bd \leq 1.5$), region dominated by surface tension, inertia, and viscous force ($1.5 < Bd \leq 11$), and region without surface tension effect ($Bd > 11$). Kim and Mudawar (2012) developed a universal correlation to predict adiabatic two-phase pressure drop in mini and microchannels based on a consolidated database covering 7115 data points from 36 sources. The Chisholm parameter was modified with appropriate dimensionless parameters involving liquid-only Reynolds number, gas-only Suratman number, and liquid-gas density ratio for each of the four flow regimes. Kim and Mudawar (2013) constructed universal correlation of flow boiling pressure drop in mini and microchannels by modifying their previous model (Kim and Mudawar, 2012) which was proposed for non-boiling flow. The authors replaced the C parameter with a function of dimensionless groups containing Weber number and Boiling number as well as the previous C parameter for non-boiling flow. They also took account of the effects of small channel size, different working fluids, and comprehensive ranges of flow parameters. Huang and Thome (2017) proposed empirical flow boiling pressure drop model for high mass flux conditions by fitting Chisholm's parameter with the vapour Reynolds number and liquid only Reynolds number based on the 184 experimental data points of stable flow boiling in a microchannel.

There are other formulations of two-phase pressure drop models that were different from preceding models. Chisholm (1973a) depended upon the influence of mass velocity on two-phase flow as well as vapour quality, liquid-only and gas-only single-phase pressure drop to develop the two-phase frictional multiplier. Friedel (1979) introduced the Weber number, and Froude number to modify two-phase frictional multiplier in terms of liquid-only. Where the model includes the effect of gravitational force through the Froude number, the effects of surface tension force and total mass flux through the Weber number. Grönnerud (1979) proposed two-phase pressure drop correlation based on the variety of refrigerants and operating conditions. The author used the Froude number, viscosity ratio, density ratio and vapour quality to develop the two-phase frictional liquid-only multiplier. Müller-Steinhagen and Heck (1986) suggested a correlation based on databank involving 9300 measurements of frictional pressure drop. They employed the pressure gradient of the respective single-phase flow (i.e. liquid-only and gas-only) in addition to the implementation of an empirical two-phase extrapolation between all liquid flow and all vapour flow. They also took into account the influence of flow parameters such as vapour quality, mass flux and system pressure. Recently, Xu and Fang (2012) proposed a correlation based on 2622 experimental data points of 15 refrigerants with hydraulic diameter from 0.81 to 19.1 mm. The authors modified the correlation of Müller-Steinhagen and Heck (1986) using the Laplace constant. Del Col et al. (2013a) proposed a predictive model based on the correlation of Friedel (1979) and their experimental data including broad operating conditions for mini and microchannels. The authors focused on the effects of surface roughness, mass flux, fluid properties, channel size, reduced pressure and eventually vapour quality to develop their predictive models.

From the above review, it is concluded that much work has been carried out to predict the friction pressure drop during two-phase flow. Most of the investigations in developing the separated flow model can be divided into two groups. One sought to keep the original two-phase multiplier format with empirically modifying Chisholm's parameter *C* according to their experimental database, while the second focused directly on correlating the two-phase multiplier with influential parameters and their experimental data. Nevertheless, nearly all these models depended on limited test fluids and channel dimensions under limited parametric conditions. Although the researchers have proposed and employed various approaches with various levels of complexity to predict two-phase

pressure drop in mini and microscale channel, the influences of some parameters such as fluid properties, channel size, surface roughness, channel geometry and heat flux are still unclear. The effects of these parameters on the frictional pressure drop of two-phase flow in mini and microtubes should be studied in detail. This work considered as an attempting to develop or find the recommended correlation for flow boiling pressure drop in vertical small tubes using R245fa as working fluid.

2.9 Two-phase heat transfer coefficient

The flow boiling applications used small-scale channels as a cooling technique of high heat flux systems is of great interest to the community of heat transfer engineers. The progress in this field is, as a matter of fact, restricted by a limited knowledge of heat transfer mechanisms and the ability to predict the heat transfer rates. Generally, for conventional channels, two-phase flow boiling heat transfer combines nucleate boiling and convective contributions. Nucleate boiling is a heat transfer mechanism resembling pool boiling within the continuous fluid flow. Further, the fluid flow has a strong effect on the growth and departure of bubbles. The heat transfer increases effectively with increasing heat flux as in the process of pool boiling where the magnitude of heat flux does not exceed the certain critical heat flux. The relative influence of nucleate boiling decreases during the flow boiling process in the channel when the mass flow rate and mass fraction of vapour phase increase. At high mass flow rates and high vapour qualities, this influence of nucleate boiling mechanism is suppressed because of the inception of the convection mechanism. The thin liquid film forms on the wall channel with some small zones having effective superheat and bubble nucleation. The vapour phase is formed in the channel core. The heat transfer between the hot wall and the fluid occurs during evaporation at the vapour-liquid interface of the liquid film layer. The mean density of both phases decreases and consequently the velocity of fluid increases. Thus, the effect of convective boiling on the heat transfer process increases resulting in increasing two-phase heat transfer coefficient with vapour quality.

The researchers have realized that the heat transfer characteristics and mechanism in a small-scale channel are noticeably different from those of conventional channel, and

only parts of principal knowledge attained in macroscale investigations are found to be applicable to microscale cooling systems. Most research has been performed to understand the heat transfer mechanism of flow boiling in small passages, and a lot of researchers have mentioned that the nucleation mechanism is the prevailing factor for evaporation in small and micro channels. Since the flow boiling heat transfer in conventional channels, both nucleate and convective boiling are considered influential, the current correlations rather over- or under-predict the heat transfer coefficient for mini and microchannels. This results from the laminar flow characteristics in smaller channels (Lim et al., 2015).

2.10 Key Factors influencing heat transfer coefficient

Flow pattern and pressure drop characteristics are an important aspect for understanding the basic principles of the flow boiling process and were discussed in the former sections. There are other major parameters affecting the two-phase heat transfer process including the contribution of nucleate and convective boiling. Several studies focused on the dominant mechanism of flow boiling heat transfer and the effect of operating parameters. The flow boiling studies in the literature described below which pertain to the influences of key parameters on flow boiling heat transfer and are summarized in Table 2.8. In this work, we look into the local heat transfer coefficient inside small tubes with coating and upward flow in the vertical orientation.

2.10.1 Effect of channel size

The channel diameter is among the most important parameters to enhance the values of the flow boiling heat transfer coefficient. Choi et al. (2009) studied experimentally the effect of tube diameter on flow boiling mechanisms for propane flowing inside 1.5 and 3.0 mm tubes with 5 – 20 kW/m^2 heat flux, 50 – 400 kg/m^{2}s mass flux at 0 – 10 °C saturation temperature. They found that the tube diameter influences significantly the heat transfer coefficient. Namely, the decrease of inner tube diameter gives rise to increasing heat transfer coefficient. They attributed this case to (i) the increase of the contact surface area for heat transfer with reducing tube diameter, and (ii) nucleate boiling became more active in a reduced diameter tube. The effect of inner tube diameter (channel confinement)

Table 2.8 Summary of experimental flow boiling studies in small and micro-scale tubes.

Author(s)	Fluid	Diameter, mm	Orientation	Conditions
Shin et al. (1997)	R22 R32 R134a R290 R600a Refrigerant mixtures	7.7	Horizontal	*T_{sat} = 12 °C* *G = 265–742 kg/m^{2}s* *q = 10–30 kW/m^2* *x = 0.1–0.8*
Huo et al. (2004)	R134a	2.01 4.26	Vertical	*P= 800-1200 kPa* *G = 265–742 kg/m^{2}s* *q = 13–150 kW/m^2* *x = 0–0.9*
Choi et al. (2009)	Propane	1.5 3	Horizontal	*T_{sat} = 0–10 °C* *G = 50–400 kg/m^{2}s* *q = 5–20 kW/m^2* *x = 0–1*
Ong and Thome (2011b)	R134a R236fa R245fa	1.03–3.04	Horizontal	*T_{sat} = 25–35 °C* *G = 200–1600 kg/m^{2}s* *q = 4.8–1290 kW/m^2* *x = 0–1*
Saitoh et al. (2011)	R1234yf	2	Horizontal	*DC power* *T_{sat} = 15 °C* *G = 100-400 kg/m^{2}s* *q = 6-24 kW/m^2* *x = 0-0.25*
Ong and Thome (2011a)	R134a R236fa R245fa	1.03–3.04	Horizontal	*T_{sat} = 25–35 °C* *G = 200–1600 kg/m^{2}s* *q = 4.8–1290 kW/m^2* *x = 0–1*
Maqbool et al. (2012a)	Ammonia	1.7 1.224	Vertical	*T_{sat} = 23–43 °C* *G = 100–500 kg/m^{2}s* *q = 15–355 kW/m^2* *x = 0–1.1*
Tibiriçá et al. (2012)	R1234ze(E)	1-2.2	horizontal	*DC power* *T_{sat} = 25-35 °C* *G = 50-1500 kg/m^{2}s* *q = 10-300 kW/m^2* *x = 0.05-0.99*
Copetti et al. (2013)	R600a	2.6	Horizontal	*T_{sat} = 22 °C* *G = 240-440 kg/m^{2}s* *q = 44-95 kW/m^2* *x = 0.02-0.7*
Del Col et al. (2013b)	R1234yf	0.96	horizontal	*Heat exchanger* *T_{sat} = 31 °C* *G = 200-600 kg/m^{2}s* *q = 10-125 kW/m^2* *x = 0.02-0.73*
Choi et al. (2013)	R1234yf R134a R22	1.5 3	Horizontal	*T_{sat} = 5–15 °C* *G = 100-650 kg/m^{2}s* *q = 10-35 kW/m^2* *x = 0–1*
Choi et al. (2014)	R744 R717 R290 R1234yf	1-3	horizontal	*Electric power* *T_{sat} = 0-10 °C* *G = 50-600 kg/m^{2}s* *q = 5-60 kW/m^2* *x = 0-1*

Charnay et al. (2015b)	R245fa	3	horizontal	*q = 10 – 50 kW/m²* *x = 0 – 1* *G = 100 – 1500 kg/m²s* *T_{sat} = 100 – 120 °C*
Anwar et al. (2015b)	R1234yf	1.6	vertical	*DC power* *T_{sat} = 27-32 °C* *G = 100-500 kg/m²s* *q = 5-135 kW/m²* *x = 0-0.95*
Anwar et al. (2015a)	R600a	1.6	vertical	*DC power* *T_{sat} = 27-32 °C* *G = 50-350 kg/m²s* *q = 5-135 kW/m²* *x = 0-0.77*
De Oliveira et al. (2016)	R600a	1	Horizontal	*T_{sat} = 25 °C* *G = 240-480 kg/m²s* *q = 5-60 kW/m²* *x = 0-0.92*
Abadi et al. (2016)	R245fa	3	Vertical Horizontal	*T_{sat} = 5–20 °C* *G = 200–700 kg/m²s* *q = 10–40 kW/m²* *x = 0.1–0 .7*
Longo et al. (2016a)	R32 R410a	4	Horizontal	*T_{sat} = 5–20 °C* *G = 196.1–821.3 kg/m²s* *q = 11.7–51.4 kW/m²* *x = 0.06–0.9*
Longo et al. (2016b)	R134a R1234ze(E)	4	Horizontal	*T_{sat} = 5–20 °C* *G = 196.1–610.4 kg/m²s* *q = 10.1–30.6 kW/m²* *x = 0.08–0.97*
Xu et al. (2016b)	R134a	1.002–4.065	Horizontal	*P = 578–820 kPa* *G = 185–935 kg/m²s* *q = 18–35.5 kW/m²* *x = 0.03–1*
Kanizawa et al. (2016)	R134a R245fa R600a	0.38-2.6	Horizontal	*T_{sat} = 21.5–58.3 °C* *G = 49–2200 kg/m²s* *q = 5–185 kW/m²* *x = 0.05–0.93*
Sempértegui-Tapia and Ribatski (2017a)	R134a R1234ze(E) R1234yf R600a	1.1	Horizontal	*T_{sat} = 31-41 °C* *G = 200-800 kg/m²s* *q = 15-145 kW/m²* *x = 0.05-0.95*
Linlin et al. (2017)	R744	0.6 1.5	Horizontal	*T_{sat} = 233-273 K* *G = 300-600 kg/m²s* *q = 7.5-30 kW/m²* *x = 0.05-0.95*

on two-phase heat transfer was assessed in the experimental studies of Ong and Thome (2011a, 2011b). They performed flow boiling experiments of R134a, R236fa and R245fa inside three horizontal tubes with a diameter of 1.03, 2.20 and 3.04 mm. They noticed that the channel confinement influences appreciably the two-phase flow pattern transitions. That is, when the Confinement number increased more than 1, the annular flow regime expanded gradually to lower vapour qualities, while the isolated bubble and

coalescing bubble regimes were suppressed gradually. In addition, for Confinement number less than 0.34, the slug/plug regime was observed at the lower mass flux range. For the case of R236fa, the heat transfer coefficient of the 1.03 mm tube was lower than that of 2.2 and 3.04 mm tubes in the isolated bubble regime. However, the effect of tube diameter on heat transfer coefficient was most clearly pronounced in the higher quality region which was controlled by the annular flow. They suggested the predominance of convection mechanism in the higher vapour quality region. For the case of R245fa, the trend of the heat transfer coefficient versus the vapour quality converged to one line of the heat transfer coefficient increasing with vapour quality irrespective of heat flux. This heat transfer coefficient trend occurred at lower vapour quality with decreasing channel size as shown in Figure 2.17. Maqbool et al. (2012a) presented an experimental investigation on the influence of channel size on heat transfer coefficient of R717 inside 1.70 mm and 1.224 mm vertical tubes. The operating conditions included mass flux varying from 100 to 500 kg/m^{2}s and heat flux varying from 15 to 355 kW/m^2 with saturation temperature ranging from 23 to 43 °C. They found that the 1.224 mm tube has a greater effect on the heat transfer coefficient rather than that of 1.70 mm tube i.e. the heat transfer coefficient was higher in the 1.224 mm tube. They attributed this behaviour to the thinner film of liquid phase on the heated tube wall accounting for high heat transfer coefficient. Choi et al. (2013) performed a comparison of the heat transfer coefficient data for R1234yf, R134a, and R22 flowing in horizontal round small tubes with the 1.5 and 3 mm internal diameter. The experimental data were acquired for 10–35 kW/m^2 heat flux, 100–650 kg/m^{2}s mass flux, saturation temperatures of 5, 10 and 15 °C, and vapour quality up to 1. Their experimental results demonstrated that the highest enhancement of heat transfer coefficient occurs at the low vapour quality region when the internal tube diameter was reduced from 3 to 1.5 mm. They explained that this enhancement is due to more active nucleate boiling in a smaller tube size, which rendered early the appearance of dry spots. Moreover, the reduced tube diameter assisted in increasing the contact area of the surface for flow boiling heat transfer.

Recently, Xu et al. (2016b) conducted an experimental investigation on the effect of tube diameter on flow boiling heat transfer coefficient using R134a refrigerant. The three horizontal test tubes were made of copper with an internal diameter of 1.002, 2.168, and

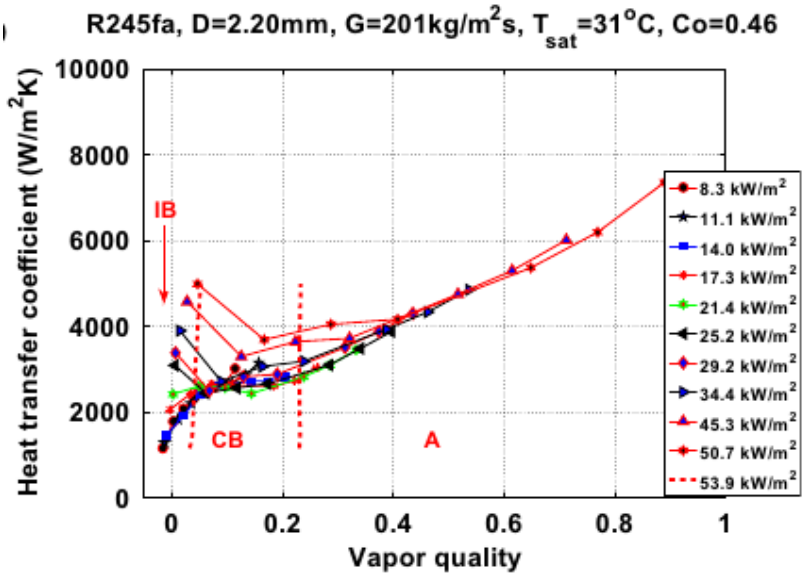

(a)

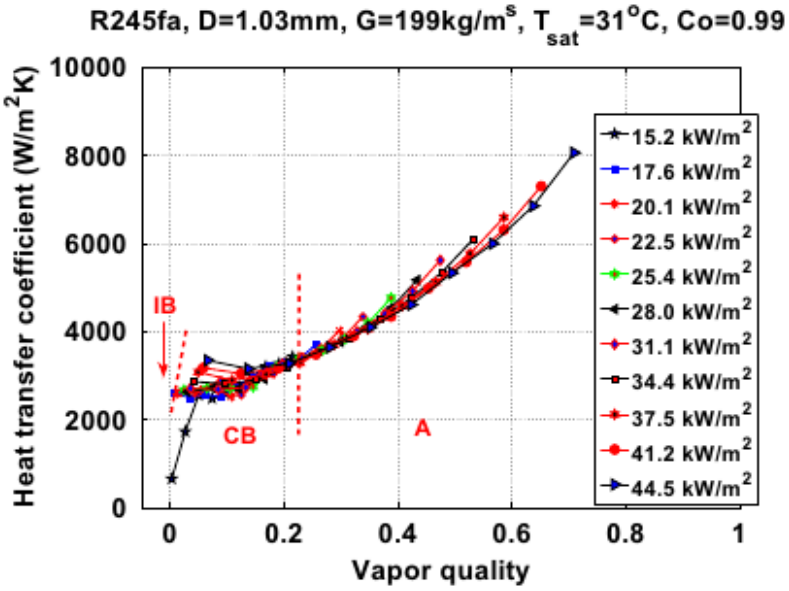

(b)

Figure 2.17 The effect of inner tube diameter on saturated boiling heat transfer coefficient: (a) for 2.2 mm tube and (b) for 1.03 mm tube, (Ong and Thome, 2011b).

4.065 mm. The experimental data were attained for a mass flux of 185 – 935 kg/m^{2}s, heat flux of 18.0 – 35.5 kW/m^2, pressure of 578 – 820 kPa, and vapour quality at the exit from 0.03 up to 1. They detected that the characteristics of flow boiling heat transfer in the 4.065 mm tube are entirely different from those in the 1.002 and 2.168 mm tubes. The heat transfer coefficient for 1.002 mm tube was higher than that for 2.168 and 4.065 mm tube at the similar test conditions. Kanizawa et al. (2016) analysed parametrically experimental flow boiling data for refrigerants R134a, R245fa and R600a flowing in

small-diameter tubes. The experimental data covered internal tube diameter from 0.38 to 2.6 mm, mass flux from 49 to 2200 kg/m^{2}s, heat fluxes from 5 to 185 kW/m^2 and quality up to 0.93. They inferred generally that the heat transfer coefficient before the dryout increased as the inner tube diameter reduced from 1 to 0.38 mm. Nevertheless, the tube diameter greater than 1 mm had a negligible effect on heat transfer coefficient. On the other hand, they found that the reduction of tube diameter results in the occurrence of earlier dryout, as shown in Figure 2.18. Linlin et al. (2017) presented an experimental investigation on flow boiling heat transfer for carbon dioxide (R744) as the refrigerant in two different horizontal small-diameter tubes at the low saturation temperature of 233 – 273 K. The test tubes had 0.6 and 1.5 mm inner diameters and made of stainless steel. The experimental conditions included 7.5 – 30 kW/m^2 heat flux and 300 – 600 kg/m^{2}s mass flux. The experimental results revealed that heat transfer coefficient increases with the decrease of inner tube diameter. They explained the reason for this phenomenon could be due to the dominance of nucleate boiling.

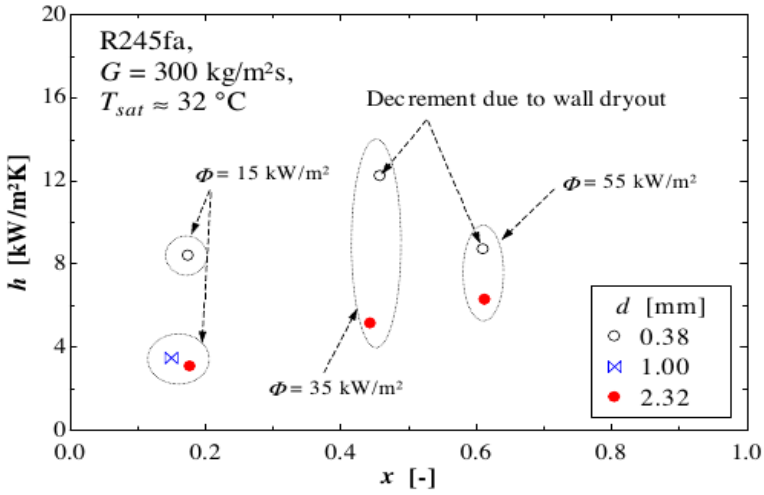

Figure 2.18 The effect of inner tube diameter on flow boiling heat transfer coefficient, (Kanizawa et al., 2016).

It can be concluded from the above, that all researchers agreed that the channel diameter has a significant effect on saturated boiling heat transfer coefficient and consequently on the contributions of the nucleate boiling and convective boiling mechanisms in small-scale channels. Also, the small channel plays an important role in changing the distributions of vapour and liquid phases inside the channel. That is, the decreased channel diameter leads to an increased heat transfer coefficient due to strongly

contributing to the bubble nucleation in flow boiling and the changes of flow patterns. In this work, the effect of four diameter tubes on local heat transfer coefficient for R245fa were studied, including 1.1 mm, 2.01 mm, 2.88 mm, 4.26 mm inner diameter tubes. The decrease of diameter tube causes an enhancement in the local heat transfer coefficient. This enhancement of two-phase flow heat transfer rates in small to microscale tubes is very important for the design of small-scale shell and tube heat exchangers.

2.10.2 Effect of pressure and fluid properties

Several studies have shown that the pressure and saturation temperature significantly influence the flow boiling heat transfer coefficient because the variations of pressure and saturation temperature affect the thermophysical properties of fluids. In addition, the fluid type affects the heat transfer coefficient due to its influential properties. As a result, this affects the heat transfer process and then the transitions of flow patterns. Huo et al. (2004) researched the pressure effect on the two-phase heat transfer coefficient of R134a evaporation in small diameter tubes. The test results revealed that the pressure affected positively the heat transfer coefficient. They attributed the increase of heat transfer coefficient with the increased pressure to the influence of pressure on the evaporation latent heat. The influence of saturation temperature on heat transfer coefficient was investigated by Choi et al. (2009). They observed that the heat transfer coefficient of propane is enhanced with the increased saturation temperature because of the contribution of nucleate boiling, which has a significant influence. They clarified that the higher saturation temperature results in higher pressure and lower surface tension. Therefore, the vapour forms in the boiling process leading to an increase in heat transfer rate and consequently yielding the higher heat transfer coefficient. Ong and Thome (2011b) presented in detail the experimental study of the transition from macro to microchannel flow boiling for R134a, R236fa and R245fa refrigerants at the saturation temperature of 31 and 35 °C. They concluded that the heat transfer coefficient during the transition of flow pattern is increased with increasing saturation temperature from 31 to 35 °C. Maqbool et al. (2012a) obtained experimental flow boiling results of R717 during evaporation inside 1.224 and 1.7 mm tubes. They conducted the flow boiling experiments at the 23, 33 and 43°C saturation temperature with a mass flux of 100 – 500 kg/m^{2}s and 15 – 355 kW/m^2 in heat flux. The results exhibited that the heat transfer coefficient

increases with saturation temperature at the low vapour quality region for both tubes. For higher vapour quality, the increased saturation temperature had an insignificant influence. They explained that the heat transfer coefficient increases with saturation temperature due to the increased nucleation with an increment in saturation temperature. Further, when saturation temperature increases, the bubble departure diameter reduces. As a result, the bubble formation and the bubble frequency may increase. This, in turn, enhances the contribution of nucleation mechanism. Choi et al. (2013) studied the effect of saturation temperature on two-phase heat transfer coefficient for R1234yf, R134a, and R22 in 1.5 and 3 mm inner diameter. The test parameters were 10–35 kW/m^2 heat flux, 100–650 kg/m^{2}s mass flux, saturation temperatures of 5, 10 and 15 °C, and exit vapour quality up to 1. They reported that the higher saturation temperature provided the higher two-phase heat transfer coefficient. They considered significantly the effect of saturation temperature on the physical properties of refrigerants such as surface tension, liquid-vapour density ratio, liquid-vapour viscosity ratio and pressure. These properties contributed to the effect on the heat transfer coefficient.

Recently, Xu et al. (2016b) conducted an experimental study to investigate the effect of pressure on the heat transfer coefficient of R134a boiling inside three horizontal small copper tubes with an inner diameter of 1.002 – 4.065 mm. They found that the saturated boiling heat transfer coefficient increases with increasing saturation pressure. The test conditions covered pressure ranging from 578 to 820 kPa, mass flux from 185 to 935 kg/m^{2}s and heat flux from 18.0 to 35.5 kW/m^2. They explained that the increasing heat transfer coefficient with saturation pressure results from the effect of pressure on the thermodynamic properties of refrigerants. They reported that the rise of pressure results in a reduction of surface tension and an increase of vapour-liquid density ratio. The advantage is due to the decreasing surface tension in contrast with the increase of vapour-liquid density ratio for flow boiling. As a result, the influence of pressure is associated with the contributions of these two significant effects which could, in turn, affect the heat transfer coefficient. Longo et al. (2016a) presented the comparative study of R32 and R410a during flow boiling in a 4 mm horizontal tube under three different saturation temperatures (5, 10, and 20 °C). The experimental results demonstrated that the heat transfer coefficient of R32 is about 17% higher than that of R410a under the same operating conditions and also the heat transfer coefficient increases with increasing

saturation temperature. The authors considered that the differences in thermophysical properties such as liquid thermal conductivity, dynamic viscosity and surface tension as well as thermodynamic properties such as reduced pressure, latent heat of vaporization between both refrigerants can explain this increase in the heat transfer coefficient of R23. In addition, Longo et al. (2016b) studied the effects of saturation temperature and fluid properties on saturation boiling heat transfer coefficients for R134a and R1234ze(E) flowing in a 4 mm tube. They observed similar findings to Longo et al. (2016a) regarding the effect of saturation temperature, but the effect of fluid properties was different. R1234ze(E) exhibited heat transfer coefficients similar to those of R134a under the same operating conditions. Kanizawa et al. (2016) presented experimental results of R134a during flow boiling in a 2.32 mm tube at saturation temperatures of 22, 31 and 41 °C. They concluded that the dependence of the heat transfer coefficient on saturation temperature is significant as the nucleation mechanism become the predominant heat transfer process. But, this effect becomes negligible under circumstances of prevailing convective boiling. The experimental study of Sempértegui-Tapia and Ribatski (2017a) for R134a revealed that the heat transfer coefficient increases from 5 to 15% with increasing pressure from 793 to 1045 kPa. However, they detected that the heat transfer coefficient for R600a increased with system pressure at low quality, whilst at high quality, the trends were opposite i.e. it decreased with pressure. They attributed this behaviour to the influences of mass and heat flux.

In conclusion, these studies show that the saturation temperature corresponding to operating pressure is an influential parameter. All researchers have presented a unified agreement on the increase of two-phase heat transfer coefficient with increasing pressure because the pressure has a strong influence on the thermophysical fluid properties. This, in turn, affects the distributions of both phases in the flow channel, especially, for mini and micro channels. In addition, the differences in thermophysical and thermodynamic properties between different working fluids can result in an increase in heat transfer coefficient. In this work, the experimental data for three low pressures were used to study their effects on flow boiling heat transfer rates in small to microscale tubes, including those for 185, 245 and 310 kPa.

2.10.3 Effect of mass flux and vapour quality

Mass flux and vapour quality are considered influential parameters in the flow boiling, since they influence the two-phase heat transfer mechanism, specifically in convective boiling. It is notable that the convection mechanism dominates in annular flow due to the dependence of the heat transfer coefficient on mass flux. Shin et al. (1997) carried out investigation on flow boiling for pure refrigerants and refrigerant mixtures at 12 °C saturation temperature. They reported that the heat transfer coefficient for R22 working fluid increases with increasing mass flux and vapour quality under conditions of constant heat flux except for the entry region. They illustrated that this phenomenon takes place due to the increase in the velocity of the refrigerant in the flow path with developing flow patterns to stable annular flow. Thus, the heat transfer coefficient increases, leading to the rapid removal of the heat transfer imposed on the tube. Meanwhile, when the refrigerant velocity became high, the nucleation mechanism diminished in the higher vapour quality region. Huo et al. (2004) conducted study of R134a flow boiling inside 4.26 and 2.01 mm internal tube diameter at system pressure of 800–1200 kPa. The test parameters covered heat flux of 13–150 kW/m^2, mass flux of 100–500 kg/m^{2}s and quality up to 0.9. They reported that the mass flux has insignificant effect on heat transfer coefficient in both tubes. Choi et al. (2009) presented an experimental investigation to study the effect of mass flux on flow boiling mechanisms for propane flowing inside 1.5 and 3.0 mm tubes with 5 – 20 kW/m^2 heat flux, 50 – 400 kg/m^{2}s mass flux at 0 – 10 °C saturation temperature. The test data revealed that the effect of mass flux on the heat transfer coefficient was insignificant in the low vapour quality region. The authors report that this implies the predominance of nucleation mechanism in this region. They also attributed the dominant nucleate boiling to the fluid properties and state (such as surface tension, pressure) and the geometric influence of the channel. In addition, they mentioned that the flow boiling heat transfer coefficient increases as the mass flux increases at moderate and high vapour quality regions because of the dominance of the convective boiling mechanism. The dependence of heat transfer coefficient of R134a, R236fa and R245fa refrigerants on mass flux in macro-to-micro channel was investigated by Ong and Thome (2011a, 2011b). Firstly, they noticed that the occurrence of the two-phase flow pattern transitions moves to lower quality values with increasing mass flux in the low vapour quality region. Therefore, annular flow expanded from high to low vapour quality region, especially at higher mass fluxes. Simultaneously, the isolated bubble and

coalescing bubble flow regimes gradually vanished. They thought that with the expansion of the annular flow, the dominance of forced convection is also expanded from high to low vapour quality region. Consequently, this could be generally accompanied by the enhanced heat transfer coefficient against vapour quality. Secondly, they observed that the heat transfer coefficient in the coalescing bubble regime distinctively declines for all mass fluxes. They employed the same explanation of Thome et al. (2004), which attributed the reason to thin liquid film evaporation with dry spot formation and rewetting in these situations. Generally, the heat transfer coefficient increased with increased mass flux under conditions of the completed transition from coalescing bubble to annular flow as seemed in Figure 2.19. Maqbool et al. (2012a) investigated flow boiling of R717 in two vertical tubes with the diameters 1.224 and 1.7 mm. The test sections were heated uniformly with a range of 15 – 355 kW/m^2 in heat flux and a mass flux range of 100 – 500 kg/m^{2}s at saturation temperature of 23 – 43 °C. Their experimental results showed that the independence of local heat transfer coefficient in 1.7 mm tube from mass flux and vapour quality is due to the dominance of the nucleate boiling. For the flow boiling in the 1.224 mm tube, they observed that the local heat transfer coefficient is slightly dependent on mass flux at the lower vapour quality region in contrast with the region of intermediate up to high vapour quality values, it depends on mass flux and vapour quality. They suggested the same explanation of Choi et al. (2007) to illustrate this case, where the nucleate boiling was earlier suppressed because of convective contributions under conditions of high mass flux. Copetti et al. (2013) conducted an experimental investigation to study the mass flux effect on the heat transfer coefficient for flow boiling of R600a in a 2.6 mm tube at 22 °C with mass flux of 240 and 440 kg/m^{2}s and heat flux of 44 – 95 kW/m^2. They observed that the heat transfer coefficient slightly depends on the mass flux with lower heat fluxes. However, the dependence of heat transfer coefficient on the higher mass flux becomes strong with higher heat fluxes due to the dominant convective boiling and then becomes weak due to the occurrence of dryout.

De Oliveira et al. (2016) presented an experimental study for flow boiling of R600a inside a horizontal micro-tube with an inner diameter of 1 mm. They reported that the strong dependence of heat transfer coefficient on mass flux is obvious. The convective boiling became more dominant with increasing mass flux and vapour quality in addition to the absence of the heat flux impact. Abadi et al. (2016) conducted an experimental

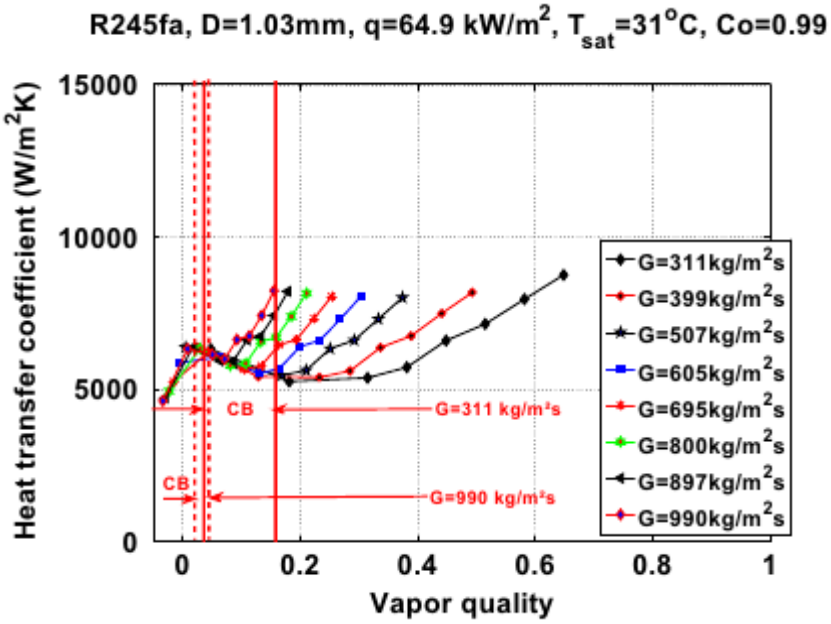

Figure 2.19 The effect of mass flux on flow boiling heat transfer coefficient, (Ong and Thome, 2011b).

investigation on flow boiling for R245fa inside a 3 mm stainless-steel tube with a different orientation. They found that the two-phase heat transfer coefficient depends strongly on mass flux especially in annular flow and high vapour qualities. Conversely, in the low vapour quality region, the mass flux has a slight effect on the heat transfer coefficient. They reported that this behaviour conforms the contribution of the convective boiling. Xu et al. (2016b) performed flow boiling test for R134a in three horizontal tubes with diameter ranging from 1.002 to 4.065 mm. The experimental findings revealed that the heat transfer coefficients for 1.002 and 2.168 mm tubes increase with vapour quality in intermittent and annular flows, but the mass flux has a very little influence on the heat transfer coefficient of 1.002 mm tube as opposed to that of 2.168 mm tube. However, for the 4.065 mm tube, the heat transfer coefficient decreased with vapour quality in intermittent and annular flow and it was nearly not influenced by mass flux. Kanizawa et al. (2016) carried out flow boiling experiments for R134a, R245fa and R600a in small diameter tubes ranging from 0.38 to 2.6 mm at the saturation temperature of 21.5 –58.3 °C. The mass flux was varied between 49 and 2200 kg/m^{2}s, the heat flux was up to 185 kW/m^2 and vapour quality reached up to 0.93. They deduced that the heat transfer coefficient for R134a increases with increasing mass flux in the high vapour quality region. For R600a, the heat transfer coefficient increased over the entire quality values until it reached dryout, while, for R245fa, the effect of mass flux was almost insignificant.

They imputed the dependence of the heat transfer coefficient on mass flux and quality to the predominance of convective flow boiling. An insignificant effect of mass flux and vapour quality on R32 and R410a heat transfer coefficients in a 4 mm tube was obtained by the investigation of Longo et al. (2016a) due to the dominance of nucleate boiling heat transfer regime. However, the study of Longo et al. (2016b) proved the contrary for R134a and R1234ze(E) heat transfer coefficients. That is, the heat transfer depended strongly on mass flux and vapour quality resulting in the prevailing of convective boiling heat transfer regime in their experimental tests. Sempértegui-Tapia and Ribatski (2017a) presented the flow boiling results for R1244yf and R600a in the internal diameter of 1.1 mm. They observed that the heat transfer coefficient increases with mass flux in mild and high vapour quality where convective boiling prevails.

It can be concluded from the above that the mass flux and vapour quality play an important role in flow boiling process, especially, on the two-phase heat transfer coefficient. The saturated boiling heat transfer coefficient increases when the mass flux and vapour quality increase. This means that the convective mechanism is dominant in flow boiling after the suppression of nucleate boiling. This occurs in an intermediate up to high vapour quality region in macro channels, while in mini and micro channels, there is controversy among researchers about this point. The reason ascribes to the effect of channel size and surface tension. In this work, the changes of mass flux for vertical tubes and their effects on flow boiling heat transfer rate were experimentally investigated with the range of 200 – 500 kg/m^{2}s and vapour quality up to onset of dryout. The initial stage of the present study aims to understand the flow boiling mechanisms in small to microscale tubes through the effects of mass flux and vapour quality on local heat transfer coefficient (representing the contribution of convective boiling).

2.10.4 Effect of heat flux

Generally, the heat flux parameter plays an important role in increasing two-phase heat transfer coefficient, thus the nucleate boiling mechanism becomes dominant in flow boiling. Shin et al. (1997) studied experimentally flow boiling heat transfer in a horizontal round tube with internal diameter of 7.7 mm (large tube) utilising pure refrigerants of R22, R32, R134a, R290 and R600a and refrigerant mixtures. Their experiments were

fulfilled under saturation temperature of 12 °C, mass flux range of 265 – 742 kg/m^{2}s and heat flux rang of 10 – 30 kW/m^2. It was noticed that for the R22, the heat transfer coefficient exhibits a significant dependence on the heat flux in the region with low vapour quality and this dependence disappears as vapour quality increases. Namely, the nucleate boiling dominated at low vapour quality location, in particular for high heat flux. When the vapour quality incremented due to the reduced liquid film thickness. The vapour phase velocity increased and thus, the convection mechanism became prevailing. Huo et al. (2004) investigated experimentally flow boiling heat transfer of R134a in vertical macro/mini tubes. The test sections were made from stainless steel tubes of 4.26 and 2.01 mm internal diameter. The experimental parameters included 13 – 150 kW/m^2 heat flux, 100 – 500 kg/m^{2}s mass flux, 800 – 1200 kPa pressure and quality up to 0.9. The experimental results revealed that the effect of heat flux on heat transfer coefficient is significant clearly within a region of vapour quality less than 0.5 and 0.3 for the 4.26 mm and 2.01 mm tubes, respectively. Afterwards, the trend of heat transfer coefficient was declined sharply with increasing vapour quality over values mentioned above (0.5 and 0.3 for the 4.26 mm and 2.01 mm tubes, respectively) due to dryout. They clarified an increase in the effect of heat flux in low and intermediate vapour quality region to be due to the predominance of nucleate boiling. They thought that the nucleation mechanism may be suppressed due to the increase of the bubble generation frequency giving rise to the more bubbles that occupy the inner tube wall particularly, in churn and annular flow regimes. Choi et al. (2009) researched the characteristics of two-phase heat transfer for flow boiling of R290 (propane) inside two different horizontal tubes of 1.5 and 3.0 mm inner diameter. The experiments were conducted for a heat flux range of 5 – 20 kW/m^2, mass flux range of 50 – 400 kg/m^{2}s and vapour quality reached 1 at saturation temperatures of 0, 5 and 10 °C. Thus, it was found that the large effect of heat flux on flow boiling heat transfer coefficients in the low and middle vapour quality region. This referred to the contribution of the nucleate boiling domination. Furthermore, the contribution of convective boiling at the higher vapour quality region inferred suppression of nucleate boiling with a minimal impact of heat flux on heat transfer coefficient. Ong and Thome (2011b) performed flow boiling tests for R134a, R236fa and R245fa flowing in horizontal tubes with diameter range of 1.03 – 3.04 mm in order to study the effect of Confinement number on flow boiling heat transfer. They stated that the influence of heat flux on the heat transfer coefficient is gradually diminished, while

the spanning prevalence of convective evaporation increases with reducing the tube diameter (i.e. increasing Confinement number). Further, these findings were classified with respect to the effect of fluid surface tension on Confinement number. This means that a higher surface tension shows a higher Confinement number. Maqbool et al. (2012a) carried out practically an investigation on the flow boiling heat transfer of R717 in vertical mini-tubes. The test parameters included the two mini tubes of 1.224 and 1.7 mm inner diameter, the 100 – 500 kg/m^{2}s mass flux, the 15 – 355 kW/m^2 heat flux and the 23, 33 and 43°C saturation temperature. They noticed that the heat flux affected strongly the local heat transfer coefficient for the 1.7 mm tube in all values of vapour quality. Conversely, the effect of vapour quality on the heat transfer coefficient was insignificant. For the 1.7 mm tube, the influences of heat flux and quality was ascribed to the dominant nucleate boiling mechanism with a lesser convection effect. They quoted this clarification from the suggestion of Thome et al. (2004). Thome et al. (2004) reported that the main factors that enhanced the heat transfer coefficient were nucleation and liquid film evaporation. For the 1.22 mm tube, the trends of heat transfer coefficient increased with increasing heat flux at low quality region and they then increased with increasing local vapour quality. The authors considered the predominance of nucleate boiling in low quality and the major prevalence of convective boiling from middle until higher vapour quality.

In a follow-up research, Copetti et al. (2013) introduced an experimental study of flow boiling for R600a during a horizontal tube with inner diameter tube of 2.6 mm at saturation temperature of 22 °C. The mass flux was varied from 240 to 440 kg/m^{2}s with the range of heat flux between 44 and 95 kW/m^2. The test results exhibited that the heat flux has a significant influence on the heat transfer coefficient at low vapour quality conditions. When the vapour quality and mass flux become higher, the effect of heat flux vanishes. They relied on the hypothesis of Jacobi and Thome (2002) to illustrate their experimental results. The influence of heat flux on the heat transfer coefficient can only be related to mechanism of nucleate boiling at bubbly flow pattern with very low vapour quality. For the slug flow pattern, the influence of heat flux on the heat transfer coefficient arises from the thin-film evaporation process around elongated bubbles with lacking nucleation sites. The flow boiling experiments for R1234yf and R134a was followed out by Choi et al. (2013) inside 1.5 and 3 mm tubes at saturation temperature of 5 – 15 °C

with heat flux ranging from 10 to 35 kW/m^2, mass flux ranging from 100 to 650 kg/m^{2}s and vapour quality up to 1. The authors drew a conclusion from their experimental results that the trends of the heat transfer coefficients depend significantly on heat flux in the low vapour quality region for both R1234yf and R134a. They illustrated that an increase in heat transfer coefficient at low quality with increasing heat flux was attributed to the dominance of nucleate boiling on evaporation inception. Afterwards, this dominance vanished with increasing vapour quality. De Oliveira et al. (2016) performed an experimental study for flow boiling of R600a in a 1 mm horizontal tube. The test conditions comprised of 5–60 kW/m^2 heat flux, 240–480 kg/m^{2}s mass flux, saturation temperature of 25 °C and vapour quality up to 0.92. They found that the heat transfer coefficient increases with increasing vapour quality. In addition, the heat flux has a strong effect on local heat transfer coefficient at the low vapour quality region for all mass fluxes. The authors observed the plug, slug and churn flow pattern in low quality region, which related to the predominance of nucleate boiling. Contrarily, in high vapour quality, the nucleate boiling suppressed and annular regime was apparent at which the convective boiling dominated. They clarified the occurrence of this phenomenon due to the increased velocities of two-phase flow and participation of flow patterns pertaining to convective boiling. Longo et al. (2016a) carried out experimental study to investigate the effect of heat flux on R32 and R410a heat transfer coefficients inside 4 mm tube. They observed that the heat transfer coefficients for both refrigerants are significantly dependent on the heat flux. They concluded that the R32 and R410a flow boiling are dominated by the nucleate boiling mechanism. The effect of heat flux on heat transfer coefficient was noticed by Xu et al. (2016b) with range of heat flux from 18 to 35.5 kW/m^2. They found that the dependence of heat transfer coefficient on mass flux clearly appears in 2.168 and 4.065 mm tubes, while it declined with increasing heat flux in the 1.002 mm tube. The flow boiling and heat transfer mechanism of R245fa in a 3 mm stainless-steel tube were experimentally studied by Abadi et al. (2016). They inferred that the heat transfer coefficient increases with heat flux in the intermittent flow and especially for lower qualities. The effect of heat flux becomes minor in higher vapour qualities and annular flow. The authors thought that the nucleate boiling and convective boiling contribute in flow boiling heat transfer process. Kanizawa et al. (2016) performed an investigation to study the characteristics of flow boiling of R245fa, R600a and R134a refrigerants in small diameter tubes. The test data were obtained under 21.5 – 58.3 °C saturation temperature,

5–185 kW/m^2 heat flux and 49 – 2200 kg/m^{2}s mass flux. The effect of heat flux on the heat transfer coefficient of R134a was significant. For R600a, the heat transfer coefficient increased with heat flux at low to moderate quality region. In the case of R245fa, the heat transfer coefficient depended only on heat flux in the lower vapour quality. Figure 2.20 displays the dependence of heat transfer coefficient on heat flux in the lower vapour quality region only and then the trends merge on one line and linearly increasing with vapour quality. They attributed this behaviour to the predominance of nucleate boiling mechanism at low vapour quality region and afterward the nucleate boiling was suppressed with the increasing vapour quality due to the convective boiling heat transfer contribution. Sempértegui-Tapia and Ribatski (2017a) carried out flow boiling experiments for R1234ze(E) and R600a in horizontal tube with 1.1 mm inner diameter. The experimental condition covered saturation temperature of 31 and 41 °C, 200 – 800 kg/m^{2}s range of mass flux, 15 – 145 kW/m^2 heat flux, and 0.05 – 0.95 vapour quality. They found that the local heat transfer coefficient increases as the heat flux increases in the region of low and intermediary local vapour quality. However, the heat flux did not have any influence on heat transfer coefficient in the high vapour quality region. They reported that these conditions correspond to the dominant nucleate boiling mechanism at

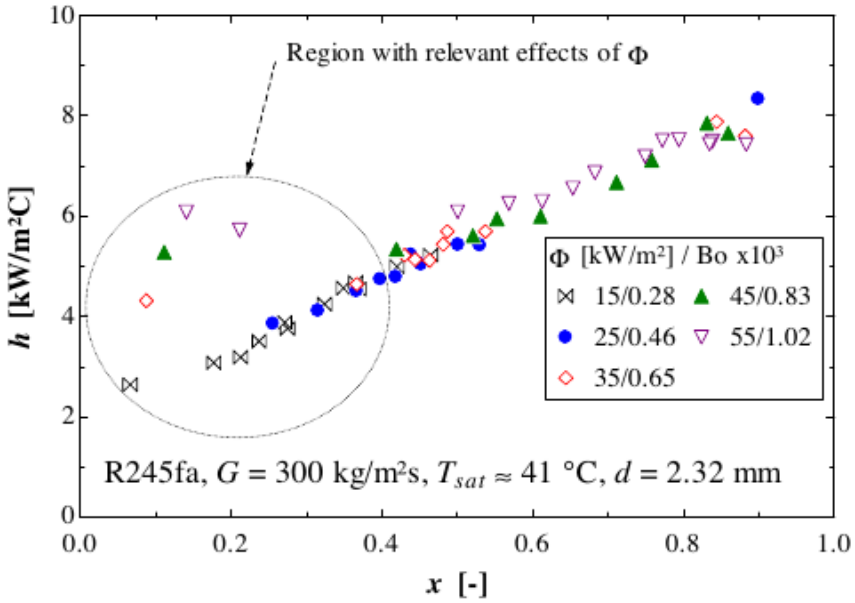

Figure 2.20 The effect of heat flux on flow boiling heat transfer coefficient, (Kanizawa et al., 2016)

low quality with high heat flux, while the nucleate boiling is suppressed at high quality with increasing the velocity of two-phase flow. This in turn enhanced the

convective influence. They mentioned that this behaviour results from the appearance of bubble nucleation in elongated bubbles and annular flow patterns.

It can be concluded from this review that there were some controversial points in the effect of heat flux on two-phase heat transfer coefficient and flow boiling process corroborated by the observations of flow patterns. That is, the heat flux has a strong effect on heat transfer coefficient in the low quality region, where bubble nucleation dominates. This behaviour may continue with increasing vapour quality if the bubble nucleation occurs under conditions of slug, churn and annular flow. The dominance of surface tension in small size tubes supports the dominance of nucleate boiling in flow boiling process. If this does not happen, the convective boiling becomes dominant, i.e. the mass flux and vapour quality have a strong effect on heat transfer coefficient. In this work, the changes of heat flux for vertical tubes and their effects on flow boiling heat transfer rate were experimentally researched with the range of 3 – 188 kW/m^2. The main aim of the present work is to understand the flow boiling mechanisms in small to microscale tubes through the effects of heat flux on local heat transfer coefficient (representing the contribution of nucleate boiling).

2.11 Two-phase heat transfer correlations

For flow boiling in tubular channels, the correlations of heat transfer coefficient can be classified according to the study of Webb and Gupte (1992) into three different groups: enhancement, superposition, and asymptotic models. The enhancement models assessed the two-phase heat transfer coefficient (α_{tp}) by enhancing single-phase heat transfer coefficient (α_{sp}) as $\alpha_{tp} = E\ \alpha_{sp}$ where E is enhancement factor. The single-phase heat transfer coefficient (α_{sp}) was commonly determined by the Dittus and Boelter (1930) correlation. This model was firstly proposed by Shah (1982) for flow boiling in conventional vertical tubes. The superposition models simulated the two-phase heat transfer coefficient with the contribution of a nucleate boiling component (α_{nb}) and a convective boiling component (α_{cb}). These models expressed as $\alpha_{tp} = \alpha_{nb} + \alpha_{cb}$. Chen (1966) used this model to develop his well-known correlation for flow boiling in conventional vertical tubes. The asymptotic models were essentially identical with the

superposition models but by adding a power function as $\alpha_{tp}^{n} = \alpha_{nb}^{n} + \alpha_{cb}^{n}$ where $n > 1$. This model was first suggested by Kutateladze (1961) for flow in plain tubes and with using exponent $n = 2$. Several investigations in the literature were experimentally conducted to study flow boiling characteristics in conventional channels. Also, there are numerous studies which have proposed empirical correlations to predict flow boiling heat transfer coefficient for vertical and horizontal channels so far, although most of them focus on the effect of channel size with different working fluids such as water and refrigerants. Moreover, they rarely give precise predictions of the heat transfer coefficients in small scale channels. These studies can be divided according to the criterion of Kandlikar (2002) into two groups, namely macroscale and microscale channels.

Several studies available in the literature over the past decades have provided significant knowledge for two-phase heat transfer in regard to the flow in conventional channels. These studies are primarily the starting point for the transition to small channels. An early study of flow boiling in the conventional vertical channel was conducted by Chen (1966). He developed the first correlation on the basis of the superposition model. He suggested the use of the Forster and Zuber (1955) and Dittus and Boelter (1930) correlations to predict nucleate and convective boiling component, respectively. Chen (1966) correlated the enhancement factor (*E*) as a function of the reciprocal of the Lockhart-Martinelli parameter (X_{tt}), which was proposed by Lockhart and Martinelli (1949) for turbulent-turbulent mixture flow. Moreover, he hypothesized that the nucleate boiling mechanism is suppressed by the liquid phase velocity. Therefore, the author proposed the suppression factor (*S*) which accounted for this phenomenon. He correlated the suppression factor (*S*) as a function of the two-phase Reynolds number ($Re_{tp} = E^{1.25}\, Re_{l}$) by using curve fitting method of least squares. He used an iterative solution to obtain the *S* and *E* factors from the empirical data. This model was later become outdated by more recent pool boiling correlations such as Cooper (1984) correlation. Shah (1982) proposed the enhancement model, as mentioned above, based on 780 data points covering eight fluids (water, cyclohexane, and refrigerants) in vertical and horizontal tubes and annuli. Further, he presented the enhancement factor (*E*) which was as a function of the Convection number (*Cov*) and the Boiling number (*Bo*) in order to enhance the single-phase heat transfer coefficient for the liquid phase flowing alone. To distinguish the tube

orientation, he employed the Froude number (*Fr*) which accounted for the dry part of the tube circumference (partial wall wetting) which may appear in horizontal channels. Thus, when $Fr < 0.04$, the correlation was applied only to horizontal tubes. Kandlikar and Thakur (1982) developed an enhancement factor for the Shah (1982) correlation to combine the contributions of nucleate boiling and convective boiling mechanisms for the entire range of flow boiling. They selected the Dittus and Boelter (1930) equation for liquid flow alone. The predictions of their correlation covered 510 data points for water, cyclohexane, R11 and R113 flowing vertical and horizontal tubes with a diameter range of 11.93 – 18.26 mm. They also used the Boiling number, Convection number and Froude number to predict the two-phase heat transfer coefficient. Gungor and Winterton (1986) improved the *S* and *E* factors in Chen (1966) correlation to predict heat transfer coefficient for flow boiling in vertical and horizontal flow in tubes and annuli. They collected an empirical databank from the literature including 4300 data point for ethylene glycol, water and refrigerants flowing in tubes with a diameter range of 2.95 – 32 mm. Further, they suggested the use of the Cooper (1984) equation instead of the Forster and Zuber (1955) equation to evaluate nucleate boiling term. They added the Boiling number with the Lockhart-Martinelli parameter (X_{tt}) in the *E* factor. For horizontal tubes, they also used the Froude number, i.e. if *Fr* is less than 0.05, the *S* and *E* factors must be multiplied by $\sqrt{Fr}$ and $Fr^{(0.1-2Fr)}$, respectively. Kandlikar (1990) extended the Shah (1982) correlation to include the effect of fluid by using fluid dependent parameter (F_{fl}) which he incorporated with the nucleate boiling term. He suggested the use of an additive correlation with contributions of nucleate boiling and convective boiling and then selected the large value accounting for heat transfer coefficient. The correlation was modified on the basis saturation flow boiling heat transfer for different fluid flowing in vertical and horizontal tubes. The author employed the Boiling number, Convection number and Froude number in the modification. The used database consisted of 5264 data points covering inner diameter range from 4.6 to 32 mm, water, and refrigerants.

The evolution of the small-scale cooling systems has led to increased demand for the development of correlations which predict the heat transfer coefficient for saturated flow boiling in small channels. This resulted in the emergence of several studies in the literature which added significant knowledge for heat transfer during the flow boiling in small-diameter tubes. Among these studies, Lazarek and Black (1982) conducted an

experimental test to measure the heat transfer coefficient of saturated boiling of R113 flowing in a vertical tube of 3.17 mm inner diameter. They deduced that the heat transfer coefficient depends strongly on heat flux leading to the dominant nucleate boiling mechanism in all tests. They suggested a simple correlation for local saturated boiling heat transfer coefficients based on 728 experimental data points, where the Nusselt number is a function of the liquid Reynolds number and the Boiling number. Kew and Cornwell (1997) performed an experimental study to develop a correlation based on measurements of saturated boiling heat transfer of R141b flowing in tubes with a diameter range of 1.39 – 3.69 mm. They found the contribution of nucleate boiling at low vapour quality region and convective boiling in the high vapour quality region. This was based on the dependence of heat transfer coefficient on heat flux in the low quality region, while its dependence on vapour quality and its independence from heat flux were in the high quality region. Therefore, they decided to modify the Lazarek and Black (1982) correlation, at which Nusselt number became a function of liquid Reynolds number, Boiling number and vapour quality. Bertsch et al. (2009) presented a composite heat transfer correlation for saturated flow boiling including the effect of channel size. This correlation was modified according to Chen (1966) model by applying a superposition of nucleate boiling and convection contributions. Further, the enhancement factor (E) considered the effect of bubble confinement in small channels, while the suppression factor (S) appeared to be independent of the channel size. The correlation was developed based on a database of 3899 data points from 14 studies in the literature involving 12 different wetting and non-wetting fluids, vertical and horizontal channels with hydraulic diameters ranging from 0.16 to 2.92 mm. Li and Wu (2010b) proposed heat transfer correlation for flow boiling in mini and micro channels. The correlation developed from 769 experimental databanks covering 12 fluid types and tubes with diameters ranging from 0.148 to 3.25 mm. The authors depended on the Lazarek and Black (1982) model to propose their correlation which embodied in Nusselt number as a function of liquid Reynolds number, Boiling number and Bond number. It considered the effect of channel size through the Reynolds number accounting for inertia and viscous forces and Bond number accounting for gravitational force and surface tension. Mahmoud and Karayiannis (2012) proposed boiling heat transfer correlation depending on the improvement of the Lazarek-Black model. The correlation was represented by Nusselt number as a function of the Boiling number, liquid Weber number, liquid Reynolds

number and Confinement number in addition to conjunct constant and function exponents. It took into account the influence of channel size within the Confinement number accounting for confined bubble size and channel size. The model was formed by using a non-linear least square fitting method to fit a multi-parameter with databank consisting of 5152 experimental data of R134a flowing in vertical tubes with inner diameter ranging from 1.1 to 4.26 mm. Mahmoud and Karayiannis (2013) introduced another correlation for boiling heat transfer on the basis of the superposition model of Chen (1966) and aforementioned databank. They used the Cooper (1984) equation rather than the Forster and Zuber (1955) equation. They correlated the enhancement factor (*E*) as a function of the Lockhart-Martinelli parameter and the Confinement number by the approach of linear least square fitting with experimental data for R134a. Additionally, the values of this enhancement factor turned out to be larger than the original enhancement factor of Chen (1966). It considered the effect of bubble confinement in small channels with the Confinement number. The suppression factor (*S*) was adapted from the Chen (1966) model as a function of the two-phase Reynolds number ($Re_{tp} = F^{1.25}\, Re_l$) by using linear curve fitting method of least squares. Its value decreased gradually with the two-phase Reynolds number giving rise to larger value.

Recently, Fang et al. (2015) proposed specific expression of the heat transfer correlation for saturated flow boiling of water in micro and mini-channels. Further, they compiled 1055 experimental data points from nine independent studies in the open literature. The correlation was developed based on collecting dimensionless parameters from the fifteen correlations that have better performances. The selected dimensionless parameters were Nusselt number, liquid Reynolds number, Boiling number, Convection number, and liquid Prandtl number. They also defined a new dimensionless number, $Fa = (\rho_l - \rho_v)\sigma/G^2 D$, Fang number ($Fa$) which was associated with the formation and departure of bubbles. Moreover, they presented two factors (*S* and *E*), where *S* factor included the Boiling number, liquid-vapour density ratio and molecular weight and the *E* factor included the vapour quality and the liquid-vapour density ratio. The correlation was a Nusselt number as a function of the additive model of two factors (*S* and *E*), liquid Reynolds number, Fang number, and liquid Prandtl number as well as the ratio of the liquid viscosity at the fluid temperature ($\mu_{l,l}$) to the inside wall temperature ($\mu_{l,w}$). Furthermore, this correlation also works well for R22, R134a, R410A and R717. Turgut

et al. (2016) developed an asymptotic model (with n = 2) of the correlation for saturated boiling heat transfer coefficient in micro- and macro-tubes based on the consolidated database consisting of 3594 data points of R134a compiled from 19 sources. Ranges of the database cover hydraulic diameter between 0.5 and 13.84 mm and saturation temperatures between −8.8 and 52.4 °C. They took into account the effects of channels and surface roughness of the channel wall. Further, they suggested the use of the fluid-specific reduced pressure correlation proposed by Gorenflo (1993) and Dittus and Boelter (1930) correlations to predict nucleate boiling and convective mechanisms, respectively. They correlated the enhancement factor as a function of the reciprocal of the Lockhart-Martinelli parameter which was proposed by Lockhart and Martinelli (1949) for turbulent-turbulent mixture flow. Also, they correlated the suppression factor as a function of the vapour quality and the reduced pressure. Experimental results for the heat transfer coefficient during flow boiling of R134a, R245fa and R600a in small diameter tubes with the addition of a boiling heat transfer correlation were presented by Kanizawa et al. (2016). The experimental database involved 2047 data points covering tube diameter range of 0.38 – 2.6 mm. The authors developed a superposition model, similar to Saitoh et al. (2007) with contributions of nucleate boiling and convective boiling. The nucleate boiling effects were estimated by the correlation of Stephan and Abdelsalam (1980) for pool boiling of organic refrigerants, while the convective effects were estimated by the correlation of Dittus and Boelter (1930) by assuming only the liquid phase flowing in the tube. Further, the enhancement factor was a function of the multiplicative constant, the reciprocal of the Lockhart-Martinelli parameter, and the Weber number based on the gas in situ velocity, while the suppression factor appeared to be dependent on the Bond number and two-phase modified Reynolds number. The enhancement factor took into account the cross-sectional velocities distribution of both phases. The suppression factor accounted for capturing effects of confined bubble growth on the suppression of nucleate boiling. Fang et al. (2017) extended Fang et al. (2015) correlation to involve other fluids by evaluating the fluid dependent parameter (F_{fl}) for that fluid from the experimental data. The new correlation was developed based on the first database consisting of 17778 experimental data points from 101 sources and 13 different fluids. Also, it was validated with the second database containing 6664 experimental data points from 60 sources and 18 different fluids. The validation results showed that the new correlation has a mean absolute deviation (MAD) of 4.4% against the second database. The correlation gave the

Nusselt number as a function of the fluid dependent parameter (F_{fl}), molecular weight, Boiling number, liquid only Froude number, Bond number, liquid-vapour density ratio, and reduced pressure as well as the ratio of the liquid viscosity at the fluid temperature ($\mu_{l,l}$) to the inside wall temperature ($\mu_{l,w}$). Shah (2017) also extended the author's old correlation to indicate the boundary between conventional and mini/micro channels for boiling inside channels as a function of vapour Weber number and Boiling number. Therefore, the author suggested the E factor, $E = 2.1 - 0.008We_v - 110Bo$, to multiply by his old correlation and if the E factor is less than 1, use $F = 1$. The new correlation developed was based on 4852 experimental data points from 81 independent sources in the literature including the diameter ranging from 0.38 to 27.1 mm and 30 different fluids.

From the above review, it seems that much effort has been made to develop a simple, general correlation for determining the heat transfer coefficient during flow boiling inside mini and micro channels. Most of the studies have to do with the development of saturated boiling heat transfer correlation can be divided into three groups: a) enhancement models such as Shah (1982), Kandlikar and Thakur (1982), and Kandlikar (1990), b) superposition models such as Chen (1966), Gungor and Winterton (1986), Bertsch et al. (2009), Mahmoud and Karayiannis (2013), and Kanizawa et al. (2016), and c) asymptotic models such as Kutateladze (1961), and Turgut et al. (2016). According to existing correlations, the investigators focused directly on correlating the dimensionless numbers based on their experimental data to represent the contributions of nucleate boiling and convective mechanisms in flow boiling heat transfer. These dimensionless numbers included influential parameters accounting for the effects of confined bubbles, channel size, surface tension, viscosity, and surface roughness of channel wall. Nevertheless, the researchers have proposed various approaches with various levels of complexity to predict the heat transfer coefficient in a small channel, the influences of some parameters (such as fluid properties, channel geometry, and surface roughness on channel walls) are still unclear. Thus, the effects of these parameters on the flow boiling mechanisms and heat transfer coefficient of two-phase flow in mini and microtubes should be extensively investigated. This work considered as an attempting to develop correlation for local heat transfer coefficient in vertical small tubes and also to provide a guide for selecting an apposite correlation which has the best accuracy of prediction for R245fa.

Chapter 3

Experimental Test Facility and Methodology

3.1 Introduction

The experimental facility described in this chapter, includes the conceptualisation, construction, related instrumentation, modifications and commissioning of the experimental setup utilized during the present work. This project is past of a long-term project in Brunel's heat transfer research group that aims to investigate flow boiling heat transfer of different fluids (R134a and R245fa) in vertical small-diameter tubes. This experimental test facility was originally designed and constructed by Huo (2005) and was used by Chen (2006) for studying the flow boiling characteristics of R134a in small-diameter tubes. It was subsequently developed by Shiferaw (2008), Mahmoud (2011) and Pike-Wilson (2014) for their experimental research. For this current study, the flow visualisations, flow boiling heat transfer coefficient valuations, and two-phase flow pressure drop assessments have been carried out on the same experimental rig. In parallel, the two-phase flow regimes were characterized. The initial stage of the present study aims at acquiring adequate and precise experimental data of flow boiling in different diameter tubes. The data reduction procedure for parameters of interest is also presented in this chapter. Afterwards, the method adopted for assessment of uncertainty in the experimental data is elucidated, followed by the single-phase flow validation of the facility. Finally, the experimental procedure is described.

3.2 Experimental setup

3.2.1 Experimental test facility

The Experimental test facility used to perform the two-phase flow boiling study of fluid R245fa in small-diameter tubes is shown schematically in Figure 3.1. A photo of the facility is presented in Figure 3.2. The facility is comprised of a closed fluid R245fa flow

loop, an external cooling or heating system, and a data acquisition system. The main fluid R245fa flow loop consists of a controlled-temperature R245fa tank (for utilizing the collection of coolant), a circulating gear pump, a filter dryer, a sight glass, two Coriolis flow meters (for low and high mass flow rates), a sub-cooler, a preheater, a test section (consisting of a calming section, a heating section, and an observation section), a liquid separator and a condenser. The experimental facility is insulated to ensure relative stability during the experiments by reducing the loss of heat and insulating the system against external influences. Therefore, the main parts of the facility and all system pipes are wrapped with a layer of synthetic nitrile rubber insulation, with particular care given to all test sections. The experimental test facility was developed to control the fluid characteristics at the inlet of the test sections (i.e. saturation pressure, mass flow rate and inlet subcooling). Also, consideration was given in the design of the entire facility with regard to the required heat and mass flux values, and with the wide range of temperatures, from superheating to subcooling.

The controlled-temperature R245fa tank is a cylindrical shape, which comprises of a pressure gauge, a thermocouple, a safety valve, two floating ball sight glasses (to see the R245fa level), a cooling coil and a cartridge heater (3 kW). The tank contains the majority of the coolant in the main fluid R245fa flow loop. However, the state of the working fluid in this tank is maintained at two-phase conditions (liquid and vapour phase). The amount of vapour in the R245fa tank also helps to minimize the fluctuations in a pressure of the test system. The desired pressure in the whole system depends on the degree of saturated temperature for two-phase fluid in the tank, which is heated to regulate the pressure to the point of matching the required saturated temperature via setting the variac of the tank heater manually. The cartridge heater is positioned at a low level of the floating ball sight glass so as not to burn out the heater when the R254fa is at a low level in the tank. The cooling coil is placed in the centre of the tank above the cartridge heater. It is used with a low thermal load to ensure that the pressure of the test system is more stable as the larger condenser before the R245fa tank causes instability in the system pressure. Namely, the system pressure is controlled through controlling the temperature inside the tank by regulating the electric power of the heater and the flow rate of R22 in the cooling coil. Finally, the safety valve is used to reduce the excess pressure in the tank

and superheated conditions are tracked via the thermocouple, which is positioned at the top of the tank.

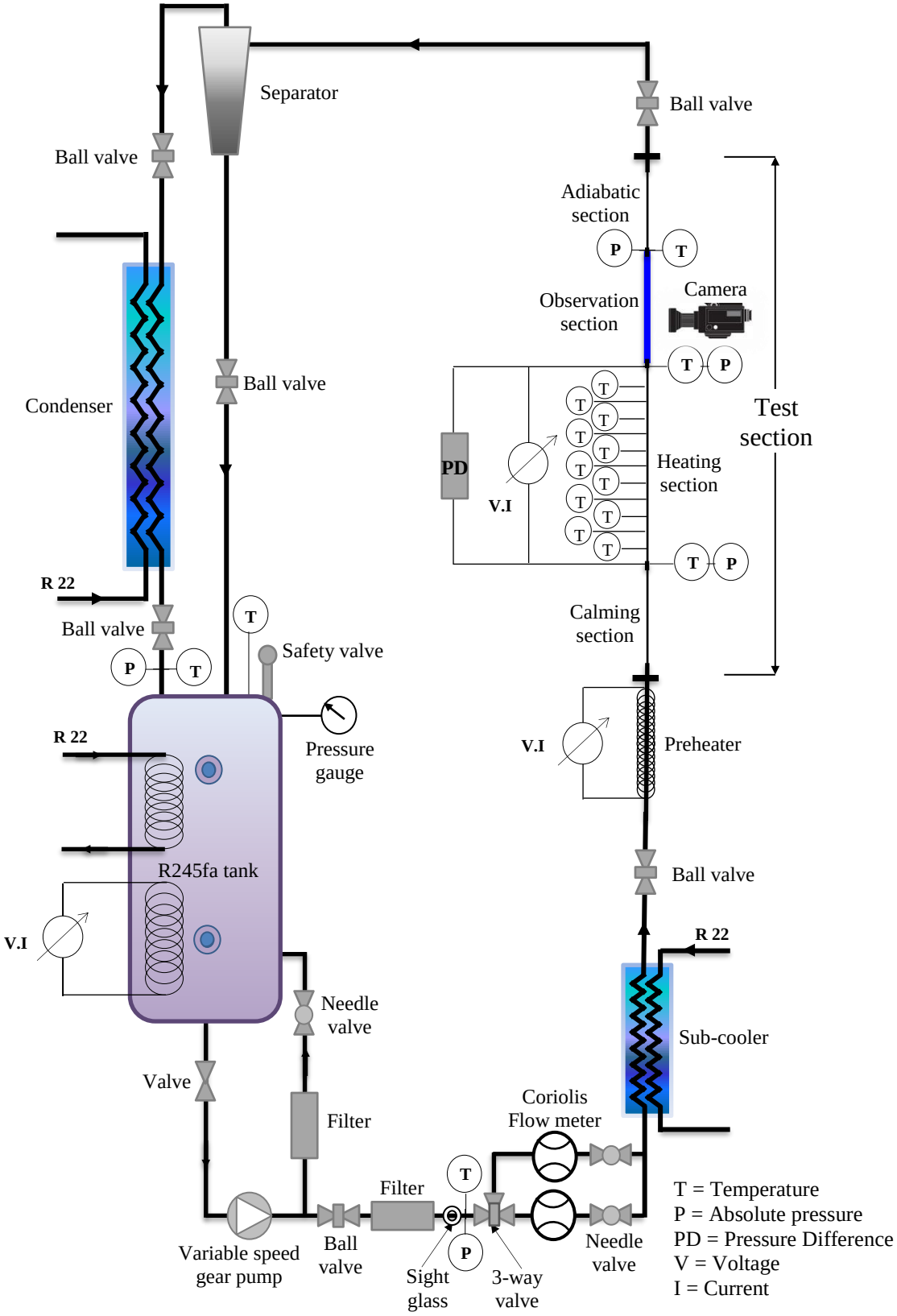

Figure 3.1 Schematic diagram of the R245fa test facility.

Figure 3.2 photograph of the R245fa test facility.

A gear pump (Tuthill 1010) is located after the tank to circulate the working fluid from the tank through a filter drier, a sight glass, two Coriolis mass flow meters, a needle valve and then pass through a sub-cooler, a preheater, a test section, a separator, a condenser and eventually the controlled-temperature R245fa tank. The mass flow rate of the system is adjusted by varying the speed of the gear pump. A bypass loop is also a part of the experimental facility with a needle valve, after the pump, to ease the pressure on the pump and to return excess fluid to the tank. The other objective of this bypass and valve is to combine with the two valves after the Coriolis mass flow meters in the main loop, to control the mass flow rates. The filter dryer removes moisture and solid particles from the working fluid. The sight glass is used to make sure that there are no bubbles in the liquid line before the flow meters. A pressure transducer and a thermocouple are connected to the main loop via compression fitting before the mass meters. They are used to measure the extent of subcooling from the saturated condition of the working fluid in the tank. The fluid flow must be maintained in a single-phase condition which it passes through the mass meters to attain higher accuracy for measurements. The two Coriolis flow meters, CMF010M and CMF025M are used to measure the high or low mass flow

rates of R245fa liquid, respectively. The two precision metering valves are situated after the flow meters. One is used to control a high range of flow rate and the other for a low range. Afterwards, a continuous stream of R245fa liquid flows to a sub-cooler, which is designed as a tube-in-tube heat exchanger. Thus, heat is removed from R245fa through the sub-cooler, which utilizes an R22 cooling system to attain the desired subcooling. The preheater which follows, is installed, as a rope heater (Omegalux FGR-080, 400 W) wrapped around a conductive stainless-steel tubing to apply heat to working fluid. In addition, the desired vapour quality and the subcooled temperature of R245fa prior to entering the test section are regulated using the preheater and adjusted by the variac. In other words, the degree of sub-cooling at the test section inlet (fluid temperature) is controlled by regulating the flow rate of R22 in the sub-cooler and the electric power to the preheater.

After the preheater, the fluid enters to the stainless-steel test sections oriented in a vertical direction during the flow boiling experiment. Thus, the experiments are executed under upward flow conditions (i.e. see Figure 3.1). The DC current is directly supplied to both ends of the heating section to ensure uniform heat flux conditions. Consequently, the R245fa fluid turns into two-phase flow due to heating and the vapour quality changes along the heating section. The variation of temperature and pressure can be measured via the thermocouples and the pressure transducers, respectively, which are set at both ends of the heating section, see Figure 3.1. At the end of the test section, the two-phase flow regime is visualised and recorded using a Phantom high-speed camera (Photo-Sonics, Model Phantom V4 B/W, 1000 frames/s and 512 × 512 pixels) through the borosilicate glass tube which is installed after the heating section.

Following the test section, the separator is used to separate the two-phase stream to vapour and pure liquid of R245fa and gravity plays an important role in the separation process. It is considered that the pressure drop in the condenser tubes is sequentially reduced by means of the separator. The R245fa vapour flows mostly to the condenser with the R245fa liquid settling in the bottom of the separator and then immediately returns to the R245fa tank. On the one hand, the condenser can be used to absorb heat from R245fa vapour via the R22 cooling system and the condensed vapour flows into the

R245fa tank. The pressure balance takes place between the condenser inlet and the R245fa tank through the 6 mm diameter bypass pipe in order to avoid and reduce pressure fluctuations in the condenser inlet. Thus, the pressure throughout the system can be more stable. On the other hand, the condenser has another function to control the system pressure by decreasing the pressure up to a desired saturated pressure value. Finally, most of working fluid returns to the R245fa tank. In the data acquisition system, the fluid temperature, pressure signals, mass flow rate and the test section wall temperatures were acquired by the IMP S13595 1C and IMP S13595 1E instruments allowing for multiple measurements of up to 40 channels. A LabVIEW program was used to simultaneously acquire and save the data. Besides, this LabVIEW program is employed to monitor and control the facility. The limitations of operating conditions for the experimental test facility are listed in Table 3.1.

Table 3.1 The limitations of the test facility conditions.

Parameter	Unit	Range
Mass flux	kg/m^2s	20 – 3000
Heat flux	kW/m^2	0.4 - 800
Pressure	kPa	100 – 1000
Saturation temperature	°C	-20 – 50
Diameter of test tube	mm	0.5 – 5
Subcooling	K	75
Vapour quality	–	0 – 1

3.2.2 Upgrading of the experimental test facility

In the existing experimental setup, the test facility was upgraded. The upgrade included the circulating gear pump, the absolute and differential pressure transducers and the data of fluid properties in LabVIEW software. The old gear pump was run on a high speed and generally led to high oscillations in the reading of Coriolis mass flow meters. This is attributed to the high flow rate of R245fa fluid before a needle valve causing a high pressure drop inside the system. In the current study, the old gear pump was replaced with the new gear pump (Tuthill 1010) and the speed regulator. Thus, the mass flow rate of the system is adjusted by varying the speed of the gear pump. In addition, the old pressure transducers connected to the inlet and outlet of test section had a range of 0 – 2000 kPa full scale. Since R245fa is a low-pressure refrigerant, the old pressure transducers were replaced with the pressure transducers having a range of 0 – 1000 kPa

full scale. This leads to a high accuracy in pressure reading. Also, the pressure drop between the inlet and outlet of the test section was measured by a differential pressure transducer with a range of 0 – 24.91 kPa full scale. It was replaced with a new differential pressure transducer having a range of 0 – 103.421 kPa full scale because the properties of R245fa yields high pressure drop in the flow path. Finally, the experimental recording system using LabVIEW software has been updated with the data of fluid properties for R245fa as the working fluid and parameters for each test section.

3.2.3 External cooling system

The R22 cooling system is utilized to regulate the system pressure and the subcooled temperature of R245fa prior to entering the test section, within the main fluid R245fa test flow loop. This cooling system contains a condenser unit and an evaporation unit. The condenser unit consists of a compressor (BITZER), an oil separator, an air-cooled condenser, an R22 liquid receiver, a filter dryer and a sight glass. The evaporation unit consists of an R22 tank, a gear pump, an R22 small cooling coil which is inside the R245fa tank, an R245fa sub-cooler, and an R245fa condenser. The air-cooled condenser was set up outside the lab, while others were set up next to the R245fa experimental test facility inside the lab. Figure 3.3 and Figure 3.4 show respectively a schematic diagram and photo of the R22 cooling system.

The R22 liquid is driven by a gear pump from the R22 tank into the R245fa condenser, R245fa sub-cooler and the R22 small cooling coil inside the R245fa tank to supply the R245fa test system with the needed cooling capacity. The stream of cold R22 fluid directed into the R245fa test system is regulated by needle valves and a by-pass line. Afterwards, the R22 flow returns to the R22 tank in two-phase flow (vapour and liquid phase). The liquid remains in an R22 tank, while the vapour is absorbed by the compressor and it compresses as high-pressure hot vapour into the oil separator. Most of the recovered oil comes back to the compressor, while R22 hot vapour flows to an air-cooled condenser which has six fans. The condensation capacity of the air-cooled condenser can be adjusted by controlling the fans individually. The R22 liquid flows to the R22 liquid receiver and then passes through a filter dryer, a sight glass, a solenoid valve and a thermostatic liquid level controller. Eventually, it returns back to the R22 tank.

The thermostatic liquid level controller is utilized to reduce the pressure in the R22 tank by decreasing the R22 liquid temperature to around - 40 °C and it is also utilized to regulate the level of R22 liquid inside the R22 tank. The bulb is set up at the desired position within the R22 tank. When the liquid level drops below this position, the temperature of the gas inside the bulb rises. This rise in temperature makes the gas expand inside the bulb. Thus, the gas expansion assists in the opening valve and allows the R22 liquid to flow into the tank until it reaches the level of the bulb. Consequently, the temperature of bulb goes down leading to gas shrinkage within it and then the valve shuts off. The extra R22 liquid remains in the R22 liquid receiver for storage. On the other hand, there is a hot vapour bypass line which connects the compressor after the oil separator with the R22 tank. The hot vapour passes through a solenoid valve and a regulator and returns into the R22 tank. This bypass line supports the compressor running continuously irrespective of load changes. The regulator is set at a pressure of about 2 bar, whereas the temperature inside the tank is – 25 °C. The high pressure before the regulator and the decreased temperature inside the tank, below – 25 °C, make the valve to open. The hot vapour is enabled to flow into the R22 tank until the temperature inside the tank reaches roughly – 25 °C. The pressure regulator closes the hot gas valve.

Although much of the oil is removed from the R22 fluid by the oil separator, it still flows with the R22 fluid into the R22 tank and then settles at the bottom of the tank. The oil return system is subsequently employed to separate that oil and return it to the compressor. This is executed by using an oil tank which includes a cartridge heater. The heater evaporates the R22 fluid. The R22 vapour returns to the loop, while oil can be utilized to replenish the compressor as needed.

3.2.4 Test section

In the present study, five test sections with internal diameters of 1.1, 2.01, 2.88, and two tubes of 4.26 mm (uncoated and coated tubes) are tested for the investigation of flow boiling heat transfer, pressure drop, and flow patterns. The typical tube size used in the current experiments depends on commercially obtainable tube diameters and an initial valuation proposed by Kew and Cornwell (1997) using the Confinement number as follows:

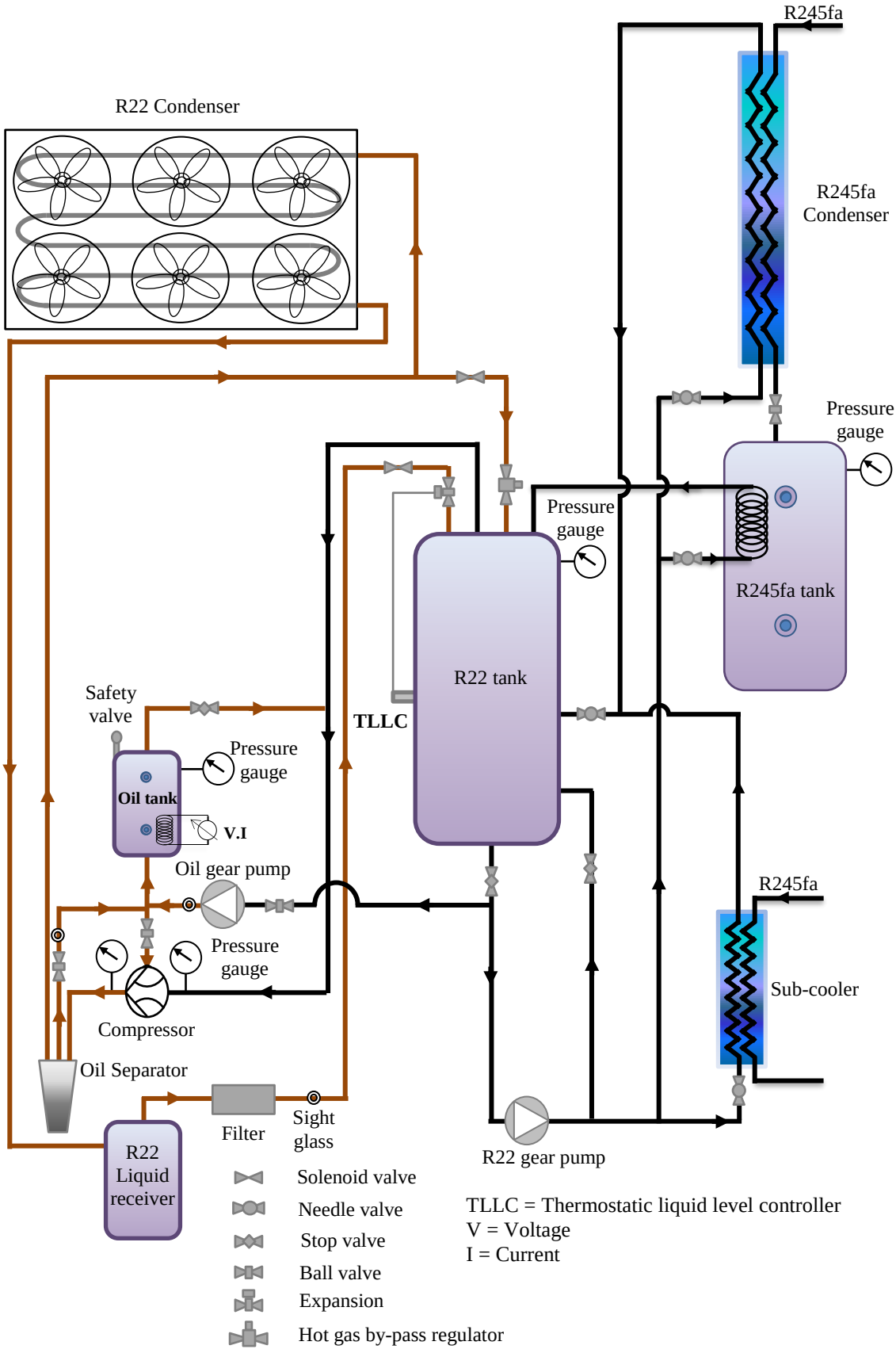

Figure 3.3 Schematic diagram of the external cooling system.

Figure 3.4 Photograph of the external cooling system.

$$Co = \frac{\sqrt{\sigma / g(\rho_l - \rho_v)}}{D_{inner}} \tag{3.1}$$

where the Confinement number (*Co*) is a function of hydraulic diameter and physical properties (surface tension, liquid density and vapour density). Since saturation pressure is an important parameter that affects physical properties, the Confinement number increases with decreasing saturation pressure, as shown in Figure 3.5. According to the figure, the threshold value for the transition from a small diameter to micro diameter is 0.5. Thus, the tube diameter of 4.26, 2.88, and 2.01 mm is considered a mini-channel

while the tube diameter of 1.1 mm represents a micro-channel. The test sections are manufactured from stainless steel cold drawn tubes. They include three sections namely; adiabatic calming section (hydrodynamic developing section), heating section and observation section as shown in Figure 3.6. All sections have the same inner diameter. Table 3.2 summarizes the details of the test sections. They are vertically connected with the main experimental facility by two flanges in order to remove and install easily. All parts of the test section, except the observation section, are insulated from its surroundings by wrapping them with two layers of alumina ceramic fibre and nitrile rubber insulation.

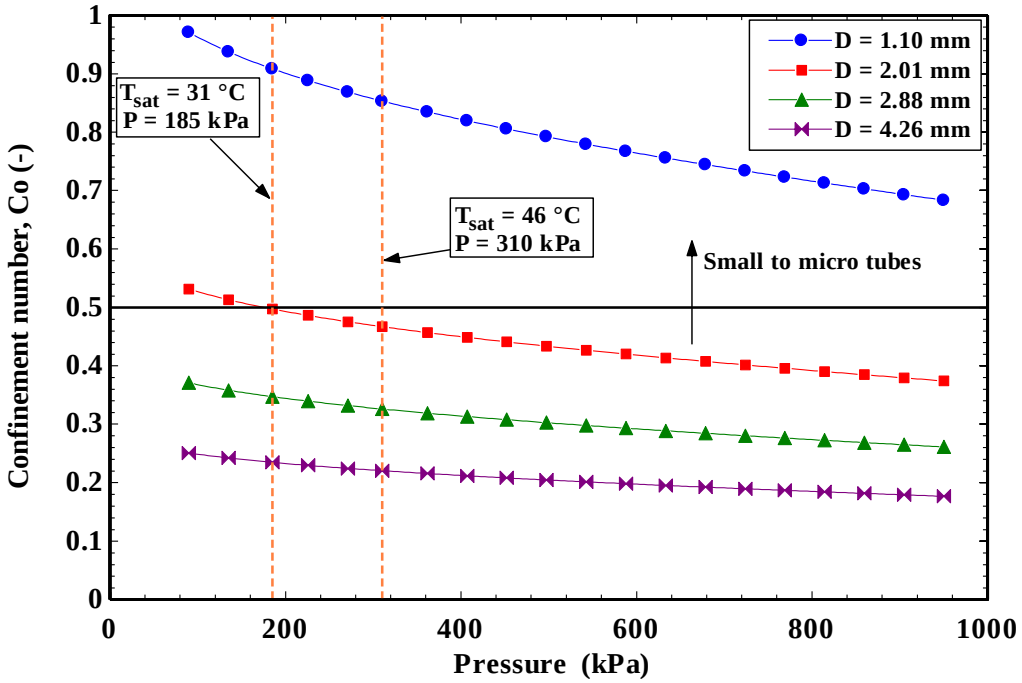

Figure 3.5 The effect pressure on Confinement number.

The adiabatic calming section is made of the same tube as the heating section. It is connected before the heating section inlet to provide a hydrodynamic developing length. The length of the calming section is based on the laminar and turbulent hydrodynamic developing length. The hydrodynamic entry length of laminar flow with Reynolds number less than 2300 can be obtained from the correlation of Langhaar (1942) which is cited in Bergman et al. (2011) as given in following:

$$\frac{L_{h,fd}}{D_{inner}} = 0.05Re \tag{3.2}$$

Whilst, the hydrodynamic entry length for turbulent flow can be approximately obtained from following expression (Kays and Crawford (1993), which is also cited in Bergman et al. (2011)):

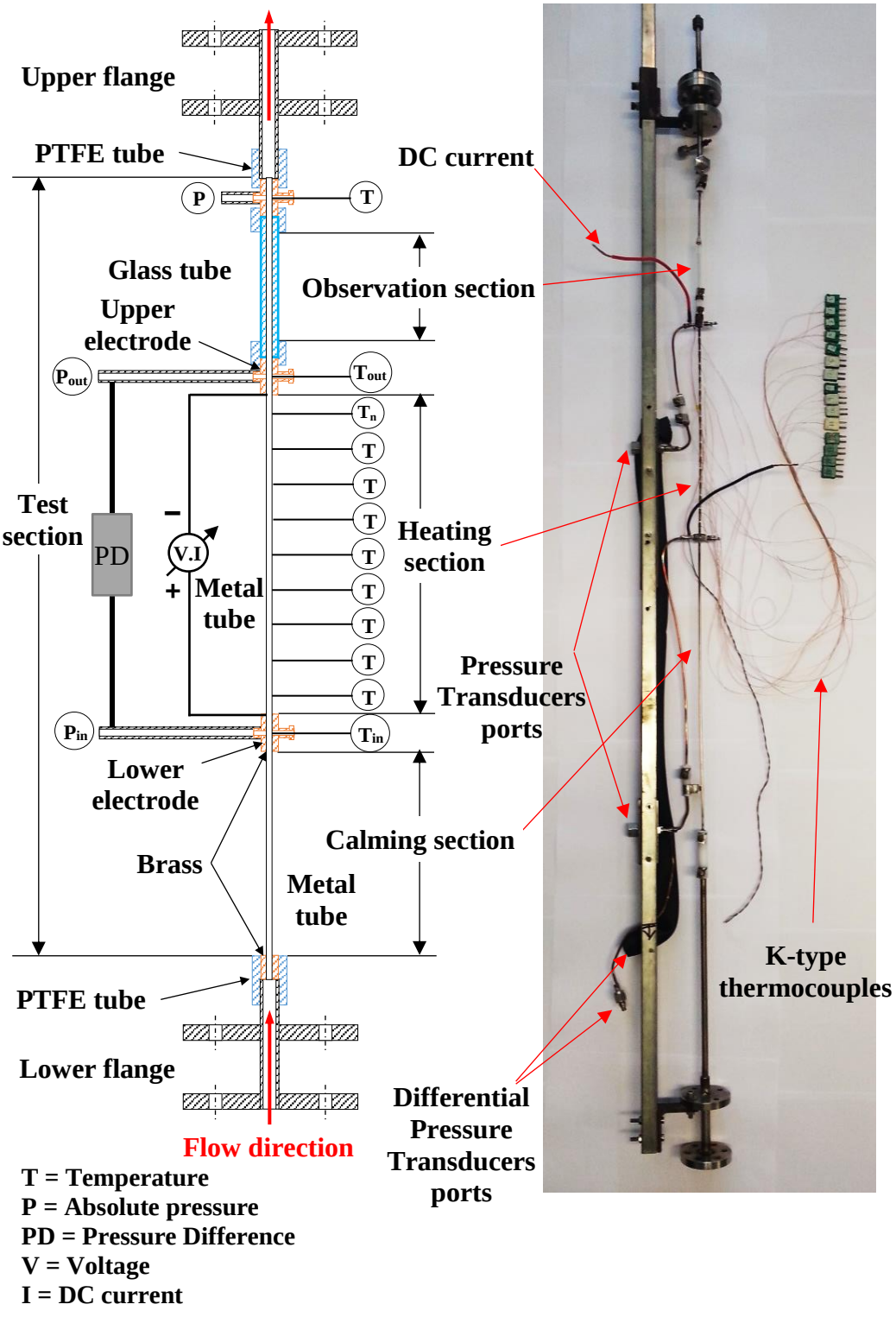

(a) (b)

Figure 3.6 Test section: (a) schematic view of the vertical tube, (b) photograph before thermal insulation.

$$10 \leq \frac{L_{h,fd}}{D_{inner}} \leq 60 \tag{3.3}$$

Therefore, the length has to be sufficiently long to ensure fully developed flow in the heating section entrance. The calming section typically requires a minimum length of 60 times the hydraulic diameter.

Table 3.2 The test sections investigated in the current study

Inner Diameter (mm)	1.1	2.01	2.88	4.26	4.26*
Wall thickness (mm)	0.225	0.19	0.13	0.245	0.245
Wall thickness of glass tube (mm)	3.325	2.695	2.46	2.57	2.57
Length of glass tube, (mm)	185	300	185	120	120
Heated length, (mm)	150	210	300	500	500
Pressure drop length, (mm)	170	218	310	515	515
Entry length, (mm)	110	121	173	256	256
Calming section length, (mm)	150	200	230	260	260

* represents coated tube.

Two-phase flow boiling with the desired vapour quality is generated in the heating section by supplying DC current through the tube wall (Joule's effect). The DC current is supplied by DELTA ELEKTRONIKA BV, Model SM30-300 power supply. This provides the tube wall with a uniform heat flux boundary condition. The realized heat fluxes are recalculated with DC current and voltage measurements by Yokogawa WT110 digital power meter. The brass electrode and the stainless-steel tube are welded by using soldering to ensure good contact. Also, the soft soldering method is utilized to weld the two electrodes from the DC power supply to the brass pieces at the inlet and outlet of the heating section. The test section is electrically insulated from the rest of the test facility using a small dielectric PTFE tubing which is installed at both inlet and outlet ends of the test-section tube. The external wall surface temperatures are measured using fifteen K-type thermocouples. These thermocouples are stuck on the external surface at fifteen axial positions along the heating section with uniform spacing, as demonstrated in Figure 3.6. They are affixed to external tube wall by means of a special thermally conductive and electrically insulating epoxy adhesive. Table 3.3 gives the details of thermocouple locations on the external tube wall surface. The first and last K-type thermocouples are affixed far from the brass electrodes at a sufficient distance to obviate any possible thermal conduction losses to the electrodes. Two T-type thermocouples (Omega) and two pressure transducers (Druck PDCR 910-0826) are fixed at the inlet and outlet of the

heating section to measure the fluid temperatures and pressures. A differential pressure transducer (Omega Model PX409-015DWUI) is installed between the inlet and outlet of the heating section to measure directly the pressure drop. As a consequence, the measurements of pressure drop and heat transfer coefficients could be obtained simultaneously.

Table 3.3 The details of the wall temperature thermocouples locations

Diameter of the test tubes (mm)	1.1	2.01	2.88	4.26	4.26*
Heated length (mm)	150	210	300	500	500
Number of thermocouples	15	15	15	15	15
Spacing between thermocouples (mm)	10	13	19	32	32
Spacing from the lower electrode (mm)	5	14	17	26	26
Spacing from the upper electrode (mm)	5	14	17	26	26

* represents coated tube.

The observation section is a transparent borosilicate glass tube with the same inner diameter as the stainless-steel tube of the heating section. It is connected directly after the heating section to allow flow visualisations. The dimensions of five glass observation sections are included in Table 3.2. As mentioned before, the visualisation of the flow patterns was recorded employing a digital high-speed camera (Photo-Sonics, Model Phantom V4 B/W, 1000 frames/s and 512 × 512 pixels). The recorded flow patterns are converted into pictures via the software for the camera. They are analysed to further explain the heat transfer results.

In this study, the surface roughness of the test sections is taken into account in order to study its influence on the characteristics of bubble nucleation in flow boiling heat transfer and pressure drop. As a result, the knowledge of the internal surface characteristics of the test tubes will help to explain the performance of flow boiling heat transfer in small-diameter tubes. The measurements of internal surface roughness are therefore conducted for all the five test sections. For the 2.88 mm to 1.1 mm tubes, a small sample is taken from the test section tube and is scanned using a Zygo NewView 5000 optical surface profiler to measure its internal surface roughness. However, the estimation technique of the internal surface roughness for coated and uncoated tubes of 4.26 mm is different from the rest of the tubes. It is performed at the Brunel University London

Experimental Techniques Centre (ETC). Veeco Dimension 3100 Atomic Force Microscope (AFM) is used to measure the surface roughness for both tubes. The values of key roughness parameters for the five tubes are summarized in Table 3.4. Also, the ISO standard definitions used in the description of the roughness parameters are displayed in the table to understand the measured values. A copper coating was used to enhance the coated tube surface. Oxford Nanosystems Ltd. used the OnS nanoFLUX® process to coat the tube surface with copper.

Table 3.4 Roughness characteristics of the heating surface.

Parameter	Description	Formula	Inner tube diameter (mm)				
			1.1	2.01	2.88	4.26	4.26*
R_a	Arithmetic average of absolute values	$R_a = \frac{1}{N}\sum_{i=1}^{N}\lvert X_i \rvert$	1.698	1.356	0.422	0.197	0.675
R_q	Root mean square (rms) values	$R_q = \sqrt{\frac{1}{N}\sum_{i=1}^{N} X_i^2}$	2.142	1.737	0.534	0.240	0.838
R_v	Maximum valley depth	$R_v = \min X_i$	6.913	5.34	2.04	0.528	1.523
R_p	Maximum peak height	$R_p = \max X_i$	11.13	7.903	2.515	0.803	1.988

The unit of roughness values is (μm), * represents coated tube.

The Scanning Electron Microscope (SEM) analysis was also conducted for a sample of the coated and uncoated tubes. The grinding method is carefully used to cut each tube sample into two halves without touching their internal surface. The SEM analysis results of coated and uncoated tubes are presented in Figure 3.7. It is seen in Figure 3.7c that the uncoated tube has a very smooth surface with the appearance of random scratches with some cavities. Figure 3.7d shows that the internal surface characteristics of the coated tube are entirely different from those of the uncoated tube. There are more of fissures and pits in the internal surface of the coated tube. They could play an influential role in nucleation characteristics compared to the uncoated tube.

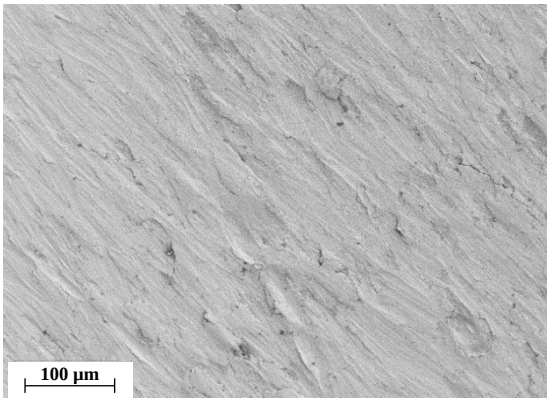

(a) Uncoated tube with length 100 µm.

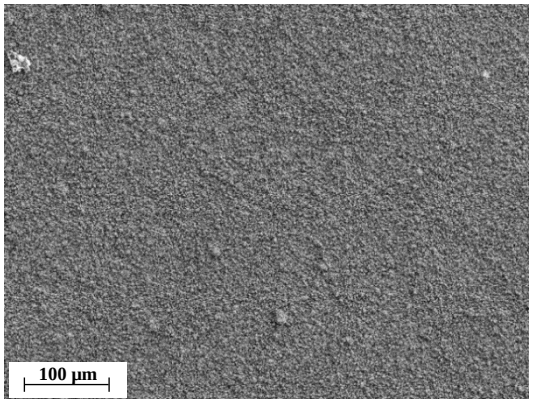

(b) Coated tube with length 100 µm.

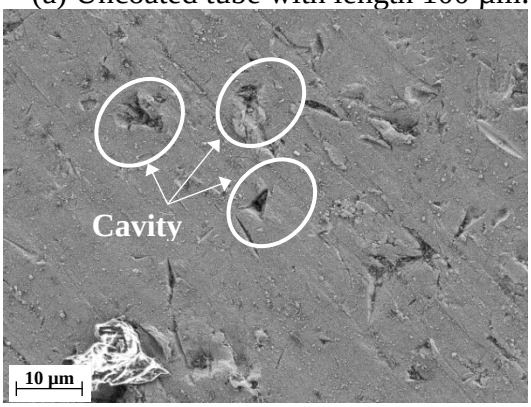

(c) Uncoated tube with length 10 µm.

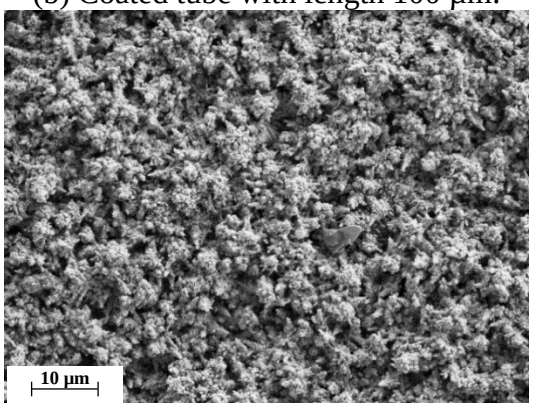

(d) Coated tube with length 10 µm.

Figure 3.7 The samples of uncoated and coated surface are scanned with a Scanning Electron Microscope (SEM), (Al-Gaheeshi et al., 2016).

3.3 Experimental test conditions

The R245fa fluid was tested in five test sections under three system pressures (185, 245 and 310 kPa) and inlet subcooling (5 K). The key thermo-physical properties of the R245fa fluid are summarized in Table 3.5. The flow boiling tests are carried out by setting the mass flux and increasing the heat flux step by step. The ranges of mass flux and heat flux tested are 200 to 500 kg/m^{2}s and 3 to 188 kW/m^2 (with a step of 7 to 90), respectively. Before logging the data for each test case, the system can take a sufficient time (2 – 3 hours) for stability. The test conditions are summarized in Table 3.6.

3.4 Measurements and uncertainty analysis

In this section, the various techniques of measurement, the calibration procedure and the experimental accuracy are described. The uncertainty in a measurement concerns systematic errors (bias) and random errors (precision) which affect the experimental

Table 3.5 The thermodynamic properties of R245fa fluid at different saturation temperatures are based on the Engineering Equation Solver (EES) program.

Property	Pressure (kPa)		
	185	245	310
Saturation temperature, T_{sat} (°C)	31.22	39.44	46.73
Liquid density, ρ_l (kg/m^3)	1321	1298	1277
Vapour density, ρ_v (kg/m^3)	10.56	13.82	17.35
Density ratio, (ρ_l/ρ_v)	125.2	93.94	73.62
Liquid viscosity, μ_l (μPa·s)	372.8	333.2	302.1
Vapour viscosity, μ_v (μPa·s)	10.4	10.73	11.03
Liquid enthalpy, h_l (kJ/kg)	240.7	251.8	261.8
Vapour enthalpy, h_v (kJ/kg)	427.3	433.3	438.6
Latent heat of vaporization, h_{lv} (kJ/kg)	186.6	181.5	176.8
Liquid thermal conductivity, k_l (W/m·K)	0.07929	0.07686	0.07471
Vapour thermal conductivity, k_v (W/m·K)	0.01446	0.01514	0.01577
Surface tension, σ (N/m)	0.01284	0.01179	0.01088

Table 3.6 The ranges of flow boiling test conditions.

Condition	Inner tube diameter (mm)				
	1.1	2.01	2.88	4.26	4.26*
Heat flux, q (kW/m^2)	3.41 – 135.7	5.95 – 175.9	5.19 – 186.9	5.16 – 188.5	5.18 – 149.9
Mass flux, G (kg/m^{2}s)	200 – 500	200 – 500	200 – 500	200 – 500	200 – 500
Saturation temperature, T_{sat} (°C)	31, 39, 46	31, 39, 46	31, 39, 46	31, 39, 46	31, 39, 46
System pressure, P_{in} (kPa)	185, 245, 310	185, 245, 310	185, 245, 310	185, 245, 310	185, 245, 310
Inlet subcooling, ΔT_{sub} (K)	5	5	5	5	5
Exit quality, x_e (–)	0 – 0.92	0 – 0.86	0 – 0.88	0 – 1	0 – 0.89

* represents coated tube.

accuracy. Systematic errors are constant and recurring errors which occur because of a bias in the measuring apparatuses and instruments. Thus, the instrumentation is calibrated to reduce systematic errors. Random errors can be unknown entities that are reduced by collecting a large number of readings over time. Coleman and Steele (2009) introduced the methodology to account for random errors using statistical analysis, see also Moffat (1988), where the sample of N measurements are statistically analysed by using a normal or Gaussian distribution within the interval at 95% confidence level. The random uncertainties are determined directly from the N set of data as follows:

$$u_{random} = t_{95\%} S_X \tag{3.4}$$

$$S_X = \sqrt{\frac{\sum_{i=1}^{N}(X_i - \bar{X})^2}{N-1}} \tag{3.5}$$

$$\bar{X} = \frac{\sum_{i=1}^{N} X_i}{N} \tag{3.6}$$

where X_i is the ith measured variable, $\bar{X}$ is mean value of measured parameters, S_x is standard deviation and $t_{95\%}$ is the degree of freedom. The systematic uncertainties are estimated by the root-sum-square (RSS) method for k components of biases B_x (see Equation (3.7)). These biases are often taken from the manufacturers, as accuracy of instrument. Coleman and Steele (2009) offered Equation (3.8) to evaluate S_{Bx}, the standard deviation of systematic uncertainty.

$$B_X = \sqrt{\sum_{i=1}^{N}(B_x)_i^2} \tag{3.7}$$

$$S_{Bx} = \frac{B_X}{2} \tag{3.8}$$

As previously mentioned, a combination of systematic and random errors results in the total uncertainty of variable U, that is calculated by RSS method of ISO guide (1993) cited from Coleman and Steele (2009), as given in the following expression:

$$u_c = \sqrt{S_{Bx}^2 + S_X^2} \tag{3.9}$$

$$U = t_{95\%} u_c \tag{3.10}$$

The general uncertainty analysis considers the propagation of all uncertainties in measured or calculated variables X_i to estimate the overall uncertainty of the experimental result R. The propagation of uncertainties in experimental results is numerically calculated from the data reduction equation, where R is a function of measured variables:

$$R = R(X_1, X_2, X_3, X_4, \ldots, X_N) \tag{3.11}$$

$$U_R = \left[\left(\frac{\partial R}{\partial X_1}\right)^2 U_{X_1}^2 + \left(\frac{\partial R}{\partial X_2}\right)^2 U_{X_2}^2 + \left(\frac{\partial R}{\partial X_3}\right)^2 U_{X_3}^2 + \cdots + \left(\frac{\partial R}{\partial X_J}\right)^2 U_{X_N}^2\right]^{1/2} \tag{3.12}$$

Equation (3.12) is can be written as a dimensionless form:

$$\frac{U_R}{R} = \left[\left(\frac{X_1}{R}\frac{\partial R}{\partial X_1}\right)^2\left(\frac{U_{X_1}}{X_1}\right)^2 + \left(\frac{X_2}{R}\frac{\partial R}{\partial X_2}\right)^2\left(\frac{U_{X_2}}{X_2}\right)^2 + \left(\frac{X_3}{R}\frac{\partial R}{\partial X_3}\right)^2\left(\frac{U_{X_3}}{X_3}\right)^2 + \cdots + \left(\frac{X_N}{R}\frac{\partial R}{\partial X_N}\right)^2\left(\frac{U_{X_N}}{X_N}\right)^2\right]^{1/2} \quad (3.13)$$

The methodology mentioned above was applied to compute the uncertainties with ranges of experimental parameters that are shown in Table 3.6. The uncertainty of measured parameters is estimated by either manufacturer or through calibration at which all instruments are calibrated before testing. The thermocouples and pressure sensors were individually calibrated for each test section. The acquired data from calibration methods were statistically analysed using linear regression curve fitting. It was modelled

Table 3.7 The uncertainty value for each measured parameter with the used instrumentation.

Parameter	Measuring instrument	Unit	Range	Uncertainty
Outside diameter, D_{outer}	Digital Vernier Caliper Micrometer	mm	–	±0.01mm
Heated length, L_h	Tape meter	mm	–	±1mm
Fluid temperature, T_{in}	T-Type thermocouple	°C	- 200 – 160	± 0.04 °C (calibration)
Fluid temperature, T_{out}	T-Type thermocouple	°C	- 200 – 160	± 0.04 °C (calibration)
Wall temperature, $T_{w,outer}$	K-Type thermocouple	°C	- 267 – 260	± 0.07 °C (calibration)
Inlet pressure, P_{in}	Druck PDCR 910-0826 absolute pressure transducer	kPa	0 – 1000	± 0.16 %
Outlet pressure, P_{out}	Druck PDCR 910-0826 absolute pressure transducer	kPa	0 – 1000	± 0.17 %
Observation section outlet pressure	DRUCK PDCR 4010	kPa	0 – 2000	± 0.16 %
Differential pressure, ΔP_{total}	Ω Omega PX409-015DWUI differential pressure transducer	kPa	0 – 103.42	± 0.18 %
Mass flow rate, m	Coriolis flowmeter (CFM010 and CFM025)	Kg/h	0 – 8000	± 0.03 % (manufacturer)
DC Voltage, V	Yokogawa digital power meter WT110	V	0 – 30	± 0.20 % (manufacturer)
DC Current, I		A	0 – 200	± 0.20 % (manufacturer)

by a best-fit linear equation as a relationship between actual and measured variables. The difference between the actual value and the value which was determined from the fit

linear equation is the error in the instrument, and thus the largest error was considered the uncertainty in a measured parameter. The uncertainty for each measured parameter with its type of measuring instrument is listed in Table 3.7.

The process measurements consist of four types that can be made for recording data from the experimental flow boiling tests. The process measurements are wall and fluid temperature, absolute and differential pressure, mass flow rate, voltage and DC current measurements (to calculate heating power supplied to the test section). The measuring instruments used for each of these process measurements are described above in Table 3.7.

3.4.1 Tube diameters and tube lengths

The inside diameter for both the seamless cold drawn stainless-steel tubes and the borosilicate glass tubes are estimated before manufacturing the test sections. The same method mentioned in Chen (2006) is followed for the inside diameter estimation. The inside diameter of glass tubes is assessed by measuring a weight difference between empty tube and tube filled with water. A highly precise analytical balance is employed for this estimation with a five-decimal place resolution with an accuracy of ± 0.00001 g. Initially, the empty tube is weighed. The same empty tube is then filled with water and weighed again. For stainless-steel tubes, the known outside diameter D_{outer}, length L and weight W for a sample of the tube, the volume as the annular shape is estimated, as follows:

$$\frac{\pi}{4}(D_{outer}^2 - D_{inner}^2)L = \frac{W}{\rho} \tag{3.14}$$

The inside diameter is then calculated according to the following equation:

$$D_{inner} = \sqrt{D_{outer}^2 - \frac{4W}{\pi L \rho}} \tag{3.15}$$

The absolute uncertainty is calculated from Equation (3.16), as follows:

$$U_{D_{inner}} = \frac{1}{D_{inner}} \sqrt{D_{outer}^2 U_{D_{outer}}^2 + \left(\frac{-2}{\pi L \rho}\right)^2 U_W^2 + \left(\frac{2W}{\pi L^2 \rho}\right)^2 U_L^2 + \left(\frac{2W}{\pi L \rho^2}\right)^2 U_\rho^2} \quad (3.16)$$

where ρ is the density of stainless steel tube, which it considers without the uncertainty. The outside diameter is measured by utilizing a Vernier Calliper with an accuracy of ± 0.01 mm at several different locations. A tape measure with an accuracy of ± 1 mm is utilized to measure both the length of a sample from each test section and the heated length of test sections. The relative uncertainty results for the inside diameter are summarized in Table 3.8, while the relative uncertainty of heated length is shown in Table 3.9.

Table 3.8 The uncertainties in the tube diameter for the investigated test sections.

Tube	Outer diameter (mm)	Inner diameter (mm)	Uncertainty
stainless-steel	4.75	4.26	± 0.26 %
stainless-steel	4.75*	4.26*	± 0.26 %
stainless-steel	3.14	2.88	± 0.37 %
stainless-steel	2.39	2.01	± 0.59 %
stainless-steel	1.6	1.1	± 1.37 %
glass	9.4	4.26	± 0.41 %
glass	7.8	2.88	± 0.26 %
glass	7.4	2.01	± 0.16 %
glass	7.8	1.1	± 0.27 %

* represents coated tube.

Table 3.9 The uncertainty of the heated length.

Inside diameter (mm)	heated length (mm)	Uncertainty
4.26	500	± 0.20 %
4.26*	500	± 0.20 %
2.88	300	± 0.33 %
2.01	210	± 0.48 %
1.1	150	± 0.67 %

* represents coated tube.

3.4.2 Temperature

The most significant temperature measurements in the present study are measured by two types of rapid-response thermocouples; T-type (Copper-Constantan) and K-type

(Chromel-Alumel). Three T-type thermocouple needle probes are installed in the test sections to measure the fluid temperatures directly. Fifteen K-type thermocouple wires are distributed uniformly along the outside wall surface of the heating section and affixed by Epoxy adhesive glue with a thermal conductivity of 1.038 W/mK. These thermocouples are utilized to measure the temperature distribution of the wall surface at fifteen locations. The other temperature measurements of the fluid from the rest of the facility are obtained by means of K-type thermocouple probes. An error in the temperature measurements for the test sections can arise because of fluctuations in ambient temperature when using the room-temperature as a reference point. Thus, the external reference temperature can be employed to improve accuracy. This is attained by using the triple point of water through an ice bath (– 0.01 K). For constant triple point, the cold junctions are placed in individual glass tubes containing transformer oil, which are then submerged in an ice-water bath. However, the internal reference temperature (ambient temperature) compensates automatically through the data logger (3595 Series IMP), which is called automatic cold junction compensation. This method is only adopted for the temperature measurements, which is used to control the system, see Table 3.10.

Table 3.10 Absolute uncertainties for thermocouples.

Position	Thermocouple type	Reference point	Accuracy
Condenser outlet	K type probe	Ambient	± 0.07 K
R245fa tank	K type probe	Ambient	± 0.03 K
Flow meter inlet	K type probe	Ambient	± 0.05 K
Test section inlet	T type needle probe	Ice bath	± 0.04 K
Test section outlet	T type needle probe	Ice bath	± 0.04 K
Glass test section outlet	T type needle probe	Ice bath	± 0.04 K
Insulation tube wall	K type probe	Ambient	± 0.05 K
Test section tube wall ($Tw_{1\text{-}15}$)	K type wire	Ice bath	± 0.05 K

The thermocouples are calibrated in an omega constant-temperature liquid circulating bath with a precision thermometer (ASL F250 MKII), as shown in Figure 3.8. The omega circulation bath comprises of digital thermoregulator (HCTB-3030) and refrigerated cooler (RCTB-3050). The digital thermoregulator is equipped with an immersion heater, a stirrer and a temperature controller. The circulation bath fills with a mixture of 60 % water, 40 % antifreeze liquid having a freezing point of – 35 ºC. A precision thermometer (ASL F250 MKII) has platinum resistance thermometer (PRT) with ± 0.005 K uncertainty

and a measurement range of – 200 °C to 962 °C. The thermocouples and the thermometer are immersed in uniform-temperature calibration zone. The thermocouples are connected to the two data acquisition loggers (3595 Series IMP), while both data loggers are connected to a computer to simultaneously record the temperature readings via the LabVIEW software. The readings of temperature from the thermocouples are compared with the readings of the F250 MKII precision thermometer. The range of calibration temperature is from – 1 °C to 90 °C with increment steps of 5 °C. The best-fit linear equation is then produced for each thermocouple to integrate into the LabVIEW software. The uncertainties and positions for thermocouples are summarized in Table 3.10. The thermocouple systematic error is ± 0.03 – 0.07 K, while the error due to the resolution of the data logger (Solartron's IMP S13595) was ± 0.1 K. Thus, the overall uncertainty in the temperature readings was conservatively estimated to be ± 0.1 K.

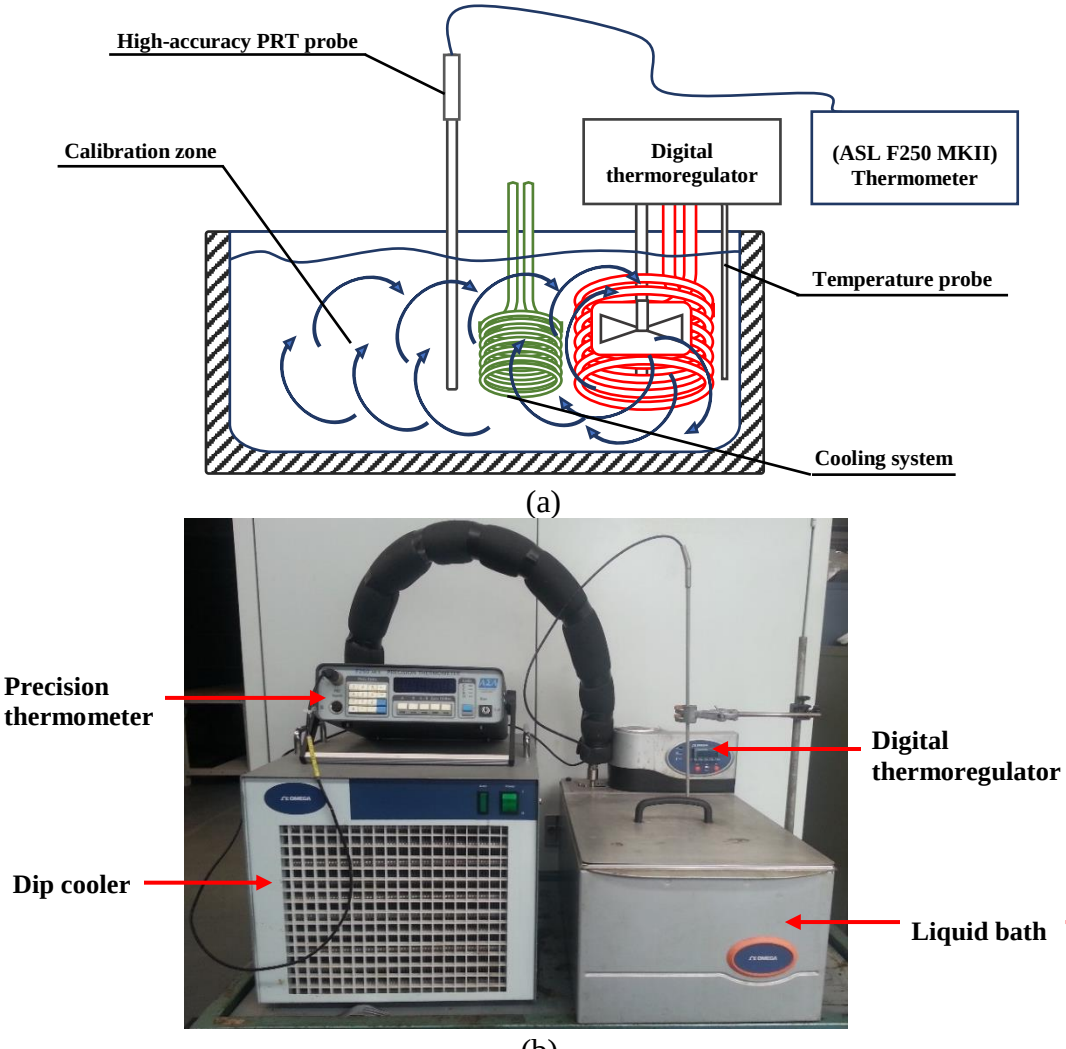

Figure 3.8 (a) Sketch and (b) photograph of the thermocouple-calibration equipment.

3.4.3 Absolute and differential pressure

In the current study, there are five pressure transducers, which fit into the facility at different locations as listed in Table 3.11. They are supplied with a DC power supply of 12 V. The pressure transducers convert pressure readings to analogue signals which are acquired by the IMP S135951C data logger. The voltage signals convert from the data logger to pressure according to the particular calibration equations. These signals are then monitored via the computer by the LabVIEW software. All pressure transducers are calibrated by utilizing a dead weight pressure gauge tester (Bryans Aeroquipment Ltd, Series No 616, Standard range 10 – 5000 psi, accuracy ±0.1%), see Figure 3.9. The test range of applied oil pressure is from 10 to 90 psi (i.e. 172 – 724 kPa), which cover the experimental pressure range between 185 and 310 kPa. The best-fit linear equations are formed precisely by the comparison between the output signals from the LabVIEW software and the actual applied pressures. The calibration equations for each pressure transducer are incorporated into the LabVIEW software. The relative uncertainties and specifications for pressure transducers are presented in Table 3.11.

Table 3.11 Relative uncertainties for pressure transducers

Position	Sensor (manufacturer)	Range	Accuracy
After condenser	GP series (RS)	0-2000 kPa	± 0.34 %
Before flow meter	GP series (RS)	0-2000 kPa	± 0.31 %
Test section inlet	PDCR 910-0826 (Druck)	0-1000 kPa	± 0.17 %
Test section outlet	PDCR 910-0826 (Druck)	0-1000 kPa	± 0.29 %
Glass section outlet	PDCR 4010 (Druck)	0-1000 kPa	± 0.16 %

The pressure drop between the inlet and outlet of the test sections is measured by an Omega differential pressure transducer (PX409-015DWUI). This transducer is supplied by 24 VDC power supply. It has a range of 0 – 15 psi (0 – 103.421 kPa), an accuracy of ± 0.18 % full scale and an output signal of 4 – 20 mA. However, its signal is converted from DC current to DC voltage through a 500 Ω resistor (± 0.1 % accuracy). The analogue signal of the differential pressure transducer is then acquired by the IMP S135951C data logger and send to the computer. This signal is then converted to a pressure reading by LabVIEW software according to the linear calibration equation. The Omega PX409-015DWUI transducer is also calibrated by means of a dead weight pressure gauge tester. The best-fit linear equation is obtained from the calibration data. The result of relative

uncertainty after the process of calibration is ± 0.18 %. It is worth mentioning that this value is close to the accuracy in the calibration certificate by the manufacturer.

Figure 3.9 Photograph of dead weight pressure gauge tester.

3.4.4 Mass flow rate and mass flux

The mass flow rate in this experimental facility is measured by means of two Coriolis mass flow meters with ± 0.03 % accuracy. The smaller Coriolis mass flow meter (CMF010) that has a range of (0 - 25 kg/h) is used to measure the low mass flow rate, while the high mass flow rate is measured by larger Coriolis mass flow meter (CMF025) with range of (0 - 500 kg/h). The calibration process for both mass flow rates was accomplished at the manufacturer's location due to the fact that the standard measuring technique was not available in the current laboratory. Therefore, the linear calibration equation for each mass flow meter provided by the manufacturer was used for the present experiments. The mass flux can be expressed for a circular tube as:

$$G = \frac{4\dot{m}}{\pi D_{inner}^2} \tag{3.17}$$

The uncertainty for mass flux *G* is:

$$U_G = \sqrt{\left(\frac{4}{\pi D_{inner}^2}\right)^2 U_{\dot{m}}^2 + \left(\frac{-8\dot{m}}{\pi D_{inner}^3}\right)^2 U_{D_{inne}}^2} \tag{3.18}$$

The mass flux ranges from 200 kg/m^{2}s to 500 kg/m^{2}s. Thus, the uncertainties for the extreme values of mass flux *G* are listed in Table 3.12.

Table 3.12 The uncertainty of the mass flux for each test section.

Test section (mm)	Mass flux range (kg/m^{2}s)	Uncertainty
4.26	200 – 500	± 0.74 %
4.26*	200 – 500	± 0.78 %
2.88	200 – 500	± 0.93 %
2.01	200 – 500	± 1.63 %
1.1	200 – 500	± 4.34 %

* represents coated tube.

3.4.5 Heat flux

The uniform heat flux imposed on the heating section can be calculated from the total supplied power, heat loss from the heating section to the ambient and inner surface area, as follows:

$$q = \frac{IV - Q_{loss}}{\pi D_{inner} L_h} \tag{3.19}$$

where the total supplied power to the heating section is determined from the measurements of the DC current *I* and the DC voltage *V*. A digital power meter (Yokogawa WT110) is utilized to measure current and voltage. The accuracy of the voltage and current measurement provided by the manufacturer is ± 0.2 %. The value of heat loss Q_{loss} from the heating section to the surroundings can be estimated by the identical method as presented in the work of Huo (2005) and Chen (2006) and will be tested by evaluating the energy balance for the heating section. The main objective of the energy balance analysis in single-phase flow is also to help evaluate the net heat absorbed by the fluid during evaporation. The single-phase energy balance is checked for various mass fluxes and heat fluxes. It is represented by the following expressions:

$$Q_{loss} = \overline{K}\,\Delta\overline{T} \tag{3.20}$$

$$\overline{K} = \frac{IV - \dot{m}\, Cp(T_{out} - T_{in})}{\Delta\overline{T}} \tag{3.21}$$

$$\Delta\overline{T} = \frac{1}{N}\sum_{i=1}^{N} T_{w,outer,i} - T_{ins} \tag{3.22}$$

where $\overline{K}$ is the thermal loss coefficient, which is presumed constant and obtained from single phase flow, $\Delta\overline{T}$ is the average surface temperature difference between the inside and the outside of the insulation, *Cp* is liquid specific heat, T_{out} is the fluid outlet temperature, T_{in} is the fluid inlet temperature, $T_{w,outer,i}$ is the local outside wall surface temperature of the heating section and T_{ins} is the outside surface temperature of the insulation (the ambient temperature). The heat loss from the heating section is roughly estimated to be 1 % – 3 % of the total supplied power.

The uncertainties in the heat flux are determined by the following expression:

$$U_q = \sqrt{\left(\frac{I}{\pi D_{inner} L_h}\right)^2 U_V^2 + \left(\frac{V}{\pi D_{inner} L_h}\right)^2 U_I^2 + \left(\frac{-1}{\pi D_{inner} L_h}\right)^2 U_{Q_{loss}}^2 + \left(\frac{-q}{D_{inner}}\right)^2 U_{D_{inner}}^2 + \left(\frac{-q}{L_h}\right)^2 U_{L_h}^2} \tag{3.23}$$

where the uncertainties in heat loss correspond to the following expressions:

$$U_{Q_{loss}} = \sqrt{\Delta\overline{T}^2 U_{\overline{K}}^2 + \overline{K}^2 U_{\Delta\overline{T}}^2} \tag{3.24}$$

$$U_{\overline{K}} = \sqrt{\begin{array}{c}\left(\frac{I}{\Delta\overline{T}}\right)^2 U_V^2 + \left(\frac{V}{\Delta\overline{T}}\right)^2 U_I^2 + \left(\frac{-Cp_l(T_{out} - T_{in})}{\Delta\overline{T}}\right)^2 U_{\dot{m}}^2 \\ + \left(\frac{-\dot{m}(T_{out} - T_{in})}{\Delta\overline{T}}\right)^2 U_{Cp_l}^2 + \left(\frac{-\dot{m}Cp_l}{\Delta\overline{T}}\right)^2 U_{T_{out}}^2 \\ + \left(\frac{\dot{m}Cp_l}{\Delta\overline{T}}\right)^2 U_{T_{in}}^2 + \left(\frac{-\left(VI - \dot{m}Cp_l(T_{out} - T_{in})\right)}{\Delta\overline{T}^2}\right)^2 U_{\Delta\overline{T}}^2\end{array}} \tag{3.25}$$

$$U_{\Delta\overline{T}} = \sqrt{\left(\frac{1}{N}\right)^2 \sum_{i=1}^{N} U_{T_{wi}}^2 + U_{T_{ins}}^2} \tag{3.26}$$

The uncertainties in the heat flux are summarized in Table 3.13.

Table 3.13 The uncertainties in heat flux for all test sections

Test section diameter (mm)	Heat flux range (kW/m^2)	Uncertainty %
4.26	5 – 189	± 0.51 – 2.32 %
4.26*	5 – 150	± 0.50 – 2.20 %
2.88	5 – 187	± 0.64 – 1.19 %
2.01	6 – 176	± 0.99 – 2.96 %
1.1	3 – 136	± 2.29 – 4.70 %

* represents coated tube.

Finally, the computations of uncertainty analysis using the technique proposed by Coleman and Steele (2009) are implemented in this study. The uncertainty propagation is taken into account during the data reduction methodology.

3.5 Data reduction

The methodology of specific data reduction is very important for obtaining the final experimental results. In this subsection, the procedure of data reduction covering the characteristics for both single-phase flow and flow boiling is presented in detail. The overall measurements in the current experiments provide experimental data to calculate local two-phase heat transfer coefficient, flow boiling pressure drop and superficial velocities for flow patterns. For flow boiling, the data reduction method of vapour quality x is introduced taking into account the fact that the fluid enters into the heating section as a subcooled liquid. Subsequently, the data reduction method of heat transfer coefficient α is detailed for both single-phase flow and flow boiling. The data reduction method for the frictional pressure drop ΔP_{fr} is presented. Finally, the liquid and vapour superficial velocities for flow pattern regimes are presented.

3.5.1 Single-phase flow

Pressure drop

In the current experimental set up, the test sections do not have any sudden contraction and expansion at its inlet and outlet, as shown in Figure 3.6. In the single-phase flow, the pressure drop along the test section is divided into developing and developed regions. The pressure drop in the developing region results from both wall shear stress and fluid acceleration, whilst the pressure drop in the fully developed region

results only from friction. The boundary between the developing and developed flow is defined by the hydraulic entrance length which is related to the channel diameter. Thus, the fully developed flow is completely actualized in each test section after the calming section, as previously mentioned it can be characterized by the Fanning friction factor. The experimental friction factor is deduced from the following expression:

$$f = \frac{\Delta P D_{inner} \rho_l}{2 l_{\Delta P} G^2} \tag{3.27}$$

where f is the friction factor, ΔP is the measured pressure drop, D_{inner} is the tube inside diameter, ρ_l is the liquid density, $\dot{m}$ is the mass flow rate and $l_{\Delta P}$ is the length between the two pressure ports.

The uncertainty of the experimental friction factor is obtained from the following:

$$U_f = f \sqrt{\begin{array}{c} \left(\frac{1}{\Delta P}\right)^2 U_{\Delta P}^2 + \left(\frac{1}{D_{inner}}\right)^2 U_{D_{inner}}^2 + \left(\frac{1}{\rho_l}\right)^2 U_{\rho_l}^2 \\ + \left(\frac{-1}{L_{\Delta P}}\right)^2 U_{L_{\Delta P}}^2 + \left(\frac{-2}{G}\right)^2 U_G^2 \end{array}} \tag{3.28}$$

Heat transfer coefficient

The local single-phase heat transfer coefficient α_{sp} at each axial temperature measurement position is determined from the following equation:

$$\alpha_{sp}(z) = \frac{q}{\left(T_{w,inner}(z) - T_f(z)\right)} \tag{3.29}$$

where $T_{w,inner}(z)$ is the local inner wall temperature, and $T_{f,}(z)$ is the local fluid bulk temperature. The local inner wall temperature is calculated using Equation (3.30), which was obtained by solving the one-dimensional heat conduction equation with volumetric heat generation in cylindrical coordinates.

$$\begin{array}{c} T_{w,inner}(z) = T_{w,outer}(z) + \frac{\dot{q}}{16 k_{ss}} (D_{outer}^2 - D_{inner}^2) \\ - \left(\frac{\dot{q}}{8 k_{ss}} D_{outer}^2\right) \ln\left(\frac{D_{outer}}{D_{inter}}\right) \end{array} \tag{3.30}$$

where $\dot{q}$ is the volumetric heat generation at the heating section, D_{outer} and D_{inner} are the outer and the inner diameters, respectively, and k_{ss} is the thermal conductivity of the stainless-steel tube, which depends on its temperature and was obtained using the EES program. The uncertainties of the inner wall temperature can be attained from the following expression:

$$U_{T_{w,inner}} = \sqrt{\begin{matrix} U_{T_{w,outer}}^2 + \left[\frac{(D_{outer}^2 - D_{inner}^2)}{16k_{ss}} - \left(\frac{D_{outer}^2}{8k_{ss}}\right)\ln\left(\frac{D_{outer}}{D_{inter}}\right)\right]^2 U_{\dot{q}}^2 \\ + \left[\frac{-\dot{q}D_{outer}}{4k_{ss}}\ln\left(\frac{D_{outer}}{D_{inner}}\right)\right]^2 U_{D_{outer}}^2 + \left[\frac{\dot{q}(D_{outer}^2 - D_{inner}^2)}{8k_{ss}D_{inner}}\right]^2 U_{D_{inner}}^2 \\ + \left[\frac{\dot{q}(D_{outer}^2 - D_{inner}^2)}{16k_{ss}^2} - \left(\frac{\dot{q}D_{outer}^2}{8k_{ss}^2}\right)ln\left(\frac{D_{outer}}{D_{inter}}\right)\right]^2 U_{k_{ss}}^2 \end{matrix}} \quad (3.31)$$

The fluid bulk temperature can be evaluated locally by using an energy balance for the heating section to reduce the data by assuming a linear variation in temperature along the flow direction, as follows:

$$T_f(z) = T_{in} + \frac{q\pi D_{inner} z}{\dot{m}Cp_l} \quad (3.32)$$

where z is the axial distance. The uncertainties of the fluid bulk temperature can be obtained from the following equation:

$$U_{T_f} = \sqrt{\begin{matrix} U_{T_{in}}^2 + \left(\frac{\pi D_{inner} z}{\dot{m}Cp_l}\right)^2 U_q^2 + \left(\frac{q\pi z}{\dot{m}Cp_l}\right)^2 U_{D_{inner}}^2 + \left(\frac{q\pi D_{inner}}{\dot{m}Cp_l}\right)^2 U_z^2 \\ + \left(\frac{-q\pi D_{inner} z}{\dot{m}^2 Cp_l}\right)^2 U_{\dot{m}}^2 + \left(\frac{-q\pi D_{inner} z}{\dot{m}Cp_l^2}\right)^2 U_{Cp_l}^2 \end{matrix}} \quad (3.33)$$

The uncertainty on the local single-phase heat transfer coefficient α_{sp} is given by the following equation:

$$U_{\alpha_{sp}} = \sqrt{\begin{matrix} \left(\frac{1}{T_{w,inner} - T_f}\right)^2 U_q^2 + \left(\frac{-q}{\left(T_{w,inner} - T_f\right)^2}\right)^2 U_{T_{w,inner}}^2 \\ + \left(\frac{q}{\left(T_{w,inner} - T_f\right)^2}\right)^2 U_{T_f}^2 \end{matrix}} \quad (3.34)$$

where U_q is calculated from Equation (3.23), $U_{T_{w,inner}}$ and U_{T_f} are obtained by applying the error propagation method using Equations (3.30) and (3.32), respectively.

The single-phase heat transfer coefficient in the dimensionless Nusselt number form Nu_{sp} is given by Equation (3.35), which is utilized in a comparison with single-phase heat transfer correlations.

$$Nu_{sp} = \frac{\alpha_{sp} D_{inner}}{k_l} \tag{3.35}$$

where α_{sp} is the single-phase flow heat transfer coefficient calculated by Equation (3.29) and k_l is the liquid thermal conductivity of R245fa. The uncertainty on the experimental Nusselt number is expressed as:

$$U_{Nu_{sp}} = \sqrt{\left(\frac{D_{inner}}{k_l}\right)^2 U_{\alpha_{sp}}^2 + \left(\frac{\alpha_{sp}}{k_l}\right)^2 U_{D_{inner}}^2 + \left(-\frac{\alpha_{sp} D_{inner}}{k_l^2}\right)^2 U_{k_l}^2} \tag{3.36}$$

The average Nusselt number can be derived from integrating Equation (3.35) with a distance, as follows:

$$\overline{Nu}_{sp} = \frac{1}{L_T} \int_0^{L_T} Nu_{sp}(z)\, dz \tag{3.37}$$

where L_T is the distance between the first and last thermocouples, the precision of the local heat transfer coefficients through the error propagation analysis is estimated to be within ±6.96%.

Finally, the Reynolds number is given by Equation (3.38), which is used in a comparison with single-phase heat transfer and friction factor correlations. The uncertainty on the Reynolds number is expressed as Equation (3.39). The specific uncertainties of the main parameters for single-phase flow are summarized in Table 3.14.

$$Re = \frac{G D_{inner}}{\mu_l} \tag{3.38}$$

$$U_{Re} = \sqrt{\left(\frac{D_{inner}}{\mu_l}\right)^2 U_G^2 + \left(\frac{G}{\mu_l}\right)^2 U_{D_{inner}}^2 + \left(-\frac{G D_{inner}}{\mu_l^2}\right)^2 U_{\mu_l}^2} \tag{3.39}$$

Table 3.14 The specific uncertainties of main parameters for single-phase flow.

Parameter	Unit	Test range	Uncertainty
Re	–	569 – 72467	± 3.04 %
f	–	0.004716 – 0.01219	± 6.52 %
Nu_{sp}	–	6.8 – 283.6	± 24.68 %

3.5.2 Two-phase flow

During the two-phase flow tests, the fluid enters the inlet heating section at the subcooled condition. Consequently, the heated tube is normally occupied by a subcooled length and a two-phase flow length. The subcooled length L_{sub} must be evaluated in order to deduce single-phase pressure drop. It is first calculated from the energy balance along heating section and can be expressed as follows:

$$L_{sub} = \frac{\dot{m}Cp_l}{q\pi D_{inner}}\left(T_{sat_{|P_{sat}}} - T_{in}\right) \tag{3.40}$$

The saturation pressure P_{sat} is determined at the end of the subcooled length, i.e. at the beginning of the two-phase flow, taking into account the single-phase pressure drop with the following expression:

$$P_{sat} = P_{in} - \Delta P_{sp} \tag{3.41}$$

where P_{in} is the absolute pressure measured at the inlet of the heating section, see Figure 3.6. The pressure drop ΔP_{sp} of single-phase flow along the subcooled length is obtained from the following expression:

$$\Delta P_{sp} = \frac{G^2}{2\rho_l} 4f \frac{L_{sub}}{D_{inner}} \tag{3.42}$$

where f is the Fanning friction factor. The subcooled length L_{sub} can be determined by solving the Equations (3.40) to (3.42) together, The calculation is accelerated by implementing a Newton-Raphson iteration until the difference between two successive iterations is very small.

The determination of a saturation pressure P_{sat} at each location z is necessary to deduce the saturation temperature $T_{sat,(z)}$ which is needed in the calculations of local heat transfer coefficient and local vapour quality. The two-phase flow pressure drop is

assumed to be linear along the tube, therefore the saturation pressure P_{sat} at any location z is calculated from the following Equation:

$$P_{sat}(z) = P_{sat} - \left(\Delta P_{total} - \Delta P_{sp}\right)\left(\frac{z - L_{sub}}{L_h - L_{sub}}\right) \tag{3.43}$$

where ΔP_{total} is the pressure drop measured along the heating section.

Heat transfer coefficient

The data reduction process postulates uniform heat flux distribution to the whole heating section. Hence, the local heat transfer coefficient of each axial location is evaluated by applying Newton's law of cooling utilizing the value of uniform heat flux, inner wall temperature and saturation temperature. The flow boiling heat transfer coefficient α_{tp} at each location z is obtained from the following equation:

$$\alpha_{tp}(z) = \frac{q}{\left(T_{w,inner}(z) - T_{sat}(z)\right)} \tag{3.44}$$

The inner wall temperature $T_{w,inner}$ at each location z is calculated from Equation (3.30) and the saturation temperature T_{sat} at each location z is deduced from the saturation pressure $P_{sat}(z)$ which is obtained from Equation (3.43). The uncertainty in $\alpha_{tp}(z)$ is determined from Equation (3.45) and presents in Table 3.15.

$$U_{\alpha_{tp}} = \sqrt{\left(\frac{1}{T_{w,inner} - T_{sat}}\right)^2 U_q^2 + \left(\frac{-q}{\left(T_{w,inner} - T_{sat}\right)^2}\right)^2 U_{T_{w,inner}}^2 + \left(\frac{q}{\left(T_{w,inner} - T_{sat}\right)^2}\right)^2 U_{T_{sat}}^2} \tag{3.45}$$

Table 3.15 The uncertainty values in the flow boiling heat transfer coefficient

Test section diameter (mm)	Uncertainty
4.26	± 0.55 – 9.20 %
4.26*	± 0.57 – 9.37 %
2.88	± 0.79 – 11.21 %
2.01	± 1.11 – 8.97 %
1.1	± 2.34 – 26.65 %

* represents coated tube.

The average heat transfer coefficient can be derived from integrating Equation (3.44) with a distance, as follows:

$$\alpha_{tp,av} = \frac{1}{L_T}\int_0^{L_T} \alpha_{tp}(z)\, dz \tag{3.46}$$

Vapour quality

The fluid enters the heating section as a subcooled liquid and the boiling starts in the heating section. Thus, the vapour quality x_{in} at the inlet of the heating section is equal to zero. The thermodynamic vapour quality at each location z in the saturated region of the heating section is expressed in terms of the local enthalpy as follows:

$$x(z) = \frac{h_{l,in} + \frac{q\pi D_{inner} z}{\dot{m}} - h_{l,sat}(z)}{h_{lv}(z)} \tag{3.47}$$

where $h_{l,in}$ is the specific enthalpy of the liquid deduced from T_{in} and P_{in}, z is the distance between the inlet of the heating section and the location z (thermocouple), $h_{l,sat}(z)$ and $h_{lv}(z)$ are the specific enthalpy of the saturated liquid and the latent heat of vaporization, respectively. They are calculated at $T_{sat}(z)$ which is deduced from the saturation pressure at the location z. The uncertainty of $x(z)$ is determined from the following equation:

$$U_{x(z)} = \sqrt{\begin{array}{c}\left(\frac{1}{h_{lv}}\right)^2 U_{h_{l,in}}^2 + \left(\frac{\pi D_{inner} z}{\dot{m} h_{lv}}\right)^2 U_q^2 + \left(\frac{q\pi z}{\dot{m} h_{lv}}\right)^2 U_{D_{inner}}^2 + \left(\frac{q\pi D_{inner}}{\dot{m} h_{lv}}\right)^2 U_z^2 \\ + \left(\frac{-q\pi D_{inner} z}{\dot{m}^2 h_{lv}}\right)^2 U_{\dot{m}}^2 + \left(\frac{-1}{h_{lv}}\right)^2 U_{h_{l,sat}}^2 + \left(\frac{-x}{h_{lv}}\right)^2 U_{h_{lv}}^2\end{array}} \tag{3.48}$$

where $U_{x(z)}$ is the uncertainty of local vapour quality, U_q is calculated from Equation (3.23), U_z is equal to ±1 mm, and $U_{\dot{m}}$ is equal to ±0.03%. $U_{h_{l,in}}$, $U_{h_{l,sat}}$ and $U_{h_{lv}}$ are calculated from the EES program with the adequate temperatures (inlet and saturation temperatures). The uncertainty of the measured temperatures is ± 0.04 – 0.1 K whereas for the deduced temperatures the uncertainties are estimated through error propagation on a case-by-case basis.

Frictional pressure drop

In two-phase flow conditions, the total pressure drop ΔP_{total} contains the contributions of single-phase pressure drop and two-phase pressure drop, as given in the following:

$$\Delta P_{total} = \Delta P_{sp} + \Delta P_{tp} \tag{3.49}$$

The single-phase pressure drop is determined by Equation (3.42). The two-phase pressure drop for the vertical tubes includes three components, namely: the frictional pressure drop ΔP_{fr}, the momentum pressure drop ΔP_{mom} and the gravitational pressure drop ΔP_{grav}. The two-phase pressure drop can be expressed as follows:

$$\Delta P_{tp} = \Delta P_{fr} + \Delta P_{mom} + \Delta P_{grav} \tag{3.50}$$

In case of using the homogeneous flow model to compare with experimental data, the momentum and gravitational components can be obtained from Equations (3.51) and (3.52), respectively (see Collier and Thome (1994)).

$$\Delta P_{mom} = G^2 x_e v_{lv} \tag{3.51}$$

$$\Delta P_{grav} = \frac{L_{tp}\, g \sin\theta}{v_{lv} x_e} \ln\left[1 + x_e \frac{v_{lv}}{v_l}\right] \tag{3.52}$$

where x_e is the exit vapour quality, v_l is the specific volume of the liquid and v_{lv} is the difference in specific volumes of liquid and vapour. For comparison using the separated flow model, the momentum pressure drop is expressed as follows:

$$\Delta P_{mom} = G^2 \left[\frac{x_e^2 v_v}{\epsilon} + \frac{(1-x_e)^2 v_l}{1-\epsilon} - 1\right] \tag{3.53}$$

while the gravitational pressure drop is expressed as follows:

$$\Delta P_{grav} = \frac{L_{tp} g \sin\theta}{x_e} \int_0^{x_e} \left[\frac{\epsilon}{v_v} + \frac{(1-\epsilon)}{v_l}\right] dx \tag{3.54}$$

These are also reported in Collier and Thome (1994). The void fraction, ϵ, can be calculated from different correlations which are summarized in Table 3.16.

Table 3.16 Void fraction correlations for two-phase flow pressure drop.

Author(s)	Correlation
Zivi (1964)	$\epsilon = \dfrac{1}{1 + \dfrac{1 - x_e}{x_e}\left(\dfrac{\rho_v}{\rho_l}\right)^{\frac{2}{3}}}$
Lockhart and Martinelli (1949)	$\epsilon = \dfrac{1}{1 + 0.28\left(\dfrac{1 - x_e}{x_e}\right)^{0.64}\left(\dfrac{\rho_v}{\rho_l}\right)^{0.36}\left(\dfrac{\mu_l}{\mu_v}\right)^{0.07}}$
Chisholm (1973b)	$\epsilon = \dfrac{1}{1 + \left(\dfrac{1 - x_e}{x_e}\right)\left(\dfrac{\rho_v}{\rho_l}\right)\sqrt{1 - x_e\left(1 - \dfrac{\rho_l}{\rho_v}\right)}}$

According to Equations (3.49) and (3.50), the two-phase frictional pressure drop is obtained by subtracting the single-phase, momentum and gravitational components from the total pressure drop. The uncertainties in two-phase frictional pressure drop ΔP_{fr} are calculated from the following equation:

$$U_{\Delta P_{fr}} = \sqrt{U^2_{\Delta P_{total}} + U^2_{\Delta P_{sp}} + U^2_{\Delta P_{mom}} + U^2_{\Delta P_{grav}}} \tag{3.55}$$

where $U_{\Delta P_{total}}$ corresponds to the uncertainty of the differential pressure transducer. $U_{\Delta P_{sp}}$, $U_{\Delta P_{mom}}$, and $U_{\Delta P_{grav}}$ are obtained by applying the error propagation method using Equations (3.40), (3.53) and (3.54), respectively.

Superficial velocity

The liquid and vapour superficial velocities are used to establish the flow pattern maps, which show the flow pattern transition lines. The liquid superficial velocity, J_l, and the vapour superficial velocity, J_v, are obtained from following equations:

$$J_l = \frac{G(1 - x_e)}{\rho_l} \tag{3.56}$$

$$J_v = \frac{G x_e}{\rho_v} \tag{3.57}$$

The uncertainty in liquid and vapour superficial velocities are estimated from the following expressions:

$$U_{J_l} = \sqrt{\left(\frac{(1-x_e)}{\rho_l}\right)^2 U_G^2 + \left(\frac{G}{\rho_l}\right)^2 U_{x_e}^2 + \left(\frac{G(1-x_e)}{\rho_l^2}\right)^2 U_{\rho_l}^2} \quad (3.58)$$

$$U_{J_v} = \sqrt{\left(\frac{(1-x_e)}{\rho_v}\right)^2 U_G^2 + \left(\frac{G}{\rho_v}\right)^2 U_{x_e}^2 + \left(\frac{G(1-x_e)}{\rho_v^2}\right)^2 U_{\rho_v}^2} \quad (3.59)$$

Finally, the specific uncertainties of the main parameters for flow boiling are summarized in Table 3.17.

Table 3.17 The specific uncertainties of main parameters for flow boiling.

Parameter	Unit	Test range	Uncertainty
ΔP_{tp}	kPa	0.014 – 58.89	± 0.18 – 32.47%
α_{tp}	kW/m^{2}K	0.2047 – 22.351	± 0.55 – 11.21%
x_e	–	0 – 1	± 0.37 – 19.70 %
J_l	m/s	0.002 – 0.460	± 0.47 – 15.04 %
J_v	m/s	0.008 – 38.98	± 0.02 – 18.22 %

3.6 Single-Phase flow validation

In this section, the experimental results of friction factor and Nusselt number for single-phase flow are presented and discussed. The experimental setup is validated by conducting single-phase pressure drop and heat transfer tests. These tests were carried out before conducting the flow boiling experiments and their experimental results of the R245fa fluid are used to compare with well-known correlations of single-phase flow from the literature. Besides, the reproducibility of the results was also assessed.

3.6.1 Pressure drop validation

The results of flow friction factor versus Reynolds number for the R245fa fluid in five test sections are shown in Figure 3.10. It can be seen that the single-phase friction factor decreases with increasing Reynolds number for all tubes. The correlations of single-phase flow listed in Table 3.18 are compared to validate the single-phase friction factor in tubes. It is shown that the correlations of Blasius (1913) and Haaland (1983) generally present the best agreement predictions with the experimental data for the single-phase friction factor irrespective of the tube diameter. These correlations largely predict

the friction factors of the 4.26 mm uncoated tube and the 2.88 mm tube. However, they slightly underpredict the experimental results of the friction factor for the 4.26 mm coated tube. The experimental friction factors of the 2.01 mm tube are slightly lower than the predictions from Blasius (1913) correlation. The experimental data of the friction factor inside the 1.1 mm tube is predicted very well by the Blasius (1913) correlation for the turbulent flow region. However, the Haaland (1983) correlation slightly overpredicts the experimental friction factors, while the Choi et al. (1991) correlation underpredicts the experimental friction factors of the 1.1 mm tube. For the laminar flow region, the experimental friction factors inside the 1.1 mm tube fit the classical equation of laminar flow theory. It can also be seen that the experimental transition from laminar to turbulent flow appears to happen for a Reynolds number between 2000 and 3000, which agrees with conventional theory. Furthermore, The experimental friction factor data of the 4.26 mm and the 2.88 mm tube are in a good agreement with these correlations as the Mean Absolute Error (MAE) is around 2 % and 3 % for the Blasius (1913) and Haaland (1983) correlations, respectively. The MAE of the predicted friction factor for the 4.26 mm coated tube is 5% for both correlations. For the 2.01 mm tube, the experimental data are predicted with an MAE of 4% and 7% for the Blasius (1913) and Haaland (1983) correlations, respectively. The experimental data for the laminar flow region inside the 1.1 mm tube are predicted with an MAE of 3% for the correlation of laminar flow theory. The experimental data for the turbulent flow region inside the 1.1 mm tube are predicted with an MAE of 4%, 9% and 19% for the correlations of Blasius (1913), Haaland (1983), and Choi et al. (1991), respectively. These values of MAE fall within the uncertainty range of the friction factor. Assessment of the experimental reproducibility is included in the results presented in Figure 3.10a. The agreement between the two sets of data conducted at different times (i.e. one day after the implementation of the experiment (1)) is very good. The results of Blasius (1913) correlation, considering the smooth tubes, appear to be much closer to the experimental data than that of Haaland (1983) correlation.

Table 3.18 Existing correlations from literature for the pressure loss.

Author(s)	correlation
Laminar flow theory	$f = 16Re^{-1}$ $(Re < 2000)$
Blasius (1913)	$f = 0.079Re^{-0.25}$ $(2000 < Re < 100000)$
Haaland (1983)	$\frac{1}{\sqrt{f}} = -3.6\, log_{10}\left[\frac{6.9}{Re} + \left(\frac{e}{3.71D}\right)^{1.11}\right]$
Choi et al. (1991)	$f = 0.035Re^{-0.182}$ $(4000 < Re < 18000)$

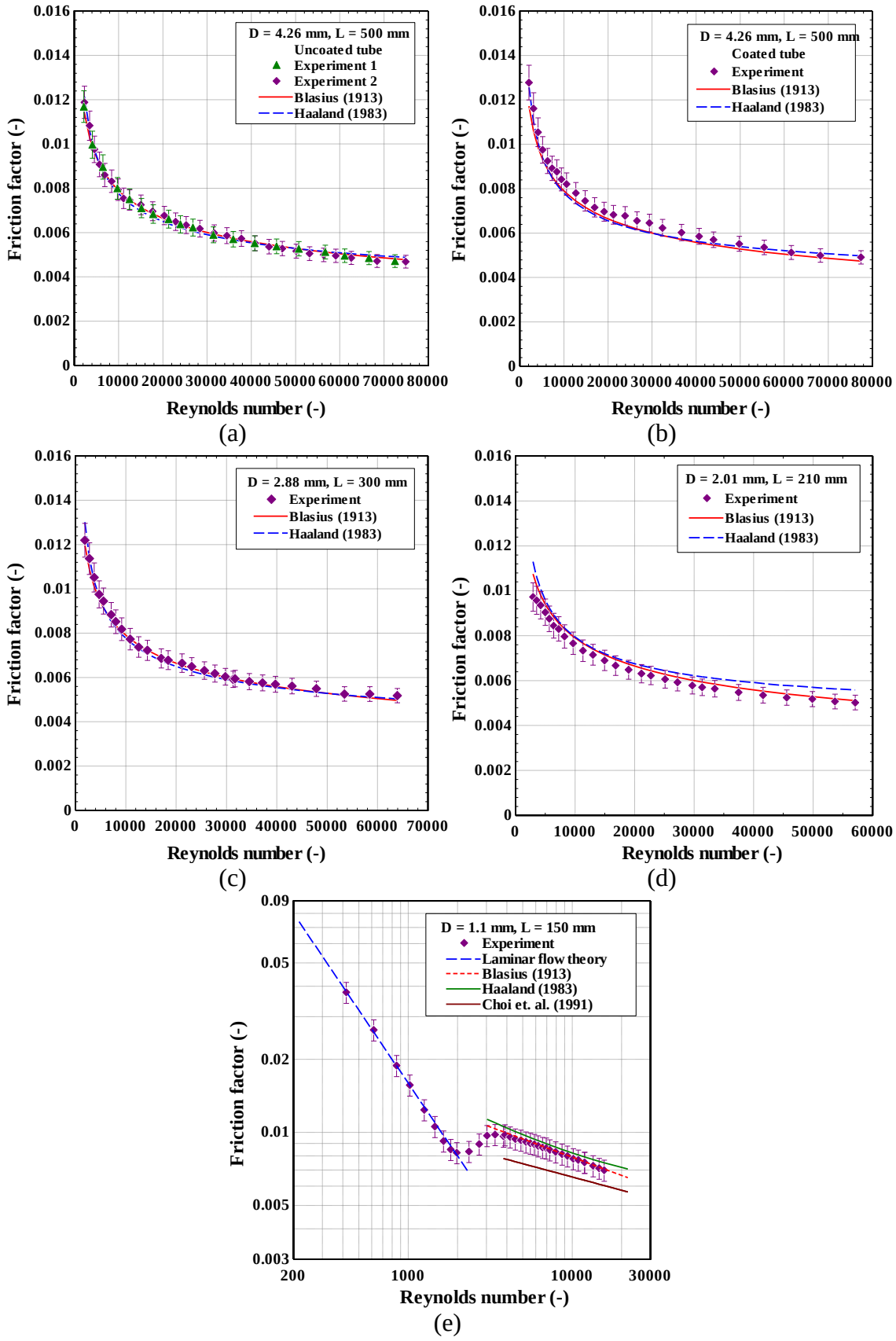

Figure 3.10 Comparison in Single-phase flow between predicted and experimental friction factor: (a) 4.26 mm uncoated tube, (b) 4.26 mm coated tube, (c) 2.88 mm tube, (d) 2.01 mm tube and (e) 1.1 mm tube.

3.6.2 Heat transfer validation

The single-phase flow validation, at the boundary condition of the uniform wall heat flux in terms of the average Nusselt number is represented in Figure 3.11. The experimental results of average Nusselt number are compared with three correlations of Dittus and Boelter (1930), Petukhov (1970) and Shah and London (1978) which are listed in Table 3.19. The Dittus and Boelter (1930) and Petukhov (1970) correlations are used to predict the turbulent flow region while the Shah and London (1978) correlation is utilized to predict the laminar flow region. The predictions of Petukhov (1970) correlation give a good agreement with the experimental Nusselt numbers for all tubes. The 2.88 mm tube results agree better with the predictions of Dittus and Boelter (1930) correlation. The correlation of Petukhov (1970) predicts the experimental data of 4.26 mm coated tube and 4.26 uncoated tube with an MAE of 4.1% and 5.3%, respectively. Also, it predicts the data of the 2.88 mm tube with an MAE of 7.8%. The results of 2.01 mm tube are predicted by Petukhov (1970) correlation with 5.1% MAE. For 1.1 mm tube, the average Nusselt number results in turbulent flow region are predicted by Petukhov (1970) correlation with 4.1% MAE. The correlation of Dittus and Boelter (1930) predicts the experimental Nusselt numbers of 4.26, 2.88 and 2.01 mm tubes with an MAE of 6.8, 5 and 5.7%, respectively. The prediction of Dittus and Boelter (1930) correlation for 4.26 mm coated tube is 6.1% MAE. The experimental Nusselt numbers of 1.1 mm tube for turbulent flow is predicted by Dittus and Boelter (1930) correlation with an MAE of 5%. The experimental Nusselt numbers for laminar flow region inside the 1.1 mm tube are predicted by Shah and London (1978) correlation with 7% MAE. All MAEs as deviations are within the uncertainty range of the average Nusselt number.

Table 3.19 Existing correlations from literature for the Nusselt number.

Author(s)	correlation
Dittus and Boelter (1930)	$Nu = 0.023Re^{0.8}Pr^{0.4}$ ($0.6 \leq Pr \leq 160$, $Re \geq 10000$ and $L/D \geq 10$)
Petukhov (1970)	$Nu = \frac{(f/8)\, Re\, Pr}{1.07 + 12.7\,(f/8)^{1/2}(Pr^{2/3} - 1)}$ $f = (0.79ln(Re) - 1.64)^{-2}$ ($10^4 < Re < 5 \times 10^6$, $0.5 < Pr < 2000$)
Shah and London (1978)	$Nu = \begin{cases} 1.953Gz^{1/3} & Gz \leq 33.3 \\ 4.364 + 0.0722Gz & Gz > 33.3 \end{cases}$ $Gz = Re\, Pr/(L/D)$

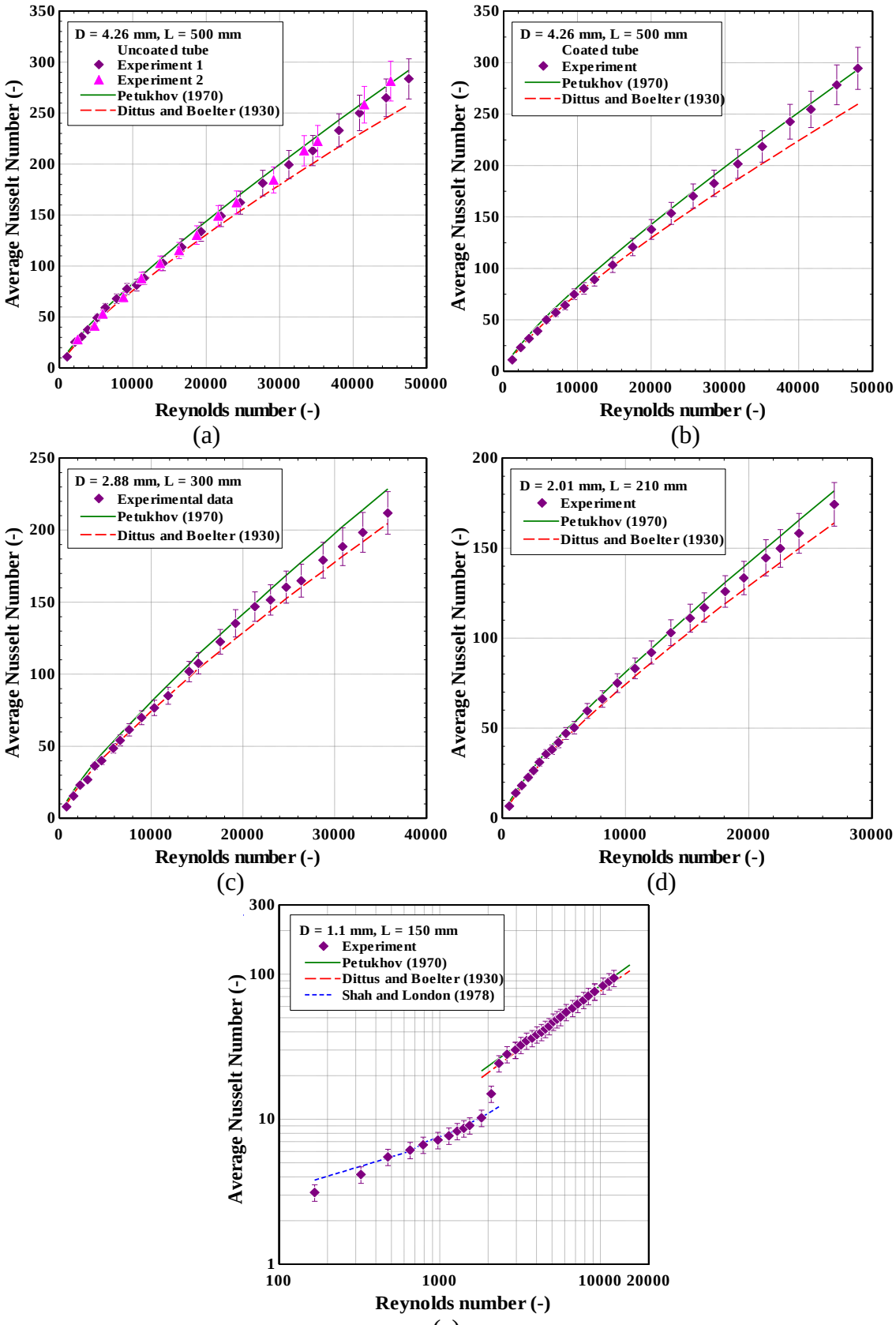

Figure 3.11 Single-phase Nusselt number validation for R245fa flowing at P = 300 kPa in: (a) 4.26 mm uncoated tube, (b) 4.26 mm coated tube, (c) 2.88 mm tube, (d) 2.01 mm tube and (e) 1.1 mm tube.

3.7 Experimental procedure

The experimental flow boiling procedure is conducted to acquire the data regarding flow pattern visualisation, local heat transfer coefficient and two-phase pressure drop simultaneously. In the beginning, the mass flux is fixed at the inlet of the test section where the system pressure is also regulated. The test facility is allowed a period of time to reach a steady state. This period experiences fluctuations of system pressure, mass flux and inlet temperature of the heating section. The R245fa fluid enters into heating section as subcooled flow with 15K subcooling. A small value of heat flux is provided to the heating section in order to do a test of single-phase flow. A single-phase flow test is carried out to determine the thermal loss coefficient which is employed to estimate the heat loss in flow boiling tests. Then, the inlet temperature is modified by adjusting the R22 flow in the sub-cooler or the power of the preheater. The subcooling temperature is reduced to become about 5 K. The facility is again given time to reach steady state. The high-speed camera is utilized for recording the visualisation of flow patterns concurrently while acquiring heat transfer data. It is worth mentioning that the test data are collected for about 90 seconds where the data acquisition frequency is within 1 Hz. The average value for the recorded sample is regarded as the nominal value for the single data point. The heat flux is increased to the heating section in equal increments. The heat flux is increased until the occurrence of dryout which is defined by monitoring the rapid signal fluctuation of the last thermocouples close to the test section outlet. When dry out occurs, the system is stopped to prevent damage to the test section. The values of the vapour quality cover a range from 0 up to 1. Then, the maximum imposed heat flux is reduced incrementally by the same magnitude that it was increased by, until a minimum value is again reached. This approach is repeated for each of the mass flux values while maintaining system pressure stability at the same value. Consequently, the experimental tests are performed by changing the heat flux while fixing the system pressure and mass flux. The acquired data are processed using the EES program for estimating the local heat transfer coefficient along the heating section and two-phase pressure drop.

3.8 Reproducibility of the experimental data

The data reproducibility is important to make sure of the reliability of the experimental data. The identical results of flow boiling heat transfer should be obtained

by reliable instrument measurements under the same conditions and procedures at different operational intervals. when decreasing the channel size, the repeatability of experimental data becomes difficult to attain. This is because that the flow boiling characteristics are significantly affected by the relative surface conditions of the inner tube wall. After one month of the first experiment, the same experimental conditions were selected for each tube to repeat the experiment. Figure 3.12 depicts the repeated data of the flow boiling experiments for each tube on a different day. The figure demonstrates

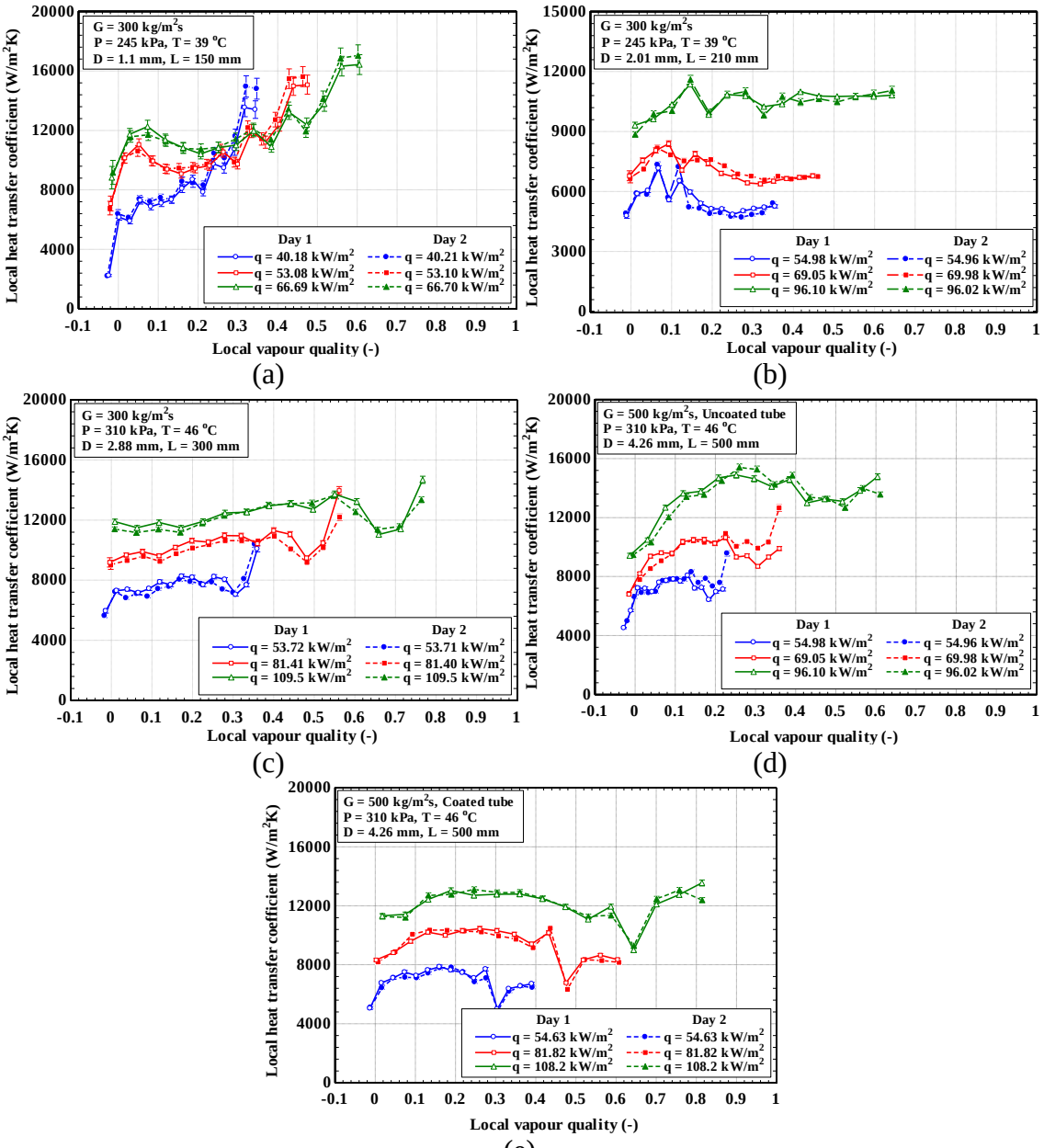

Figure 3.12 Reproducibility results of local heat transfer coefficient taken at two different times for: (a) 1.1 mm tube, (b) 2.01 mm tube, (c) 2.88 mm tube, (d) 4.26 mm uncoated tube and (e) 4.26 mm coated tube.

that the experimental data of local heat transfer coefficients are fairly repeatable with only minor deviations. These deviations may be due to the fluctuations in the system and the variation in the density of active nucleation sites. This good reproducibility of the experiments reveals appreciably the reliability and accuracy of the experimental system, i.e. reproducibility is within the experimental error.

3.9 Summary

The experimental test facility used to investigate the flow boiling of R245fa fluid in small-diameter tubes was described in this Chapter. The measuring instruments and operating procedure utilized to obtain the experimental data were also described. Five test sections have been developed to conduct flow visualisations, flow boiling heat transfer coefficient estimations and two-phase flow pressure drop measurements. The measuring instruments were carefully calibrated to reduce systematic errors and the uncertainties in key parameters were estimated through error propagation. Furthermore, single-phase flow validation was performed and the results confirm the accuracy of the measurements. In addition, the 4.26 mm smooth tube was coated with copper coating resulting in changes in its internal surface characteristics. There are more of fissures and pits in the internal surface, which could play an influential role in nucleation characteristics compared to the uncoated tube. Also, reproducibility of the flow boiling heat transfer data was checked by repeating the same experiment on a different day and satisfactory results were obtained for five tubes (1.1 - 4.26 mm). The slight deviations were in repeatability of experimental data under the same conditions and after one month of the first experiment. This may be due to the fluctuations in the system and the variation in the density of active nucleation sites. Commissioning data including flow regimes and pressure drop data are presented in Chapter 4 and Chapter 5, respectively. Heat transfer data follows in Chapter 6.

Chapter 4

Flow Patterns: Results and Discussion

4.1 Introduction

This chapter presents the flow boiling visualisation with a focus on studying basic principles of flow patterns and transition boundaries as well as the characteristics related to the flow boiling. The study has shown that a variety of flow regimes exhibits the different behaviour that affects the mechanism of heat transfer and pressure drop during flow boiling in small-diameter tubes. This chapter also presents experimental flow pattern maps. The coordinate system involves superficial liquid velocity versus superficial vapour velocity and mass flux versus vapour quality. The observed flow patterns and their transition boundaries are also compared with other flow pattern maps presented in the literature. These flow pattern maps were developed for mini- and micro-scale channels.

4.2 Experimental flow visualisation results

Flow boiling visualisation was conducted in a vertical borosilicate glass tube located after the circular stainless-steel heating section. The inner diameter of the glass tube is a similar to the inner diameter of the heating section so that the flow field is not affected by sudden contraction or expansion. This allows the investigation of the influence of heat flux, mass flux and system pressure on flow patterns and their transition boundaries. The two-phase visualisation experiments also involve increasing and decreasing heat flux to study the hysteresis influence on flow patterns in the small-diameter tube. The experimental conditions cover four inner diameter tubes of 1.1, 2.01, 2.88, and 4.26 mm, the mass flux range from 200 to 500 kg/m^{2}s, the heat flux range from 3 to 188 kW/m^2, three system pressurs of 185, 245, and 310 kPa and vapour quality range from 0 up to dryout. The dryout inception was defined by monitoring the rapid signal fluctuation of last thermocouples close to the test section outlet. When the liquid film was entirely

evaporated by convection, some hotspots started to occur near the test section outlet resulting in the inception of partial dryout. The visualisation of the flow regimes was recorded using a Phantom high-speed camera with frame rates of 1000 frames per second. The flow patterns are usually observed in flow boiling experiments for increasing and decreasing heat flux appeared in Figure 4.1 and Figure 4.2. The classification of observed flow patterns is illustrated below with some main observations, as follows:

Bubbly flow: Shortly after the departure of bubbles from nucleation sites, the bubble diameter increases to be corresponding to the tube diameter. The internal tube walls constrain the bubble growth in the radial direction. There is also heat transfer at the liquid-vapour interface for evaporation. This flow pattern is characterized by the distinctly non-spherical bubbles and almost bubbles with a shape of the cap, because of the small diameter of the tube. However, this flow regime might seem to prevail for very short lengths. In addition, this regime was only observed in situations of decreasing heat flux for all mass fluxes. It was observed that the bubbly flow regime predominates for very low vapour quality. In situations of increasing heat flux, the slug regime was observed immediately after the departure of the bubbles from the heated section. Furthermore, the bubbly regime may eventually be limited to a region near the entrance of the heat section at higher heat fluxes for a certain mass flux.

Slug flow: The confined vapour bubbles begin to grow in the axial direction and occupy nearly the full cross-section of the tube. Once the length of confined bubbles increases along the tube, the large vapour slugs are formed due to the convergence of the trailing bubble face with the back part of the leading bubble. Thus, the size of vapour slugs is very large compared to the size of the bubbles in the bubbly flow. In many cases, the tail of vapour slugs is wavy in addition to touching the tube walls, when the flow continues along the tube. Furthermore, the smaller bubbles are present between the two consecutive vapour slugs. This situation appears only in the 4.26 and 2.88 mm tube. For 2.01 and 1.1 mm tubes, the coalescence rate through the tube may be increased because of the confinement influence which leads to the disappearance of small bubbles. This flow regime is also distinguished by a very thin

liquid film that surrounds the longer vapour slug and is situated in the space between the tube walls and the longer vapour slug.

Churn flow: The flow pattern involves the occurrence of coalescing of two large vapour slugs to form the chaotic flow, and the tail of the slugs creates deformations in the liquid film which flows along the tube walls. Deformations in liquid layers are periodically observed. Occasionally, the annular flow pattern is also reached through churn flow at high mass fluxes.

Annular flow: A vapour in the tube core and a continuous flow of liquid film on the tube wall characterise the annular flow pattern. The tiny liquid droplets are entrained with vapour which flows in the tube core. The increase in vapour quality along the tube leads to a reduction in the liquid film thickness. In addition, the liquid film thickness decreases when heat flux increases in a particular location and this consequently leads to an occurrence of partial dryout.

The two-phase flow regimes in the four test sections having different internal diameter with increasing heat fluxes are presented in Figure 4.1 at the condition of 185 kPa system pressure and 200 kg/m^{2}s mass flux. According to Figure 4.1a and Figure 4.1b, some bubbles appear between successive vapour slugs as seen in the red circle. However, these bubbles vanish as the tube diameter is decreased to 2.01 mm as shown in Figure 4.1c. In addition, it is also observed that the length of slug bubbles increases when the tube diameter decreases from 4.26 mm to 2.01 mm. The slug is also distinguished by a longer tail at these conditions. This case indicates that the effect of confinement increases with a decrease in tube diameter. In other words, the reduction in tube diameter leads to increased collisions between departure bubbles and thus an increase in the coalescence rate. Furthermore, the slug, churn, and annular flows are seen in all tubes except for the 1.1 mm tube. Figure 4.1c displays only the churn and annular flow regimes inside tube 1.1 mm. The same flow regimes were observed by Consolini and Thome (2009) for R245fa in 0.51 and 0.79 mm tubes. The slug flow regime is not observed in this tube, as previously mentioned, the reason can be attributed to the effect of a reduction in tube diameter and consequently an earlier transition to annular flow. The reason for this in fact

that the Reynolds number decreases with decreasing tube size. This indicates that flow field transitions from turbulent flow into laminar flow. Also, the surface tension force has a significant influence on flow patterns as channel size becomes smaller according to two-phase flow studies in the literature, such as Kandlikar and Grande (2003) and Ong and Thome (2011a). It follows the strong surface tension forces maintain the form of vapour slug until it reaches a higher vapour quality to break up the surrounding liquid film. On the other hand, the topography of inner tube surface plays an important role in increasing the density of nucleation sites which affect the departure bubble frequency, departure bubble size and coalescence mechanism rate. This means that the number and size of active nucleation cavities existed on the surface of channel walls affect bubble generating rate, wherever the bubbles generated with a large size help to induce the occurrence of collisions between them and then coalescence. This phenomenon leads to an increase in vapour velocity, with the formation of a thin liquid film on channel walls, and subsequently an early transition to annular flow. Furthermore, the influence of tube length on vapour quality is not evident because of the mass flow rate increases with the tube diameter. In other words, the vapour quality increases as the length-diameter ratio (*L/D*) increases.

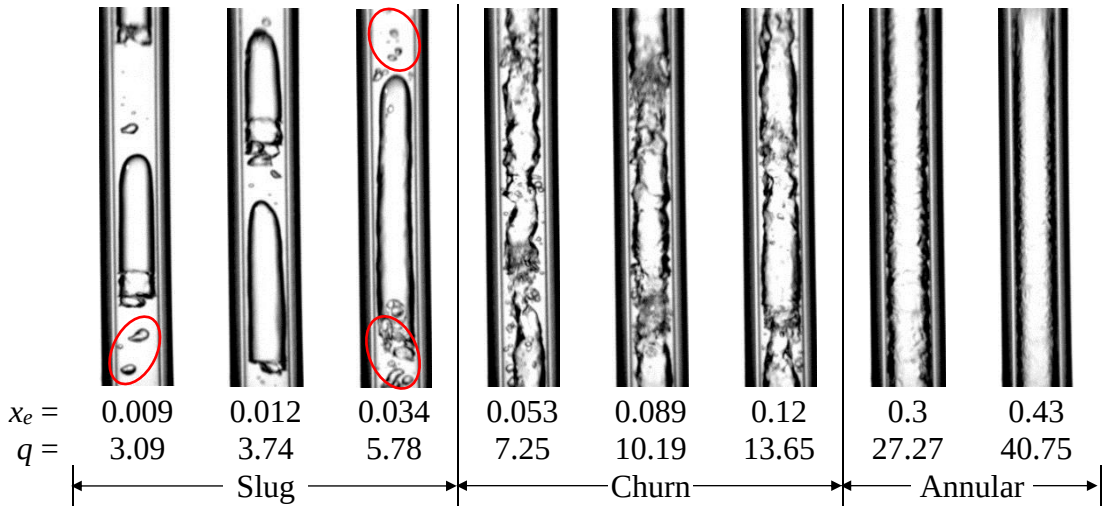

(a) 4.26 mm tube.

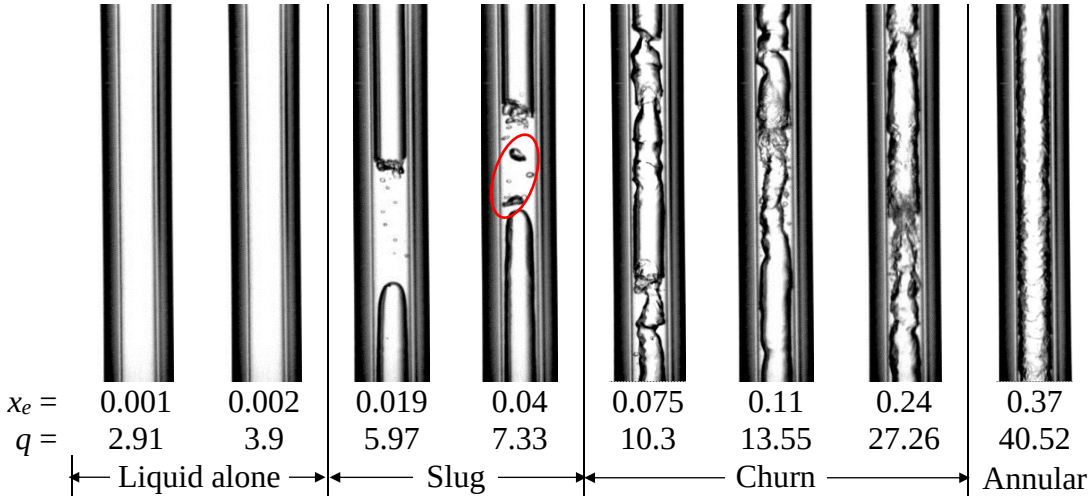

(b) 2.88 mm tube.

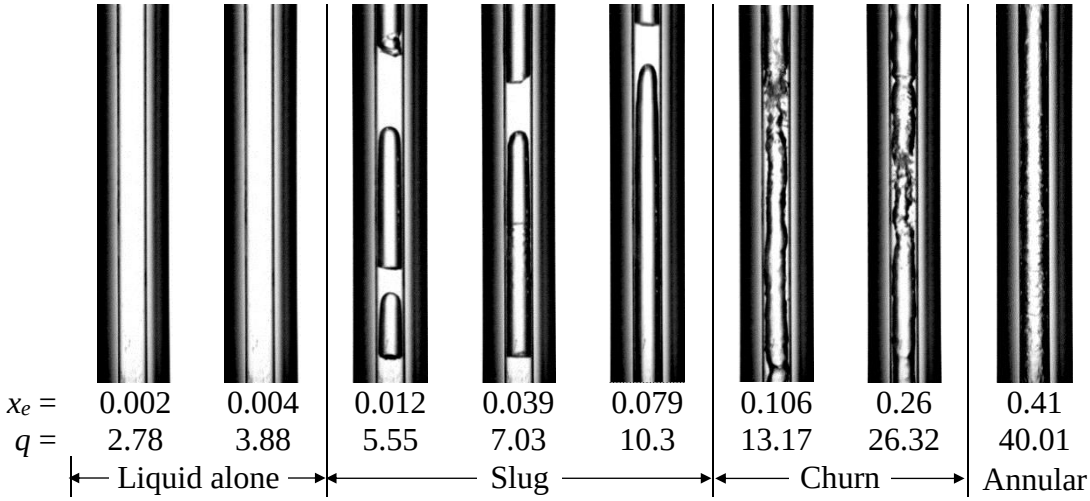

(c) 2.01 mm tube.

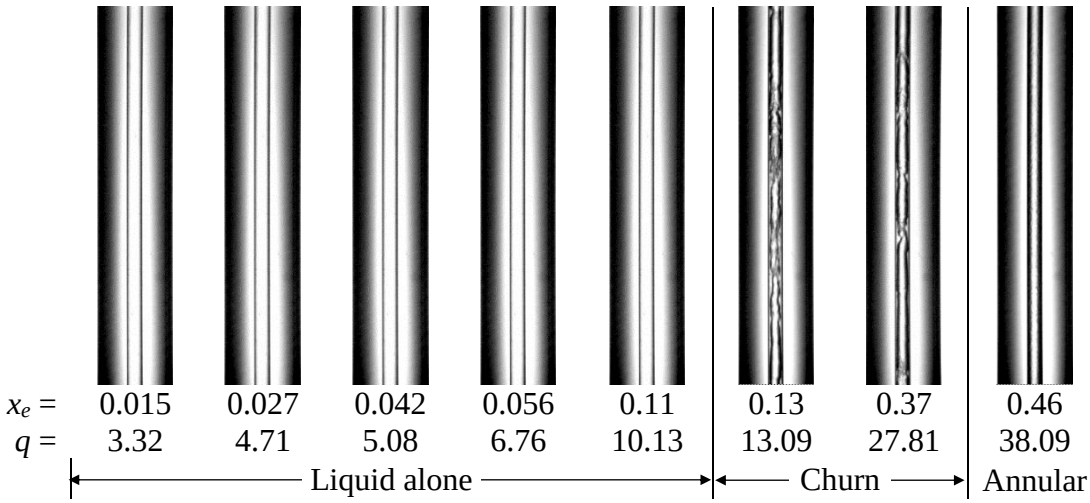

(d) 1.1 mm tube.

Figure 4.1 Flow patterns captured at P = 185 kPa and G = 200 kg/m^{2}s for increasing heat flux during the flow boiling of R245fa in diameter tube of: (a) 4.26 mm, (b) 2.88 mm, (c) 2.01 mm, and (d) 1.1 mm.

The hysteresis influence on two-phase flow patterns was also investigated by carrying out the experiments with increasing and decreasing heat flux. The observed flow patterns with decreasing heat flux are shown in Figure 4.2. The applied heat flux was reduced step by step as similar as the former procedure to increase heat flux. All the flow regimes distinguished with increasing heat flux are also observed with decreasing heat flux. However, the bubbly flow was seen in all tubes. This means that some nucleation sites become active and generate bubbles even at very low heat fluxes. The absence of these flow patterns in increasing heat flux is due to the nature of R245fa refrigerant which requires a high degree of superheat for the onset of nucleate boiling during the flow boiling process. This phenomenon is in agreement with the previous study of Karayiannis et al. (2014) which was conducted at the same facility with 1.1 mm stainless-steel tube and length of 300 mm. They reported that the hysteresis phenomenon occurs with decreasing heat flux experiments. In this case, the reason is attributed to activating more nucleation sites at higher heat flux, in the procedure of increasing heat flux experiments. Thus, these nucleation sites remain active as the heat flux is reduced. Several studies in the literature have been conducted on the density of active nucleation sites (N_a) that gave the dependence of nucleation site density as a function of heat flux, wall superheat, and radius of the available active cavity. According to the Gaertner and Westwater (1960) and the Cornwell and Brown (1978) studies, the density of active nucleation site is directly proportional to heat flux, and the wall superheat by the power of 2.1 and 4.5, respectively (i.e. $N_a \sim q^{2.1}$ and $N_a \sim \Delta T_{sat}^{4.5}$). Additionally, the nature of refrigerant R245fa required higher wall superheat to start the onset of nucleate boiling due to its thermophysical properties. Consequently, the more nucleation sites become active only until higher heat flux is reached and remain active during experiments of increasing heat flux.

4.3 Experimental flow pattern maps

A flow pattern map is a two-dimensional plot used to predict the flow regimes and transition boundaries. The coordinates employed to draw the map vary from variables such as mass flux and vapour quality to superficial velocities of both vapour and liquid phases. Several maps are present in the literature such as Cheng et al. (2008b) and Mahmoud and Karayiannis (2016) indicating that the prediction of flow regimes is still regularly updated to reflect the complexity of flow boiling patterns. To check the flow

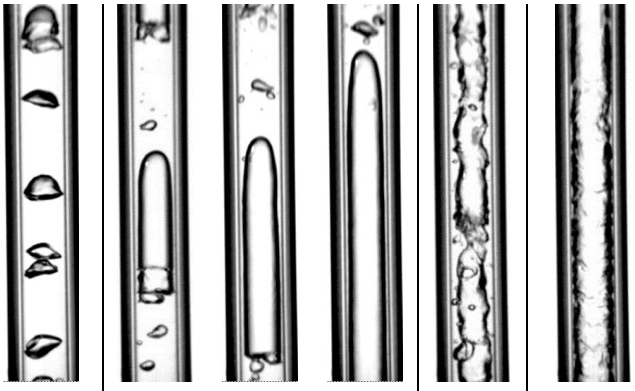

x_e =	0.001	0.01	0.031	0.038	0.052	0.302
q =	3.16	3.77	5.28	5.92	7.39	27.28
	Bubbly	← Slug →			Churn	Annular

(a) 4.26 mm tube.

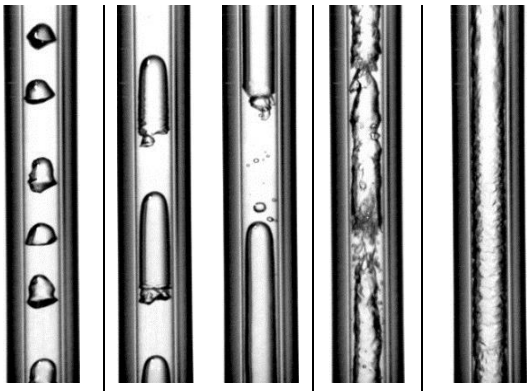

x_e =	0.003	0.028	0.043	0.078	0.456
q =	4.04	5.98	7.35	10.28	44.91
	Bubbly	← Slug →		Churn	Annular

(b) 2.88 mm tube.

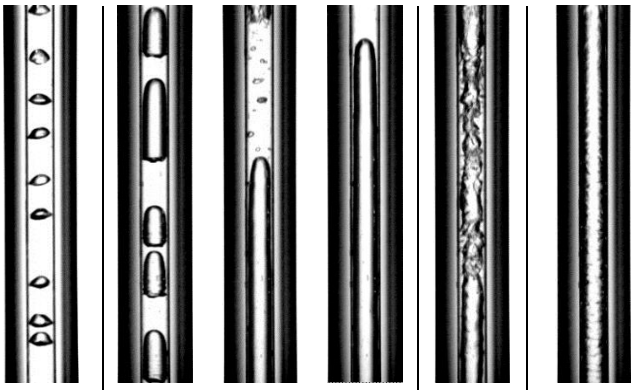

x_e =	0.002	0.018	0.041	0.075	0.109	0.401
q =	5.301	5.77	7.33	10.34	13.2	40.03
	Bubbly	← Slug →			Churn	Annular

(c) 2.01 mm tube.

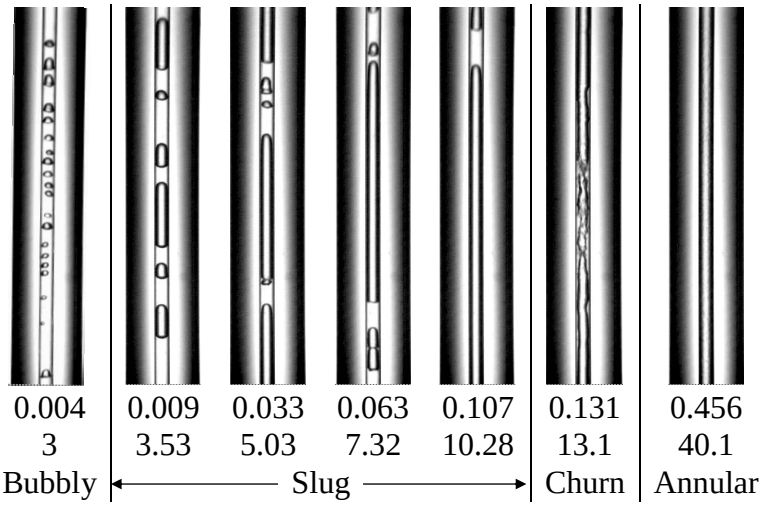

(d) 1.1 mm tube.

Figure 4.2 Flow patterns captured at P = 185 kPa and G = 200 kg/m^{2}s for decreasing heat flux during the flow boiling of R245fa in diameter tube of: (a) 4.26 mm, (b) 2.88 mm, (c) 2.01 mm, and (d) 1.1 mm.

patterns and their transitions defined in the previous section, the experimental data is plotted using the method suggested by Taitel et al. (1980) or by Revellin and Thome (2007a). The flow patterns (bubbly, slug, churn, and annular) captured during R245fa flow boiling in four vertical tubes (1.1, 2.01, 2.88, 4.26 mm) and characterised in the former section are plotted to show different flow regime zones on a graph.

The flow pattern maps in terms of liquid and vapour superficial velocities gives a clear view of flow regime variations with increasing superficial vapour velocity. Figure 4.3 – Figure 4.5 show flow pattern maps for the results of this work at a saturation temperature of 31, 39, and 46 °C, respectively, where the symbols represent the flow pattern data for increasing and decreasing heat flux experiments and the solid lines are the transition boundaries between different flow regimes. With the increase in vapour quality along the test section, the superficial vapour velocity increases. In increasing heat flux experiments, the flow patterns change from slug to churn and then to annular except in the tube of 1.1 mm diameter tube for all saturation temperatures and also a tube of 2.01 mm for saturation temperature of 46 °C. However, bubbly flow was not observed in all tubes as well as the slug flow was mostly seen at lower mass flux.

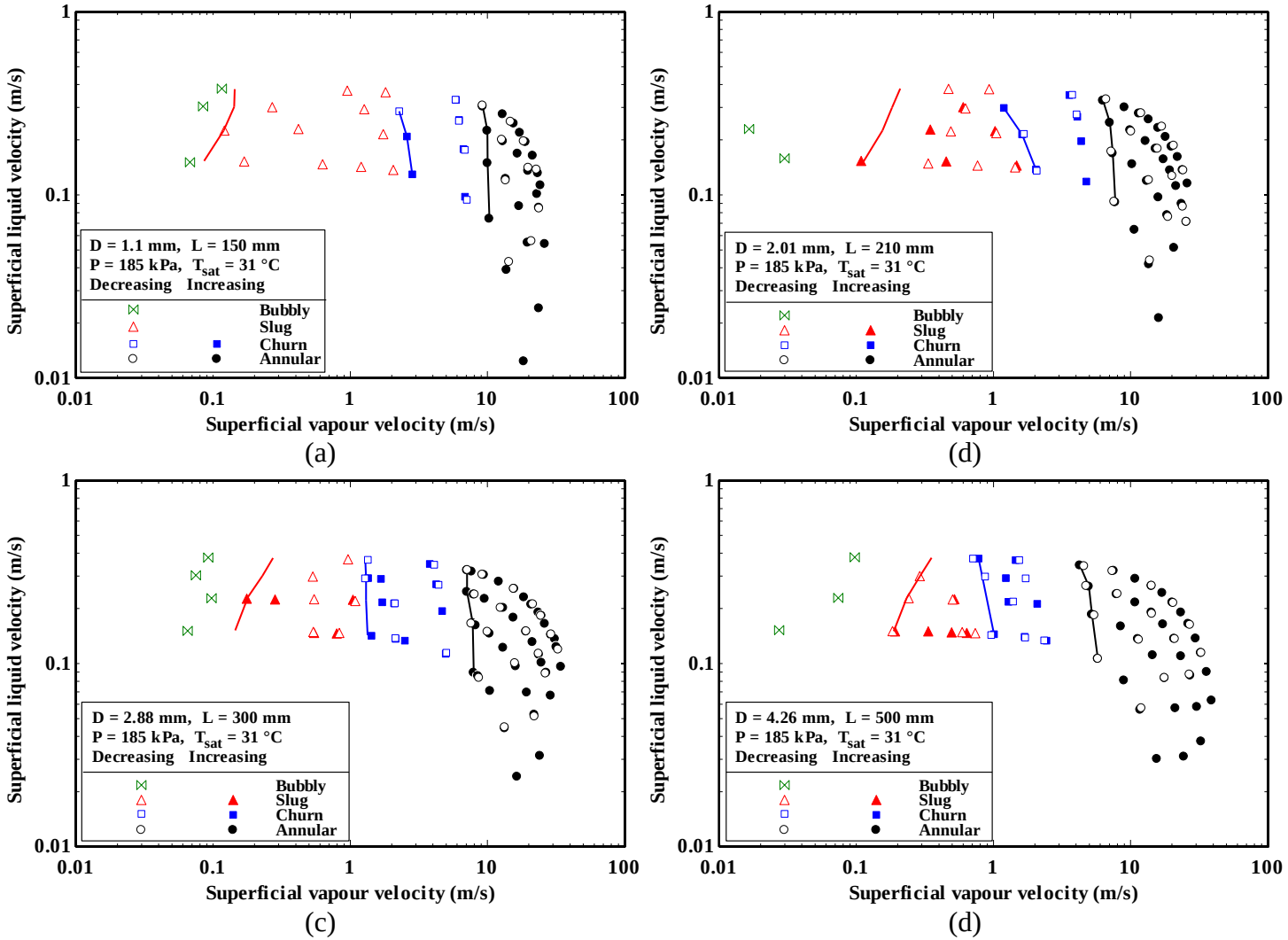

Figure 4.3 Experimental flow pattern map in terms of liquid and vapour superficial velocities at T_{sat} = 31ºC for: (a) D = 1.1 mm, (b) D = 2.01 mm, (c) D = 2.88 mm, and (d) D = 4.26 mm.

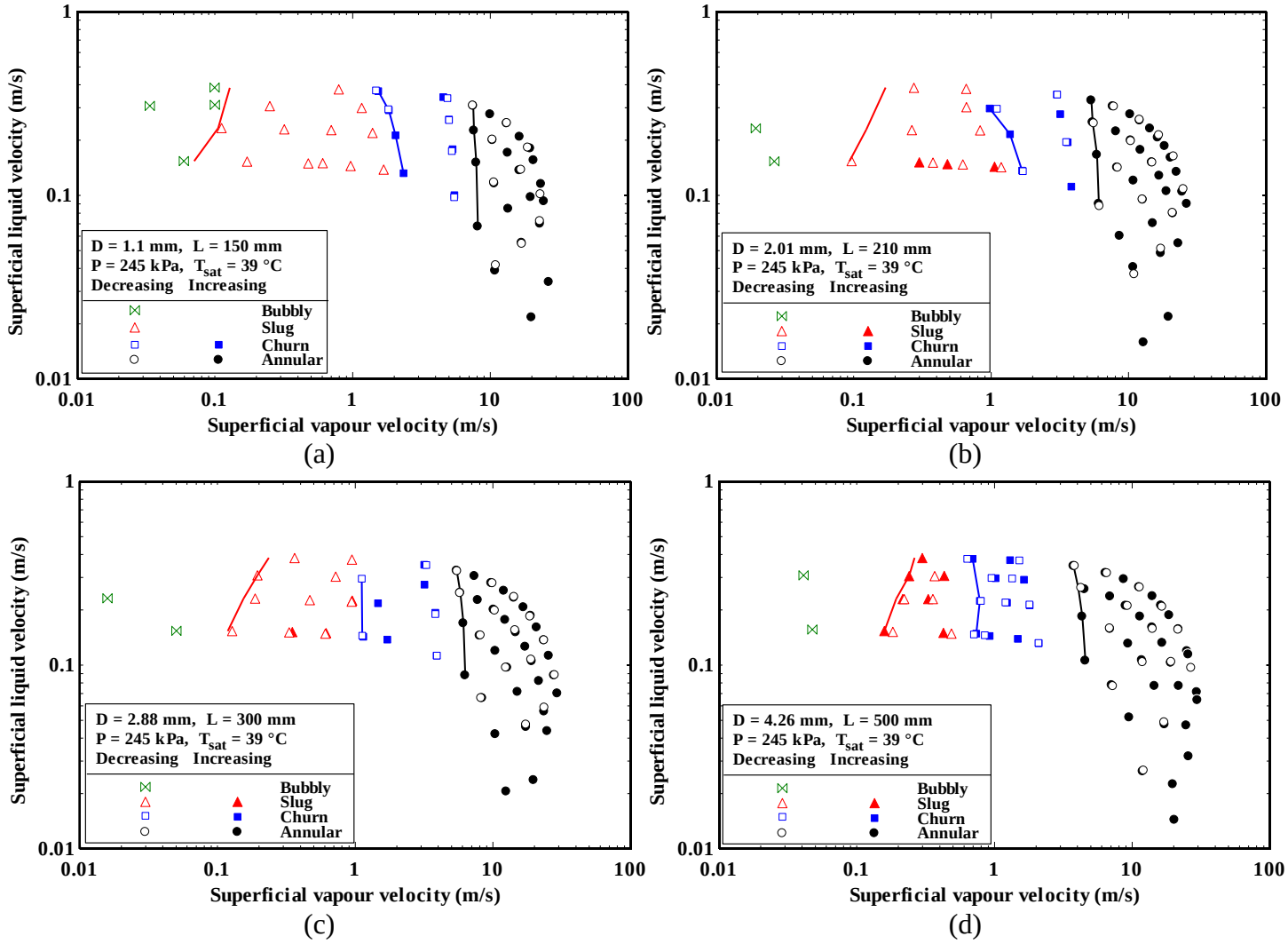

Figure 4.4 Experimental flow pattern map in terms of liquid and vapour superficial velocities at pressure corresponding to T_{sat} = 39 ºC for: (a) D = 1.1 mm, (b) D = 2.01 mm, (c) D = 2.88 mm, and (d) D = 4.26 mm.

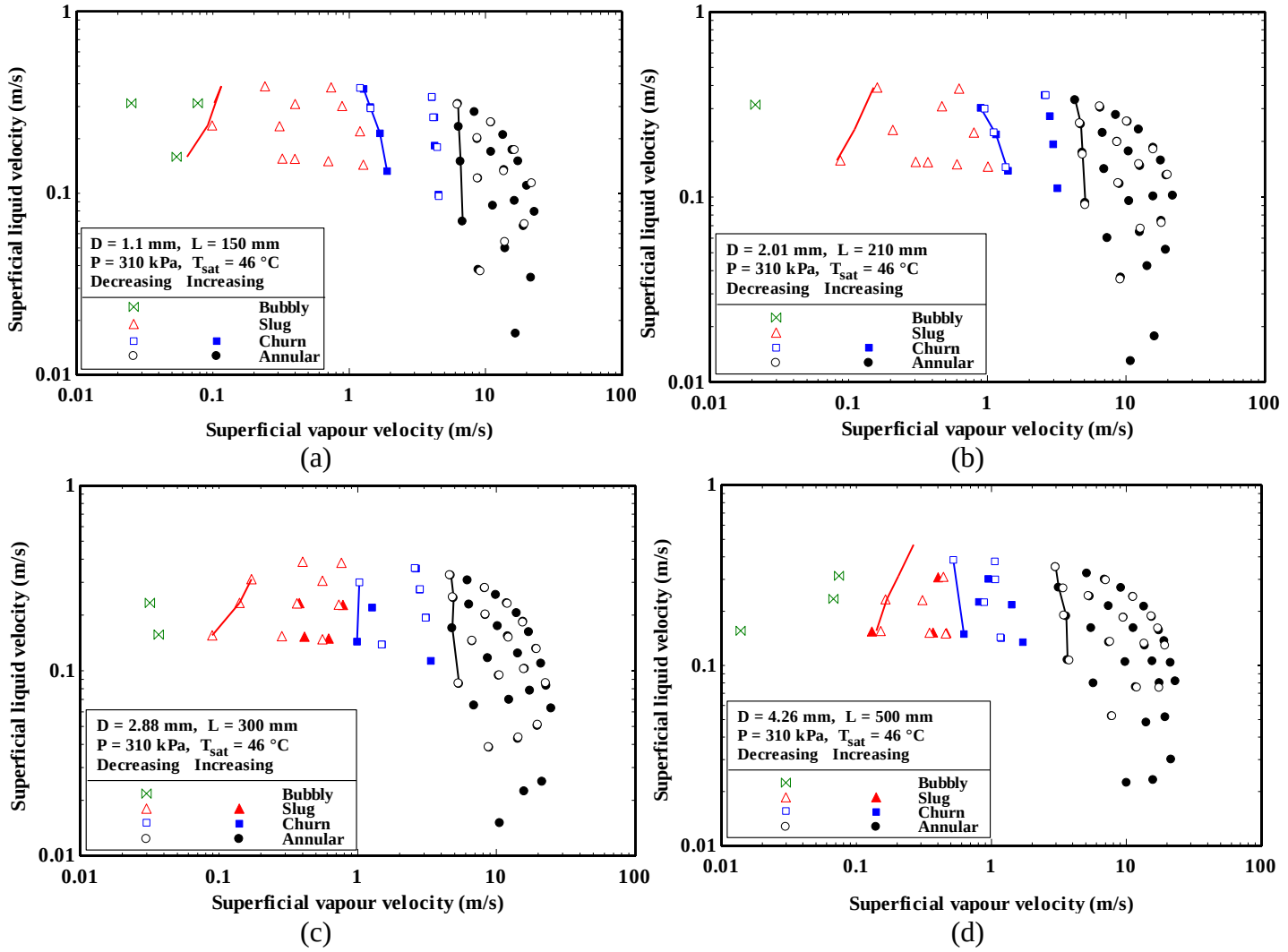

Figure 4.5 Experimental flow pattern map in terms of liquid and vapour superficial velocities at pressure corresponding to T_{sat} = 46 ºC for: (a) D = 1.1 mm, (b) D = 2.01 mm, (c) D = 2.88 mm, and (d) D = 4.26 mm.

The flow pattern maps in terms of mass flux and vapour quality are shown in Figure 4.6 – Figure 4.8 for saturation temperatures of 31, 39, and 46 °C, respectively. The annular flow is the dominant flow regime in the current tests as can be seen in these figures. The transition to annular flow shifts towards lower vapour qualities as the mass flux increases and this trend is in agreement with the previous study of Pike-Wilson (2014) or Karayiannis et al. (2014) which was conducted for a circular, vertical stainless-steel tube of 1.1 mm inner diameter.

4.4 Effect of mass flux

The flow regimes in vertical small-diameter tubes, vary with mass flux and vapour quality resembling those of other fluids such as R134a and R236fa, see Figure 4.6. The effect of mass flux on transition boundaries of flow patterns is noticeable, where the initial transition vapour qualities of flow patterns tend to decline. It is observed that the onset of transition vapour quality for annular flow is larger for the 200 kg/m^{2}s mass flux, while it is smaller for 500 kg/m^{2}s mass flux. The explanation of this case is that due to the larger mass flux is resulted a decrease in vapour quality corresponding to flow pattern transition boundaries. Consequently, the range of annular flow extends to low vapour qualities, and in contrast, the range of vapour quality relating to churn flow and slug flow becomes narrower. This behaviour of vapour quality values for flow pattern transitions was similar to other studies of Revellin and Thome (2007a), Martín-Callizo et al. (2010), Arcanjo et al. (2010), Ong and Thome (2009), Sempértegui-Tapia et al. (2013), Charnay et al. (2014a) and Abadi et al. (2016).

4.5 Effect of system pressure

The pressure influence on flow pattern transitions in terms of liquid and vapour superficial velocities is illustrated in Figure 4.9. Transition boundaries from bubbly to slug flow, slug to churn flow and churn to annular flow shift to lower superficial vapour velocities for pressure corresponding to T_{sat} = 31 ºC compared to a pressure corresponding to T_{sat} = 46 ºC. The effect of system pressure on flow pattern transitions in terms of mass flux against vapour quality can also be seen in Figure 4.10, where the transition for slug-

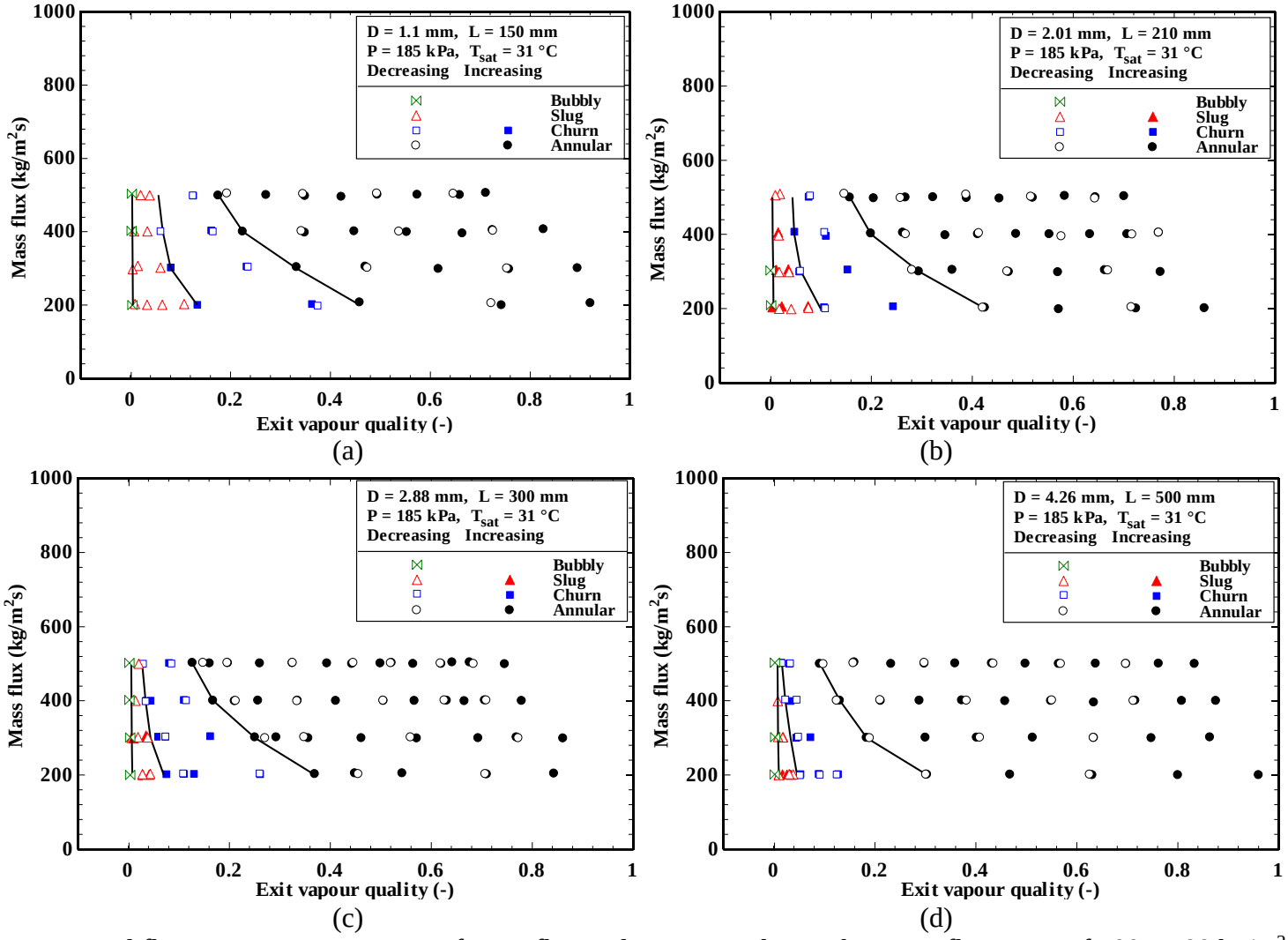

Figure 4.6 Experimental flow pattern map in terms of mass flux and vapour quality with a mass flux range of 200 – 500 kg/m^{2}s at pressure corresponding to T_{sat} = 31 ºC for: (a) D = 1.1 mm, (b) D = 2.01 mm, (c) D = 2.88 mm, and (d) D = 4.26 mm.

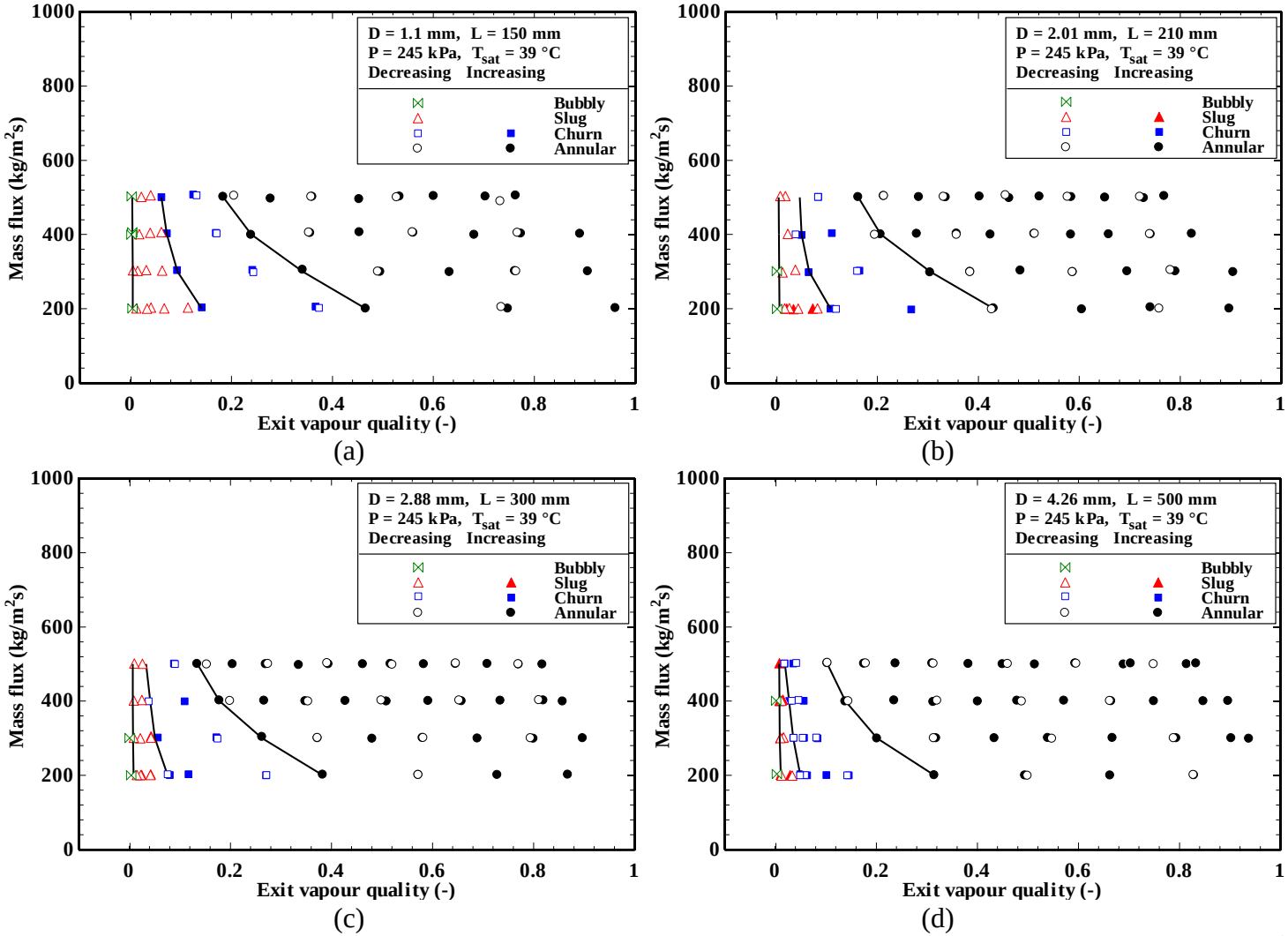

Figure 4.7 Experimental flow pattern map in terms of mass flux and vapour quality with a mass flux range of 200 – 500 kg/m^{2}s at pressure corresponding to T_{sat} = 39 ºC for: (a) D = 1.1 mm, (b) D = 2.01 mm, (c) D = 2.88 mm, and (d) D = 4.26 mm.

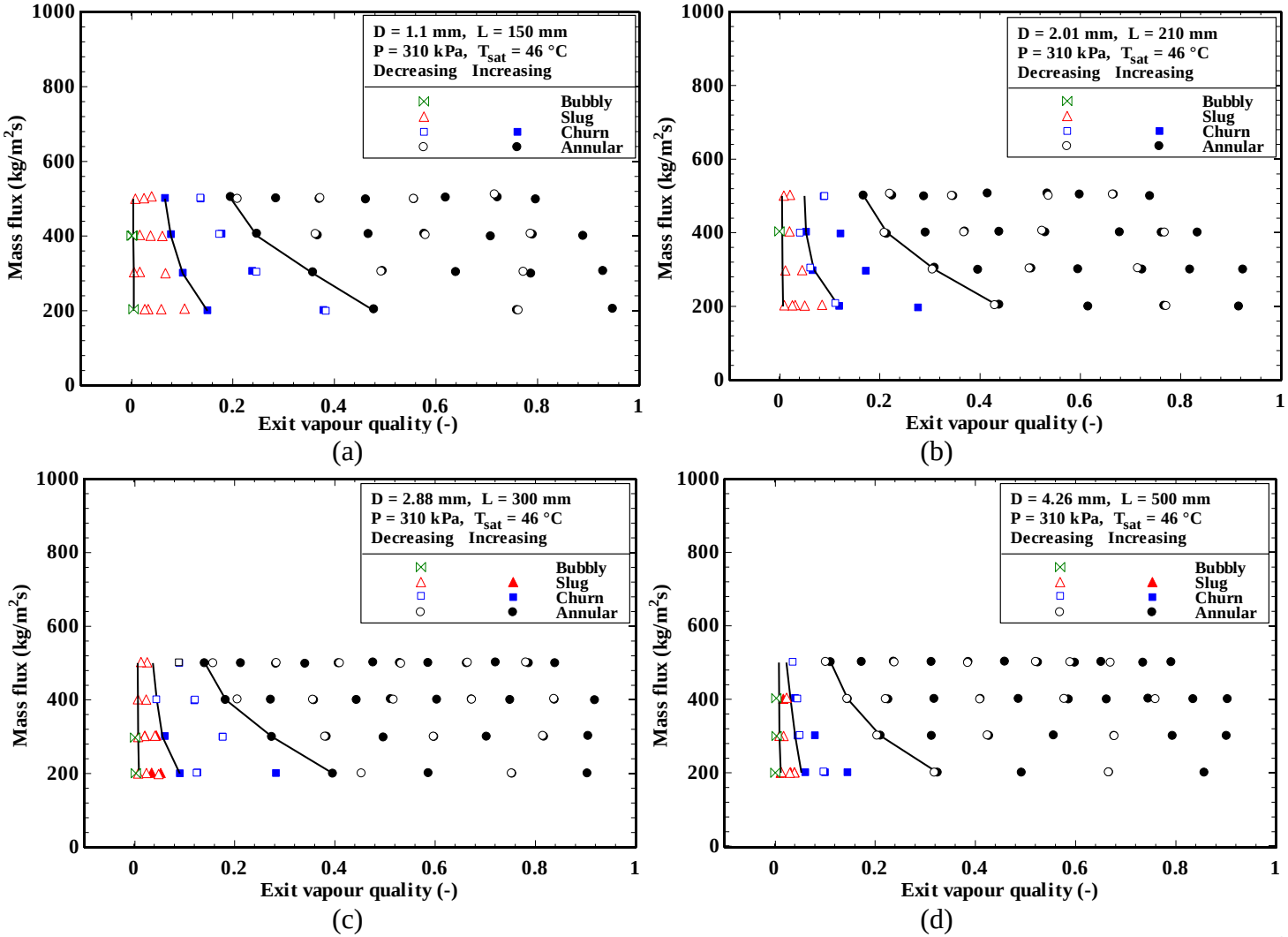

Figure 4.8 Experimental flow pattern map in terms of mass flux and vapour quality with a mass flux range of 200 – 500 kg/m^{2}s at pressure corresponding to T_{sat} = 46 ºC for: (a) D = 1.1 mm, (b) D = 2.01 mm, (c) D = 2.88 mm, and (d) D = 4.26 mm.

churn and churn-annular flow move to higher vapour qualities, for a higher pressure. The difference in flow pattern transition boundaries for the three saturation temperatures can be explained by the difference in the ratio of liquid to vapour density. In other words, the thermodynamic properties of R245fa vary with system pressures as listed in Table 3.5. For example, the vapour density will be equal to 10.56 and 17.35 kg/m^3 at system pressures corresponding to 31 and 46 ºC saturation temperatures, respectively. It can be seen that the lower the saturation temperature gives lower vapour density (i.e. higher ρ_l/ρ_v ratio). This leads to a high vapour velocity which may consequently bring about the change in a flow pattern from slug to churn and eventually transition to annular flow regime earlier than that at higher system pressure. Therefore, the vapour quality corresponding to transitions of flow regime has a tendency to increase with increasing system pressure (i.e. the transition boundaries move towards high vapour qualities). On the other hand, the effect of surface tension during flow boiling process is to keep a bubble shape and hold up of liquid on the tube walls. The decrease in system pressure leads to an increase in surface tension and liquid viscosity as shown in Table 3.5. This, in turn, results in making it difficult to change the bubble shape and difficult to form a continuous vapour core in the centre of the tube. Furthermore, the difficulty of moving the liquid film surrounding slug bubble towards churn flow and then annular flow requires high vapour velocities. Simultaneously, the thickness of the liquid film is affected by surface tension and liquid viscosity. These factors contribute to increasing vapour qualities corresponding to flow pattern transitions, with increasing system pressure. This phenomenon agrees with the similar observations in previous studies for Arcanjo et al. (2010), Zhu et al. (2017a) and Yang et al. (2018a). In addition, the shift in the flow pattern transitions towards lower superficial vapour velocities has significant effect on the two-phase pressure drop and flow boiling heat transfer coefficient. In other words, the high pressure reduces a vapour velocity and consequently reduces a void fraction. This leads to a decrease in the two-phase pressure drop. Also, the high pressure decreases the latent heat of vaporization. The vapour quality is inversely proportional to the latent heat of vaporization (see Equation (3.47)). This, in turn, results in the increase of vapour quality giving rise to the thickness of the liquid film on the hot surface to be thinner. Accordingly, the heat transfer rate between the hot surface and the liquid-vapour interface increases ($\alpha = k/thickness\ of\ liquid\ film$) and consequently increasing the heat transfer coefficient.

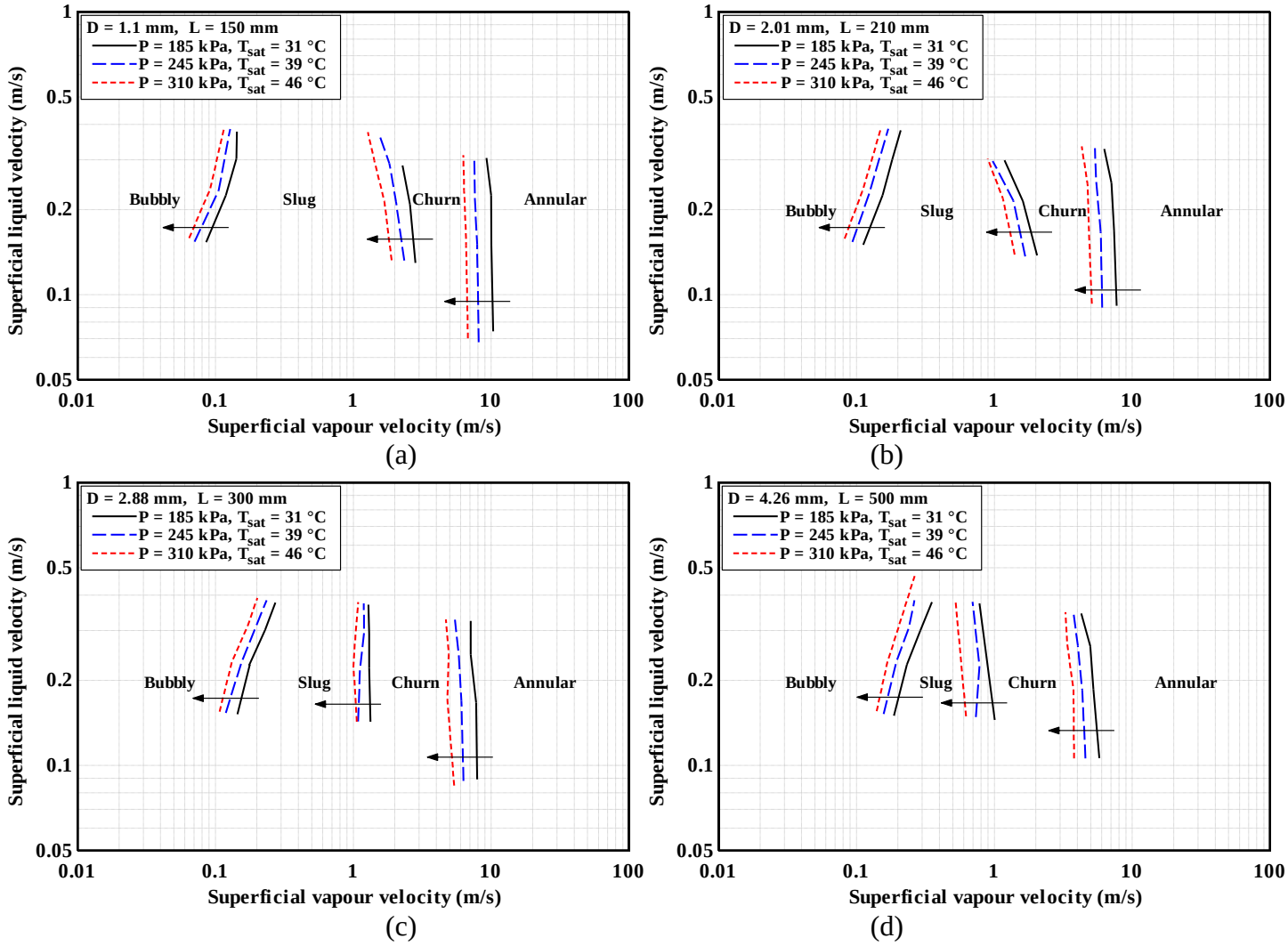

Figure 4.9 Effect of system pressure on experimental flow pattern transitions in terms of liquid and vapour superficial velocities for: (a) D = 1.1 mm, (b) D = 2.01 mm, (c) D = 2.88 mm, and (d) D = 4.26 mm.

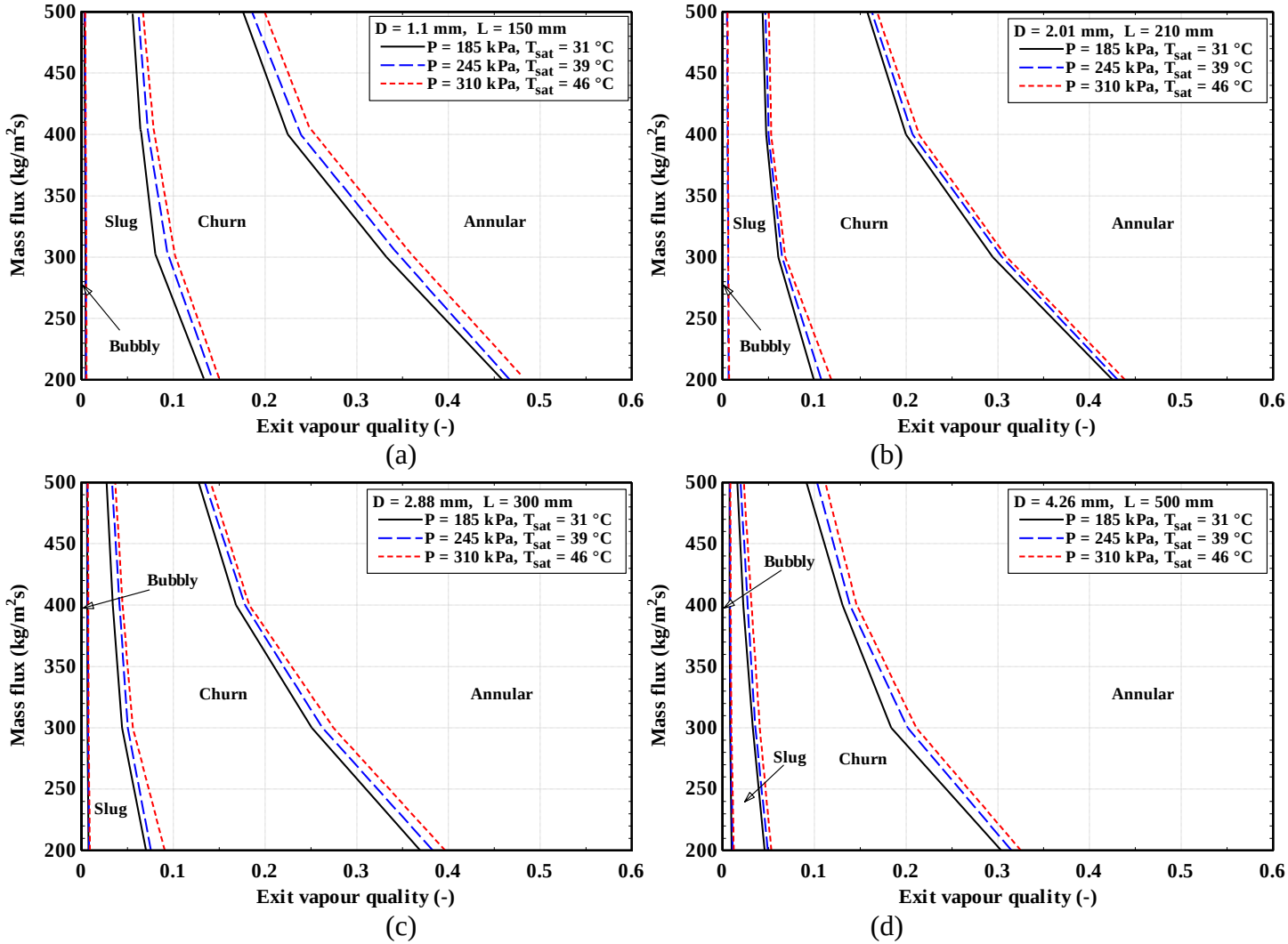

Figure 4.10 Effect of system pressure on experimental flow pattern transitions in terms of mass flux and vapour quality for: (a) D = 1.1 mm, (b) D = 2.01 mm, (c) D = 2.88 mm, and (d) D = 4.26 mm.

4.6 Effect of channel diameter

The tube diameter influence on flow pattern transitions has been assessed by comparing the four tubes of 4.26, 2.88, 2.01, and 1.1 mm inner diameter. The transition boundaries for four tubes are plotted together in terms of liquid and vapour superficial velocities, and also in terms of mass flux and vapour quality for three saturation temperatures (31, 39, and 46 ºC), as depicted in Figure 4.11 and Figure 4.12, respectively. According to Figure 4.11, the transition from bubbly to slug flow for all tubes occurs at slightly lower superficial vapour velocity. This transition also takes place at lower vapour qualities as shown in Figure 4.12. Additionally, the bubbly-slug transition line is shifted towards lower superficial vapour velocities with reducing tube diameter. This case may be attributed to increased confinement of vapour bubbles with decreasing tube diameter, leading to an increase in the coalescence rate of departure bubbles. There is another reason, the frequency of vapour bubble departure is increased by increasing active nucleation sites with increasing heat flux. According to Owhaib et al. (2007) and Ali et al. (2013), the bubble departure frequency is higher for the smaller-diameter tubes. It may mean that the transition from bubble to slug will occur earlier in smaller-diameter tubes. This result is in agreement with Ali et al. (2013), Chen et al. (2006), Coleman and Garimella (1999) and Zhao and Bi (2001). However, the slug-churn and churn-annular transition boundaries are delayed to higher vapour qualities when the tube diameter decreases, i.e. they move to higher superficial vapour velocities as channel size becomes smaller. This phenomenon is similar to the report of Ali et al. (2013) and Chen et al. (2006). According to two-phase flow studies in literature, the surface tension force has a significant influence on flow patterns as channel size becomes smaller. It follows that the strong surface tension forces maintain the form of vapour slug, until it reaches a higher superficial vapour velocity or higher vapour quality, corresponding to flow pattern transition. Moreover, the tube length has a significant influence on the exit vapour quality. That is, the vapour quality increases when the tube length increases at the same tube diameter and heat flux. However, the decrease of tube diameter results in decreasing the mass flow rate in a tube. Since the vapour quality is inversely proportional to the mass flow rate, this results in significantly lower vapour quality compared to the tube length effect. Therefore, the effect of tube length is not evident.

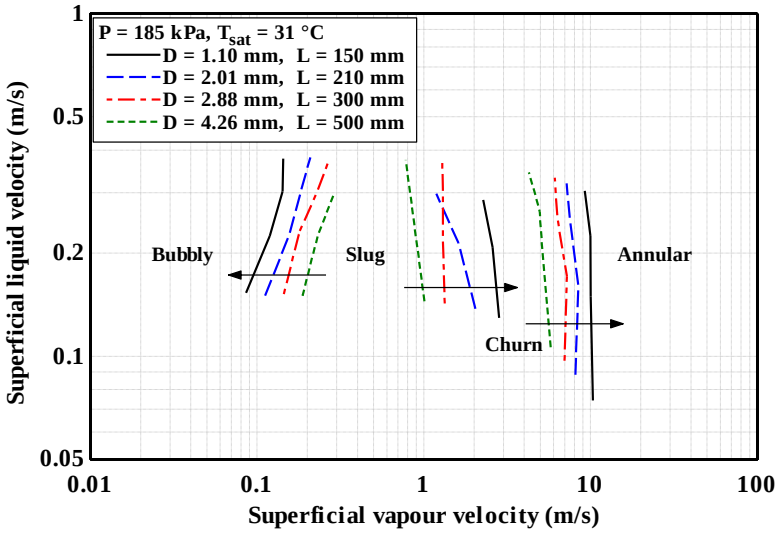

(a)

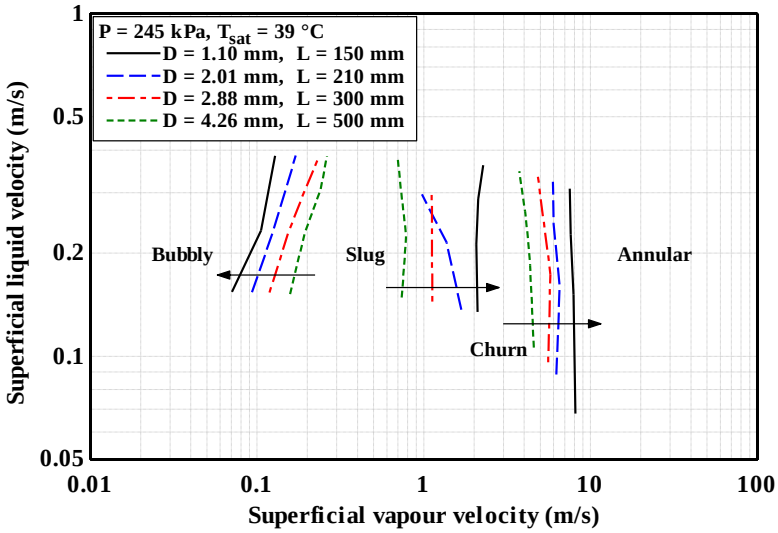

(b)

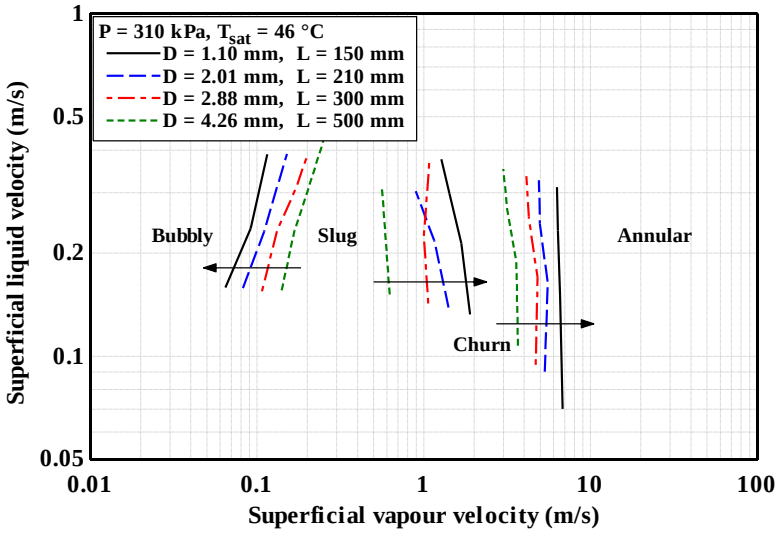

(c)

Figure 4.11 Effect of channel diameter on experimental flow pattern transition lines in terms of liquid and vapour superficial velocities for pressures corresponding to: (a) T_{sat} = 31 ºC, (b) T_{sat} = 39 ºC, and (c) T_{sat} = 46 ºC.

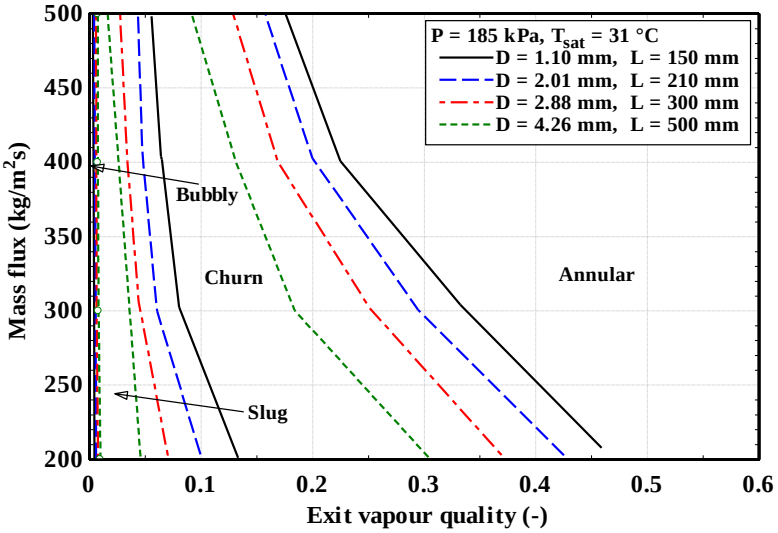

(a)

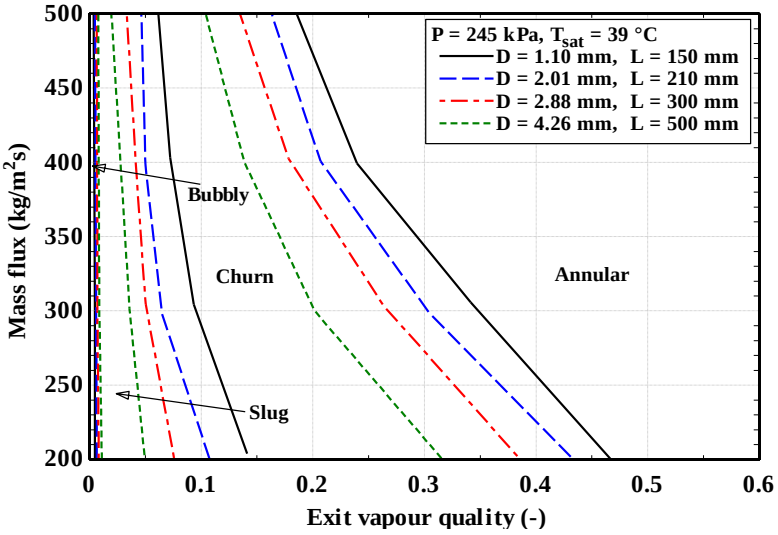

(b)

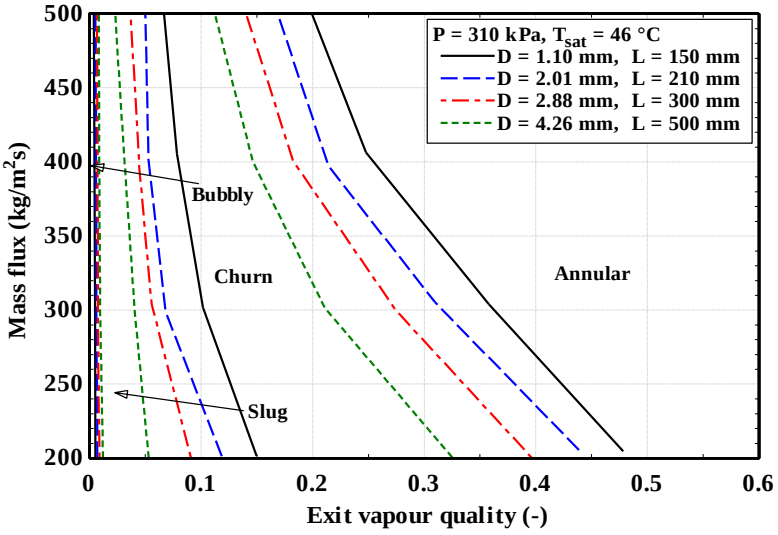

(c)

Figure 4.12 Effect of channel diameter on experimental flow pattern transition lines in terms of mass flux and vapour quality for pressures corresponding to: (a) T_{sat} = 31 ºC, (b) T_{sat} = 39 ºC, and (c) T_{sat} = 46 ºC.

4.7 Comparison with previous flow pattern maps

Comparison carried out with flow pattern maps for mini- and micro-scale channels was in order to assess the general applicability of flow patterns and flow pattern maps. As discussed earlier in Chapter 2, the Literature Review, there is no generally agreed universal flow pattern map available for small-scale tubes. In the current work, a set of R245fa flow patterns for increasing heat flux experiments is limited because this fluid needs high wall superheat in order to initiate boiling. Therefore the comparison with flow regime maps includes only the data for decreasing heat flux experiments. The present flow pattern maps of Figure 4.3 and Figure 4.6 are compared with the existing transition models and correlations for vertical and horizontal flow in the mini- and micro-channels, as follows:

4.7.1 Revellin and Thome (2007a) flow regime map

In the continued development of the flow pattern map, Revellin and Thome (2007a) provided a new map termed the diabatic coalescing bubble map based on a new classification of observed flow regimes. This classification could be very similar to the three-zone model for two-phase heat transfer predictions that was offered by Thome et al. (2004). For distinct, the observed flow regimes distinguished by three types, namely isolated bubble regime (bubbly and slug flow), coalescing bubble regime (the rate of bubble coalescence is much greater than that of bubble frequency) and annular regime (from the end of bubble coalescence process to the inception of critical heat flux). The authors developed their map for horizontal micro-evaporators based on database covering two fluids (R134a and R245fa), two microtubes (0.509 mm and 0.79 mm), three saturation temperatures (26, 30, and 35°C), mass fluxes from 200 to 2000 kg/m^{2}s, heat fluxes until 597 kW/m^2 and vapor qualities from 0 to 0.95. The authors also considered the influences of mass and heat fluxes, channel size and fluid properties on flow regimes in the establishment of flow map. The map was coordinated in terms of mass flux as ordinate and vapour quality as abscissa. The models of transition boundaries from isolated bubble flow (IB) to coalescing bubble flow (CB) and coalescing bubble flow (CB) to annular flow (A) are given in Appendix A. It is believed that the channel orientation does not significantly affect flow pattern characteristics in the vertical and horizontal micro-channels because of the diminishing of the effect of gravitational forces with the

predominance of surface tension forces. Therefore, the comparisons between the experimental data of current work and the predictions by the Revellin and Thome (2007a) flow pattern map is shown in Figure 4.13. The criterion of the IB-CB transition is located close to transition boundary from bubbly to slug flow for all tubes, especially, for high mass flux. The map predicts well the churn-annular transition only for 1.1 mm tube but not for other tubes. However, the CB-annular transition criterion moves towards high vapour quality, contrary to the churn-annular transition of the present experimental data which shifts to low vapour quality with increasing tube diameter. Accordingly, these disagreements are due to this map designated only for a microchannel with a diameter range of less than 1.

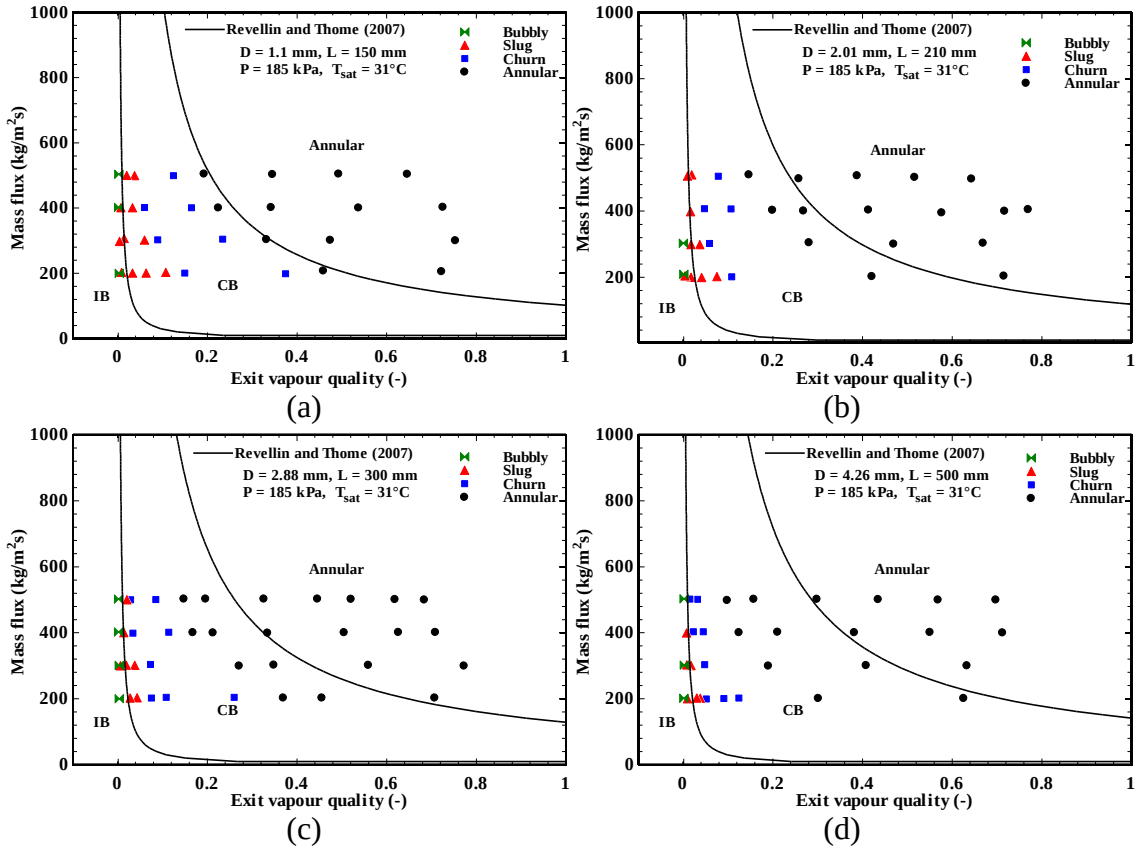

Figure 4.13 Comparison of experimental flow patterns at pressure corresponding to T_{sat} = 31ºC with Revellin and Thome (2007a) flow regime map for: (a) D = 1.1 mm, (b) D = 2.01 mm, (c) D = 2.88 mm, and (d) D = 4.26 mm.

4.7.2 Ong and Thome (2011a) flow regime map

Ong and Thome (2011a) developed the flow pattern transitions of Revellin and Thome (2007a) map by means of adding three dimensionless parameters, involving

Confinement number, vapour to liquid density ratio and vapour to liquid viscosity ratio. The authors also expanded the range of tube diameter from micro to macro channels and used three working fluids (R134a, R236fa and R245fa). The developed transitions of Ong and Thome (2011a) map with operating conditions are mentioned in Appendix A. Figure 4.14 shows the comparison of the predictive transition models of Ong and Thome (2011a), with experimental flow pattern data points. According to the figure, the predictions of IB-CB transition with current experimental bubbly to slug transition are unsatisfactory for all tubes, but they have similar trends to the present transition boundaries. Also, the bubbly flow is predicted well in the isolated bubble (IB) range. In addition, the CB-annular transition predictions are satisfactory with all tubes and the annular flow is predicted very well.

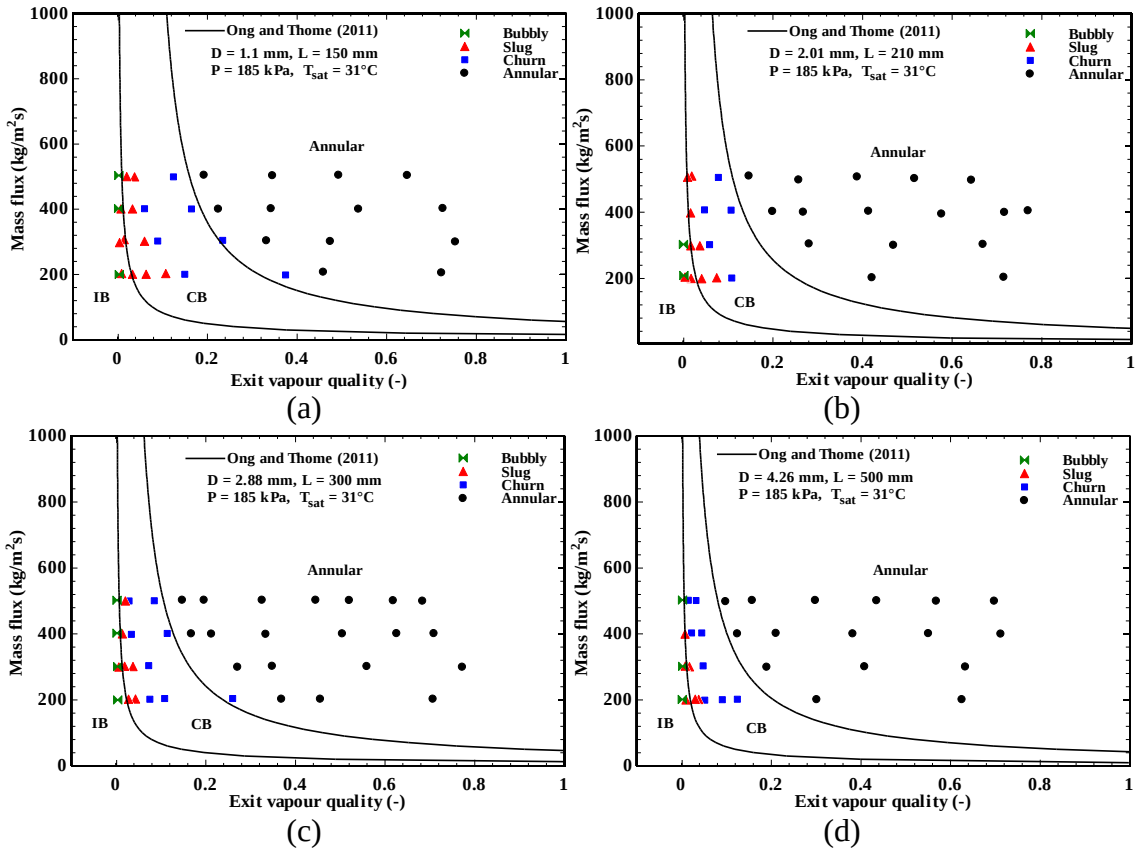

Figure 4.14 Comparison of experimental flow patterns at pressure corresponding to T_{sat} = 31ºC with Ong and Thome (2011a) flow regime map for: (a) D = 1.1 mm, (b) D = 2.01 mm, (c) D = 2.88 mm, and (d) D = 4.26 mm.

4.7.3 Costa-Patry and Thome (2013) criterion

Costa-Patry and Thome (2013) proposed a transition vapour quality representing the boundary between coalescing bubble flow (CB) and annular flow (A) in horizontal channels. This transition was established based on three sources of diabatic flow database for macro- and micro-channels. The database included experimental data for Costa-Patry et al. (2011, 2012) studies and Ong and Thome (2011a) study. The authors took into account the effects of fluid thermophysical properties, channel size, mass and heat flux in developing the CB-A boundary criterion. The ranges of database and boundary criterion are summarised in Appendix A. It can be seen from Figure 4.15 that the transition criterion predicts very well experimental data for churn flow and annular flow in 1.1, 2.88 and 2.01 mm tubes, while the experimental data for 4.26 mm tubes do not agree with this criterion. However, the CB-A transition line shifts to the annular region (i.e. towards high

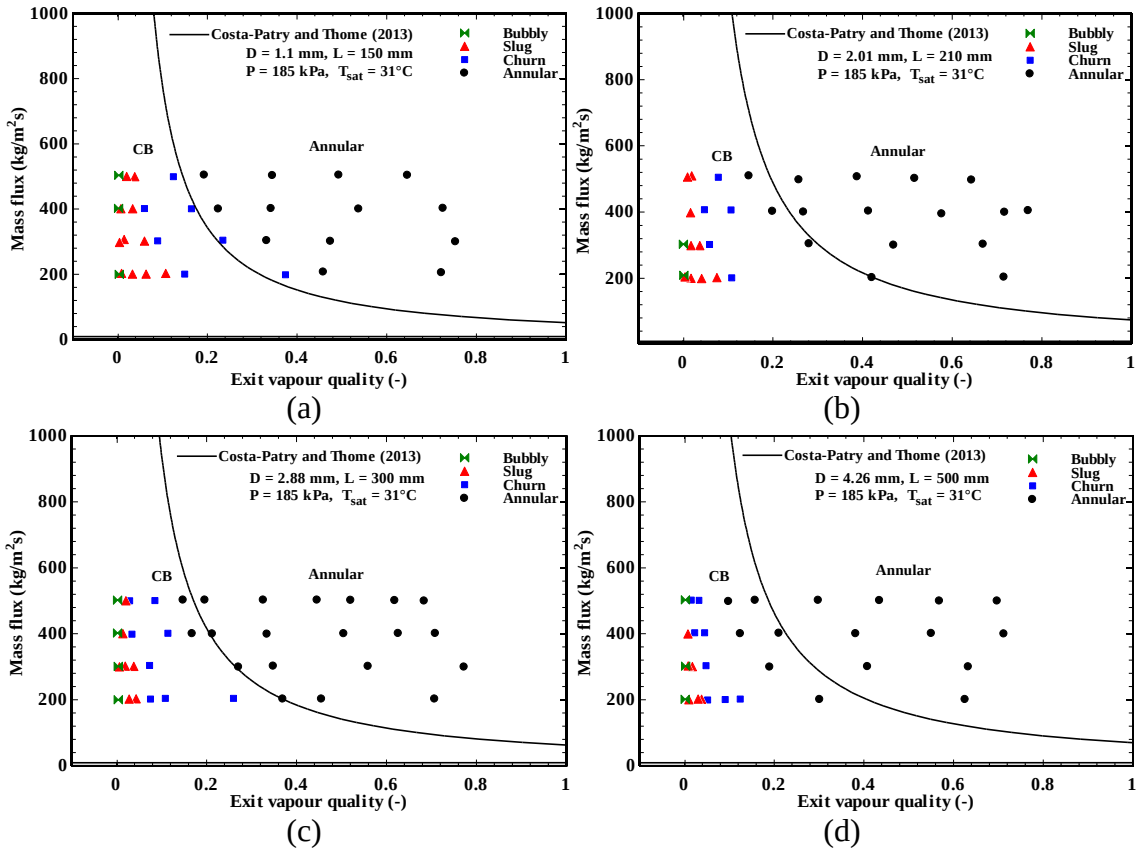

Figure 4.15 Comparison of experimental flow patterns at pressure corresponding to T_{sat} = 31ºC with Costa-Patry and Thome (2013) flow regime map for: (a) D = 1.1 mm, (b) D = 2.01 mm, (c) D = 2.88 mm, and (d) D = 4.26 mm.

vapour quality) with increasing tube diameter. This shift of transition vapour quality is caused by the increase in tube diameter leads to a decrease in bubble confinement consequently a reduction in the rate of bubble coalescence process. Also, the transition vapour quality of Costa-Patry and Thome (2013) proposed for horizontal tubes (with a diameter range of 0.146 – 3.04 mm) loses its applicability to the vertical tube as channel size increases. This means that the effect of channel orientation on flow patterns is suppressed by the predominance of surface tension force in microchannels, i.e. the orientation impact becomes insignificant while decreasing the size of the channel.

4.7.4 Karayiannis et al. (2014) flow regime map

This map was developed by Chen (2006) based on 2392 experimental data points for refrigerant R134a upward flow in four vertical tubes with the range of internal diameter from 1.1 to 4.26 mm. The map was based on vapour and liquid superficial velocities. The operating conditions of the map covered 6-14 bar system pressure, 50-6400 kg/m^{2}s mass flux and vapour quality up to 0.9. The authors relied on dimensional and dimensionless parameters to develop a typical map with transition criteria for five flow regimes. These criteria are given in Appendix A, and the observed flow patterns were dispersed bubble, bubbly, slug, churn and annular flow. Figure 4.16 depicts the comparison of experimental data of current work versus these transition criteria of Chen (2006) map which was presented in Karayiannis et al. (2014). The figure shows that the observed flow patterns of slug and annular are predicted very well. However, the bubbly and churn flow regimes are poorly predicted. The disagreement in predicting bubbly and churn flow regimes could be attributed to the fact that the reason was related to the effect of fluid and fluid properties.

4.7.5 Mahmoud and Karayiannis (2016) flow regime map

This map described elaborately in a study of Mahmoud and Karayiannis (2016) to assess models predicting flow regimes in mini-channels. The authors made improvements to bubbly-slug transition criteria in Karayiannis et al. (2014) map through a theoretical study which highlighted on the force balance on bubble moving in the flow field. The developed bubbly-slug transition boundary was expressed by

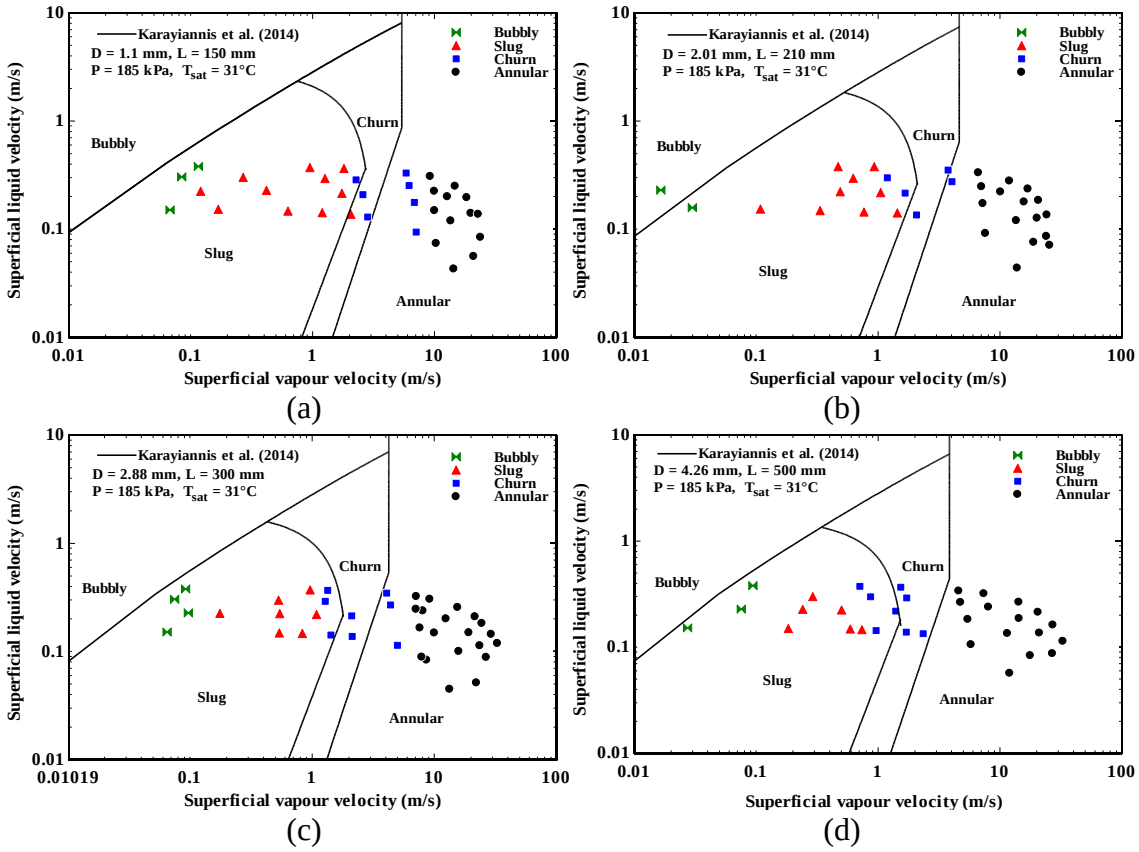

Figure 4.16 Comparison of experimental flow patterns at pressure corresponding to T_{sat} = 31 ºC with Karayiannis et al. (2014) flow regime map for: (a) D = 1.1 mm, (b) D = 2.01 mm, (c) D = 2.88 mm, and (d) D = 4.26 mm.

$$J_l = 0.33\left[\frac{J_v}{0.67} + \sqrt{\frac{4\sigma}{\rho_l D}}\right] \tag{4.1}$$

The new transition of bubbly-slug takes into account the effects of surface tension forces and tube size on bubble movement and its size according to $(\Delta P = 4\sigma/D_b)$ equation. Figure 4.17 depicts the comparison of experimental data of current work versus these transition criteria of Chen (2006) map. The figure shows that the observed flow patterns of bubbly, slug and annular are predicted very well, especially the predictions of the new bubbly-slug transition of Mahmoud and Karayiannis (2016). However, the churn flow regime is poorly predicted. As mentioned above, the disagreement in predicting churn flow regime could be attributed to the effect of fluid and fluid properties.

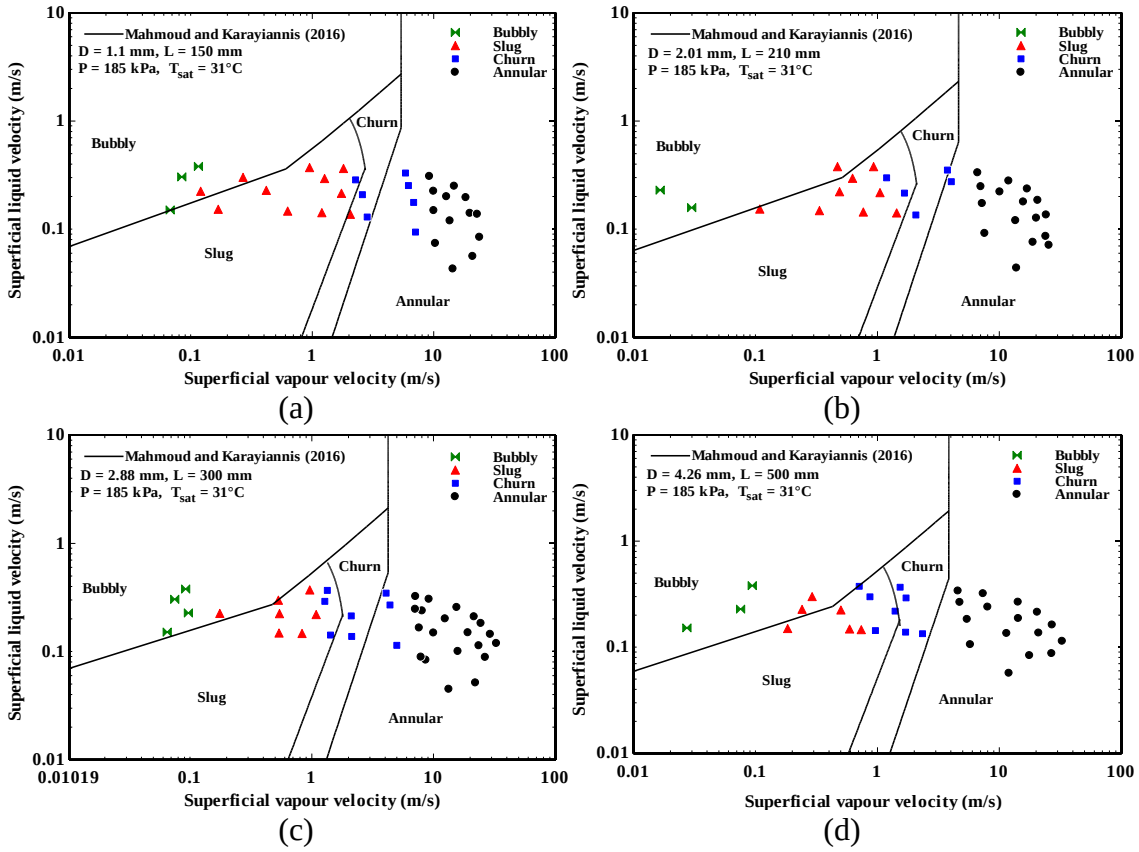

Figure 4.17 Comparison of experimental flow patterns at pressure corresponding to T_{sat} = 31 ºC with Mahmoud and Karayiannis (2016) flow regime map for: (a) D = 1.1 mm, (b) D = 2.01 mm, (c) D = 2.88 mm, and (d) D = 4.26 mm.

4.7.6 Zhu et al. (2017a) flow regime map

Recently, the complete flow regime map of Zhu et al. (2017a) was developed for R32 flow boiling in horizontal mini channels with inner diameter tube of 1 and 2 mm. The experimental parameters are summarized in Appendix A. The authors adopted highly cited flow pattern maps for flow boiling to propose a new one, such as the Costa-Patry and Thome (2013) map, the Ong and Thome (2011a) map and the Cheng et al. (2008b) map. The two transition criteria mention here, one for the slug to churn flow and another for churn to annular flow as given in Appendix A. The slug-churn transition was developed based on correlation of Costa-Patry and Thome (2013) with adding boiling number, while the churn-annular transition was developed based on correlation of Ong and Thome (2011a) with adding boiling number. Figure 4.18 shows the comparisons between the predictions of the Zhu et al. (2017a) map and the experimental results. It can be seen that a comparison with this map established for small-diameter tubes did not show a reasonable agreement with experimental data for all investigated tubes. The

disagreement might be due to large differences between the thermophysical properties of R32 and those of R245fa. For instance, the latent heat of vaporization, vapour to liquid density ratio and vapour to liquid viscosity ratio of R32 are much greater than those of R245fa at the same saturation temperature. This, in turn, makes the transitions of Zhu et al. (2017a) move to lower vapour qualities.

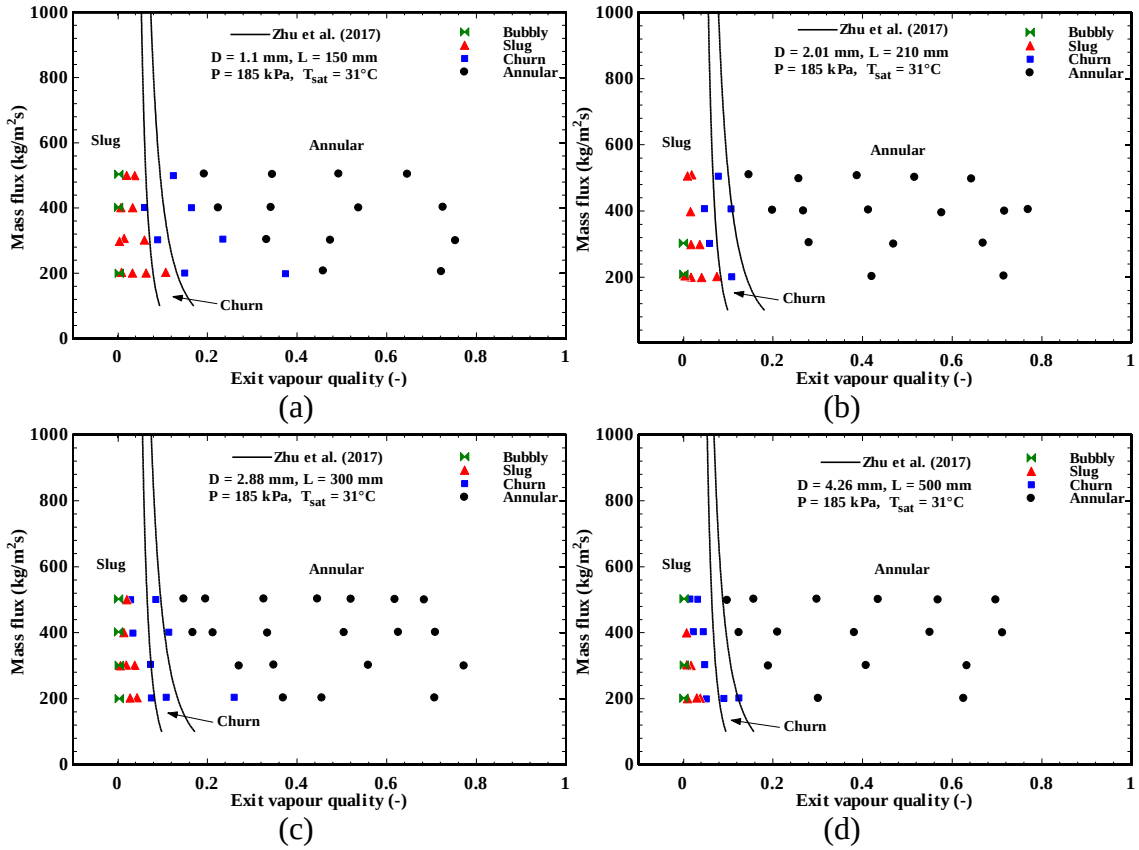

Figure 4.18 Comparison of experimental flow patterns at pressure corresponding to T_{sat} = 31ºC with Zhu et al. (2017a) flow regime map for: (a) D = 1.1 mm, (b) D = 2.01 mm, (c) D = 2.88 mm, and (d) D = 4.26 mm.

4.7.7 Tibiriçá et al. (2017) flow regime map

A recent universal flow pattern map in the macro to microscale conditions was established by Tibiriçá et al. (2017). The transition models for this new flow pattern map have been developed based on a database gathered from adiabatic and nonadiabatic flow studies for different working fluid in horizontal channels. The details of this map and its working conditions are summarised in Appendix A. The comparison of experimental flow pattern data points with the flow map of Tibiriçá et al. (2017) is depicted in Figure 4.19. The transition curves of Tibiriçá et al. (2017) predict the bubbly flow, slug flow and churn

flow very well. The predictive churn-annular transition line has a similar trend to the experimental flow pattern boundary but with few deviations toward low vapour qualities in the status of decreasing tube diameter.

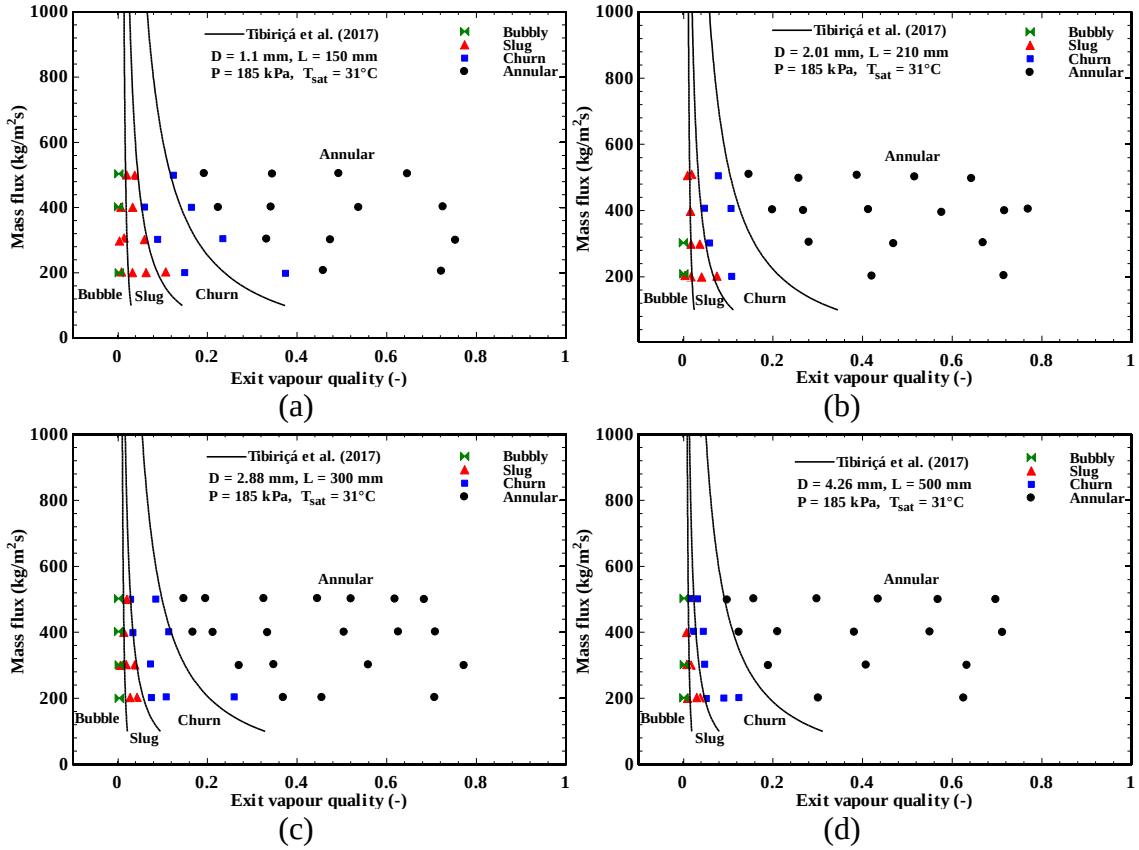

Figure 4.19 Comparison of experimental flow patterns at pressure corresponding to T_{sat} = 31 ºC with Tibiriçá et al. (2017) flow regime map for: (a) D = 1.1 mm, (b) D = 2.01 mm, (c) D = 2.88 mm, and (d) D = 4.26 mm.

4.8 Summary

The following conclusions are drawn from the discussion of the results of flow patterns and their transition boundaries presented in this chapter.

- The flow patterns in flow boiling of R245fa, inside four vertical stainless-steel tubes with different inner diameters, were investigated under a wide range of conditions. The four observed flow regimes are identified as bubbly flow, slug flow, churn flow and annular flow. The flow boiling visualisation was recorded by a high-speed camera (frame rates of 1000 f/s and 512 × 512 pixels) with

experiments of increasing and decreasing heat flux. In increasing heat flux experiments, the churn and annular flows were only the dominant patterns in all four tubes. The slug flow was often discerned at lower mass flux except for the tube of 1.1 mm, it was not observed at all. This is contrary to decreasing heat flux experiments where all flow patterns including the bubble flow were observed in all the tubes. This shows a strong impact of hysteresis.

- The flow patterns and transition boundaries for R245fa are affected by mass flux, system pressure, and tube diameter. The vapour quality corresponding to flow pattern transition boundary tends to decrease with increasing mass flux for all tubes. The system pressure corresponding to higher saturation temperature (46.7 °C which has not been tested before for the R245fa as a working fluid in the micro-tube) contributes to the flow pattern transitions shifting to lower superficial vapour velocities consequently higher initial vapour quality of flow regime transition. This situation is attributed to pressure influence on thermophysical properties of refrigerant. With decreasing tube diameter, the bubbly-slug transition moves to low superficial vapour velocities, while the slug-churn and churn-annular transitions shift towards high superficial vapour velocities (higher vapour qualities).
- The experimental flow pattern maps of R245fa were compared with seven predictive models developed for mini- and micro-channels in two-phase flow. The comparison results show that the qualitative agreement was found with bubbly-slug transition lines of Mahmoud and Karayiannis (2016) and Tibiriçá et al. (2017). However, the agreement between data of slug and churn flow with flow maps of Karayiannis et al. (2014) and in their applicability ranges appeared not to be satisfactory. Contrarily, the transition criterion given by Tibiriçá et al. (2017) can reproduce slug-churn transition well for all experimental flow maps. What is more, the predictive churn-annular transition curve of Ong and Thome (2011a) had a similar tend to the experimental transition. Also, the trend of Tibiriçá et al. (2017) transition curve was in best consistent with the churn to annular flow transition. However, this predictive transition criterion had deviation slightly towards low vapour quality with decreasing tube diameter. Generally, there is no specific flow pattern map satisfactory or able to accurately predict all the transition boundaries.

Chapter 5

Pressure Drop: Results and Discussion

5.1 Introduction

This chapter presents the characteristics of the flow boiling pressure drop in the small diameter tubes examined in this study. The parametric influence on two-phase pressure drop is also shown and discussed. This parametric influence involves mass flux, heat flux (i.e. exit vapour quality), system pressure, tube diameter, surface microstructure, and fluid thermophysical properties. The flow boiling pressure drop was obtained in this experimental study directly by measuring the pressure drop across the heated section, simultaneously with the parametric measurements related to flow boiling heat transfer. The measurements of flow boiling pressure drop were systematically conducted on five different test sections which were installed in vertical flow direction without any inlet or outlet restrictions. Moreover, the total measured pressure drop consists of four components which are single-phase, frictional, gravitational, and acceleration pressure drop. These components of the total pressure drop can be individually estimated. Also, there are two models (i.e. a homogeneous and separated model) that are widely used to predict two-phase frictional pressure drop. Furthermore, after deducting the single-phase pressure drop resulting from a subcooled liquid flow region, the contributions of the three remaining components (frictional, gravitational, and acceleration pressure drop) to the total value of two-phase pressure drop are presented and discussed. Finally, the experimental data of two-phase pressure drop are compared with the existing correlations in the open literature.

5.2 Effect of mass flux and exit vapour quality

The measurements of two-phase pressure drop under different mass fluxes are depicted in Figure 5.1 as a function of exit vapour quality for tube diameter of 1.1, 2.01,

2.88 and 4.26 mm. The experimental results demonstrate that, at a constant system pressure of 185 kPa, the two-phase pressure drops increase with increasing mass fluxes. The mass flux effect is slight in the low vapour quality (x_e < 0.1) in each tube. The influence of mass flux on two-phase pressure drop becomes significant with the increase of vapour quality (x_e > 0.1) under the same experimental conditions. According to the change in two-phase flow patterns during each test tube which was started in Chapter 4, the flow regime type, in turn, has a strong effect on two-phase flow boiling pressure drop. For vapour quality below 0.1, the bubble nucleation and slug flow are the prevailing flow regimes where the void fraction is small compared to the churn and annular flow regimes. In addition, small increases in the overall specific volume of vapour and liquid phase lead to an insignificant increase in overall flow velocity in the flow channel. Since the flow velocity depends directly on increasing mass flux and vapour quality, the mass flux influence on two-phase pressure drop is unnoticeable in the low vapour quality. With

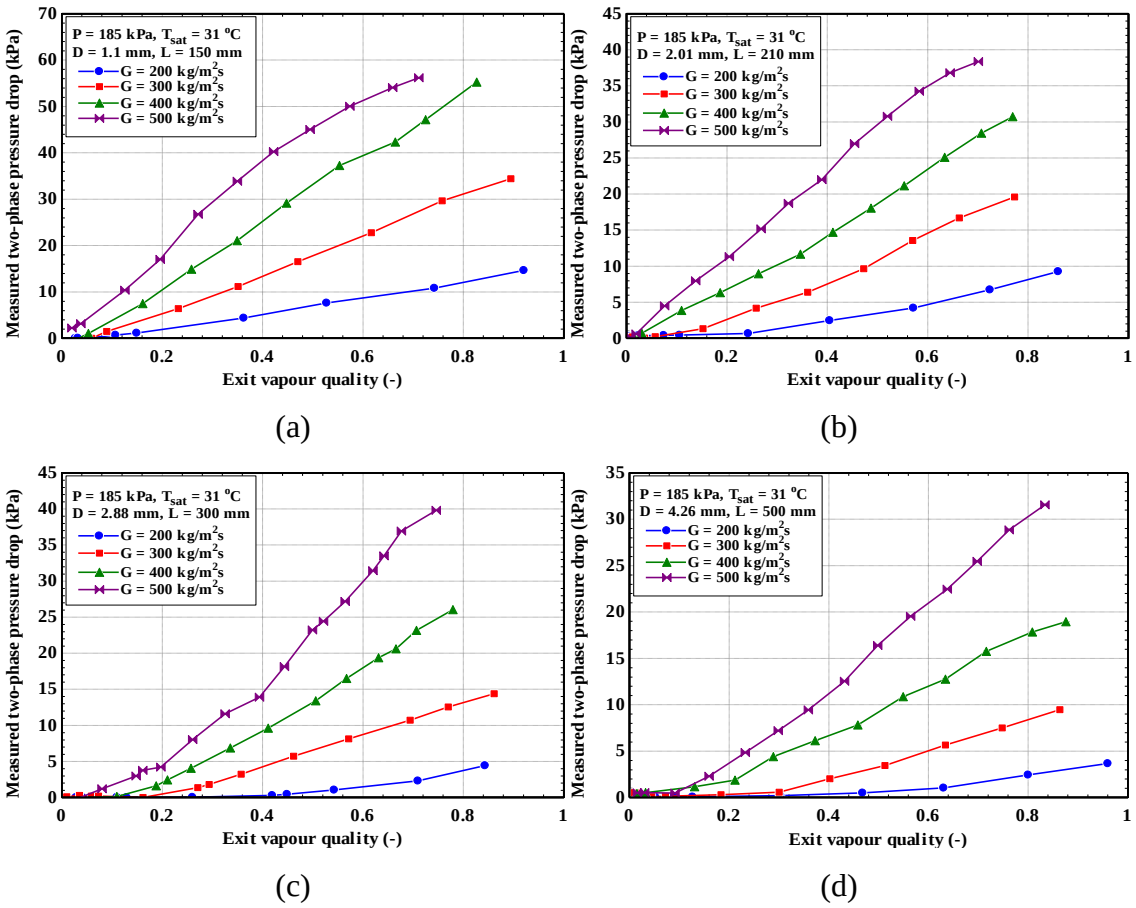

Figure 5.1 Effect of mass flux on the measured two-phase pressure drop at P = 185 kPa for different tube diameters: (a) D = 1.1 mm, (b) D = 2.01 mm, (c) D = 2.88 mm, and (d) D = 4.26 mm.

increasing vapour quality, the flow regime turns into the churn and annular flow. As a result, the formation of the vapour phase in tube core and liquid film around the tube wall periphery causes higher vapour velocity and thus increasing frictional pressure drop. Further, the increased mass flux results in the enhancement of shear forces at the tube wall as well as at the liquid-vapour interface which leads to increasing frictional pressure drop. The frictional and acceleration components are also a function of the square of the mass flux in the momentum equation indicating a quadratic increase with an increase in mass flux. This, in turn, results in increasing the flow boiling pressure drop with mass flux. Furthermore, these trends of flow boiling pressure drop are identical to other studies of Yang et al. (2018b), Saisorn et al. (2018), Sempértegui-Tapia and Ribatski (2017b), Longo et al. (2016b), Charnay et al. (2015a), Mahmoud et al. (2014a), Owhaib et al. (2008) and Quibén and Thome (2007).

5.3 Effect of heat flux

Figure 5.2 depicts the measured two-phase pressure drop as a function of exit vapour quality for four different tube diameters (1.1 - 4.26 mm) under mass flux ranging from 300-500 kg/m^{2}s and fixed pressure of 185 kPa. The experimental results show that the two-phase pressure drop increases with increasing heat flux. Indeed, this is attributed to higher vaporization in the flow channel resulting from increasing heat flux which causes an increase in the bubble nucleation and rapid transition to slug flow. This increases the vapour quality, vapour void fraction, flow velocity and flow momentum along the channel. This, in turn, gives rise to an increase in the flow boiling pressure drop. These trends agree with those in studies of Saisorn et al. (2018), Zhu et al. (2017b), Mahmoud et al. (2014a), and Pamitran et al. (2010).

5.4 Effect of system pressure

The effect of pressure on the measured two-phase pressure drop is shown in Figure 5.3 as a function of exit vapour quality for tube diameter of 1.1, 2.01, 2.88 and 4.26 mm. It is clear that at a constant mass flux of 400 kg/m^{2}s, the two-phase pressure drop decreases with increased system pressure. The two-phase pressure drop changes slightly

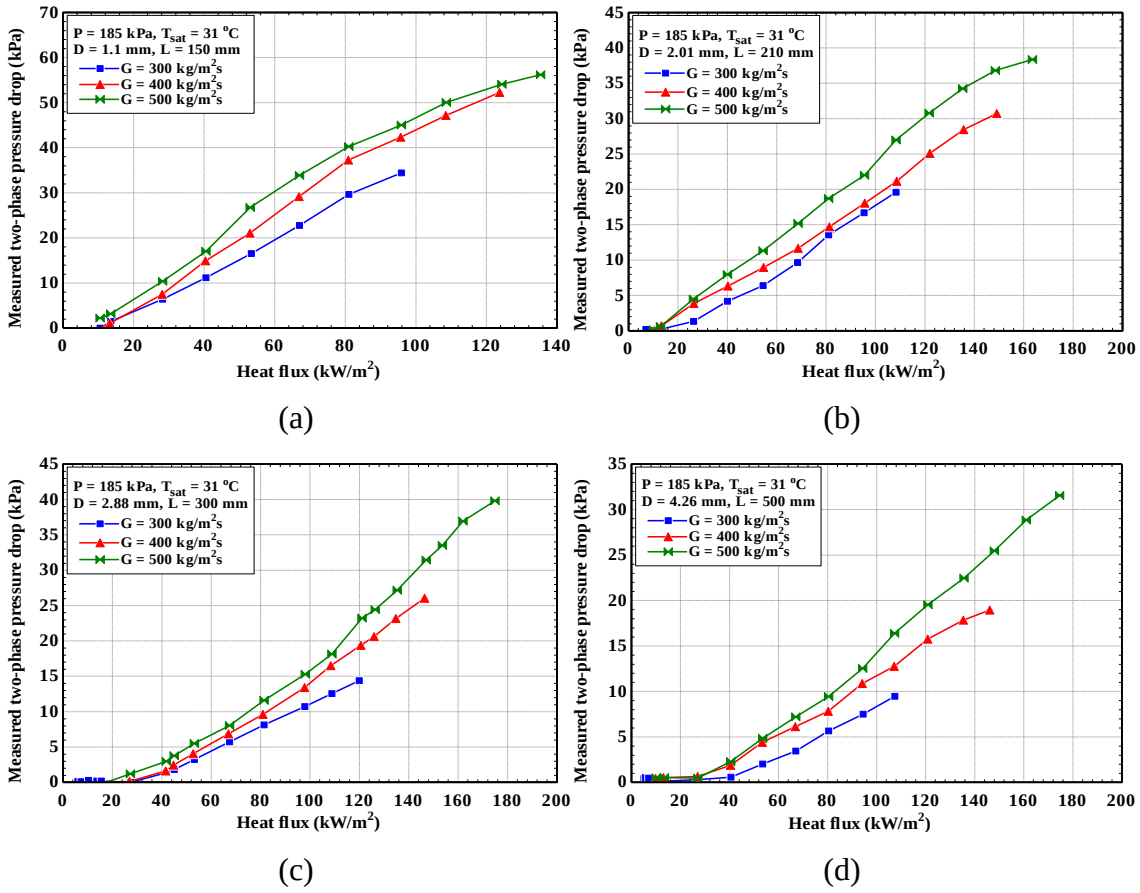

Figure 5.2 Effect of heat flux on the measured two-phase pressure drop at P = 185 kPa for different tube diameters: (a) D = 1.1 mm, (b) D = 2.01 mm, (c) D = 2.88 mm, and (d) D = 4.26 mm.

with increased system pressure at lower vapour quality (x_e < 0.1). When the vapour quality increases by more than 0.1, the two-phase pressure drop decreases significantly as the system pressure increases. This behaviour of two-phase pressure drop corresponding to the exit vapour quality is mostly similar to other conditions under different mass fluxes, as mentioned in the previous section. It is believed that the phenomenon of the decrease in two-phase pressure drop with increased system pressure is attributed to the pressure influence on the fluid thermodynamic properties. It is observed from Table 3.5 that the increase in system pressure leads to higher vapour density and lower liquid viscosity. This results in a lower vapour velocity, drop of shear stress at the liquid-tube wall and the liquid-vapour interface and consequently decrease in acceleration and frictional pressure drops. This, in turn, results in the decrease in two-phase pressure drop. In addition, the lower vapour quality causes lower void fraction. As a result, the changes of two-phase pressure drop with system pressure are not obvious at

vapour quality below 0.1. These experimental results are consistent with the observed results of other studies like Yang et al. (2018b), Huang and Thome (2017), Charnay et al. (2015a), Mahmoud et al. (2014a), Pamitran et al. (2010), and Revellin and Thome (2007b).

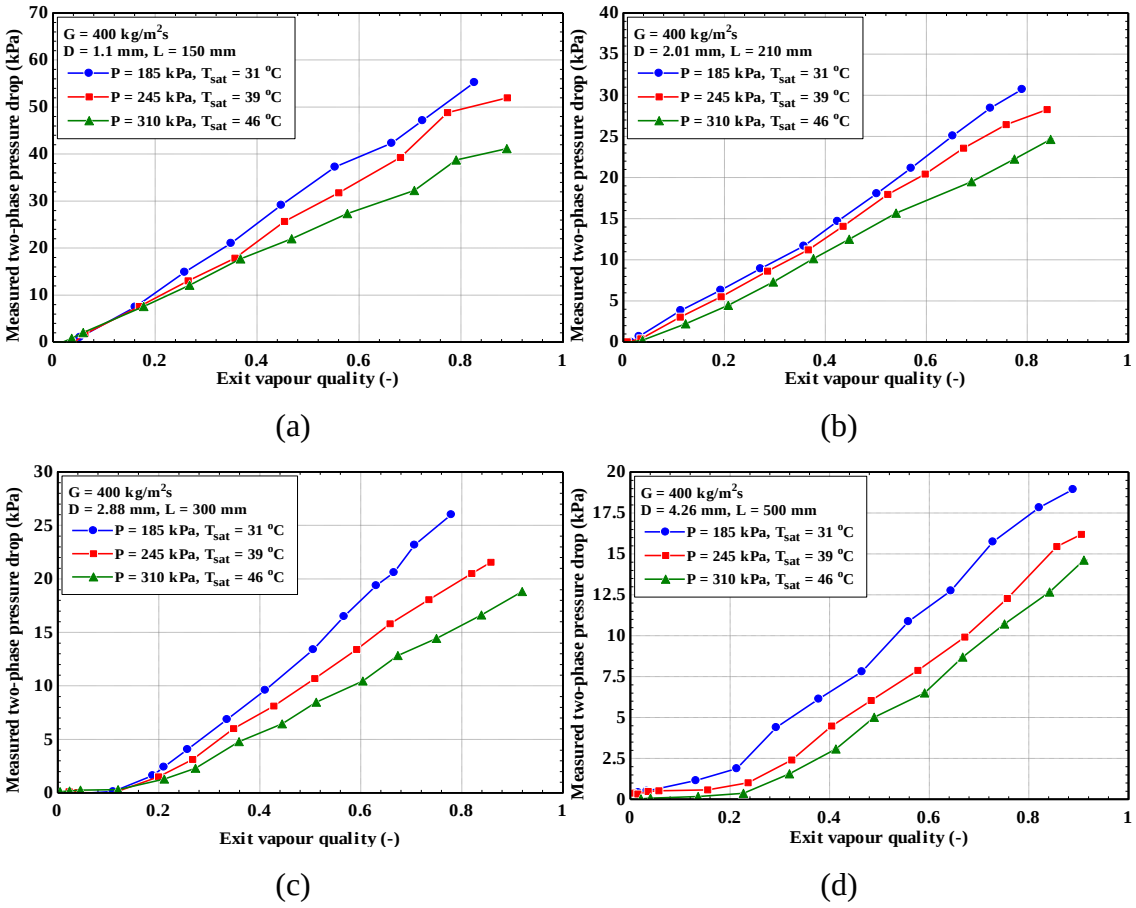

Figure 5.3 Effect of system pressure on the measured two-phase pressure drop at G = 400 kg/m^{2}s for different diameter tubes: (a) D = 1.1 mm, (b) D = 2.01 mm, (c) D = 2.88 mm, and (d) D = 4.26 mm.

5.5 Effect of tube diameter

Figure 5.4 shows the influence of tube diameter on the measured two-phase pressure drop with constant mass flux and system pressure. The comparison of two-phase pressure drop in these four tubes depends on two-phase pressure gradient instead of two-phase pressure drop because of the difference in the length of the heating section. Results show that the two-phase pressure gradient increases substantially with the decrease in tube

diameter. According to Figure 5.4, the pressure gradient in the 1.1 mm tube is about 13 times higher than that in the 4.26 mm tube at a pressure of 185 kPa and it increases to about 24 times with increasing the system pressure up to 310 kPa. These results agree with those in studies of Zhu et al. (2017b), Xu et al. (2016a), Hardik and Prabhu (2016), Mahmoud et al. (2014a), Revellin and Thome (2007b), Huo et al. (2007) and Tong et al. (1997).

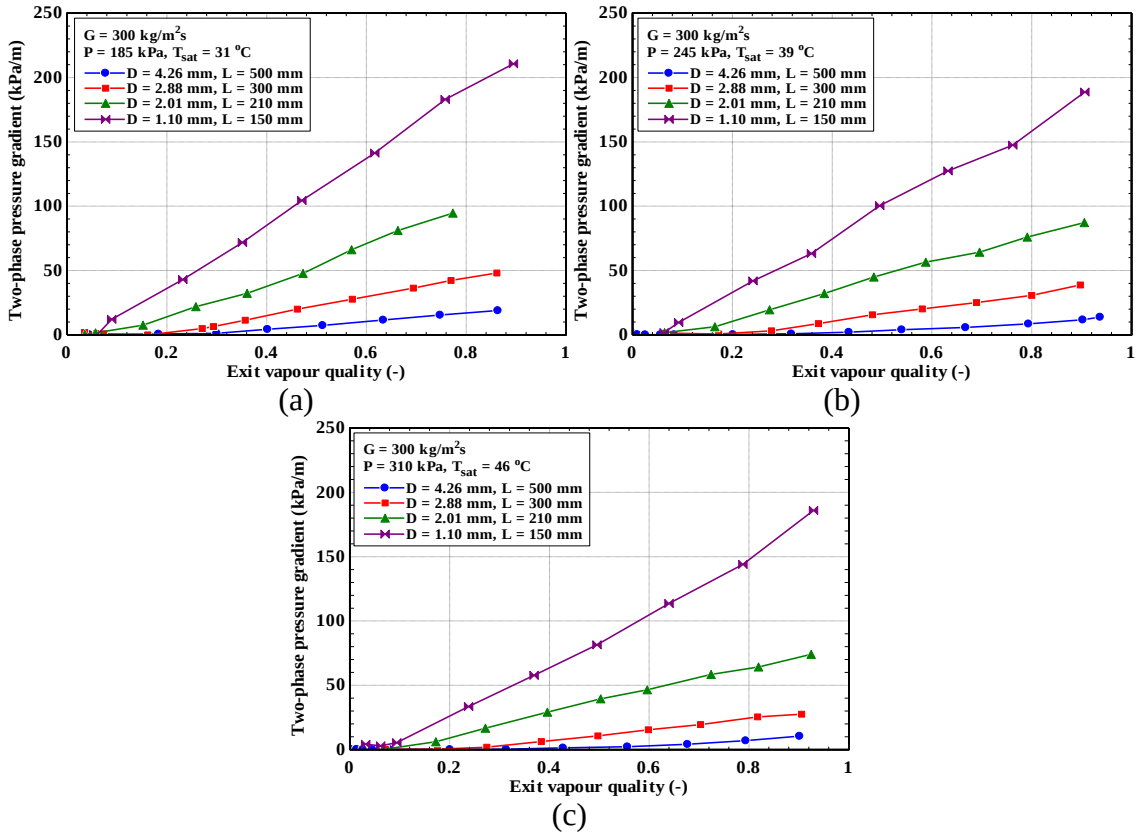

Figure 5.4 Effect of tube diameter on the measured two-phase presser gradient at G = 300 kg/m^{2}s and system pressure of: (a) P = 185 kPa, (b) P = 245 kPa, and (c) P = 310 kPa.

The increase in two-phase pressure gradient with a decrease in channel diameter could be attributed to the presence of large velocity gradient in the thin liquid film close to channel wall and consequently high wall shear stress and high interfacial shear stress, leading to the higher frictional pressure gradient. In addition, Tong et al. (1997) reported that according to the boundary-layer theory, the shear stress is directly proportional to the velocity gradient, the changes in the tube diameter give rise to a variation of the boundary-layer thickness. Small-diameter tubes have a thinner boundary layer which yields higher

velocity gradients and thus higher pressure drop. On the other hand, the tube diameter affects the distributions of the liquid and vapour phases in the tube and consequently affects flow regime transitions, see Section 4.6. Therefore, the flow regime may have an effect on the two-phase pressure drop characteristics. That is, the increased confinement of vapour bubbles with decreasing tube diameter leads to an increase in the coalescence rate of departure bubbles. Consequently, the slug flow regime is not observed in the 1.1 mm tube with occurring an earlier transition to churn and annular flow, as previously mentioned. As a result, the formation of the vapour phase in the tube core and liquid film around the tube wall periphery causes higher vapour velocity and thus increasing frictional pressure drop.

For more explanation, the contributions of the three pressure drop components for R245fa to the total measured two-phase pressure drop is depicted in Figure 5.5. The gravitational and acceleration components are individually determined by using the void fraction model of Lockhart and Martinelli (1949) (see Subsection 3.5.2), while the frictional component is obtained by subtracting the gravitational and acceleration components from the value of total measured two-phase pressure drop. As seen in Figure 5.5, the contribution of gravitational and acceleration components decreases with decreasing tube diameter in contrast to the frictional contribution which increases with decreasing tube diameter. This is in agreement with the findings for R134a obtained by Mahmoud et al. (2014a). Moreover, the frictional contribution increases with exit vapour quality, while the gravitational contribution decreases. The gravitational contribution is quite small in 1.1 mm tube compared to those of other tubes due to the dominance of surface tension forces. This also is in agreement with Kandlikar and Balasubramanian (2004), who report that the gravitational effect can be negligible for small diameter channels due to the dominance of surface tension. Further, the contribution of the acceleration component in the 1.1 and 2.01 mm tubes increases with exit vapour quality, while in the 2.88 and 4.26 mm tubes, it drops rapidly at low exit vapour quality and then increases slightly at high exit vapour quality because of the high vapour velocity.

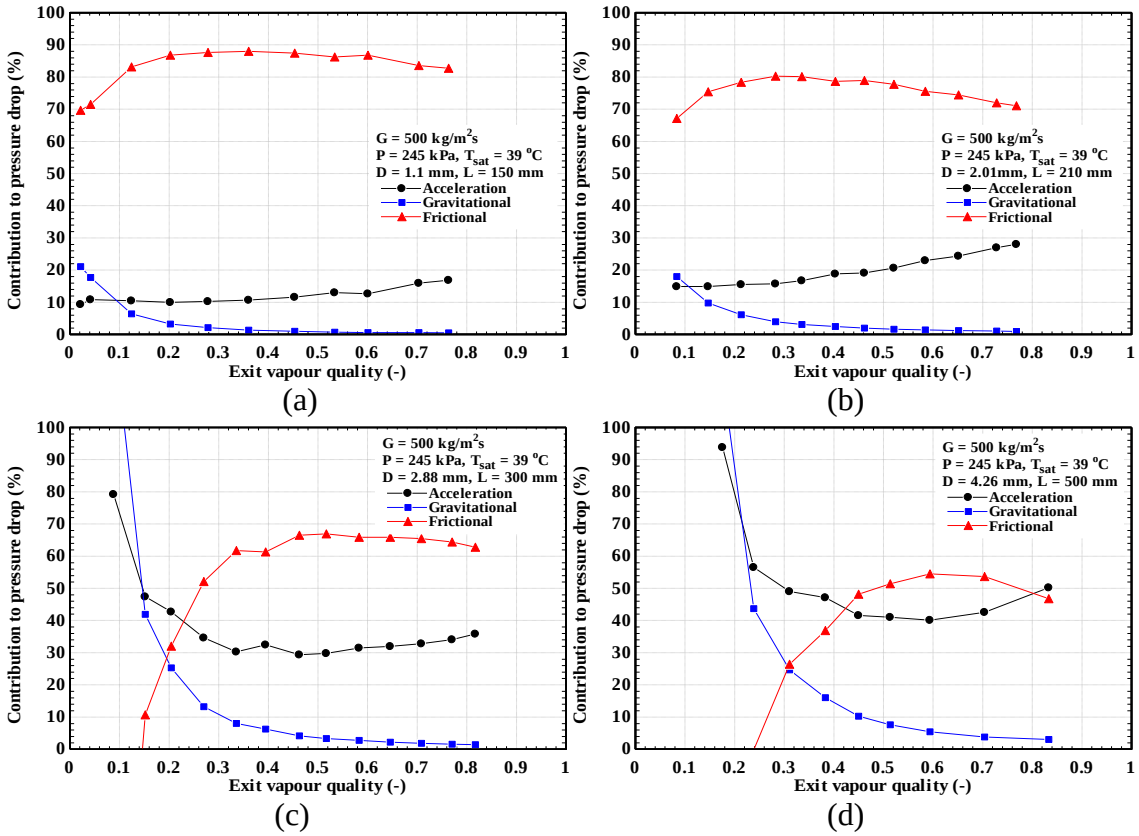

Figure 5.5 Contribution percentages from the three pressure drop components to the total measured value at G =500 kg/m^{2}s and P = 245 kPa for: (a) D = 1.1 mm, (b) D = 2.01 mm, (c) D = 2.88 mm, and (d) D = 4.26 mm.

5.6 Effect of surface condition

The influence of surface enhancements on pressure drop is investigated with two tubes having almost similar diameter and heated length. The inner diameter of tubes is 4.26 mm, while the heated length is 500 mm. The surface of one of them was enhanced by a copper coating. The measured surface roughness of uncoated tube is 0.197 μm, while the measured surface roughness of coated tube is 0.675 μm, which is about three times greater than that of the uncoated tube, see Subsection 3.2.4. Figure 5.6 shows the two-phase pressure drop variations for two different mass fluxes (200 and 500 kg/m^{2}s) at P = 185 kPa for coated and uncoated tube. The results exhibit that the two-phase pressure drop trends of the coated tube are analogous to those of uncoated tube. However, the pressure drop of the coated tube is higher than that of the uncoated tube for all mass fluxes. This is because the high density of active nucleation sites is present on the surface of coated tube wall which makes the rate of bubble generation to be higher. The bubbles generated with a large size help to induce the occurrence of random collisions between

them and then coalescence. This phenomenon leads to increased vapour velocity in the tuber core, following by increased shear stress in the liquid-vapour interface and consequently higher acceleration pressure drop. Also, with the formation of a thin liquid film on the channel walls, a higher liquid velocity in the liquid film results in an increase of wall shear stress and thus higher frictional pressure drop. This leads finally to the higher total two-phase pressure drop of coated tube comparing to that of the uncoated tube.

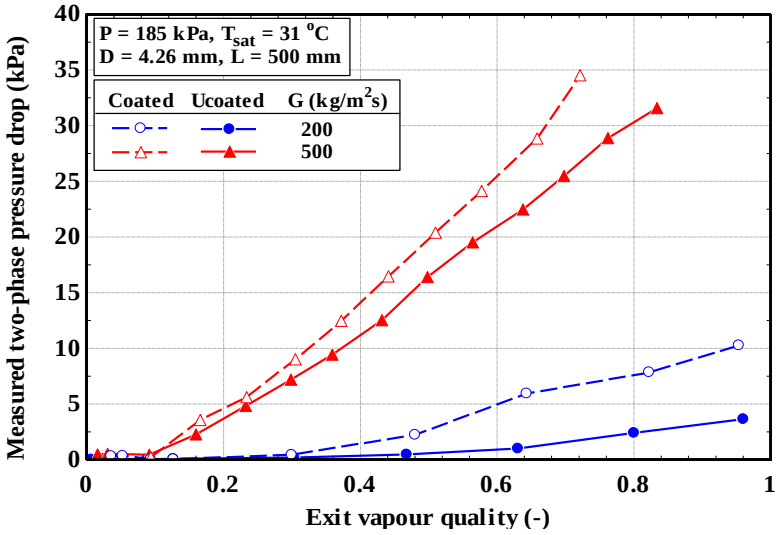

Figure 5.6 Effect of coating on the two-phase pressure drop at P = 185 kPa.

5.7 Effect of fluid properties

Figure 5.7 shows the measured two-phase pressure drop of R245fa compared to R134a for different tube diameters at operating conditions of G = 500 kg/m^{2}s and T_{sat} = 31 °C. The experimental data of R134a employed for comparison is acquired from the previous studies of Huo et al. (2007), Shiferaw et al. (2011) and Mahmoud et al. (2014a). These studies were carried out in the same experimental facility for R134a with a vertical stainless-steel tube of diameter 4.26, 2.88, 2.01 and 1.1 mm under the similar operating conditions. According to Figure 5.7, the measured two-phase pressure drop of R245fa is obviously higher than that of R134a. In the low vapour quality region and especially in 2.88 and 4.26 mm tube, the two-phase pressure drop for R245fa slightly lower than R134a. Contrarily, in high vapour quality, the two-phase pressure drop for R245fa is significantly higher than R134a. Moreover, the increase in vapour quality with the reduction in tube diameter from 1.1 to 4.26, the two-phase pressure drop difference

between R245fa and R134a increases. These results are similar to experimental data of other studies which were reported by Huang and Thome (2017), Sempértegui-Tapia and Ribatski (2017b), Yang et al. (2018b) and Ali et al. (2011). A comparison of main refrigerant properties for R245fa and R134a is shown in Table 5.1. It can be seen in this table that the R134a exhibits a vapour density about 3.7 times larger than the R245fa under similar saturation temperature. This denotes a higher vapour velocity in the flow boiling process of R245fa at the same mass flux and consequently a higher two-phase pressure drop compared to the R134a. Also, with increasing vapour quality, the large differences in two-phase pressure drop between R245fa and R134a are due to the vapour

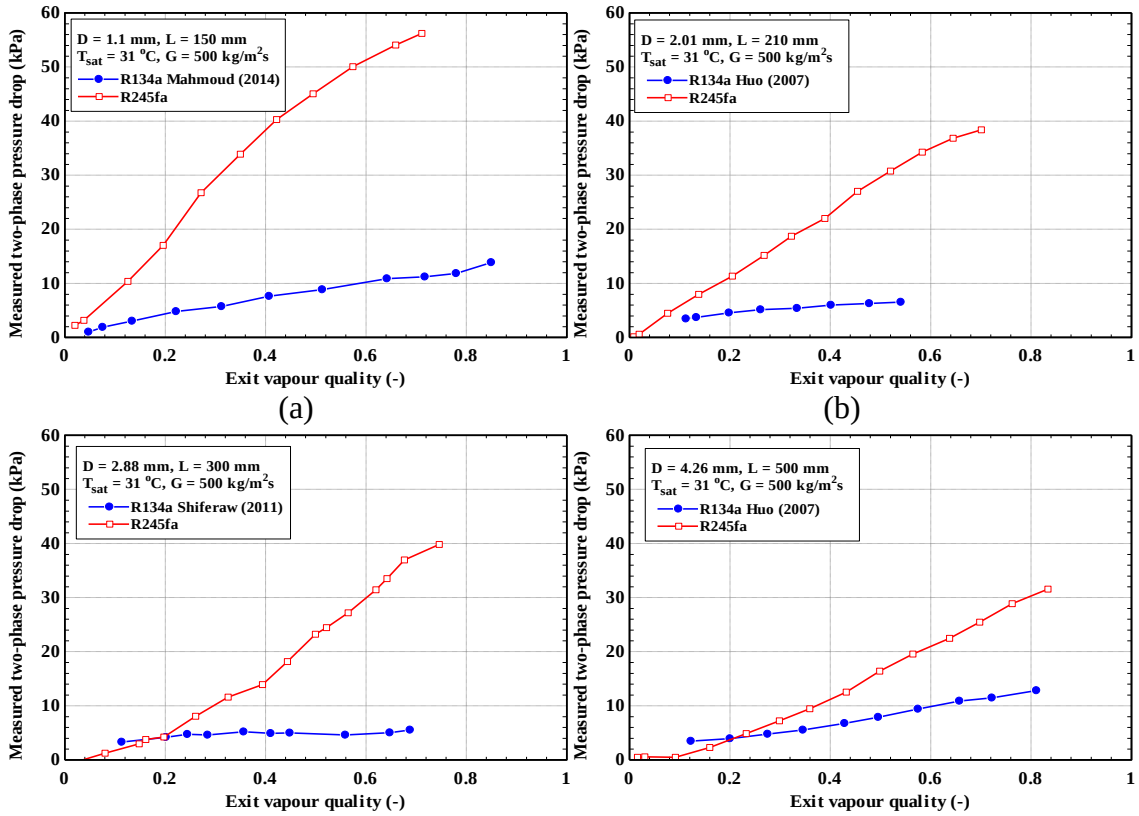

Figure 5.7 Effect of fluid on the measured two-phase pressure drop at G = 500 kg/m^{2}s and T_{sat} = 31 °C for: (a) D = 1.1 mm, (b) D = 2.01 mm, (c) D = 2.88 mm, and (d) D = 4.26 mm.

Table 5.1 The thermodynamic properties of R245fa and R134a at T_{sat} = 31 °C are based on the Engineering Equation Solver (EES) program.

Fluids	P_r	ρ_v (kg/m^3)	ρ_l (kg/m^3)	μ_v (μPa s)	μ_l (μPa s)	σ (mN/m)
R134a	0.195	38.68	1184	12.24	180.4	7.25
R245fa	0.05	10.48	1322	10.39	373.9	12.86

velocity of the R245fa being higher than the R134a. In other words, this phenomenon is mainly due to the difference in physical properties of the two refrigerants, i.e. the higher reduced pressure of R134a compared to R245fa gives rise to higher vapour density and lower liquid viscosity. As mentioned above, the higher vapour density leads to lower vapour velocity, following by drop of shear stress at the liquid-vapour interface and consequently lower acceleration pressure drop. Also, the lower liquid viscosity results in a drop of wall shear stress and consequently lower frictional pressure drop. This leads finally to lower total two-phase pressure drop of R134a comparing to R245fa.

5.8 Comparison with previous prediction methods

The experiments produced 484 data points of flow boiling pressure drop in four different tubes, including 114 data points for 1.1 mm, 118 for 2.01 mm, 124 for 2.88 mm and 128 for 4.26 mm tube. The experimental data are compared to the predictions of 15 existing correlations of two-phase pressure drop, including one model of homogeneous equilibrium flow and fourteen separated models. These correlations were chosen for the comparison based on the fact that they are relevant to the present experimental conditions. Full details for these correlations are included in Appendix B. The respective equations for the acceleration and gravitational components corresponding to each model (homogeneous and separated) were discussed in Subsection 3.5.2. The comparative results of the correlations against all four separate subsets of the experimental data for four tubes (1.1 – 4.26 mm) are listed in Table 5.2, where MAE is the mean absolute error, defined by Equation (5.1). The MAE is employed as the criterion for assessing the accuracy of the predictive model.

$$\mathrm{MAE} = \frac{1}{N}\sum_{i=1}^{N}\left|\frac{\Delta P_{pre} - \Delta P_{exp}}{\Delta P_{exp}}\right| \tag{5.1}$$

where ΔP_{pre} and ΔP_{exp} are the predicted and experimental two-phase pressure drops and N represents the total number of the data points. The parameter β is used to represent the percentage of data within ±30% error bands for each correlation. The most commonly used two-phase pressure drop correlations of conventional and mini/micro-scale are

assessed in terms of the influence of tube diameter. The macroscale and microscale pressure drop correlations are described and discussed in this section.

Table 5.2 Statistical comparison between experimental data and predictions of two-phase pressure drop correlations for conventional and small-scale tubes.

Author(s)	D (mm)	1.1	2.01	2.88	4.26	Overall
	Data points	114	118	124	128	484
McAdams et al. (1942) Homogeneous flow model	MAE (%)	78.03	72.26	54.17	20.87	55.39
	β (%)	7.89	17.80	0.00	78.91	27.07
Lockhart and Martinelli (1949)	MAE (%)	78.31	71.59	44.45	20.58	52.73
	β (%)	20.18	36.44	7.26	75.00	35.33
Chisholm (1973a)	MAE (%)	132.6	97.35	25.59	45.41	73.52
	β (%)	55.26	63.56	79.84	33.59	57.85
Grönnerud (1979)	MAE (%)	72.5	66.52	48.81	18.65	50.73
	β (%)	28.95	30.51	12.10	82.03	39.05
Friedel (1979)	MAE (%)	103.5	83.03	52.95	19.04	63.23
	β (%)	21.93	21.19	0.00	83.59	32.44
Müller-Steinhagen and Heck (1986)	MAE (%)	81.15	72.95	53.85	18.48	55.58
	β (%)	7.89	16.10	0.00	83.59	27.89
Mishima and Hibiki (1996)	MAE (%)	88.8	76.98	52.72	18.29	58.03
	β (%)	4.39	14.41	0.00	81.25	26.03
Qu and Mudawar (2003)	MAE (%)	93.9	80.37	37.47	37.17	61.14
	β (%)	8.77	50.00	33.87	44.53	34.71
Hwang and Kim (2006)	MAE (%)	78.2	62.52	25.66	85.29	62.79
	β (%)	5.26	72.03	69.35	9.37	39.05
Sun and Mishima (2009)	MAE (%)	80.05	76.47	56.65	21.36	57.66
	β (%)	15.79	14.41	0.00	77.34	27.69
Li and Wu (2010a)	MAE (%)	89.04	69.88	37.82	21.17	53.3
	β (%)	23.68	18.64	44.35	71.87	40.5
Lee et al. (2010)	MAE (%)	72.08	70.56	45.47	25.74	52.64
	β (%)	35.09	37.29	29.03	63.28	41.53
Xu and Fang (2012)	MAE (%)	86.57	81.82	76.86	48.05	72.74
	β (%)	8.77	3.39	0.00	13.28	6.405
Kim and Mudawar (2012)	MAE (%)	98.1	86.73	42.38	32.59	63.73
	β (%)	7.89	26.27	12.10	53.91	25.62
Kim and Mudawar (2013)	MAE (%)	87.68	71.38	27.86	45.46	57.22
	β (%)	21.93	75.42	62.90	32.03	48.14

5.8.1 Predictive methods for conventional tubes and comparison

Homogeneous flow model

The homogeneous equilibrium flow model postulates the liquid and vapour phase motion along the channel with the identical velocity (slip ratio = 1). This model is generally suitable for bubbly flow or slug flow, where the vapour quality is low. It depends on more complex physically-based models such as two-phase density and two-phase viscosity to predict the frictional pressure drop component, see Collier and Thome (1994). The two-phase viscosity is determined on the basis of a specific mixing law between the viscosity of liquid and vapour phase according to McAdams et al. (1942) model, as follows,

$$\frac{1}{\mu_{tp}} = \frac{x}{\mu_v} + \frac{1-x}{\mu_l} \tag{5.1}$$

The model of homogeneous equilibrium flow is implemented to predict all four separate subsets of the experimental pressure drop data for four tubes (1.1 – 4.26 mm), as depicted in Figure 5.8. As mentioned above, the velocities of liquid and vapour phases were assumed to be similar in the homogeneous equilibrium flow. Since the annular flow dominates appreciably in small-diameter tubes, the velocities of liquid and vapour phases are different. Therefore, this model is expected to provide poor accuracy. Accordingly, Figure 5.8(a-c) show the homogeneous flow model provides considerably poor predictions for most of the experimental data of three tubes (1.1, 2.01 and 2.88 mm), with MAE values of 78.03%, 72.26% and 54.17%, respectively. The model also shows significant underprediction for the data of the three tubes by much more than the –30% error band, although better prediction for only 1.1 and 2.01 mm tubes is obtained for the lower pressure drop values corresponding to low vapour quality, see Figure 5.8a and Figure 5.8b. This may be attributed to the influence of nucleate boiling at low vapour quality which gives the best mixing for both phases and consequently making the slip ratio close to unity. However, it also overpredicts the data of 4.26 mm tube with an MAE value of only 20.78%, as seen in Figure 5.8d. The performance of model improves to predict 78.91% of the experimental data within ±30% error bands when the tube diameter increases to 4.26 mm.

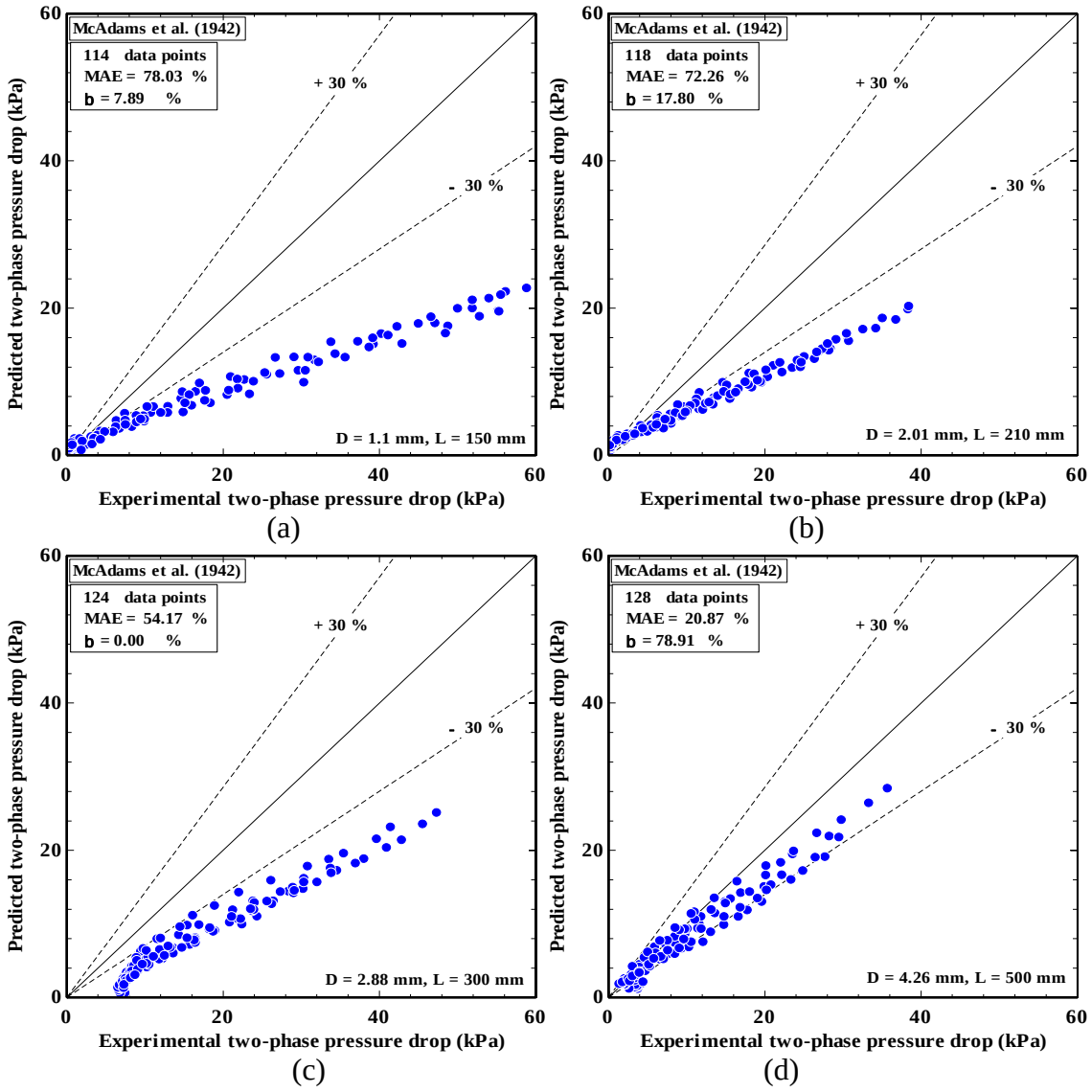

Figure 5.8 Comparison of experimental data with predictions of the Homogeneous model (McAdams et al., 1942) model for: (a) D = 1.1 mm, (b) D = 2.01 mm, (c) D = 2.88 mm, and (d) D = 4.26 mm.

Lockhart and Martinelli (1949) correlation

Lockhart and Martinelli (1949) presented a general model to predict two-phase flow pressure drop and void fraction for isothermal gas-liquid flow in conventional tubes with a diameter ranging from 1.49 – 25.83 mm. The details of correlation are expressed in Appendix B. Figure 5.9(a-c) shows that the Lockhart and Martinelli (1949) correlation recommended for conventional channel provides poor predictions for all three separate subsets of 1.1, 2.01 and 2.88 mm tubes with MAE values of 78.31%, 71.59% and 44.45%, respectively. Also, the predicted data of 1.1, 2.01 and 2.88 mm tubes are respectively 20.18%, 36.44% and 7.26% of data within the ±30% error bands. On the contrary, the

correlation performs best for the experimental data of 4.26 mm tube with an MAE value of 20.58%. It predicts 75% of data within the ±30% error bands, as shown in Figure 5.9d. That is, the performance of correlation becomes worse with decreasing tube diameter, particularly less than 3 mm. Moreover, the correlation of Lockhart and Martinelli (1949) significantly underpredicts most of the small tube data by far more than -30% error compared to the data of the 4.6 mm tube. Further, slight overprediction is observed in the pressure drop data of 4.25 mm tube. It can be seen that a comparison of this model's prediction did not show a reasonable agreement with experimental data for 1.1, 2.01 and 2.88 mm tubes. The disagreement might be due to large differences between the

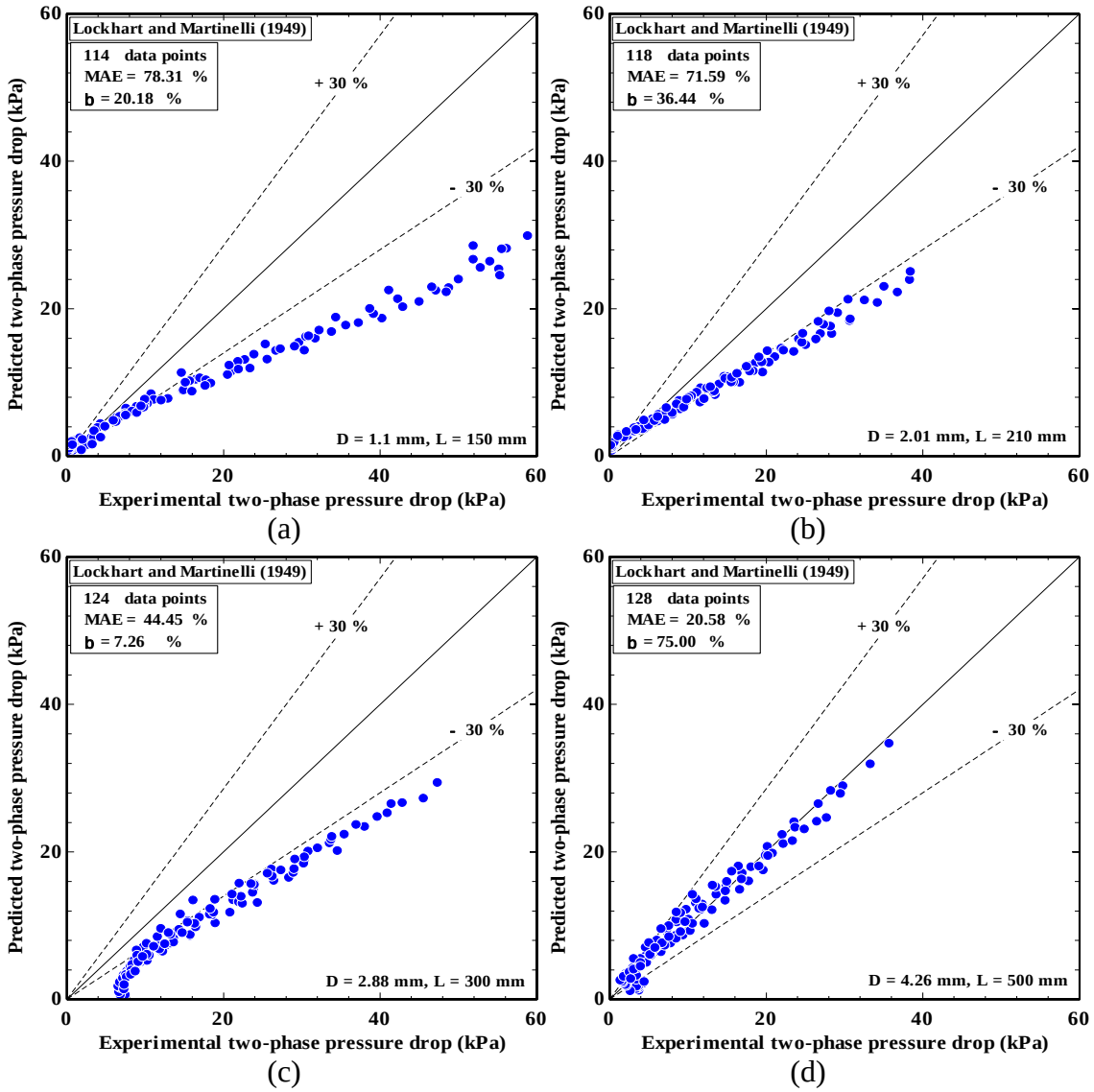

Figure 5.9 Comparison of experimental data with predictions of Lockhart and Martinelli (1949) correlation for: (a) D = 1.1 mm, (b) D = 2.01 mm, (c) D = 2.88 mm, and (d) D = 4.26 mm.

thermophysical properties of water and those of R245fa. Additionally, this model was designed for conventional channels.

Chisholm (1973a) correlation

The Chisholm (1973a) correlation depends upon the influence of mass velocity on two-phase flow as well as vapour quality and liquid-only and gas-only single-phase pressure drop of turbulent flow to develop the two-phase frictional multiplier. The expression is presented in Appendix B. This correlation shows good agreement for 1.1 and 2.01 mm tubes but with higher MAE values, see Figure 5.10a and Figure 5.10b. The β values for 1.1 and 2.01 mm tubes are 55.26% and 63.56% within ±30% error bands, respectively. The lower pressure drop data of 1.1 and 2.01 mm tube are overpredicted by slightly more than 30%, while the higher pressure drop data are underpredicted. Additionally, there is a scatter in the prediction, especially for 1.1 mm tube. It is obvious from Figure 5.10c that the correlation fairly predicts 79.84% of the experimental data for 2.88 mm tube within ±30% error bands and MAE value of only 25.59%. The correlation also provides underprediction for 2.88 mm tube, excluding the pressure drop data less than 8 kPa which falls out of -30% error band. For 4.26 mm tube, the correlation highly overpredicts the experimental data with 45.41% MAE, see Figure 5.10d. The predicted data for 4.26 mm tube is 33.59% within ±30% error bands. The disagreement between predictions of correlation and experimental data might be due to significant differences between the thermophysical properties of water and those of R245fa. In addition, this model was developed for turbulent flow in conventional channels.

Grönnerud (1979) correlation

Grönnerud (1979) proposed a two-phase pressure drop correlation based on a variety of refrigerants and operating conditions. The author used the Froude number, viscosity ratio, density ratio and vapour quality to develop the two-phase liquid-only frictional multiplier. The details of correlation expressed in Appendix B. Figure 5.11 shows that the correlation recommended for macro-channels provide poor predictions for most of the flow boiling pressure drop data of 1.1, 2.01and 2.88 mm tubes, while the correlation exhibits fair predictions for the 4.26 mm tube data. Moreover, the correlation under-

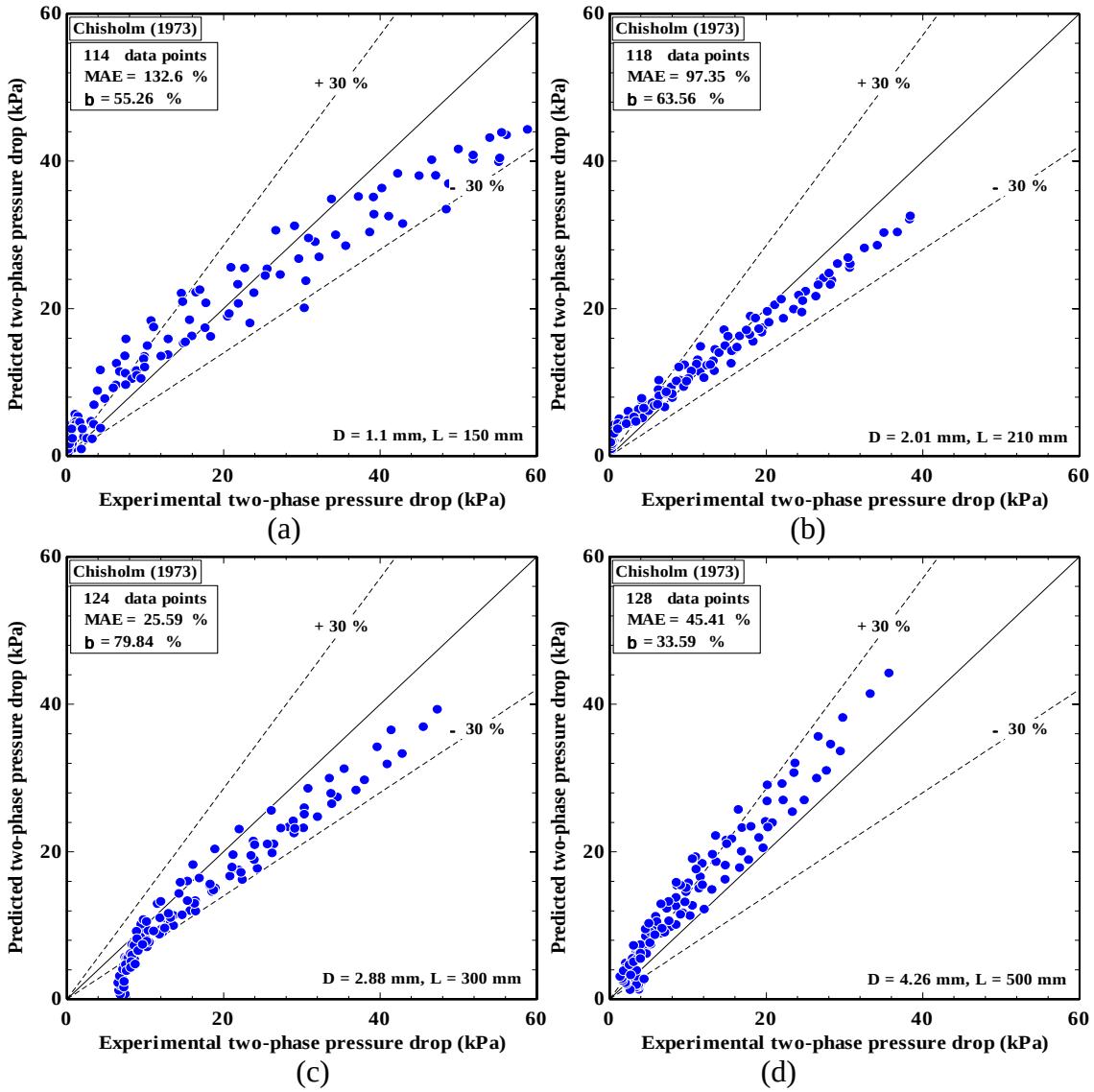

Figure 5.10 Comparison of experimental data with predictions of Chisholm (1973a) correlation for: (a) D = 1.1 mm, (b) D = 2.01 mm, (c) D = 2.88 mm, and (d) D = 4.26 mm.

predicts the data of three small tubes in general, especially for the 1.1 mm tube, by some scatter see Figure 5.11a. The MAE value of 1.1 mm tube is significantly higher compared to those of other tubes and also this value reduces with increasing the tube diameter. However, for the 4.26 mm tube, the correlation slightly overpredicts the pressure drop data with only 18.65% MAE and the β value is 82.03% within the ±30% error bands. The worse prediction of Grönnerud (1979) correlation may be attributed to using R12 and R717 as working fluid in macro channels.

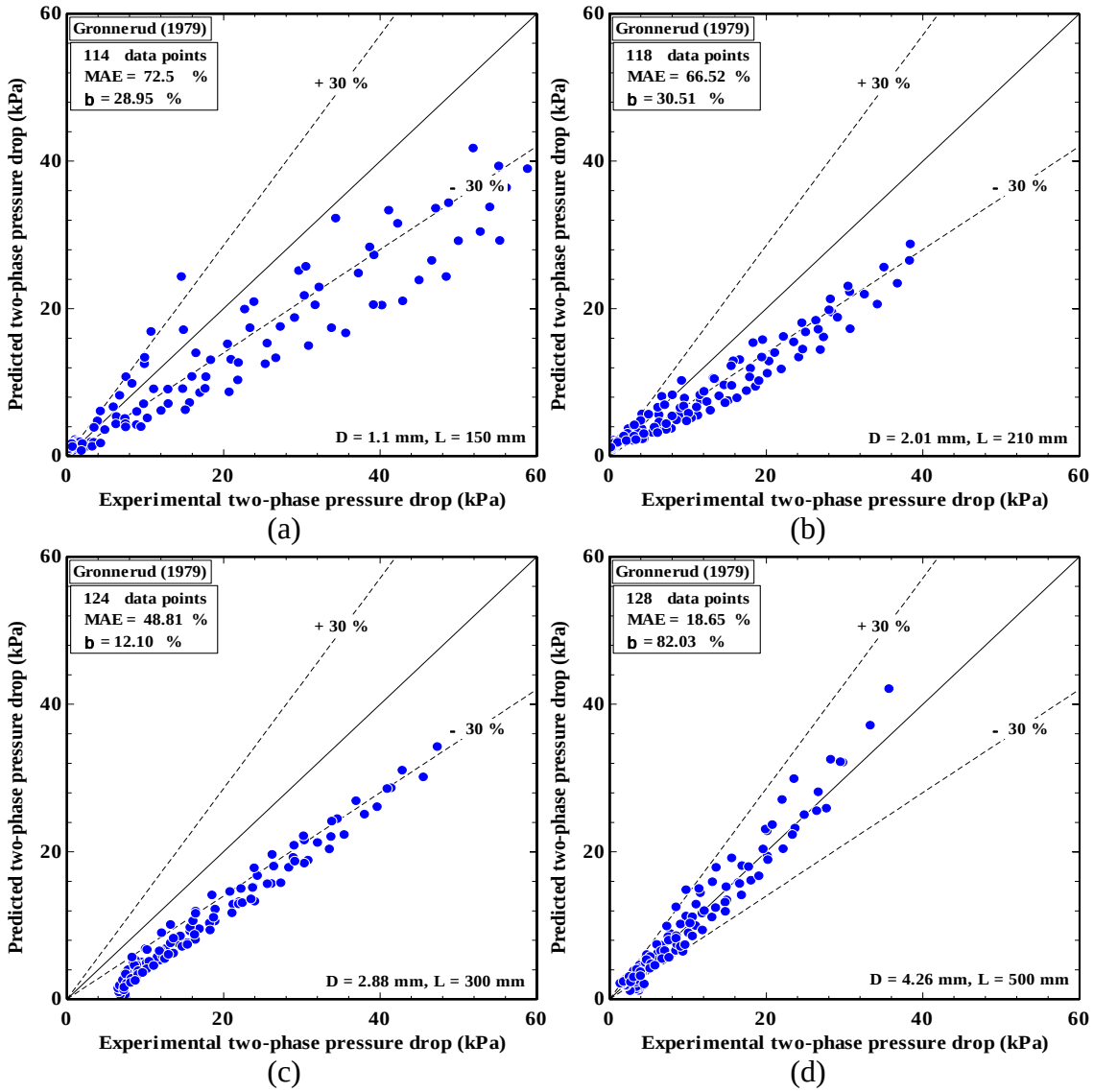

Figure 5.11 Comparison of experimental data with predictions of Grönnerud (1979) correlation for: (a) D = 1.1 mm, (b) D = 2.01 mm, (c) D = 2.88 mm, and (d) D = 4.26 mm.

Friedel (1979) correlation

Friedel (1979) introduced the Weber and Froude number to modify two-phase frictional multiplier in terms of liquid-only. This model includes the effect of gravitational force through the Froude number and the effects of surface tension force and total mass flux through the Weber number. The details of the correlation are included in Appendix B. According to Figure 5.12(a-c), the correlation presents worst accuracy for the three small tubes (1.1, 2.01 and 2.88 mm) and highly underpredicts their experimental data by MEA values of 103.5% for 1.1mm, 83.03% for 2.01 mm and 52.95% for 2.88 mm. For 4.26 mm tube, the correlation fairly predicts 83.59 % of the data at MAE value of only

19.04%, as seen in Figure 5.12d. That is, the correlation performance decreases considerably as the tube diameter is less than 4 mm. Consequently, the correlation performs considerably better for the 4.26 mm tube in comparison to 1.1 – 2.88 mm tubes. In addition, the significant underprediction for 1.1, 2.01, and 2.88 mm tubes falls outside the -30% error bands. The disagreement between predictions of model and experimental data might be because of this model designated for tubes larger than 4 mm.

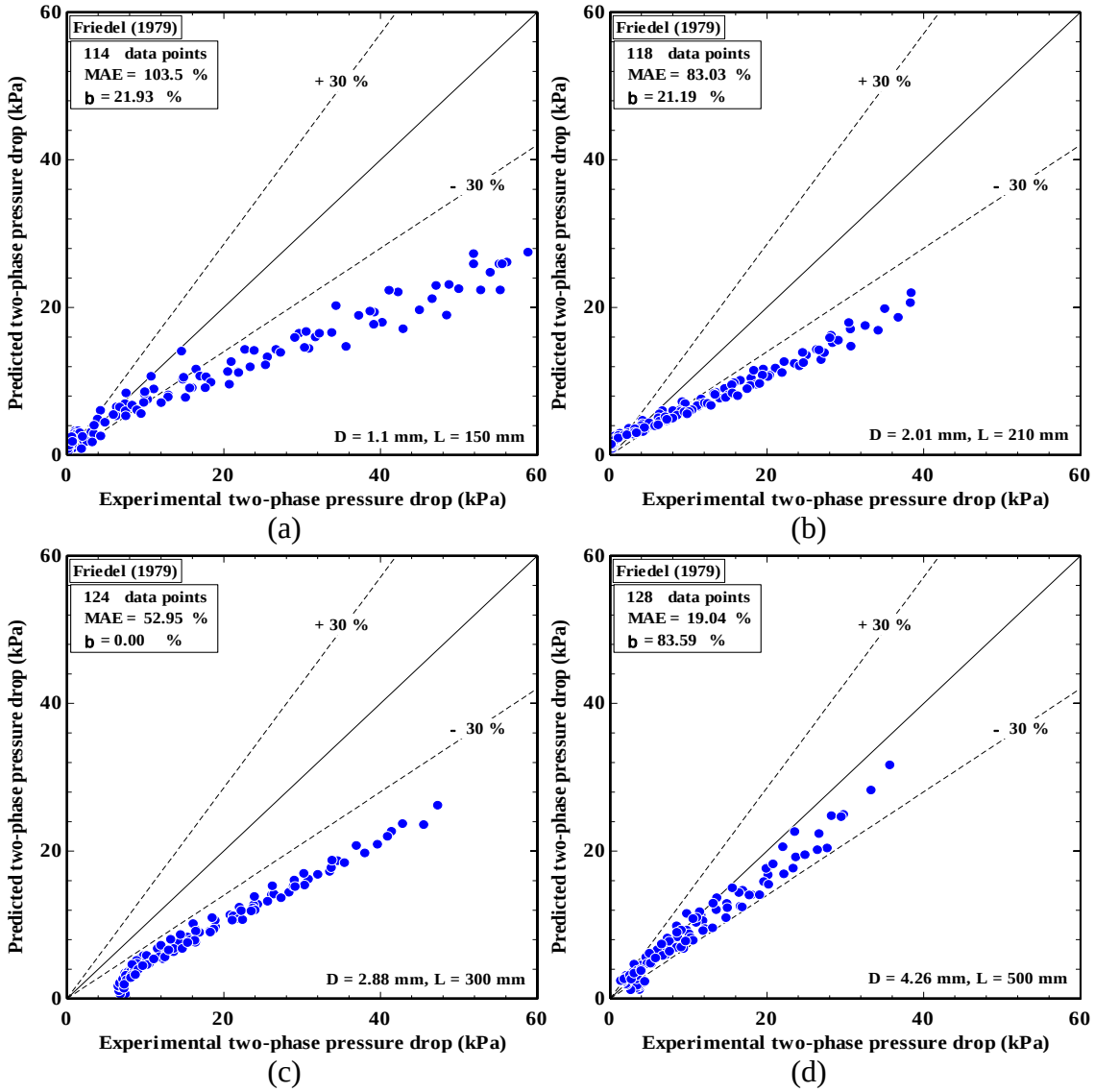

Figure 5.12 Comparison of experimental data with predictions of Friedel (1979) correlation for: (a) D = 1.1 mm, (b) D = 2.01 mm, (c) D = 2.88 mm, and (d) D = 4.26 mm.

Müller-Steinhagen and Heck (1986) correlation

Müller-Steinhagen and Heck (1986) suggested a correlation based on a databank involving 9300 measurements of frictional pressure drop. They employed the pressure gradient of the respective single-phase flow (i.e. liquid-only and gas-only) in addition to the implementation of an empirical two-phase extrapolation between all liquid flow and all vapour flow. They also took into account the influence of flow parameters such as vapour quality, mass flux and system pressure. Their relation is given in Appendix B. Figure 5.13(a-c) shows that the pressure drop data for 1.1, 2.01, and 2.88 mm tube is significantly under-predicted by more than the -30% error bands. The performance of correlation becomes low when the channel size decreases. This is due to the flow of both phases changing into the laminar flow with decreasing channel size. Also, the correlation was developed for tubes having inner diameter higher than 4 mm, see Appendix B. As seen in Figure 5.13d, for the 4.26 mm tube, the correlation predicts the experimental data very well with 83.59% of the data within the ± 30 % error bands and only 18.48% MAE. The higher value of MAE is for 1.1 mm tube, of 81.15%. Also, this value decreases with tube diameter. As mentioned before, the poor predictions of model might be because of this model developed for tubes larger than 4 mm.

5.8.2 Predictive methods for small tubes and comparison

Mishima and Hibiki (1996) correlation

Mishima and Hibiki (1996) modified the parameter of Chisholm (1967) to better match their data for air-water under turbulent-turbulent flow condition for capillary tubes with an inner diameter range of 1 – 4 mm. They tried to remove the dependence of the Chisholm's parameter *C* on Reynolds number and superficial velocity and used only the value of turbulent-turbulent flow in addition to the effect of channel hydraulic diameter. The details of the correlation are summarized in Appendix B. Figure 5.14(a-c) shows that the correlation provides poor predictions for the pressure drop data of 1.1, 2.01 and 2.88 mm tubes, evidenced by MAE values of 88.8%, 76.98%, and 52.72%, respectively. Contrarily, the correlation shows fair predictions for 4.26 mm tube with only 18.29% MAE and the β value is very higher than those of other tubes, of 81.25% within the ±30% error bands, see Figure 5.14d. It highly underpredicts the flow boiling pressure drop data for 1.1, 2.01, 2.88 mm tube by much more than -30%. The disagreement in predicting

1.1, 2.01 and 2.88 mm tubes could be attributed to the fact that the reason was related to the effect of fluid and fluid properties.

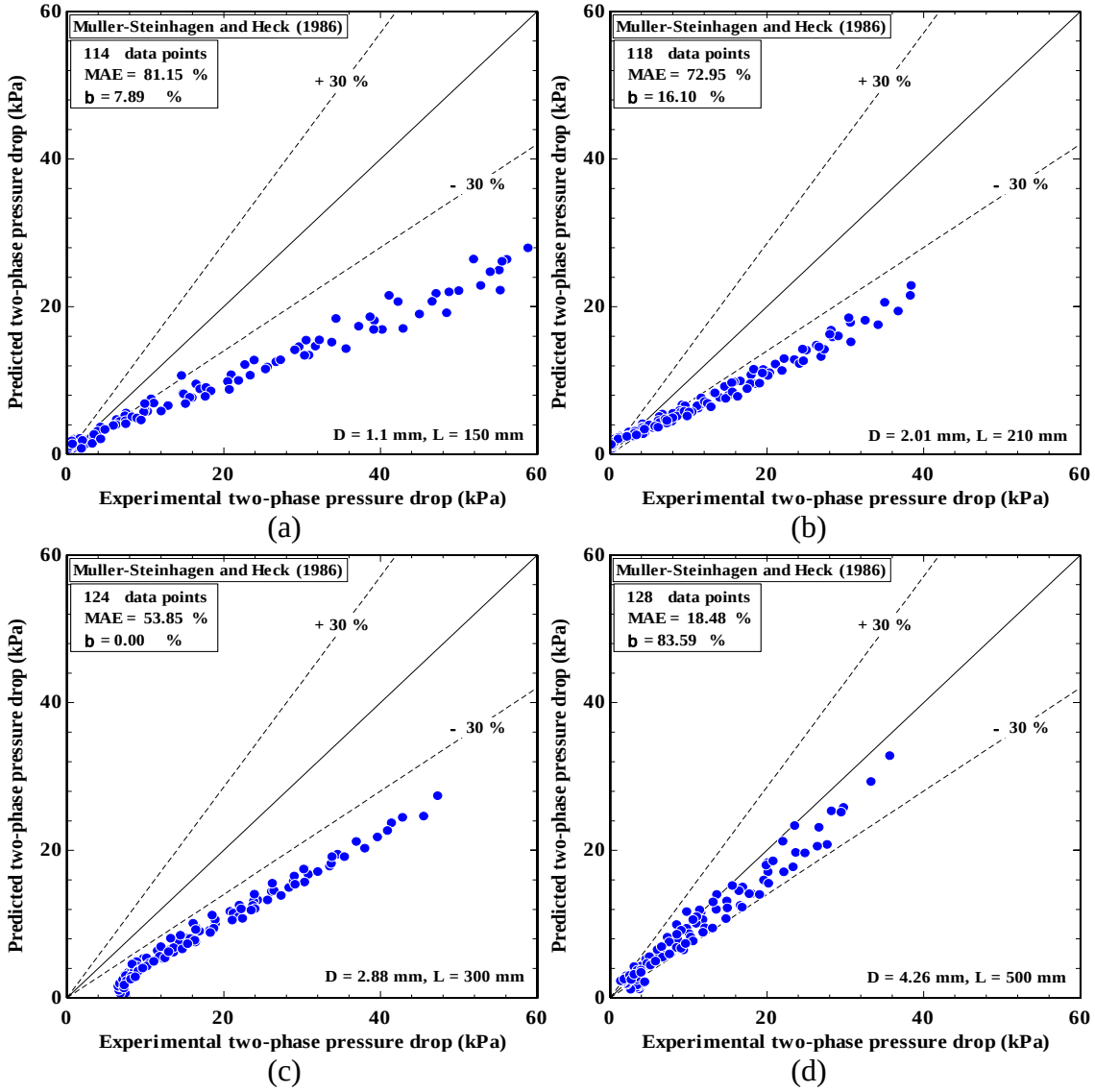

Figure 5.13 Comparison of experimental data with predictions of Müller-Steinhagen and Heck (1986) correlation for: (a) D = 1.1 mm, (b) D = 2.01 mm, (c) D = 2.88 mm, and (d) D = 4.26 mm.

Qu and Mudawar (2003) correlation

Qu and Mudawar (2003) conducted an empirical investigation on flow boiling pressure drop of water flowing in a channel with 0.35 mm hydraulic diameter. They incorporated the influences of both channel size and mass flux to improve the predictive

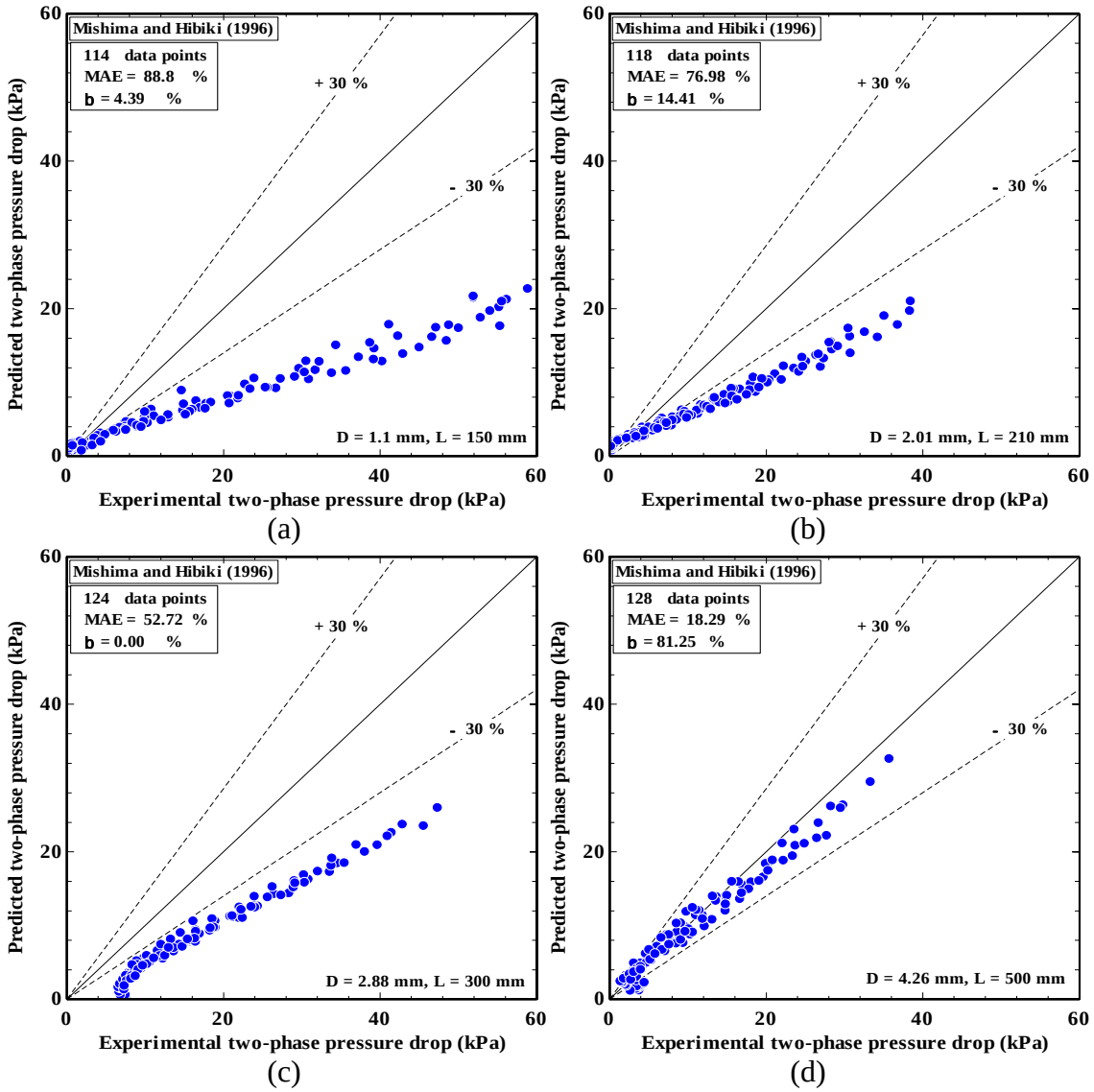

Figure 5.14 Comparison of experimental data with predictions of Mishima and Hibiki (1996) correlation for: (a) D = 1.1 mm, (b) D = 2.01 mm, (c) D = 2.88 mm, and (d) D = 4.26 mm.

performance of the Chisholm's parameter in the two-phase multiplier model of Mishima and Hibiki (1996) for mini and micro-channels. The expression is given in Appendix B. Figure 5.15 shows most of the two-phase pressure drop data are poorly predicted and the performance of the correlation becomes worse with decreasing tube diameter, evidenced by MAE value of 93.9% for 1.1 mm, 80.37% for the 2.01 mm tube, 37.47% for 2.88 mm and 37.17% for 4.26 mm. However, the β value for 2.01 mm is appreciably higher than those for the other tubes, of 50% within ±30% error bands. The correlation shows the significant underprediction for 1.1, 2.01 and 2.88 mm tube and the significant overprediction for the 4.26 mm tube. Interestingly, this correlation was a modified form

of the Mishima and Hibiki (1996)'s correlation, which underpredicted most of the data for all tubes by a large margin except the 4.26 mm tube having turbulent flow in both phases. Besides, this limited performance is ascribed to the use of a narrow range of experimental data, one working fluid and channel size less than 1 mm.

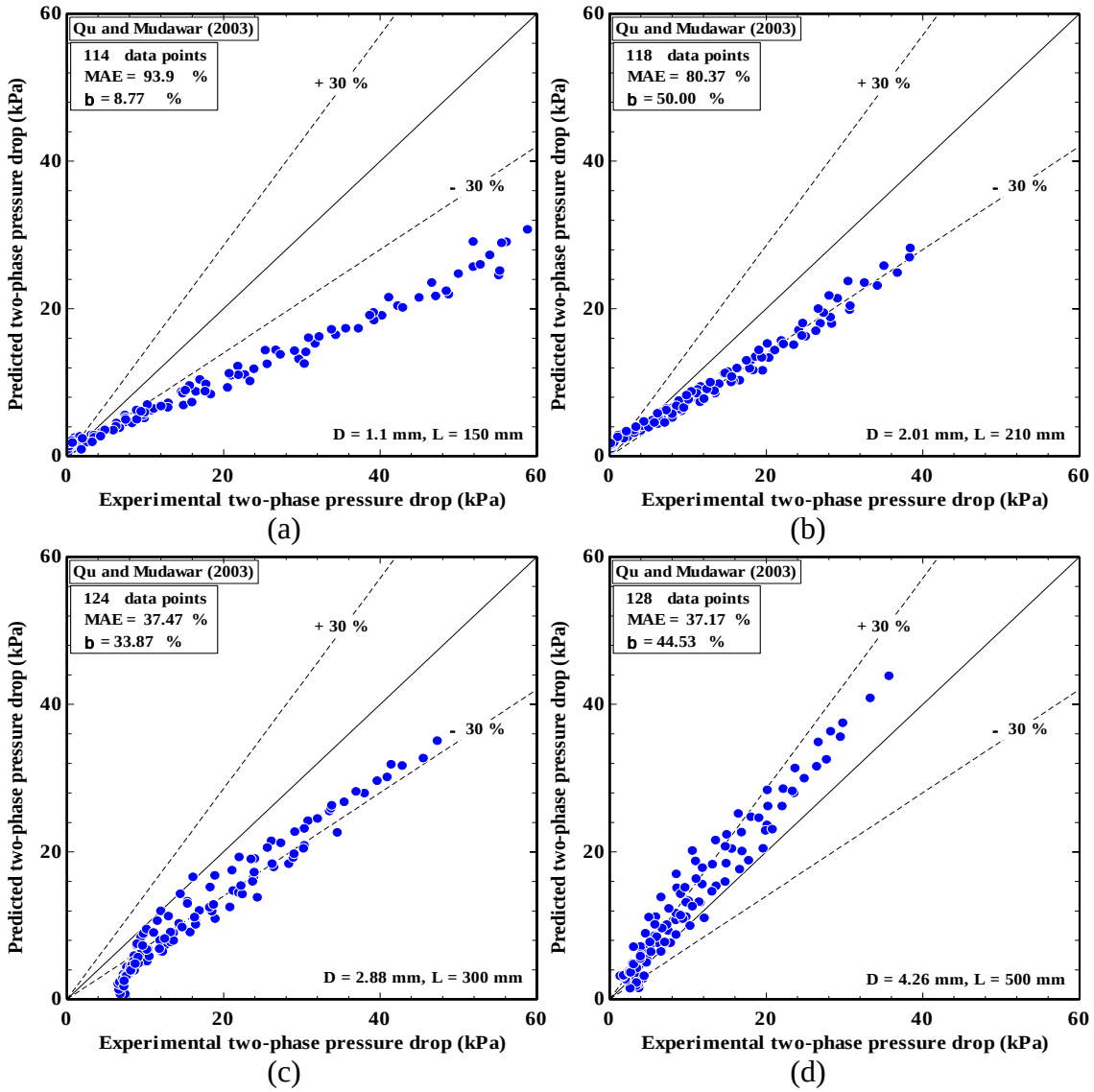

Figure 5.15 Comparison of experimental data with predictions of Qu and Mudawar (2003) correlation for: (a) D = 1.1 mm, (b) D = 2.01 mm, (c) D = 2.88 mm, and (d) D = 4.26 mm.

Hwang and Kim (2006) correlation

Hwang and Kim (2006) carried out flow boiling test of R134a in micro-tubes with a range of 0.244 – 0.792 mm. The authors found that the channel size, surface tension and

Reynolds number have a significant effect on the two-phase flow frictional pressure drop in microtubes. Therefore, they developed the Chisholm's parameter using the liquid-only Reynolds number, the Martinelli parameter, and the Confinement number. The expression is presented in Appendix B. This correlation performs well only for the 2.01 and 2.88 mm tubes with β values of 72.03% and 69.35% as well as MAE values of 62.52% and 25.66%, respectively. The correlation underpredicts the experimental data of the three small tubes (i.e. 1.1, 2.01 and 2.88 mm), while the 4.26 mm tube is highly overpredicted by this correlation, evidenced by MAE value of 85.29%, see Figure 5.16. The most

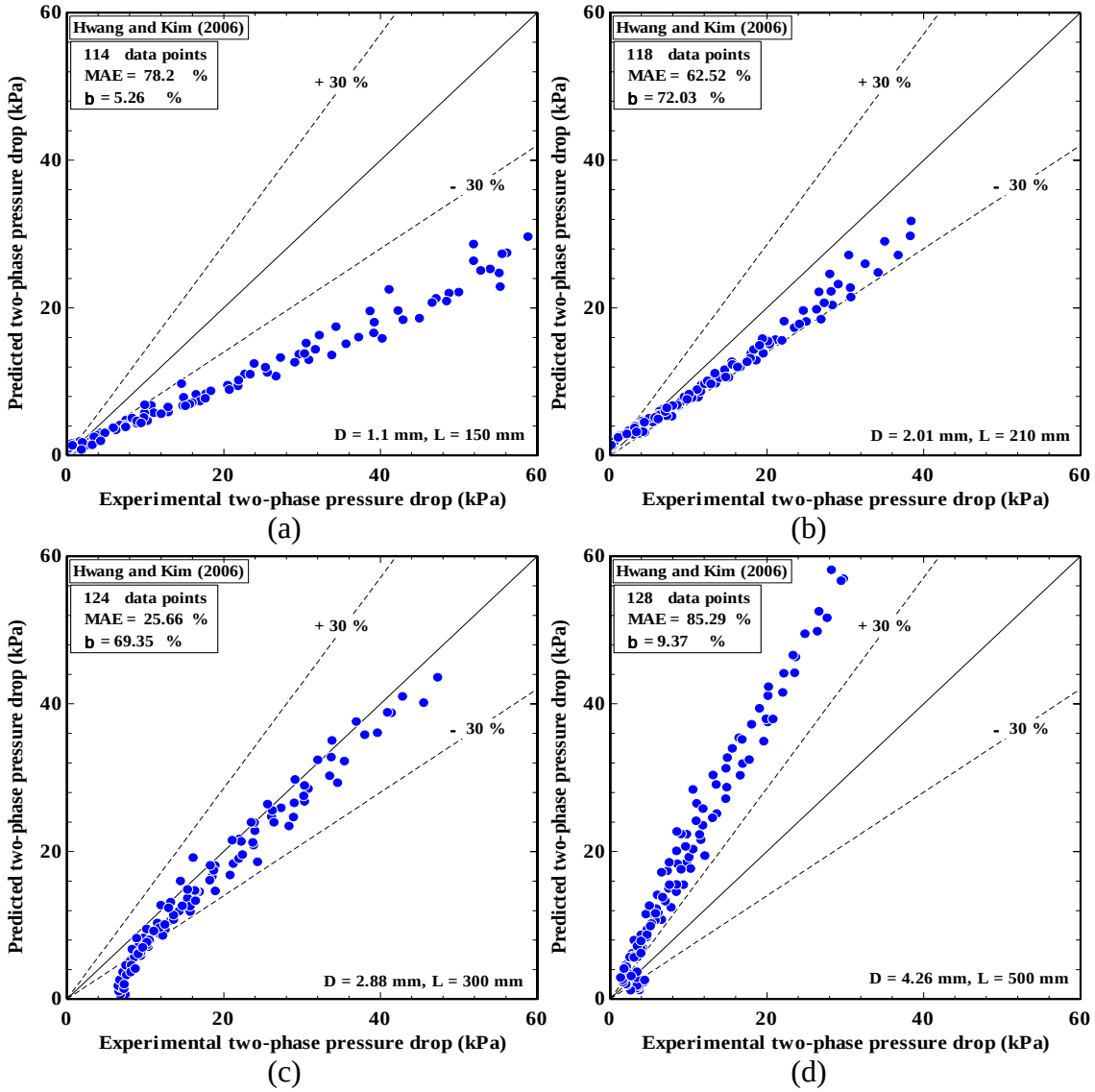

Figure 5.16 Comparison of experimental data with predictions of Hwang and Kim (2006) correlation for: (a) D = 1.1 mm, (b) D = 2.01 mm, (c) D = 2.88 mm, and (d) D = 4.26 mm.

predictions of 1.1 mm tube also fall outside of the ±30% error bands. These significant over- and under- predictions for 4.26 mm and 1.1 mm lead to an increase in the deviation between the experimental and predicted pressure drop for the entire exit vapour quality because this correlation was modified for tubes being less 1 mm with the narrow range of experimental data.

Sun and Mishima (2009) correlation

Sun and Mishima (2009) collected an experimental database from 18 sources consisting of 2092 data points, including 11 working fluids and channel size ranging from 0.506 to 12 mm. They found that the Chisholm's parameter *C* is affected by the liquid Reynolds number and Laplace number in the laminar flow region while in turbulent flow region, it significantly affected by the ratio of the gas Reynolds number to the liquid Reynolds number. Based on the results of statistical analysis, they proposed two models to modify Chisholm's parameter, one for laminar flow and another for turbulent flow, see Appendix B. This correlation provides poor predictions for the experimental data of 1.1, 2.01 and 2.88 mm tube, evidenced by MAE values of 80.05%, 76.47% and 56.65%, respectively. However, the fair predictions are provided for 4.26 mm tube with 77.34% of data within ±30% error bands and only 21.36% MAE. The correlation underpredicts most of the data, as depicted in Figure 5.17. It is interesting to note that most predicted data with diameters below 4 mm fall outside of the ±30% error bands, see Figure 5.17(a-c). This results in a large divergence between predicted and experimental data, especially for 2.88 mm tube. Besides, this limited performance is ascribed to the use of a narrow range of experimental data for R245fa flowing only in 0.509 and 0.79 mm tubes.

Li and Wu (2010a) correlation

Li and Wu (2010a) modified the Chisholm's parameter of two-phase multipliers to develop their correlation of adiabatic two-phase pressure drop across mini and microchannels based on 769 experimental data points. These data included 12 refrigerants and 0.148 – 3.25 mm tube diameter. They found that the Bond number and the liquid Reynolds number are the influential parameters. Further, they categorized the data on the

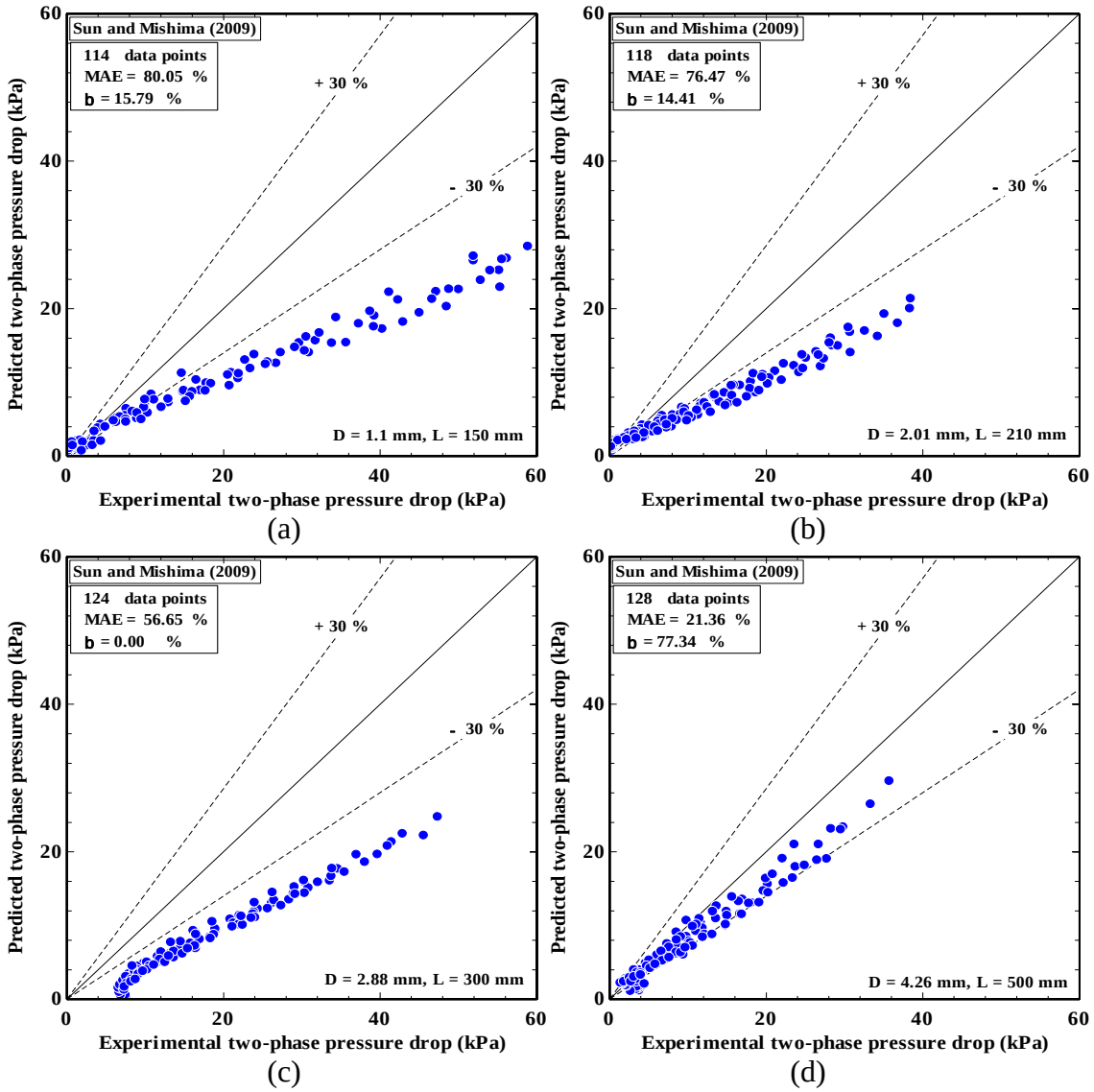

Figure 5.17 Comparison of experimental data with predictions of Sun and Mishima (2009) correlation for: (a) D = 1.1 mm, (b) D = 2.01 mm, (c) D = 2.88 mm, and (d) D = 4.26 mm.

basis of Bond number in three ranges, namely region of dominant surface tension ($Bd \leq 1.5$), region dominated by surface tension, inertia, and viscous force ($1.5 < Bd \leq 11$), and region without the surface tension effect ($Bd > 11$). The details of the correlation are summarized in Appendix B. The correlation gives the best agreement with the experimental data of the 4.26 mm tube (as shown in Figure 5.18d) where 71.87% of the data are predicted within the ±30% error bands and also 21.17% MAE. As opposed to the 4.26 mm results which are overpredicted, the performance of the correlation in the small tubes gets worse as the tube diameter decreases resulting in an underprediction of the small tube data, as seen in Figure 5.18(a-c). The MAE values of 1.1, 2.01 and 2.8 mm

tubes are respectively 89.04%, 69.88% and 37.82%. The highest MAE values of the 1.1 and 2.01 mm tubes give rise to data points falling outside of the ±30%, showing a considerable discrepancy between the experimental data and predictions. For the 2.88 mm tube (Figure 5.18a and Figure 5.18b), the correlation predicts only 44.35% of the data. In addition, this weak performance may be attributed to using a narrow range of experimental data for R245fa flowing only in 0.509 and 0.79 mm tubes.

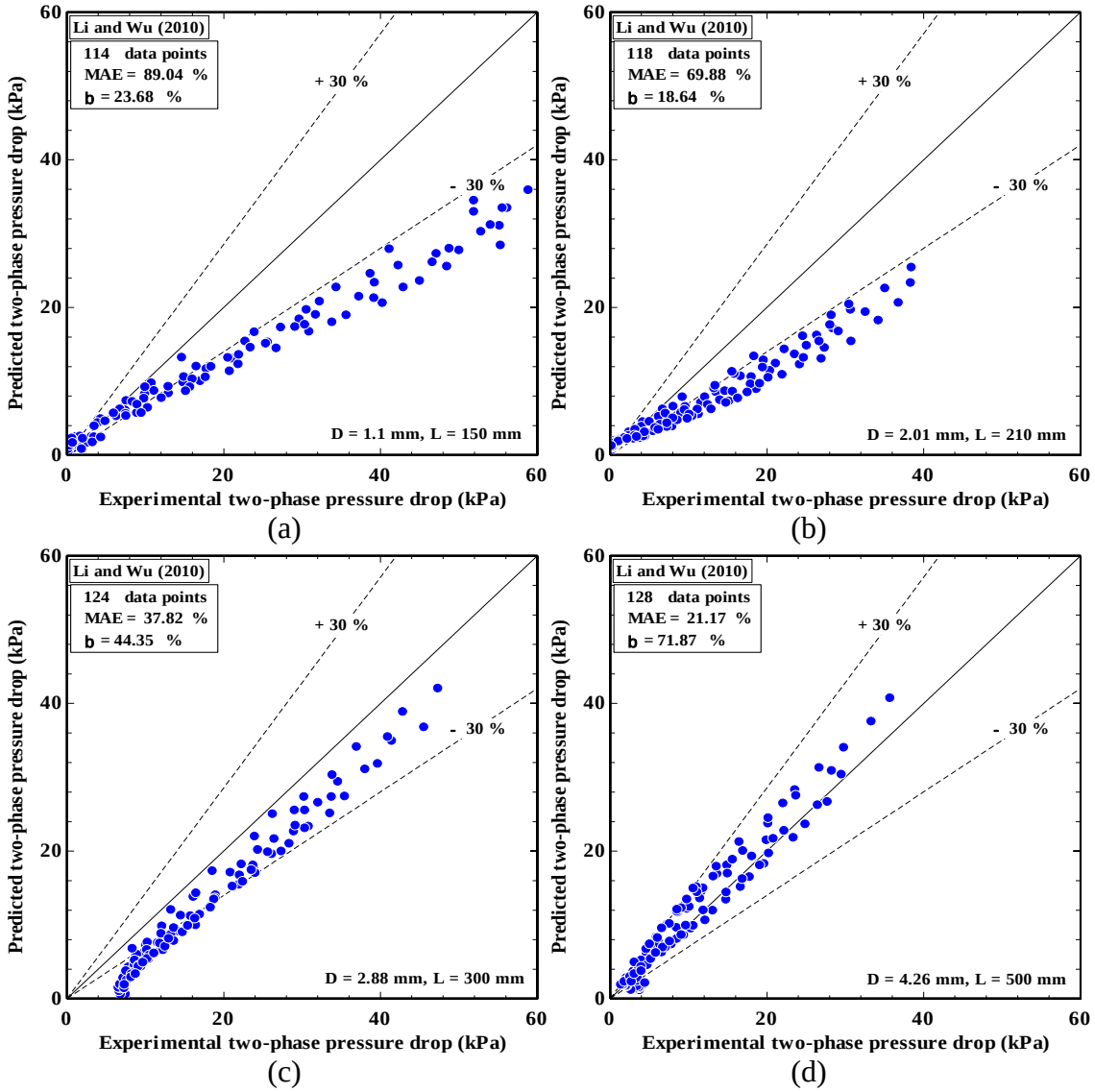

Figure 5.18 Comparison of experimental data with predictions of Li and Wu (2010a) correlation for: (a) D = 1.1 mm, (b) D = 2.01 mm, (c) D = 2.88 mm, and (d) D = 4.26 mm.

Lee et al. (2010) correlation

Lee et al. (2010) compiled 484 experimental data points from 9 different studies on flow boiling pressure drop across mini/micro channels. These data covered hydraulic diameters less than 3 mm and 7 working fluids including water and refrigerants. They adapted the Chisholm's parameter to comprise the Bond number and exit quality. They found that the Bond number is significantly influenced by interfacial interactions between the phases. A low Bond number represented the confined bubble flow with reducing the interactions between phases, while a higher Bond number measure up to more phase interactions, such as bubbly flow. This adapted parameter yields much higher values than those of the original Chisholm constants. The details of the correlation are included in Appendix B. As shown in Figure 5.19, the correlation shows large scatter against most of the entire experimental data, with significant underprediction of most of the small tube data (1.1, 2.01 and 2.88 mm). Also, the results are increasingly spread with decreasing tube diameter from 2.88 to 1.1 mm, evidenced by MAE values ranging from 72.08% to 45.47%, respectively. On the contrary, for 4.26 mm tube, the correlation provides fair predictions with only 25.74% MAE with a tendency to highly over-predict the data. The β values are considerably higher for 4.26 mm tube, of 52.64%, see Figure 5.19d. The poor performance could be attributed to the fact that the reason was related to the effect of fluid and fluid properties.

Xu and Fang (2012) correlation

Xu and Fang (2012) proposed a correlation based on 2622 experimental data points of 15 refrigerants with hydraulic diameter from 0.81 to 19.1 mm. The authors modified the correlation of Müller-Steinhagen and Heck (1986) by using the Laplace constant, see Appendix B. According to Figure 5.20, this correlation provides poor predictions for most of the experimental data: 1.1, 2.01, 2.88 and 4.26 mm tube, evidenced by MAE values of 86.57%, 81.82%, 76.86% and 48.05%, respectively. It also provides a significant underprediction of most of the data. The disagreement between predictions of correlation and experimental data might be attributed to the effect of fluid and fluid properties, i.e. the R245fa fluid was not within their chosen experimental database.

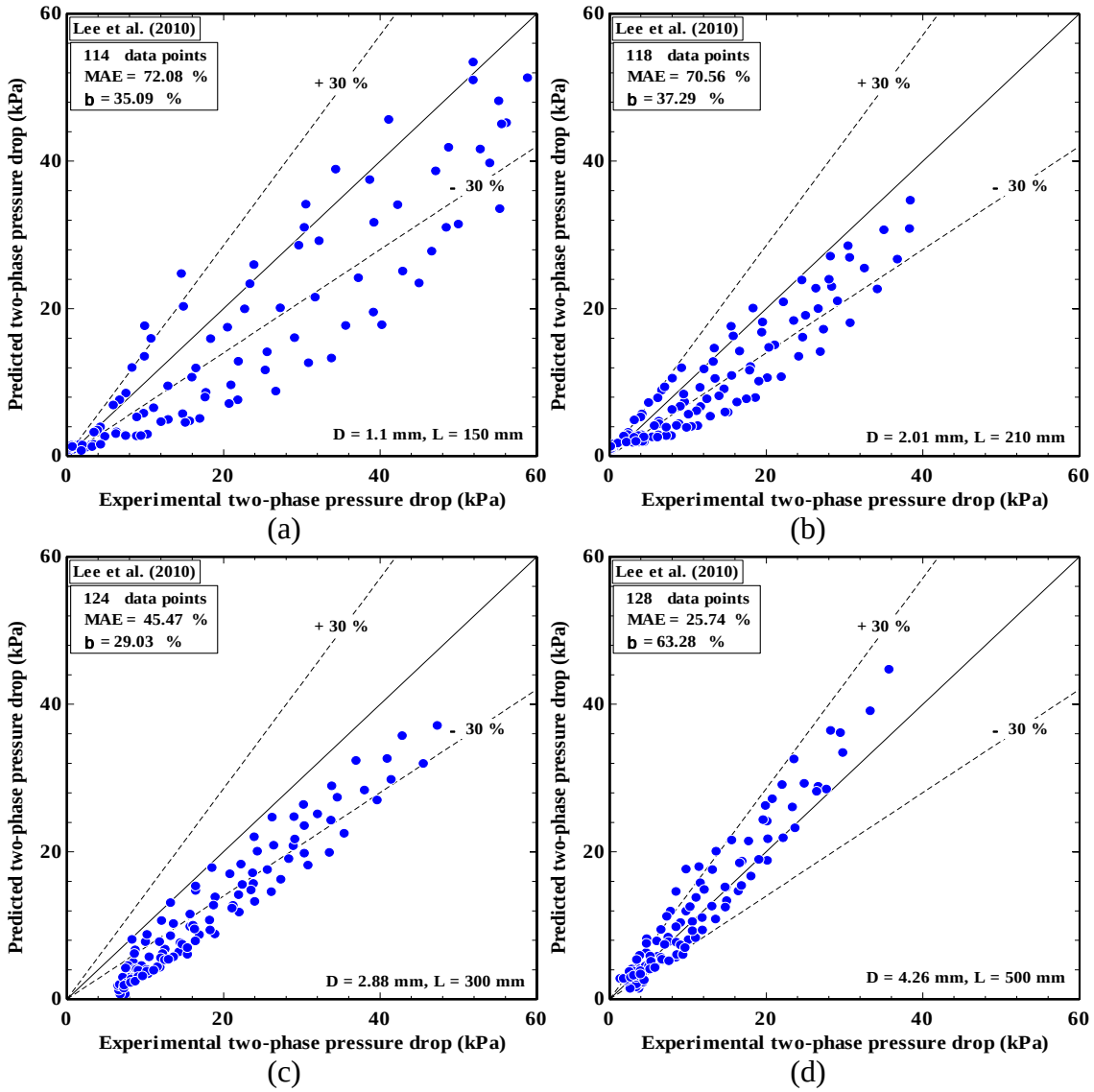

Figure 5.19 Comparison of experimental data with predictions of Lee et al. (2010) correlation for: (a) D = 1.1 mm, (b) D = 2.01 mm, (c) D = 2.88 mm, and (d) D = 4.26 mm.

Kim and Mudawar (2012) correlation

Kim and Mudawar (2012) developed a correlation to predict two-phase pressure drop in mini and microchannels based on a consolidated database covering 7115 data points from 36 sources. The Chisholm's parameter was modified with appropriate dimensionless parameters involving liquid-only Reynolds number, gas-only Suratman number, and liquid-gas density ratio for each of the four flow regimes. The details of the correlation are summarized in Appendix B. The correlation performs best for the 4.26 mm tube, predicting 53.91% of experimental data within ±30%, see Figure 5.21d. According to Figure 5.21(a-c), the values of prediction for 1.1, 2.01, 2.88 mm tube are considerably

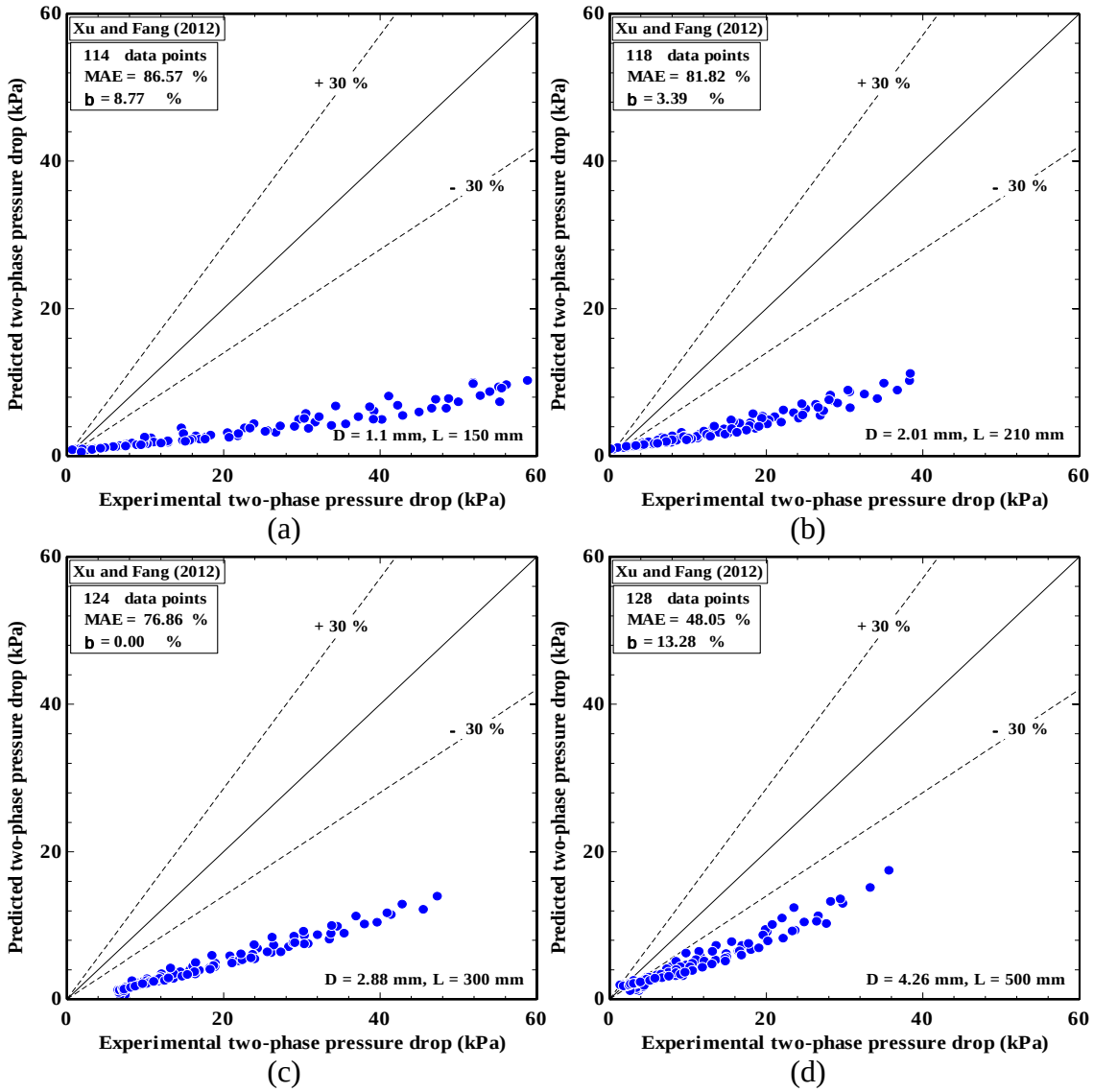

Figure 5.20 Comparison of experimental data with predictions of Xu and Fang (2012) correlation for: (a) D = 1.1 mm, (b) D = 2.01 mm, (c) D = 2.88 mm, and (d) D = 4.26 mm.

lower, of 7.89%, 26.27% and 12.1%, respectively. The 1.1 mm tube gives a large value of MAE, 98.1% compared to other tubes. The two-phase pressure drop of 4.26 mm is overpredicted by 25.11%, while the two-phase pressure drop of the other tubes is underpredicted by 21.06%, 38.78% and 42.38% for 1.1, 2.01 and 2.88 mm, respectively. The β value of entire data is very low with 25.62% and the MAE value is 63.73%. Moreover, this weak performance might be due to using a narrow range of experimental data for R245fa flowing in horizontal rectangular multi-channel.

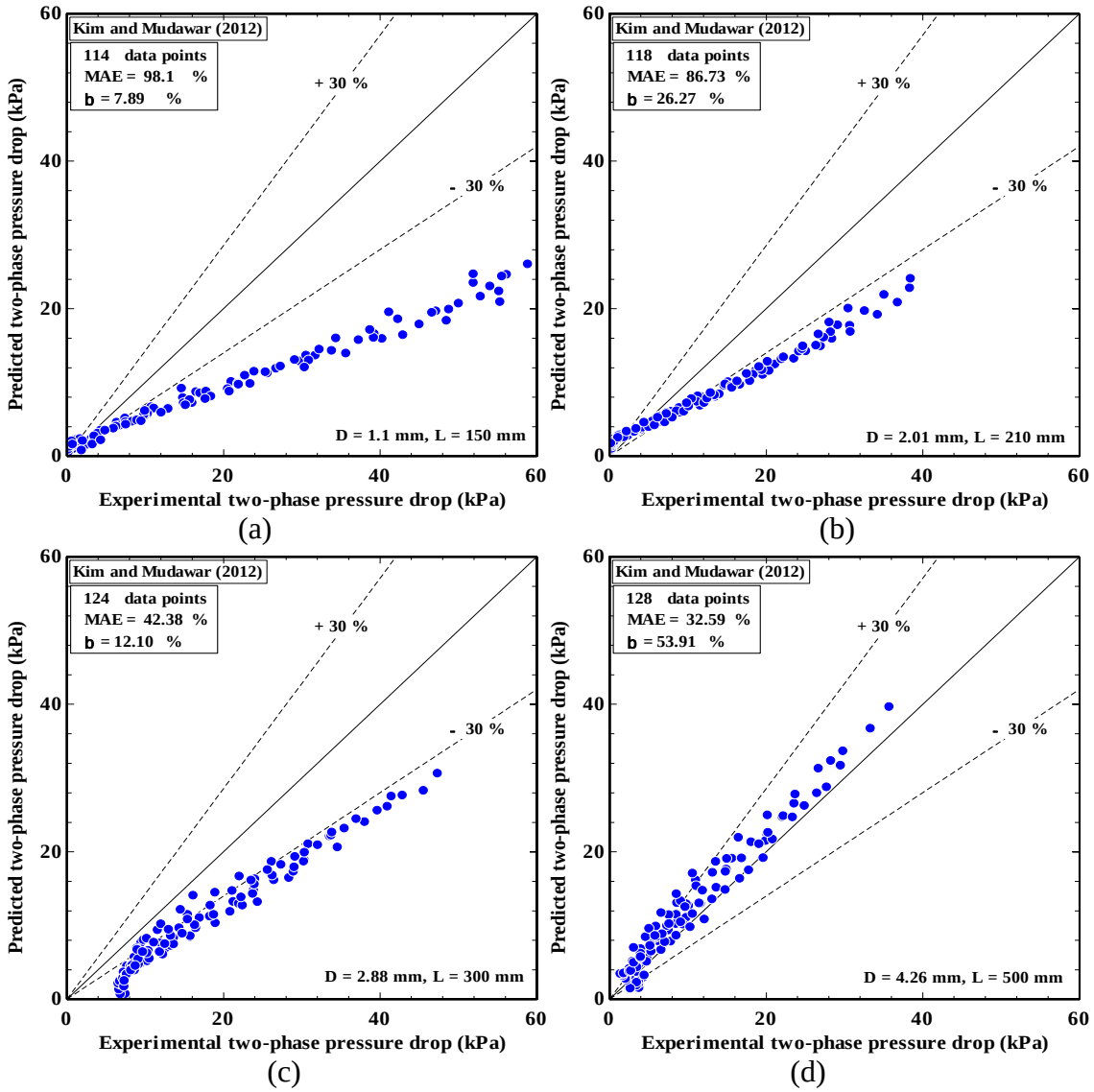

Figure 5.21 Comparison of experimental data with predictions of Kim and Mudawar (2012) correlation for: (a) D = 1.1 mm, (b) D = 2.01 mm, (c) D = 2.88 mm, and (d) D = 4.26 mm.

Kim and Mudawar (2013) correlation

Kim and Mudawar (2013) constructed a correlation of flow boiling pressure drop in mini and microchannels by modifying their previous model (Kim and Mudawar, 2012) which was proposed for non-boiling flow. The modification was based on a consolidated database of 2378 experimental points from 16 authors. They replaced the C parameter with a function of dimensionless groups containing Weber number and Boiling number as well as the previous C parameter for non-boiling flow. They also took account of the effects of small channel size, different working fluids, and comprehensive ranges of flow parameters. The correlation is given in Appendix B. Figure 5.22 shows that the trend of

the correlation agrees well with the experimental data of tubes of 2.01 mm and 2.88 mm in contrast to 1.1 mm and 4.26 mm tubes, where the correlation predicts 75.42% of experimental data for 2.01 mm and 62.9% of the data for the 2.88 mm within the ±30% error bands. This is because the authors used 142 data points regarding the R245fa flowing in a tube of only 2.32 mm within the database of this correlation. The MAE values obtained for the 2.01 and 2.88 mm tubes are 71.38% and 27.86%, respectively. When the pressure drop is less than 8 kPa. The correlation provides overprediction for the 2.01 mm tube and underprediction for 2.88 mm tube, see Figure 5.22b and Figure 5.22c. For the 1.1 mm tube, the correlation predicts only 32.03% of experimental data within the ±30% error bands and 45.46% MAE, while the correlation predicts only 21.93% of experimental data within the ±30% error bands for 4.26 mm tube with 87.68% MAE. Further, the correlation provides underprediction and overprediction for 1.1 mm and 4.26 mm, respectively, as shown in Figure 5.22a and Figure 5.22d. In addition, this weak performance may be attributed to using a narrow range of experimental data for R245fa flowing only in 2.32 mm tube.

The comparison results with selected correlations presented above demonstrated that the homogeneous flow model slightly under-predicts the data of 4.26 mm tube. However, when the tube diameter decreases from 4.26 mm to 1.1 mm, the homogeneous flow model tends to provide poor predictions for most of the small tube data (1.1 – 2.88). For the separated flow models, the correlations of Grönnerud (1979), Friedel (1979), Müller-Steinhagen and Heck (1986), and Mishima and Hibiki (1996) show best predictions for most data of 4.26 mm tube, slight overprediction of most of data by Lockhart and Martinelli (1949) and Li and Wu (2010a), and slight underprediction of most of data by Sun and Mishima (2009). Further, the data of 2.01 mm and 2.88 mm tubes are underpredicted by Chisholm (1973a), Hwang and Kim (2006) and Kim and Mudawar (2013) but with higher MAE values for the 2.01 mm tube. The data of the 1.1 mm tube are not well predicted by any of the selected predictive methods.

Generally, among the presented prediction methods, there was no predictive method that predicted all four separate subsets of the experimental data for four tubes with fair and similar accuracy. That is, there is a deviation in the prediction results with decreasing

tube diameter for most of the predictive methods. In order to improve a one comprehensive model, it is required that the consolidated database must be expanded, including different fluid properties, different channel sizes and using a wide range of experimental data for R245fa.

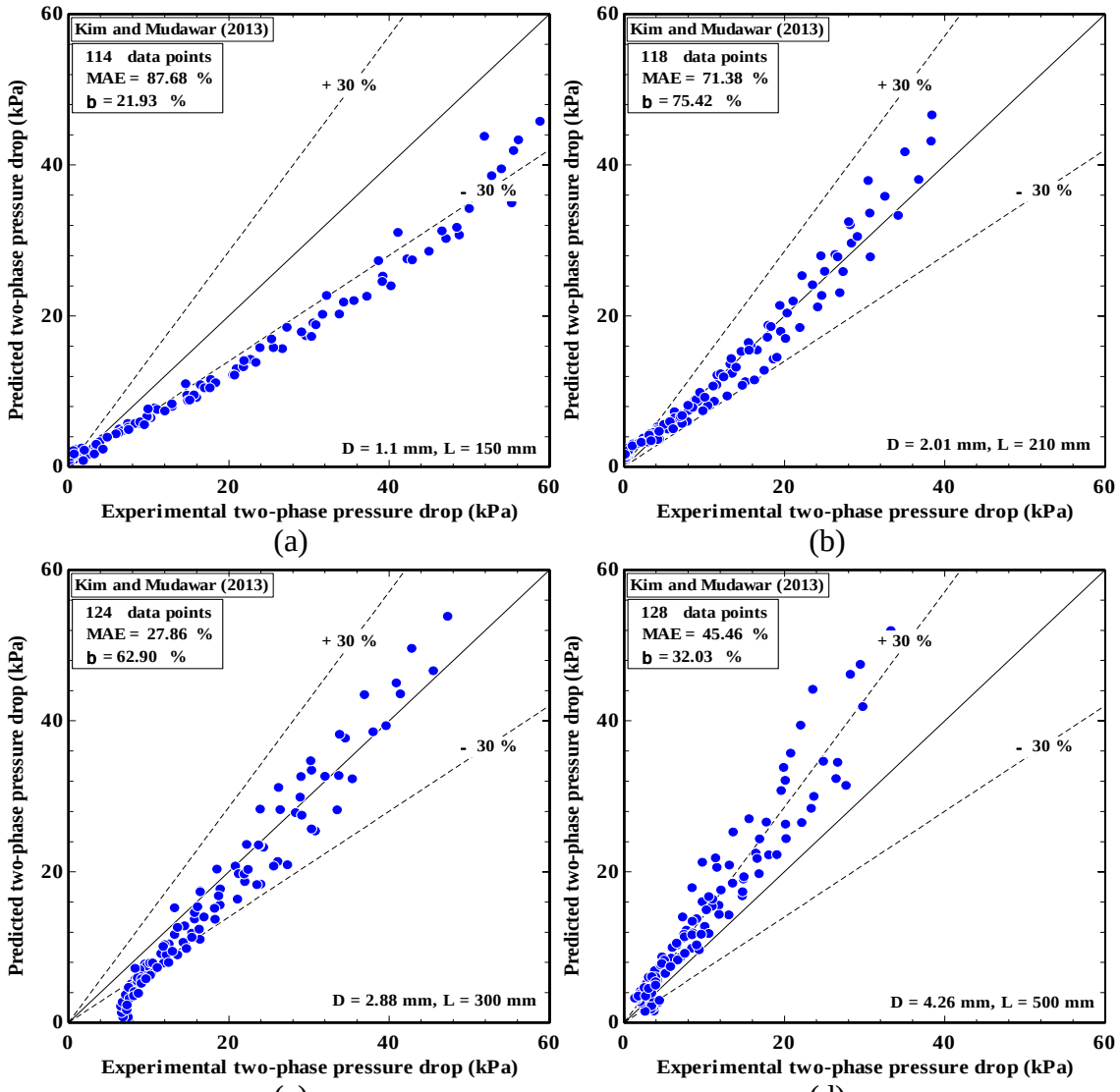

Figure 5.22 Comparison of experimental data with predictions of Kim and Mudawar (2013) correlation for: (a) D = 1.1 mm, (b) D = 2.01 mm, (c) D = 2.88 mm, and (d) D = 4.26 mm.

5.9 Summary

The following conclusions are drawn from the discussion of the experimental results of measured flow boiling pressure drop for R245fa flowing in four tubes (1.1 – 4.26 mm) and the effect of key parameters on flow boiling pressure drop which was presented in this chapter, as follows.

- The mass flux has a slight effect on the two-phase pressure drop in low exit vapour quality ($x_e < 0.1$) in all tube diameters. For higher exit vapour quality ($x_e > 0.1$), the influence of the mass flux on two-phase pressure drop becomes significant. Also, the measured two-phase pressure drop increases with exit vapour quality. This is due to the change in two-phase flow patterns during flow channel leading to higher flow velocity which depends on vapour quality and mass flux. The increase in mass flux results in increased frictional forces between fluid and tube wall and consequently increasing the two-phase pressure drop.
- The two-phase pressure drop increases with heat flux. This is attributed to higher vaporization in the flow channel resulting from increasing heat flux which causes an increase in the vapour quality and vapour phase velocity and thus the pressure drop.
- The two-phase pressure drop decreases significantly as the system pressure increases. This behaviour is attributed to the pressure influence on the thermodynamic properties of the fluid namely as vapour density and liquid viscosity.
- The two-phase pressure gradient increases substantially with the decrease in tube diameter. This could be because of the presence of large velocity gradient in the thin liquid film close to channel wall and consequently high wall shear stress and high interfacial shear stress, leading to the higher two-phase pressure gradient. The effect of coating regards as a new contribution to this study.
- The two-phase pressure drop of the coated tube is higher than that of the uncoated tube for all mass fluxes. This is a result of the surface roughness of coated tube is about three times higher than that of the uncoated tube. The effect of tube diameter with R245fa fluid in vertical orientation considers a new contribution to this work.
- The comparison of two different fluids shows that the measured two-phase pressure drop of R245fa is obviously higher than that of R134a. This phenomenon arises from the difference in physical properties of the two refrigerants, where the fluid has high

reduced pressure causing a lower pressure drop in two-phase flow. The effect of chosen working fluid on two-phase pressure drop in vertical orientation considers a new contribution to this research.

- The experimental data of two-phase pressure drop are compared with fifteen predictive models developed for the conventional to microchannels in two-phase flow. The comparison results show that the homogeneous flow model slightly under-predicts the data of 4.26 mm tube. However, the performance of homogeneous flow model become worse with decreasing the tube diameter from 4.26 mm to 1.1 mm. For the separated flow models, the correlations of Grönnerud (1979), Friedel (1979), Müller-Steinhagen and Heck (1986), and Mishima and Hibiki (1996) show best predictions for most data of 4.26 mm tube. Further, the data of 2.01 mm and 2.88 mm tubes are underpredicted by Chisholm (1973a), Hwang and Kim (2006) and Kim and Mudawar (2013) but with higher MAE and β values for 2.01 mm tube. The data of 1.1 mm tube are not well predicted by any of the selected predictive methods. Generally, there is a deviation with decreasing tube diameter for most of the predictive methods.

Chapter 6

Flow Boiling Heat Transfer: Results and Discussion

6.1 Introduction

This chapter presents the flow boiling heat transfer characteristics in small diameter tubes with a focus on the parametric effects on the local two-phase heat transfer coefficient. These parametric effects include mass flux, heat flux, system pressure, tube diameter, surface microstructure, and fluid thermophysical properties. The experimental study, which uses five different test sections, was systematically conducted to demonstrate the influence of channel diameter on the local two-phase heat transfer coefficient. Meanwhile, the characteristics of flow patterns and the flow pattern transitions corresponding to each test section are used to explain the underlying mechanisms of the flow boiling process. The description of boiling curves for each test section is also presented and discussed. Finally, the applicability of existing correlations in the literature was assessed by comparison with the experimental data of local heat transfer coefficient.

6.2 Flow boiling incipience

The boiling curves are defined for the three axial locations of wall temperature measurement at P = 310 kPa and mass flux ranging from 200 to 500 kg/m^{2}s, as plotted in Figure 6.1 - Figure 6.4. These figures depict the flow boiling curve in terms of increasing heat flux against the wall superheat for each test tube. The uniform heat flux can be calculated from Equation (3.19). Further, the wall superheat is evaluated at the location of 0.2, 0.5 and 0.8, respectively at the same increasing heat flux, the heat flux increases uniformly along the tube. The evaporation occurs on the inner surface of the tube wall. Increases in the wall temperatures during the increased heat flux activate some of the nucleation cavities and consequently bubbles arise from these cavities. This is called

'onset of nucleate boiling', which implies the transition from single-phase zone to flow boiling zone. The growth of these bubbles on the surface and their departure during the channel flow result in an augmenting in the heat transfer. According to Figure 6.1 - Figure 6.4, the nucleate boiling incipience occurs appreciably at low heat fluxes of almost similar magnitude in all tubes, but the wall superheat of nucleate boiling incipience is different

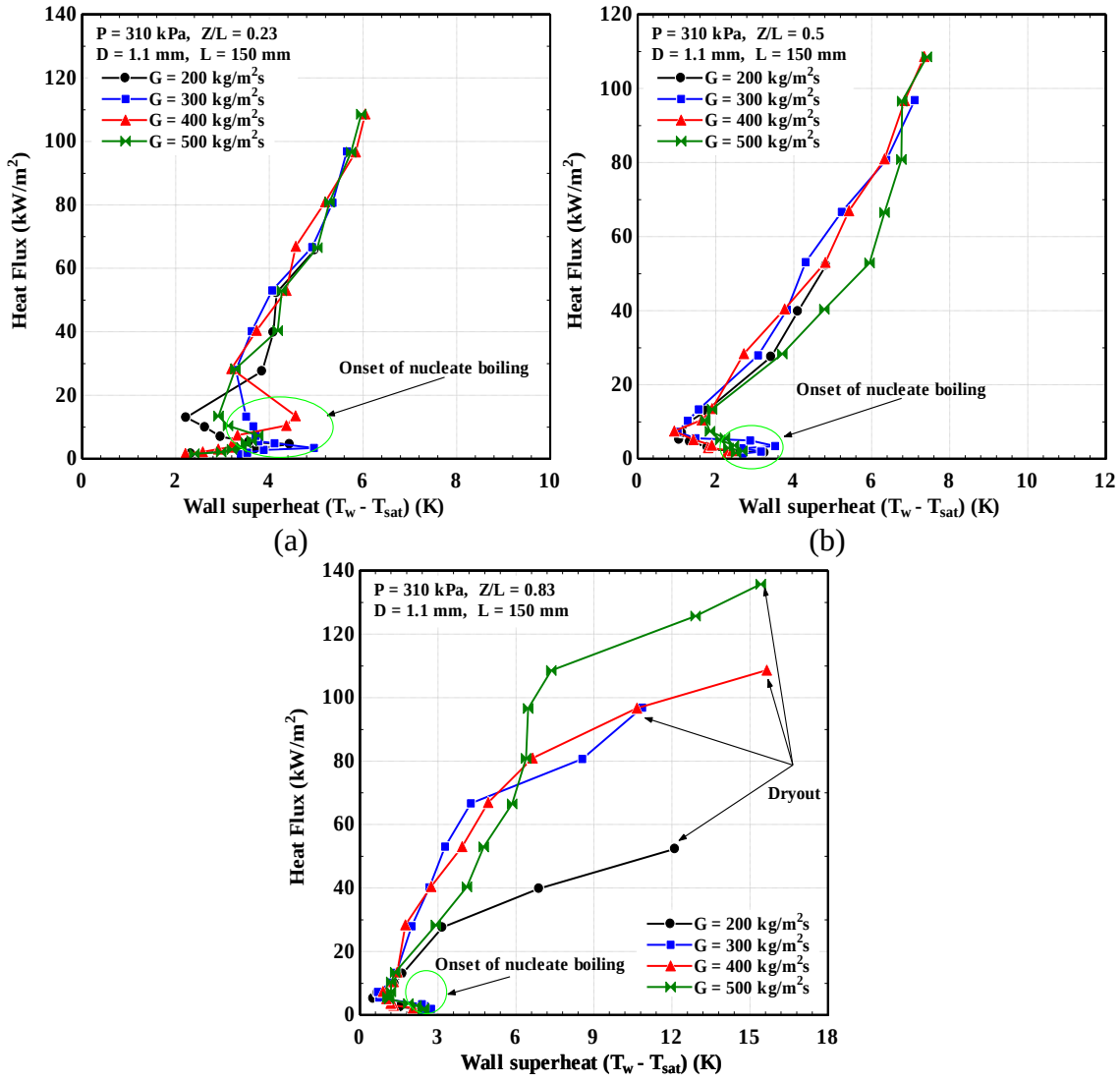

Figure 6.1 Boiling curve of the 1.1 mm tube at three locations: (a) *Z/L* = 0.23, (b) *Z/L* = 0.5, and (c) *Z/L* = 0.83.

for each tube, for each mass flux and even for each location. This may be attributed to the effect of local surface roughness and the distribution of active nucleation cavities. Additionally, there is a good indication on this, the wall superheat of boiling incipience

for the 1.1 mm tube is significantly lower than those in the rest of tubes because the surface roughness characteristics of 1.1 mm tube are much higher than those of the other tubes, see Subsection 3.2.4. The heat flux after nucleate boiling incipience increases linearly with wall superheat and at almost the same slope.

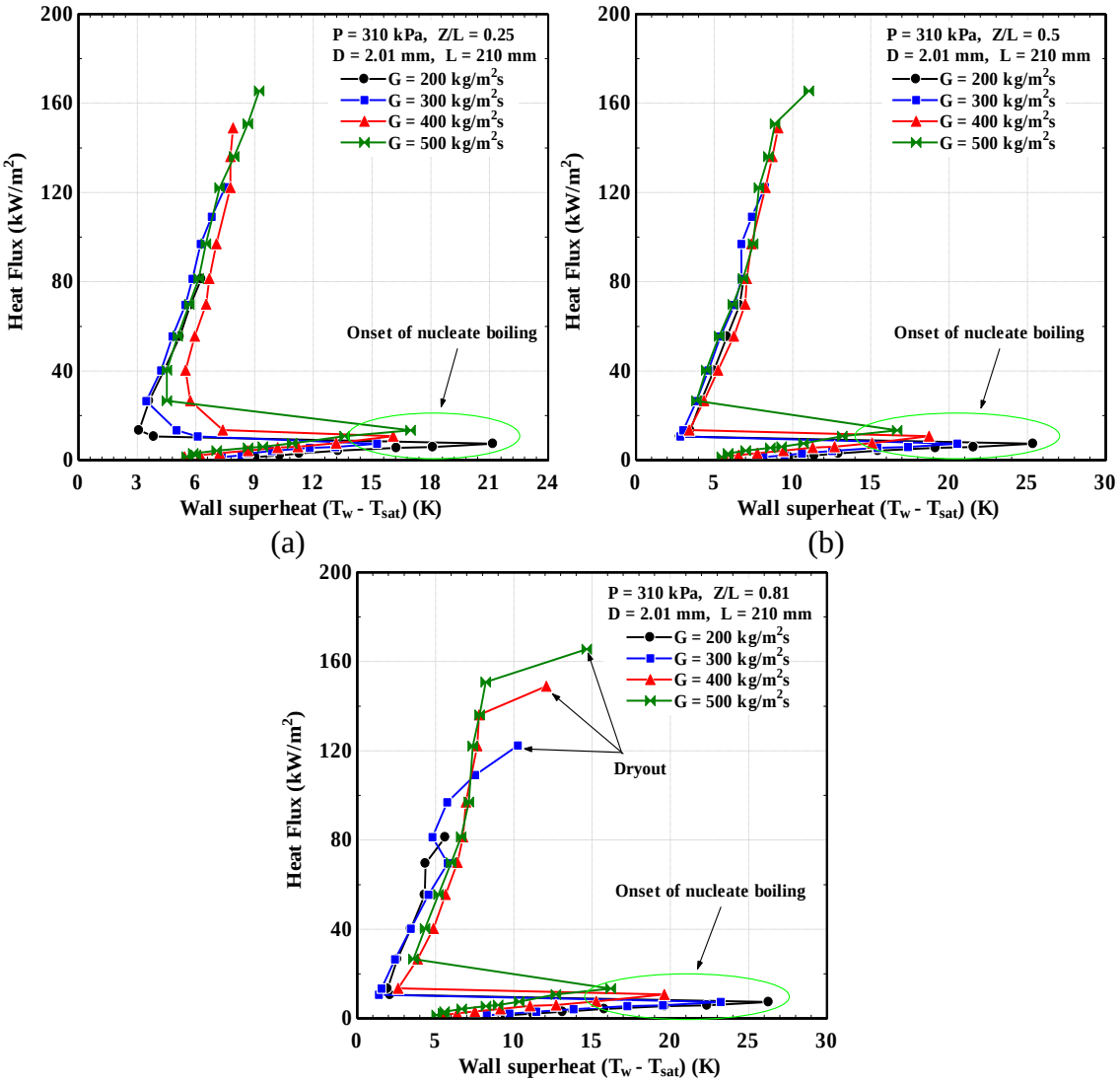

Figure 6.2 Boiling curve of the 2.01 mm tube at three locations: (a) *Z/L* = 0.25, (b) *Z/L* = 0.5, and (c) *Z/L* = 0.81.

There is also an obvious change of slope in the boiling curve for circumstances when the local dryout occurs. That is, the dryout leads to a significant change of slope in the increasing heat flux vs. the wall superheats. The flow boiling curves also reveal that the dryout occurs at higher heat fluxes and especially in the location near the exit of 1.1 mm

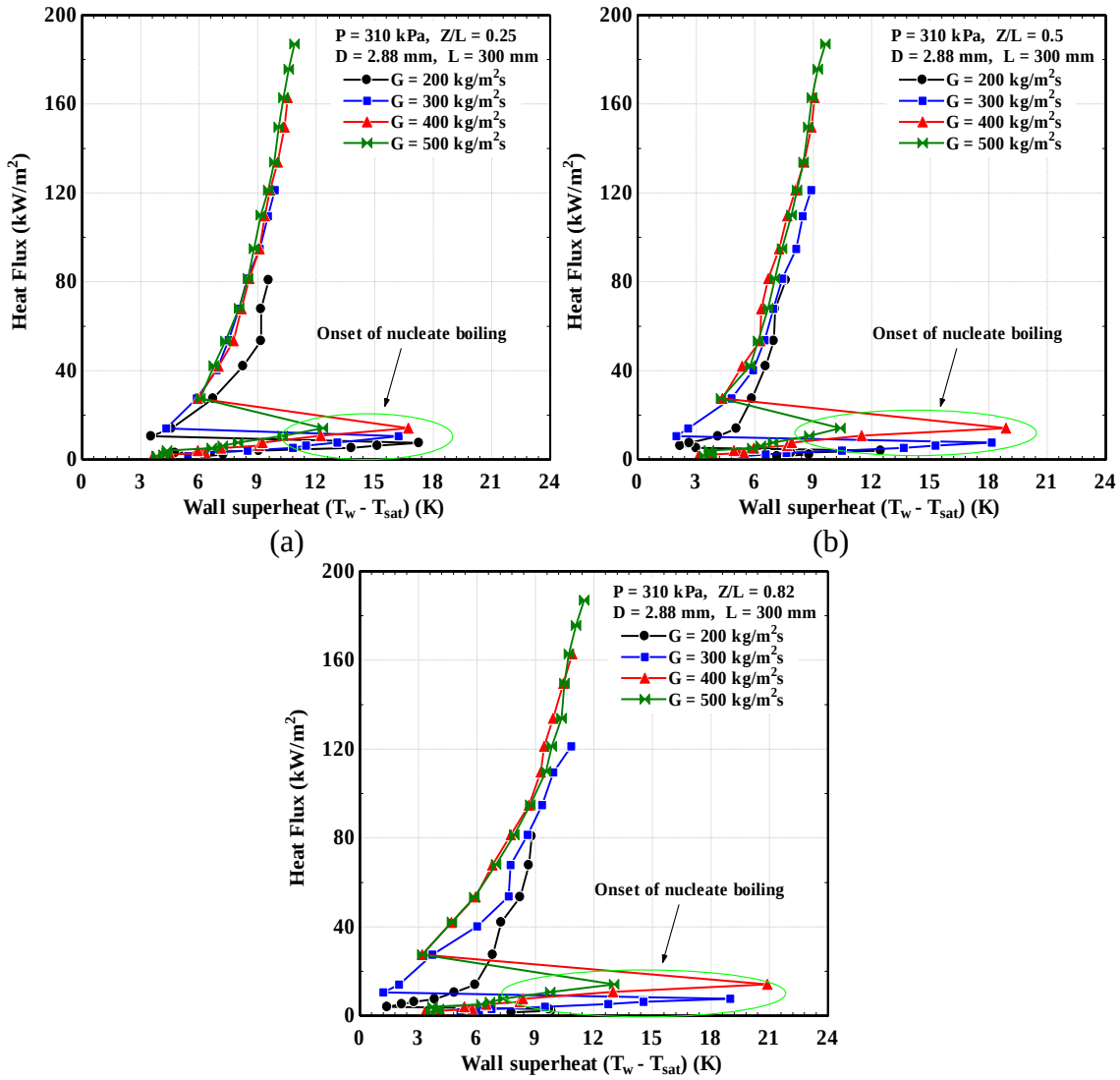

Figure 6.3 Boiling curve of the 2.88 mm tube at three locations: (a) *Z/L* = 0.25, (b) *Z/L* = 0.5, and (c) *Z/L* = 0.82.

and 2.01 mm tubes, as shown in Figure 6.1c and Figure 6.2c. Mauro et al. (2010) obtained similar behaviour for Refrigerants (R134a, R236fa and R245fa) in multi-microchannel with the 0.32 mm hydraulic diameter. The dryout is not evident in the 2.88 and 4.26 mm tubes because the heat power applied to these tubes was limited. This is due to the limitations of the R22 cooling system. In other words, the dryout requires higher heat fluxes. When the heat flux increases, the system pressure increase as well. Therefore, it is difficult to control the system pressure with the cooling system limitations. Moreover, it is obvious from Figure 6.1, Figure 6.2 and Figure 6.3 that the mass flux affects significantly the boiling curve for the 1.1, 2.01 and 2.88 mm tubes. However, the boiling curve of 4.26 mm tube is also found to be slightly dependent on mass flux.

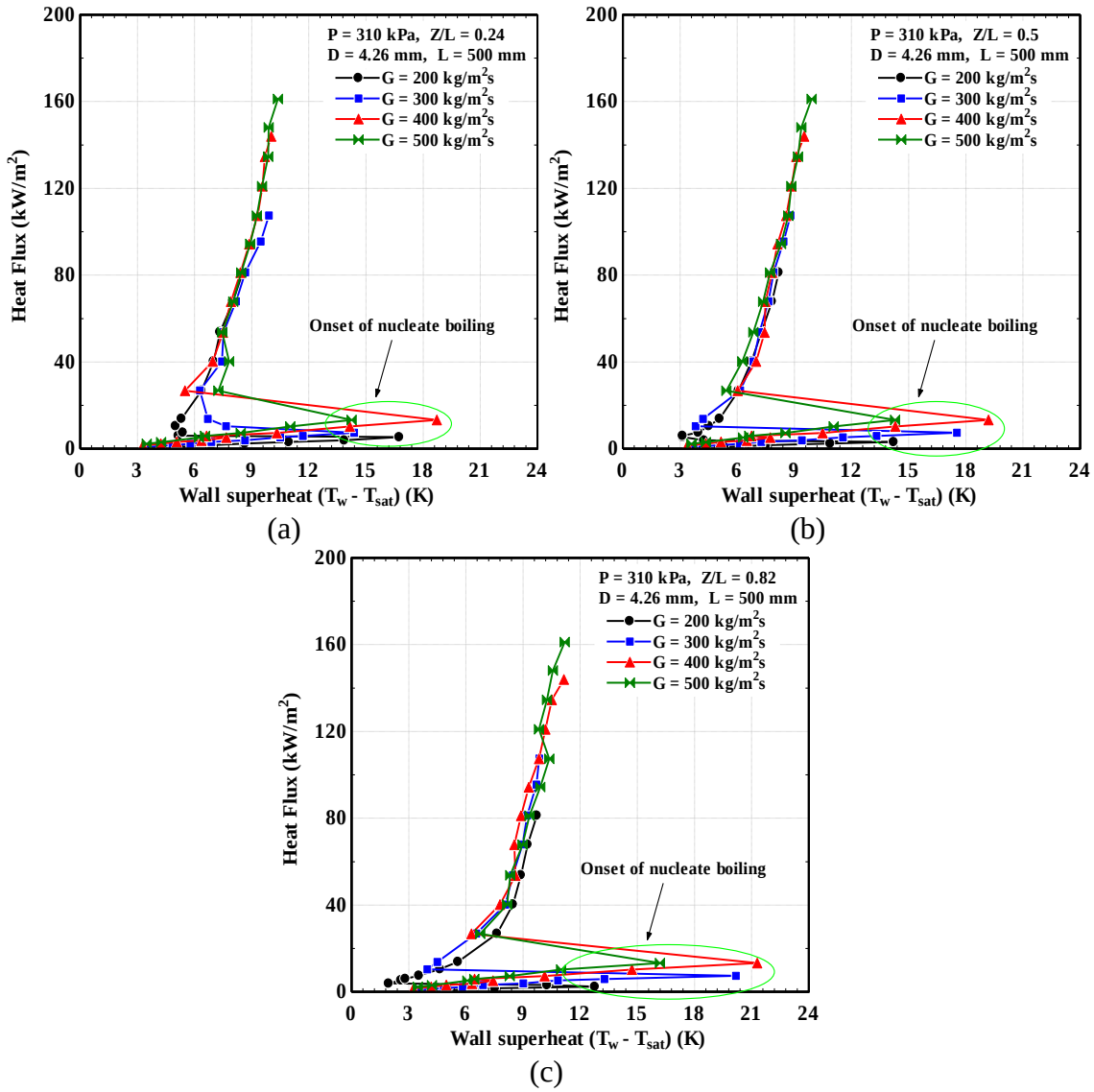

Figure 6.4 Boiling curve of the 4.26 mm tube at three locations: (a) Z/L=0.24, (b) Z/L=0.5, and (c) Z/L=0.82.

Both increasing and decreasing steps in heat flux are used in the measurements of axial wall temperature for all tubes. Figure 6.5 shows that local wall superheats are compared for three positions along heated sections with increasing and decreasing heat flux at P = 185 kPa and G = 200 kg/m^{2}s. It can be observed that the hysteresis phenomenon occurs evidently at all axial locations for all tubes. This phenomenon was also discussed previously in Section 4.2 concerning the changes in the observed flow patterns which affect directly the heat transfer coefficient. Hysteresis follows as a consequence of nucleation sites becoming activated during the increase in the heat flux. These nucleation sites also remain activated with decreasing heat flux. In addition, the

size of the active nucleation sites depends on the surface conditions inside each tube. Therefore, the active nucleation sites would vary from one tube to another.

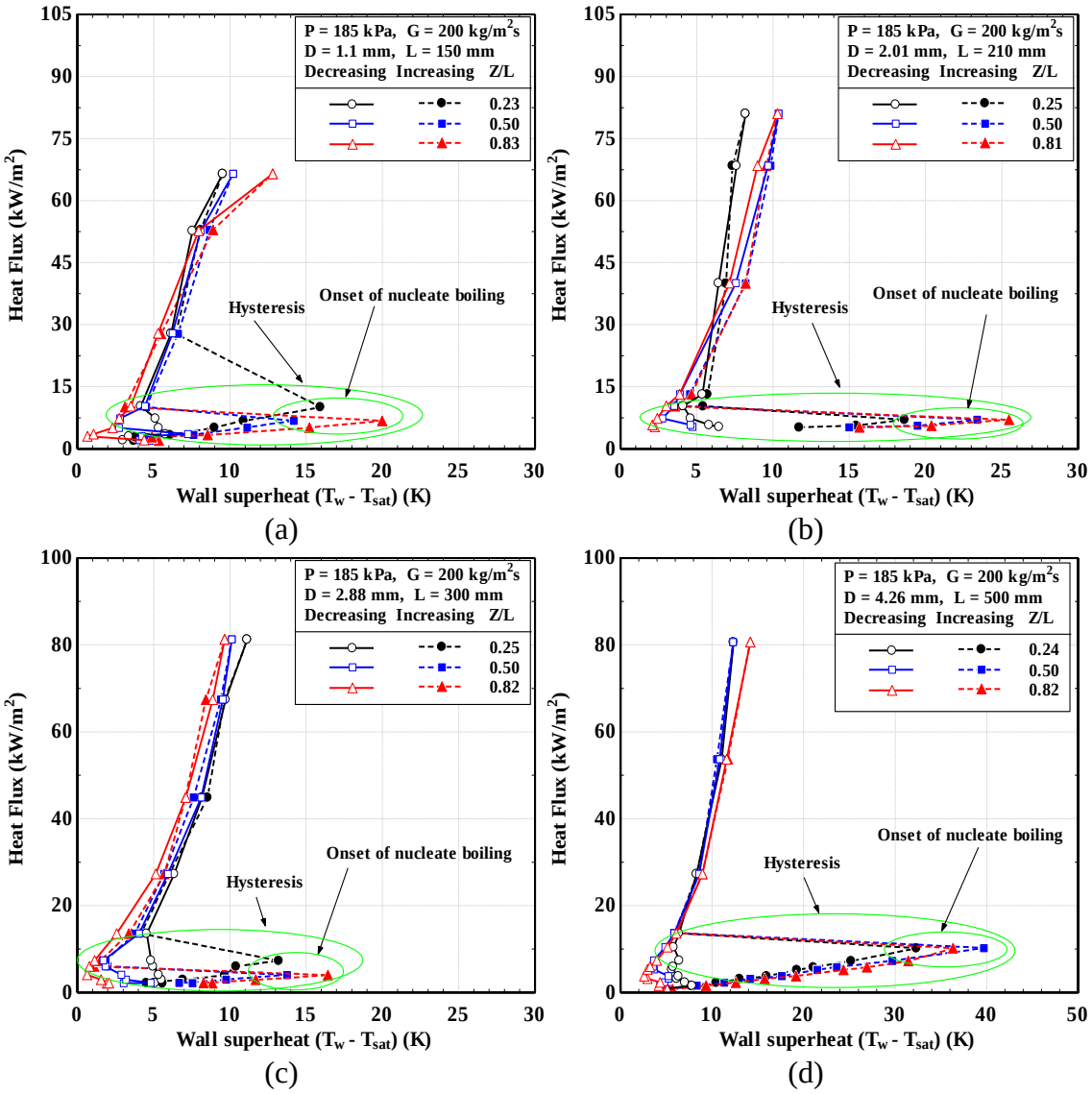

Figure 6.5 Boiling curve for comparison between increasing and decreasing heat flux at three locations for: (a) D = 1.1 mm, (b) D = 2.01 mm, (c) D = 2.88 mm, and (d) D = 4.26 mm.

Figure 6.6 shows the influence of coating on the nucleation incipience. For the coated tube, the wall superheats of nucleation incipience start early compared to those of the uncoated tube. Additionally, the heat fluxes of nucleate boiling incipience for coated tube are appreciably lower than for the uncoated tube, as shown in Figure 6.6. This is due to the influence of the active nucleate size on the onset of nucleate boiling. According to the

bubble equilibrium curve predicted by Clausius-Clapeyron equation $\left((T_w - T_{sat}) = 2\sigma T_{sat} \sin\theta / \rho_v h_{lv} r_c\right)$, the wall superheat of nucleation incipience decreases, when the active nucleate size increases. In addition, the discrepancy between coated and uncoated tube for the minimum superheat required to nucleate boiling incipience is related to active nucleate size, distribution of nucleation sites and the density of nucleation sites on the heated surface.

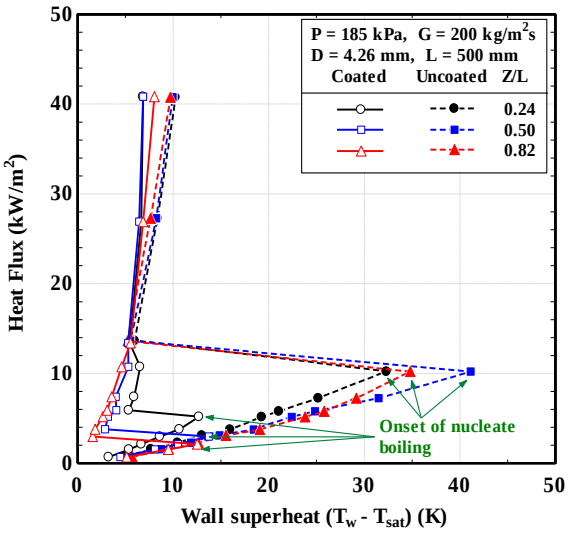

Figure 6.6 The boiling curve at three different axial locations of the tube for comparison between coated and uncoated tube.

6.3 Flow boiling instability

Flow instability always occurs with the flow boiling heat transfer during the change of fluid phase from liquid to vapour inside the heated tube, i.e. boiling incipience. There are increases occurring in the oscillation amplitude of inlet and outlet pressure and temperature, and wall temperature. This is due to the vapour bubble detachment from the active nucleation cavities on the hot wall surfaces, the growth of vapour bubble in the flow field, the occurrence of coalescence between two consecutive departure bubbles, and the bubble departing from the channel. The magnitude and amplitude of two-phase flow oscillations for each experimental parameter at mass flux 400 kg/m^{2}s are summarized in Table 6.1. The period of oscillations for each parameter is 90 s (a single reading for each second). According to this table, very small oscillations occur in all parameters during single-phase flow conditions (i.e. at a heat flux of about 3 kW/m^2). It is mean that the system has reached a steady state.

Table 6.1 The standard deviation and amplitude of oscillations for each parameter.

Tube diameter (mm)		1.1		2.01		2.88		4.26	
Measured parameters	Heat flux (kW/m^2)	3.6	80.83	2.15	81.22	2.7	80.87	3.56	80.16
Inlet temperature (°C)	Mean value	25.44	26.78	25.4	26.01	26.43	25.24	25.67	24.78
	St. de.	0.036	0.379	0.008	0.389	0.032	0.237	0.03	0.178
	Amp.	0.06	0.647	0.009	0.676	0.069	0.723	0.055	0.52
Outlet temperature (°C)	Mean value	28.72	25.56	28.98	28.52	28.35	28.21	30.27	30.13
	St. de.	0.27	0.319	0.024	0.464	0.039	0.183	0.02	0.202
	Amp.	0.047	0.573	0.048	0.958	0.073	0.397	0.04	0.543
Wall temperature at No. 15 (°C)	Mean value	34.34	34.71	33.53	43.71	32.51	38.87	34.69	41.93
	St. de.	0.013	0.038	0.021	0.046	0.056	0.061	0.078	0.081
	Amp.	0.039	0.081	0.034	0.089	0.12	0.126	0.202	0.159
Inlet pressure (kPa)	Mean value	184.2	195.9	185.3	191.6	186.7	186	187.3	185.9
	St. de.	0.084	1.31	0.161	2.818	0.349	3.781	1.48	2.151
	Amp.	0.182	3.438	0.345	5.137	0.862	6.824	4.035	7.763
Outlet pressure (kPa)	Mean value	176.9	151	177.5	169.4	180	172	183.7	174
	St. de.	1.425	2.411	1.858	2.737	3.04	4.113	0.898	1.046
	Amp.	2.989	8.492	4.736	7.601	6.413	9.692	2.363	2.642
Pressure drop (kPa)	Mean value	0.221	37.26	0.109	13.97	0.15	9.694	0.117	7.788
	St. de.	0.033	2.597	0.259	1.371	0.833	3.746	0.651	1.034
	Amp.	0.073	5.622	0.572	2.841	2.666	6.927	1.638	1.992
Mass flux (kg/m^2s)	Mean value	399.6	399.5	400.4	403.8	400.7	400	400.9	399.3
	St. de.	2.449	9.825	1.821	3.21	1.891	2.624	1.657	2.144
	Amp.	6.073	23.03	3.437	7.034	5.081	5.798	3.017	3.918

St. de. is a standard deviation and Amp. is the amplitude of oscillations.

The table also indicates that the increasing oscillations in each parameter can be observed after the transition from single-phase flow to two-phase flow condition (i.e. with increasing heat flux from 3 to 88 kW/m^2). This can be caused by phase change characteristics (periodic nucleated bubble growth, confinement, elongated, merging process), as mentioned above and transition to annular flow regime. In addition, the annular flow is defined by a vapour in tube core and a continuous flow of liquid film on the tube wall. Thus, the vapour-liquid interface stability and the liquid film thickness have an influential role in the oscillations of pressure drop and wall temperature. This is evident through increases occurring in the oscillation amplitude of inlet and outlet pressure and temperature, and last wall temperature for each test section in the range of two-phase flow conditions.

According to the literature, Ding et al. (1995), Fan and Hassan (2012) and Ruspini et al. (2014), the density wave oscillations were considered a major type of flow

oscillations which accompany the occurrence of flow boiling. The density wave oscillations arise from the dynamic interaction between mass flux, pressure drop, and local density variation. It can be observed that the single-phase flow transitions into the two-phase flow with increased heat flux leading to an increase in the mean pressure drop value. Simultaneously, the oscillation amplitude of mass flux and pressure drop also increases. Finally, the small values of all oscillation amplitude in the phase change conditions confirm the occurrence of stable boiling.

6.4 Two-phase heat transfer coefficient results

A series of experimental tests were conducted in the present study using R245fa as working fluid in small-diameter tubes. The local heat transfer coefficient is determined by Equation (3.44). In this section, the principal trends observed in this study for the two-phase heat transfer coefficient with the effects of different experimental parameters are presented and discussed.

6.4.1 Effect of heat flux

The influence of heat flux on the local heat transfer coefficient as a function of the local vapour quality for four different tube diameters is illustrated in Figure 6.7. The transition lines of the observed flow patterns presented in Section 4.3 are also included, i.e. single-phase, slug, churn and annular flow. According to Figure 6.7a, for the 1.1 mm tube, the local heat transfer coefficient increases with increasing heat flux up to vapour quality of 0.4. The vapour quality also has a significant impact on the heat transfer coefficient, especially in the slug and churn flow regions. The vapour velocity increases with increasing vapour quality. This means that both nucleate boiling and convective boiling contribute to heat transfer process for low heat fluxes (28–53 kW/m^2). However, the local heat transfer coefficient is slightly depended on vapour quality, when the heat flux is greater than 66.95 kW/m^2. Such behaviour is associated with the reduction of the liquid film thickness in an annular region. Consequently, dryout occurs after the vapour quality value of 0.4 and expands along the high vapour quality region. Sempértegui-Tapia and Ribatski (2017a) also observed the similar trend of heat transfer coefficient for R1234ze(E) flowing in 1.1 mm tube.

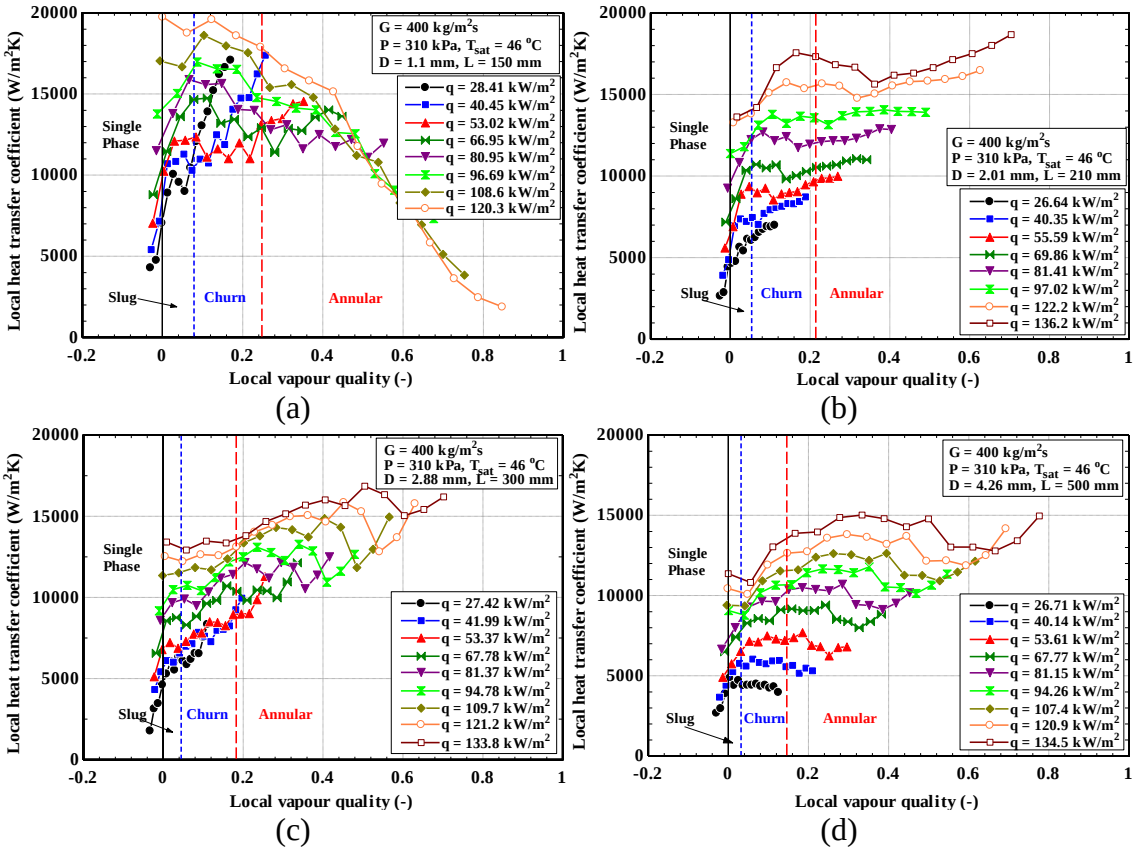

Figure 6.7 Effect of heat flux on the local heat transfer coefficient as a function of local vapour quality at P = 310 kPa and G = 400 kg/m2s for: (a) D = 1.1 mm, (b) D = 2.01 mm, (c) D = 2.88 mm, and (d) D = 4.26 mm.

The effect of heat flux on the local heat transfer coefficient with the experimental flow pattern transition lines for the 2.01 mm diameter tube is shown in Figure 6.7b. The local heat transfer coefficient increases with increasing heat flux for all vapour qualities. It is shown that as the heat flux increases, the heat transfer coefficient increases with very low vapour quality from single-phase flow to churn flow region. It then remains almost unchanged except at the last higher heat fluxes in the annular flow where it increases slightly with vapour quality. The peak values of local heat transfer coefficient in the slug and churn flow region can imply the presence of the active nucleation site densities. This behaviour gives the impression of the predominance of nucleate boiling in the flow boiling heat transfer in slug flow and churn flow regions. Additionally, the convective boiling contributes to the heat transfer in annular flow region at last higher heat fluxes. This does not mean that the nucleate boiling is entirely suppressed in this region. The local heat transfer coefficient increases appreciably when the heat flux is greater than 97.02 kW/m^2. This is due to the reduced density of liquid-vapour mixture, the flow

velocity increases leading to enhanced convective transport. The evaporation rate increases resulting in the thickness of the liquid film on the hot surface to be thinner. Thus, the thermal resistance of liquid film decreases. This also enhances heat transfer rate and consequently increasing the local heat transfer coefficient with vapour quality (Charnay et al., 2015b).

The effect of heat flux on the local heat transfer coefficient for the 2.88 mm diameter tube is depicted in Figure 6.7c. It can be seen from this figure that the trend of local heat transfer coefficient is almost identical to that obtained using the 1.1 and 2.01 mm tubes. The local heat transfer coefficient increases with increasing heat flux for vapour quality up to about 0.4. After this vapour quality value, the heat flux effect diminishes, and the curves tend to merge into one single line. The local heat transfer coefficient remained almost unchanged with vapour quality in the very low quality region and then increased moderately until the onset of annular flow. After that, the local heat transfer coefficient either increased slightly with vapour quality or remained almost unchanged except at the last three thermocouple locations where the local heat transfer coefficient increased slightly with vapour quality. The increase of local heat transfer coefficient with vapour quality is more pronounced at low heat flux values, less than 68 kW/m^2. It is worth noting that, the observed fluctuation at the last thermocouple locations seems to be due to factors other than partial dryout. It may be a result of the contribution of convection in this region. That is, the nucleate boiling and convection mechanisms contribute to the flow boiling heat transfer in this tube.

For the 4.26 mm tube, Figure 6.7d shows the effect of heat flux on the local heat transfer coefficient. Notably, this figure indicates that the trends of local heat transfer coefficient are almost identical to the local heat transfer coefficients of other tubes. The local heat transfer coefficient increases with increasing heat flux for vapour quality up to about 0.6. After this vapour quality value, the heat flux effect diminishes and the curves tend to merge into one single line. The local heat transfer coefficient did not vary significantly with vapour quality at the second lowest heat flux. As the heat flux increased, the local heat transfer coefficient increased with vapour quality in the very low quality region and then remained almost unchanged except at the last thermocouple

locations where the local heat transfer coefficient increased slightly with vapour quality. It is worth highlighting that, in the transition line from single-phase to slug flow, the heat transfer coefficient rapidly rises from its lowest value except for heat flux greater than 81.15 kW/m^2. This trend was observed before in conventional channels and also in the other tubes (1.1, 2.01, 2.88 mm), and it may be attributed to the onset of nucleate boiling.

The local heat transfer coefficient is re-plotted as a function of axial location instead of local vapour quality, as shown in Figure 6.8. This figure demonstrates clearly that the increase of heat transfer coefficient with heat flux is present at all axial thermocouple locations along the tube for all heat fluxes. It also shows that the heat transfer coefficient depends on axial location from the upstream to the downstream even at low heat fluxes. According to Figure 6.8a, the occurrence of dryout is more evident along the tube downstream with reducing the channel size to 1.1 mm at the condition of high heat fluxes.

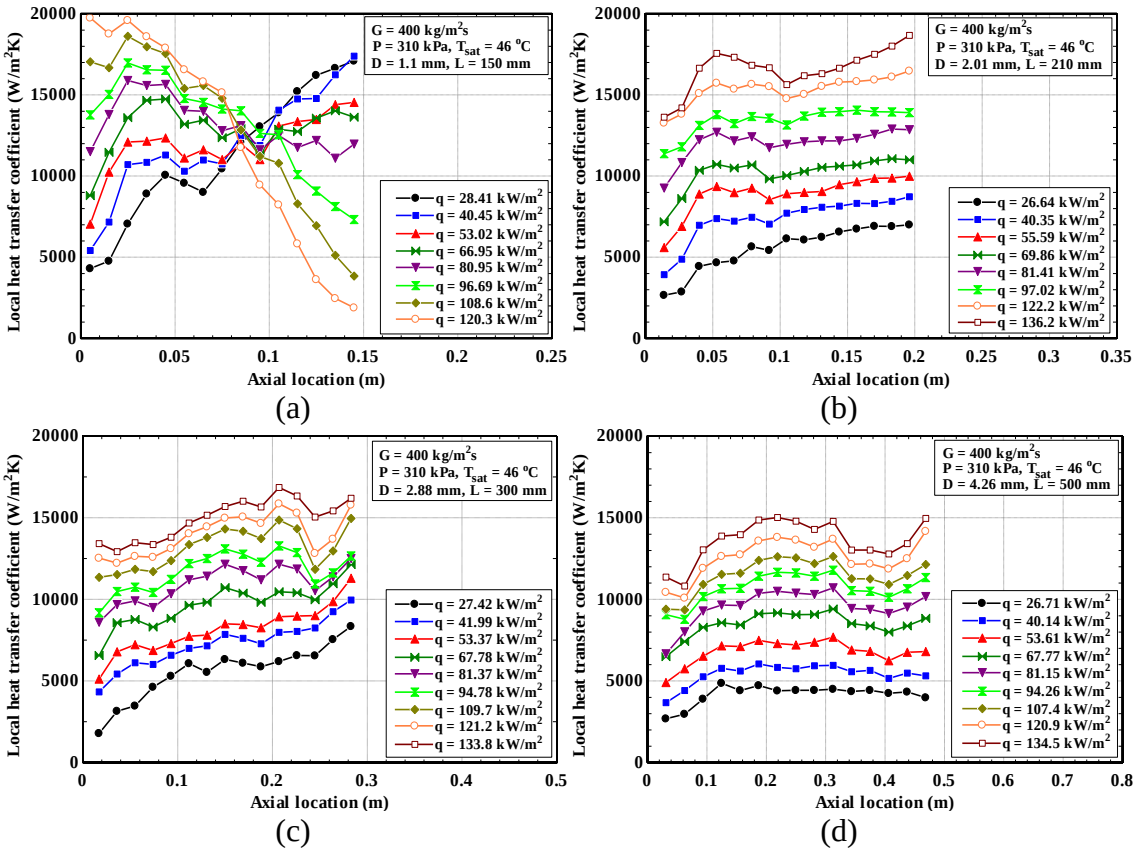

Figure 6.8 Effect of heat flux on the local heat transfer coefficient as a function of axial location at P = 310 kPa and G = 400 kg/m2s for: (a) D = 1.1 mm, (b) D = 2.01 mm, (c) D = 2.88 mm, and (d) D = 4.26 mm.

For further analysis to clarify the heat flux effect for four different tube diameters, Figure 6.9 shows a strong impact of heat flux on heat transfer coefficient by comparing three axial locations. The three positions were selected to represent the entry section (slug regime), the middle section (churn regime) and the exit section (annular regime). Figure 6.9 shows roughly the heat transfer coefficient increased linearly with heat flux. The last axial location in Figure 6.9a is excluded due to the occurrence of dryout in this region.

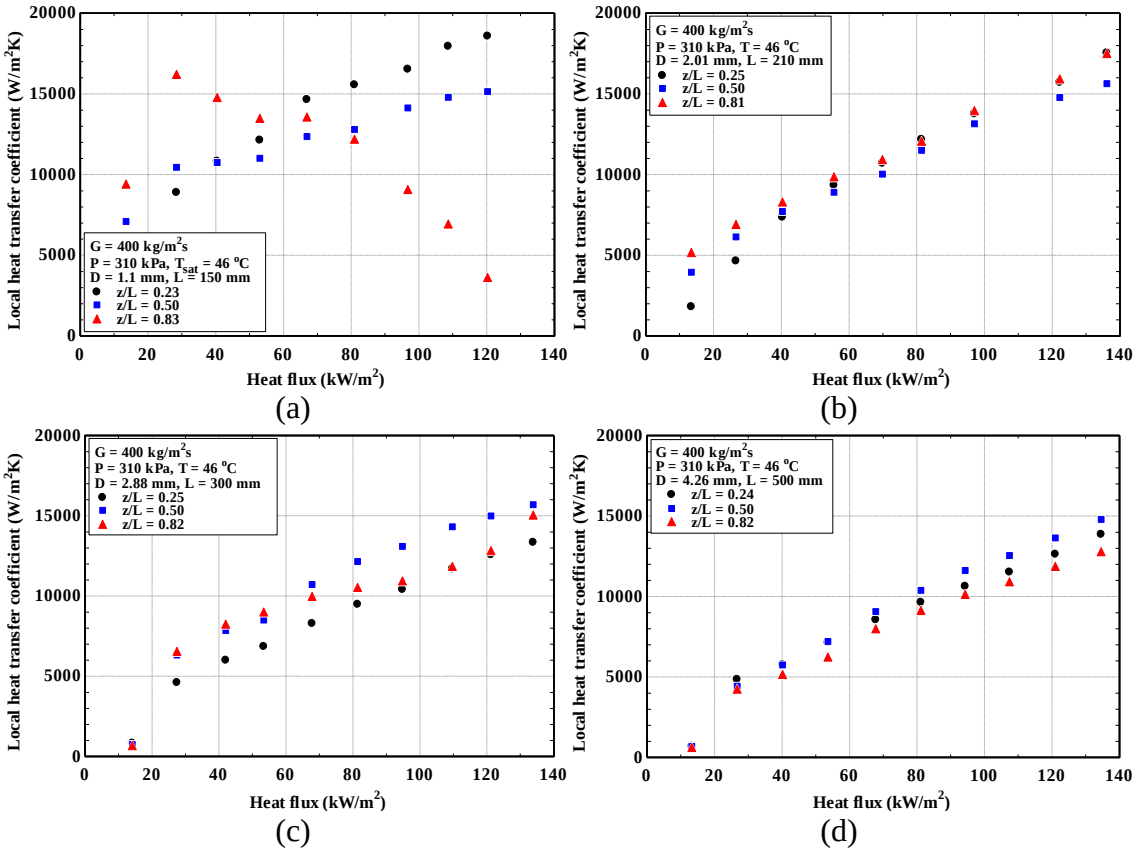

Figure 6.9 Effect of heat flux on the local heat transfer coefficient at three axial locations, P = 310 kPa and G = 400 kg/m2s for: (a) D = 1.1 mm, (b) D = 2.01 mm, (c) D = 2.88 mm, and (d) D = 4.26 mm.

6.4.2 Effect of mass flux

The influence of mass flux on the local heat transfer coefficient for the 1.1 mm tube at P = 310 kPa and q = 67 kW/m^2 is depicted in Figure 6.10a. The independence of local heat transfer coefficient from mass flux is clear in the case of heat fluxes which is equal or more than 67 kW/m^2. This gives an indication that the nucleation mechanism is dominant in the heat transfer process in low local vapour quality and before the onset of

dry out. However, according to Figure 6.7a, the mechanism of nucleate boiling is suppressed by the predominance of convective boiling in the low quality region (i.e. at $x < 0.3$) when the heat flux is less than 67 kW/m^2. There is a debate on the conventional criterion. Karayiannis and Mahmoud (2017) reported that the nucleate and convective boiling could exist simultaneously and it is difficult to segregate the contribution of each mechanism. The peak in the trend of heat transfer coefficient implies the presence of more active nucleation sites, particularly in lower vapour qualities.

Figure 6.10b illustrates the effect of mass flux on the local heat transfer coefficient for the 2.01 mm diameter tube at q = 81 kW/m^2 and P = 310 kPa. It seems that the mass flux has a slight influence on the local heat transfer coefficient in slug flow region, i.e. low quality values $x < 0.15$. In the intermediary vapour qualities, the four curves of mass flux almost merge into one line. Also, in high vapour qualities, the effect of mass flux on the heat transfer coefficient is insignificant. In this region, the heat transfer coefficient increases slightly with vapour quality in the annular flow. However, for the mass flux of 200 kg/m^{2}s, the heat transfer coefficient declines rapidly due to the normal dryout at the last thermocouple locations. It can be concluded from Figure 6.7b and Figure 6.10b that the nucleate boiling effects seem to dominate in lower and intermediary vapour qualities and the convective boiling effects also predominate in higher vapour qualities, particularly at high heat flux more than 97 kW/m^2.

The influence of mass flux on the local heat transfer coefficient for the 2.88 mm tube is depicted in Figure 6.10c. The figure indicates that the effect of mass flux is small. Based on conventional criteria, used to infer the dominant mechanism(s) in large tubes, nucleate boiling seems to be the dominant mechanism up to $x \approx 0.4$. However, as mentioned above, there is a debate on the applicability of these in small to micro scale passages (Karayiannis and Mahmoud, 2017). The contribution of nucleate boiling and convective mechanisms could also exist, even in the low quality region. This point is supported by the mass flux effect, where the heat transfer coefficient increased slightly with mass flux in the low quality region. Then, the thin liquid film layer in annular flow participates in increasing the trend of heat transfer coefficient with vapour quality, i.e. when the thickness of the liquid film on the hot surface reduces, the heat transfer rate between the hot surface and

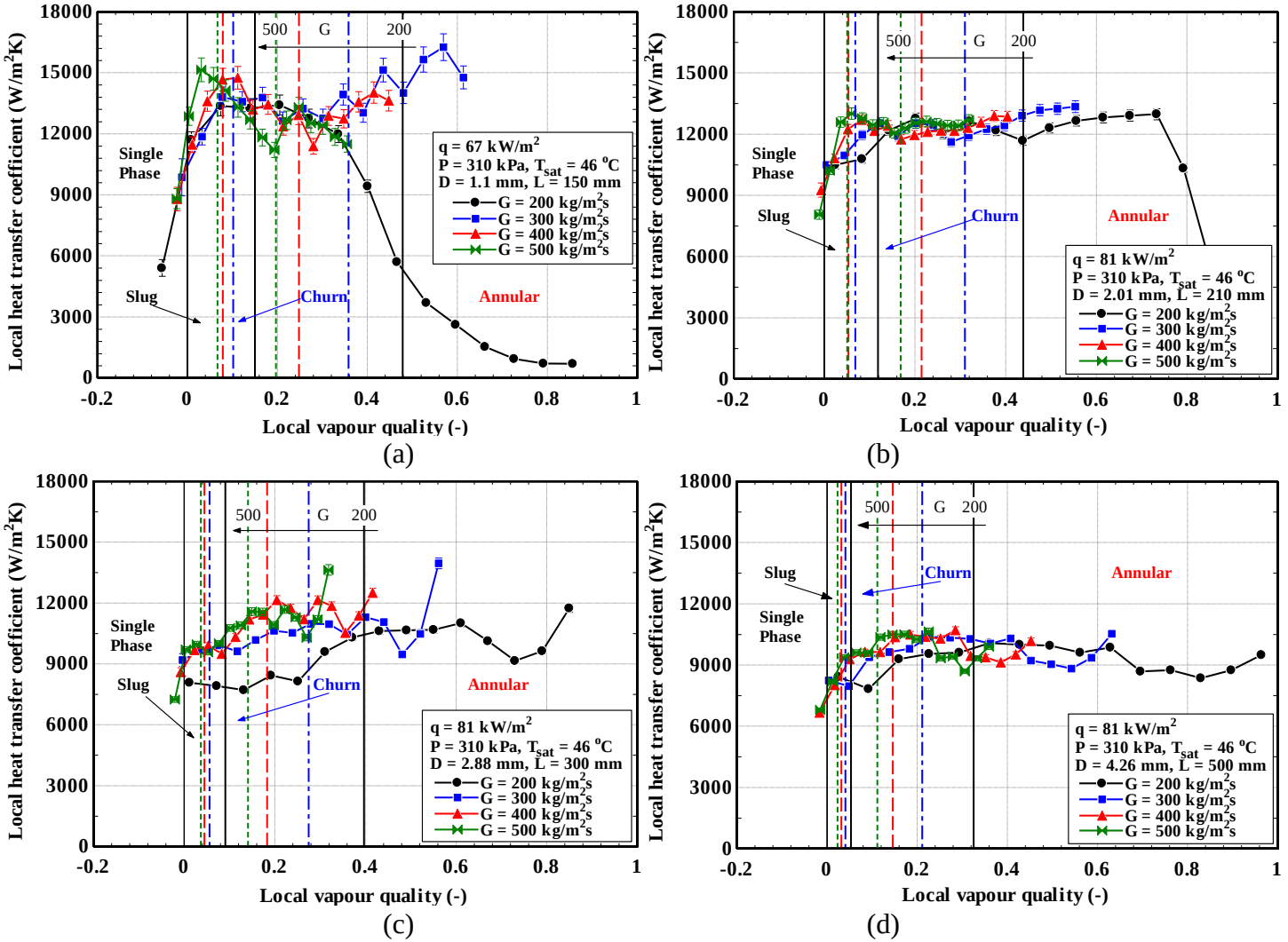

Figure 6.10 Effect of mass flux on the local heat transfer coefficient as a function of local vapour quality at P = 310 kPa for: (a) D = 1.1 mm, (b) D = 2.01 mm, (c) D = 2.88 mm, and (d) D = 4.26 mm.

the liquid-vapour interface increases ($\alpha = k/thickness\ of\ liquid\ film$) and thus the trend of heat transfer conefficent increases. This gives the indication of the dominance of convective boiling mechanism at high vapour quality and location near the tube exit.

Figure 6.10d shows the effect of mass flux on the local heat transfer coefficient for the 4.26 mm diameter tube. It can be seen from the figure that the independence of local heat transfer coefficient from mass flux is clear. The local heat transfer coefficient remained almost unchanged with vapour quality in all the vapour quality range for the four mass fluxes. This is due to the continuance of nucleate mechanism along the tube even in the annular flow. This may prevent increasing the trend of heat transfer coefficient with mass flux and vapour quality, but Figure 6.7c shows that the heat flux effect diminishes at the vapour quality of 0.6, as previously mentioned. Then, the heat transfer coefficient curves trend to increase with vapour quality for higher heat flux more than 107.4 kW/m^2. This gives an indication that a convection mechanism contributes to heat transfer process in a location near the tube outlet.

In addition, Figure 6.10 indicates that the transition to annular flow occurs at low vapour quality, as the mass flux increases. Since the superficial velocity of both phases (liquid and vapour) is directly proportional to the mass flux, the vapour velocity becomes high in the core which breaks up the liquid bridge in slug flow and results in the formation of the liquid film on the tube wall. Therefore, the annular flow extends to low vapour qualities. This behaviour has already been demonstrated and presented in Section 4.4.

6.4.3 Effect of pressure

Figure 6.11 shows the effect of pressure on the local heat transfer coefficient for the four tested tubes. As expected, the figure reveals that the local heat transfer coefficient increases with increasing system pressure. The effect of pressure on the heat transfer coefficient for all tested tubes is similar. This may be attributed to the effect of pressure on the thermophysical fluid properties, especially surface tension, liquid to vapour density ratio and latent heat of vaporization. These properties affect bubble size, bubble departure frequency and bubble growth rate during nucleation mechanism and consequently flow

patterns. For instance, the surface tension of R245fa reduces approximately by 27%, as the pressure increases from 185 to 310 kPa. This affects the size of departed bubbles generating from active nucleation sites. The bubble departure frequency is subsequently increased with increasing pressure. This enhances the nucleate boiling effects. Due to the effect of pressure on nucleation characteristics, the pronounced effect of pressure on the local heat transfer coefficient in annular flow could be an indication of the possibility of bubble nucleation in the liquid film layer next to the wall. Furthermore, Cooper (1984) confirmed this behaviour by means of his correlation, where it infers the significant influence of pressure on heat transfer coefficient through increasing the reduced pressure of the fluid. The behaviour of these experimental results is in agreement with the studies of Huo et al. (2004), Ong and Thome (2011b), Choi et al. (2013), Xu et al. (2016b) and Sempértegui-Tapia and Ribatski (2017a).

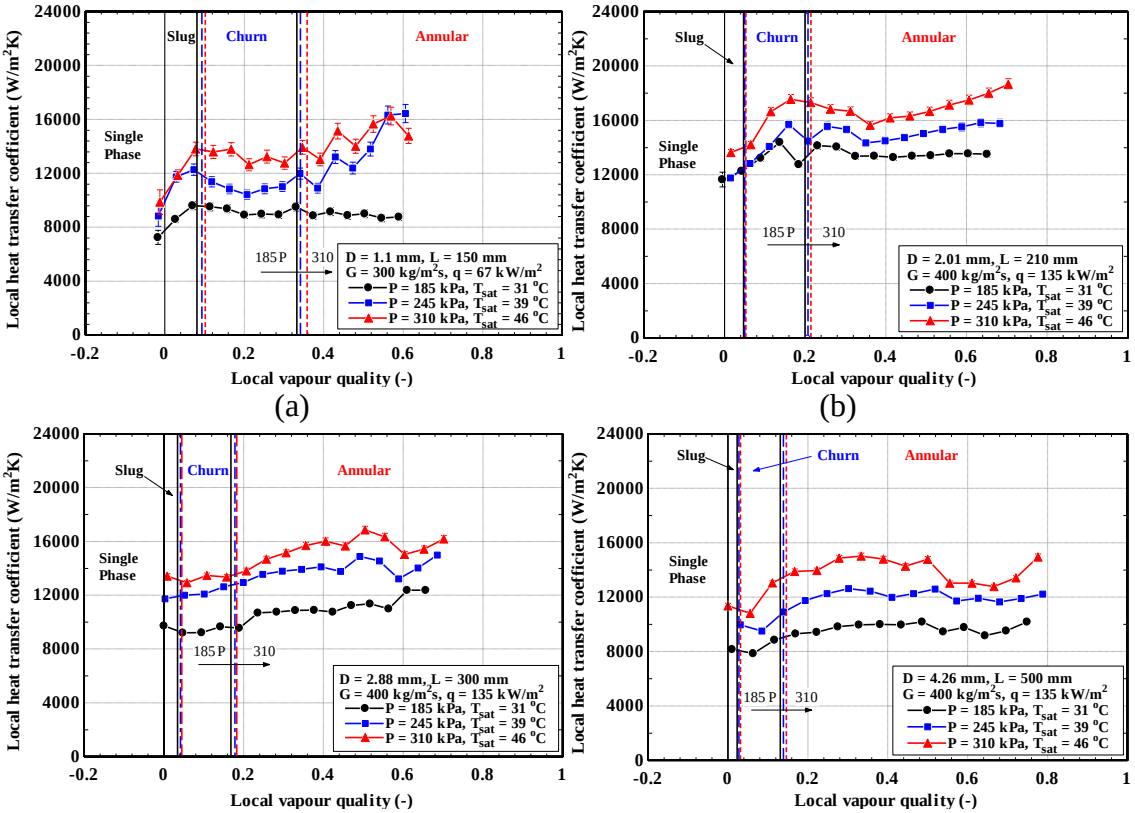

Figure 6.11 Effect of system pressure on the local heat transfer coefficient and flow patterns for different tubes: (a) D = 1.1 mm, (b) D = 2.01 mm, (c) D = 2.88 mm, and (d) D = 4.26 mm.

In addition, system pressure affects the flow patterns as reported by Chen et al. (2005). It is important to highlight that liquid to vapour density ratio and liquid viscosity are high at low pressure. This is mainly responsible for the formation of a liquid film layer between vapour core and inner tube wall surface. Thus, this leads to a high vapour velocity which may consequently bring about an early occurrence of flow pattern transitions, as previously reported in Section 4.5. Subsequently, the annular flow may be expanded towards low vapour quality.

6.4.4 Effect of channel diameter

The effect of inner tube diameter on the local heat transfer coefficient is presented in Figure 6.12 at the condition of P = 185 kPa, G = 400 kg/m^{2}s and q = 81 kW/m^2. It is clear from the figure that the channel size has a strong impact on the enhancement of the local heat transfer coefficient. In other words, the heat transfer coefficient increases with reducing the tube diameter due to an increase in the confinement effect. The effect of the confinement plays a vital role in the control of bubble departure and bubble growth rate. That is, the bubble grows in the axial direction through the tube when confinement increases leading to thinning the liquid film thickness and increasing the bubble length. This is enhanced the heat transfer cross liquid film to the liquid-vapour interface. Further, the enhancement of heat transfer coefficient with the decrease of tube diameter from 4.26 to 1.1 mm is likely to be due to essential variations which appear in the characteristics of flow patterns (such as heat transfer through the liquid film in vapour slug and heat transfer between the hot surface and liquid slug). In addition, the decreased channel size leads to increasing the coalescence of departed bubbles away from the surface and this, in turn, expedites the transitions of flow patterns as previously reported in Section 4.6. However, the transition of slug-churn and churn-annular shift toward an increase in the vapour quality as shown in Figure 6.12. This is likely to occur because of an increase in the vapour velocity in the tube core with increasing confinement (increasing the effect of surface tension force), i.e. the channel size reduction brings about an increase in the vapour velocity and consequently the vapour quality (according to $x = \rho_v J_v / G$). This gives rise to a shift in the flow pattern transitions towards the region of the high vapour quality. These results also were similar to the other studies of Xu et al. (2016b) and Choi et al. (2013).

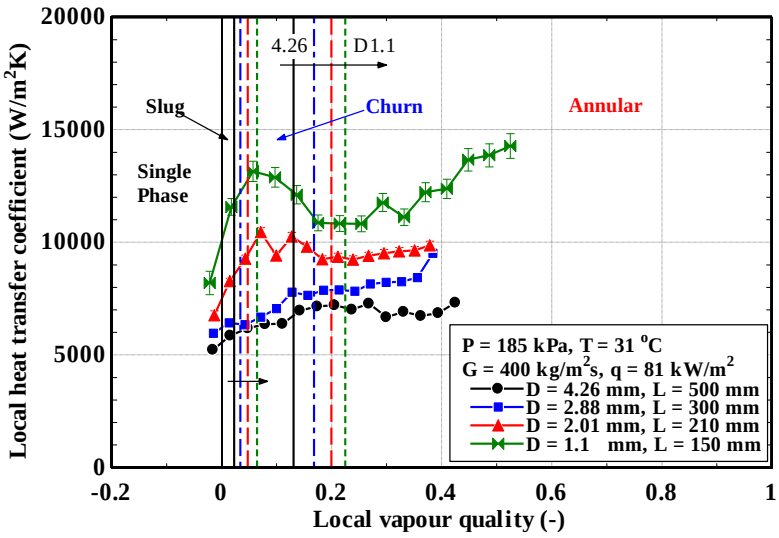

ass

Figure 6.12 Effect of tube diameter on the local heat transfer coefficient and flow patterns at P = 185 kPa.

The effect of the inner tube diameter on the average heat transfer coefficient with different mass fluxes is presented in Figure 6.13, which includes the comparison for tube diameters of 1.1, 2.01, 2.88 and 4.26 mm at P = 185 kPa. It is found that the heat transfer coefficient in the 2.88 and 2.01 mm tubes are 15% and 40%, respectively higher than that found in the 4.26 mm tube. This reduction leads to an enhancement in the average heat transfer coefficient determining by 83% when the tube diameter is further reduced from 4.26 to 1.1 mm. Mahmoud et al. (2014b) included similar data on the effect of diameter on the average heat transfer rates for R134a. Furthermore, the decreasing in tube diameter from 2.88 to 1.1 mm results in an increase of average heat transfer coefficient estimated by about 56%. The ranges of heat transfer coefficient demonstrated in Figure 6.13 for four different tube diameters represent the average values of the local heat transfer coefficient, which were determined at local vapour qualities prior to dryout inception. Consequently, these existing enhancements in heat transfer rate during the use of small-sized channel are considered further improvements in the performance and sizing of heat exchangers.

6.4.5 Effect of surface condition

The influence of surface roughness on flow boiling is investigated using a copper coating as surface enhancements. Two stainless-steel tubes are used for this target which they have a similar diameter and heated length with 4.26 mm and 500 mm, respectively.

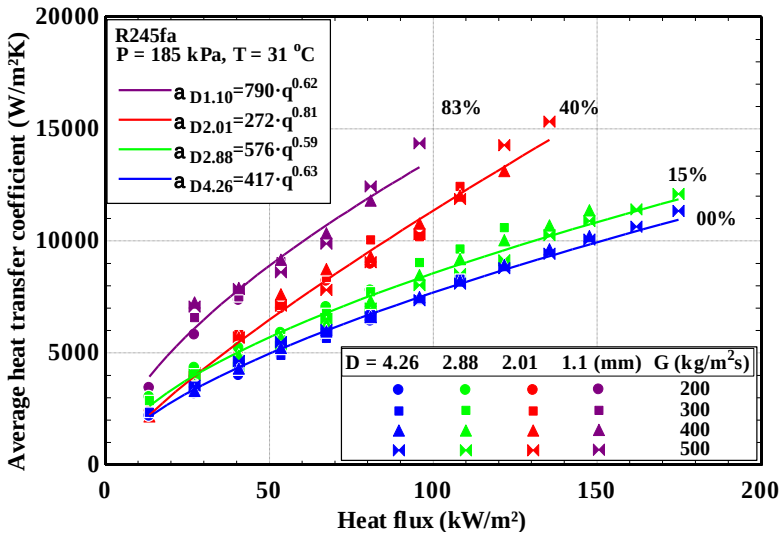

Figure 6.13 Effect of tube diameter on the average heat transfer coefficient at P = 185 kPa.

The surface of one of them is coated with copper, while another one is kept as the manufacturing process, for more details, see Subsection 3.2.4. As a result, the surface roughness of uncoated tube is increased from 0.197 to 0.675 μm with a copper coating, i.e. the surface enhancement approach to 70.82%. As expected, this leads to increasing the density of nucleation sites and consequently higher heat transfer rate (Al-Gaheeshi et al., 2016).

The comparison of the local heat transfer coefficient between uncoated and coated tubes at similar operating conditions is shown in Figure 6.14. It can be seen that the same trend of the saturated flow boiling heat transfer coefficient for the uncoated and coated tube is evident except the location of the thermocouple No. 12. It is interesting to see that the heat transfer coefficient magnitude of the coated tube in thermocouple location No. 12 suddenly drops to reach the heat transfer coefficient magnitude of the uncoated tube. Al-Gaheeshi et al. (2016) reported that this case points out to the coating lack in a small area close to this location instead of locally partial dryout. The figure also shows that the enhancement of heat transfer coefficient increases with increased heat flux because of an increase in the density of active nucleation sites on the surface of the coated tube.

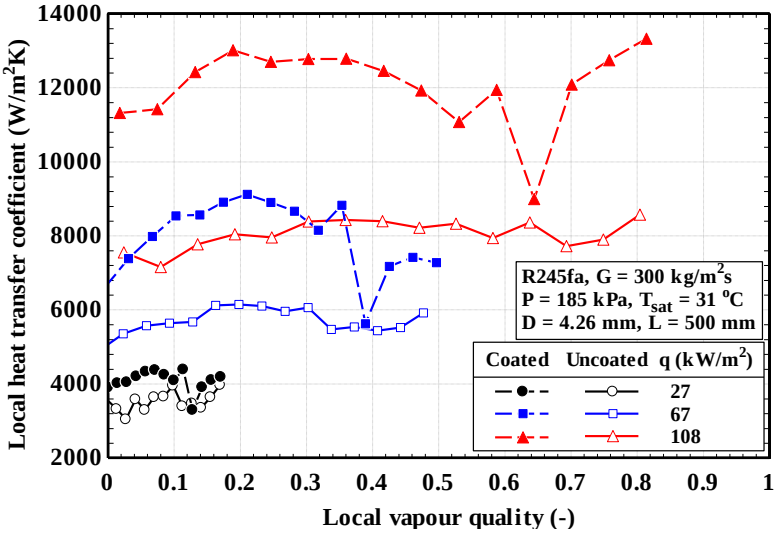

Figure 6.14 Effect of the coated surface on the local heat transfer coefficient at T_{sat} = 31°C and G = 300 kg/m^{2}s (Al-Gaheeshi et al., 2016).

Figure 6.15 demonstrates the influence of coated surface on average heat transfer coefficient as a function of the variations of heat flux with different mass fluxes. According to Figure 6.15, the average heat transfer coefficient for both two tubes increases linearly with increasing heat flux. The mass flux also has an insignificant influence on the average heat transfer coefficient for both two tubes. The average heat transfer coefficients of the coated tube are about 33% higher than those of uncoated tube.

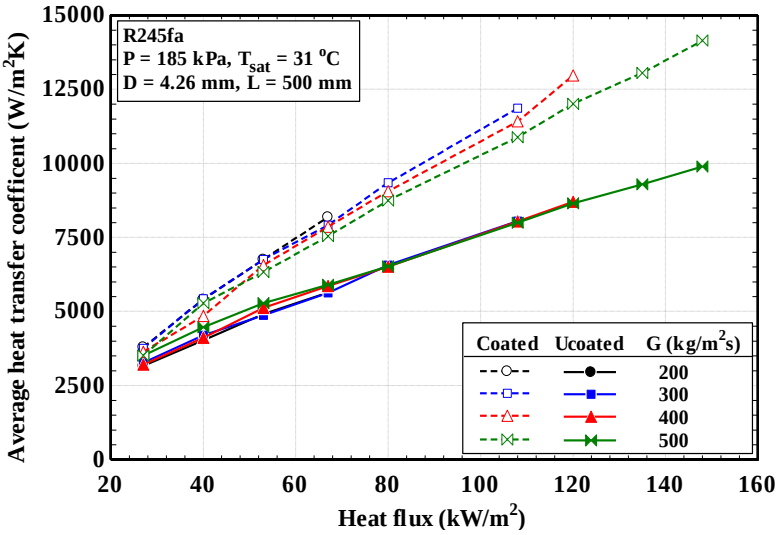

Figure 6.15 Effect of the coated surface on the average heat transfer coefficient for different mass fluxes Al-Gaheeshi et al. (2016).

6.4.6 Effect of fluid properties

Figure 6.16 shows the effect of fluid properties on the local heat transfer coefficient for R245fa and R134a at the saturation temperature of 31 °C and mass flux of 300 kg/m^{2}s. The figure also shows the transition boundaries of experimental flow patterns for both fluids. According to Figure 6.16, the local heat transfer coefficient of R245fa is weakly dependent on heat flux compared to R134a as well as without the occurrence of local dryout. The dependence of local heat transfer coefficient for R245fa on local vapour quality is insignificant. However, the local heat transfer coefficient of R134a is strongly dependent on heat flux up to $x \approx 0.5$ and then the local dryout occurs at heat fluxes more

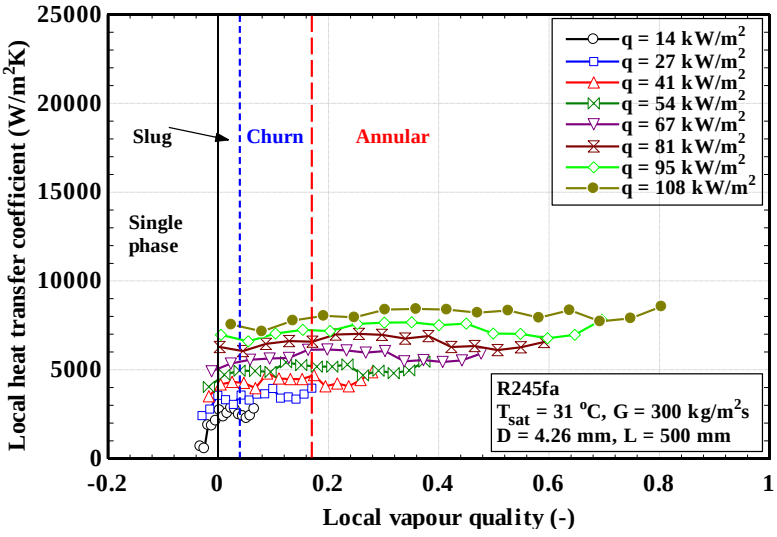

(a)

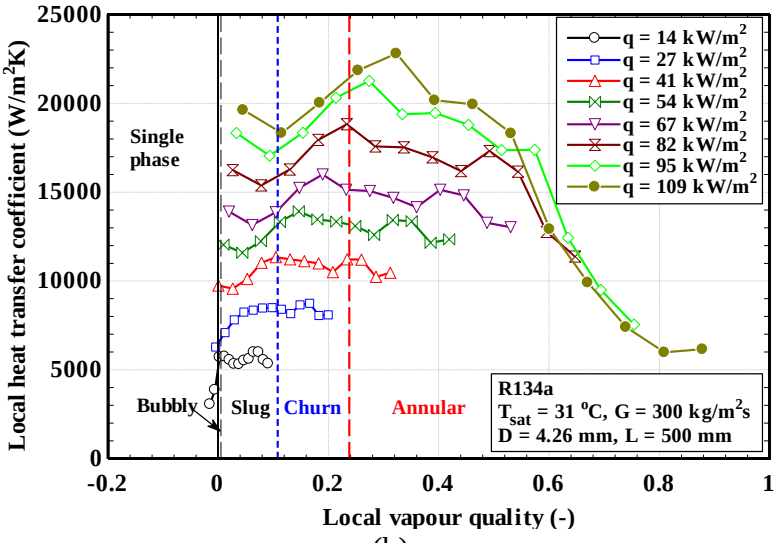

(b)

Figure 6.16 Effect of fluid properties on the local heat transfer coefficient at G = 300 kg/m^{2}s and T_{sat} = 31 °C for: (a) R245fa and (b) R134a, (Al-Gaheeshi et al., 2016).

than 67 kW/m^2 making the heat transfer coefficient drops sharply. There also are small variations of the R134a heat transfer coefficient with local vapour quality (Al-Gaheeshi et al., 2016).

Figure 6.17 shows the effect of fluid properties on the average heat transfer coefficient for both 31 and 39 °C saturation temperature. It is clear from the figure that the average heat transfer coefficient increases as the heat flux increases. The mass flux has a minor influence on the average heat transfer coefficient. In addition, the enhanced values of the average heat transfer coefficient for R134a are appreciably higher than those

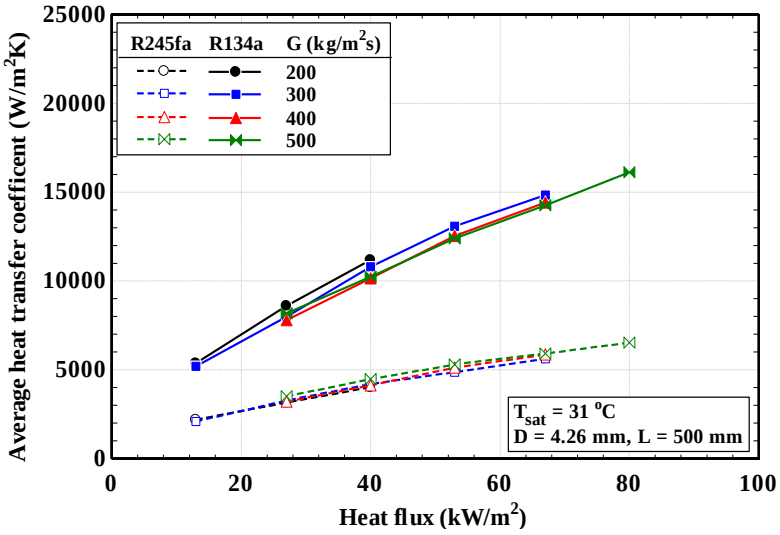

(a)

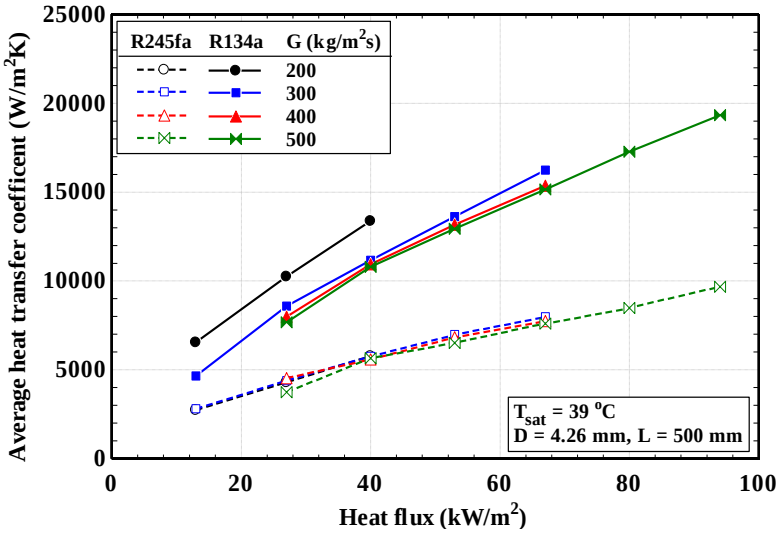

(b)

Figure 6.17 Effect of fluid properties on the average heat transfer coefficient from Al-Gaheeshi et al. (2016) for: (a) T_{sat} = 31 °C, (b) T_{sat} = 39 °C.

for the R245fa, which are estimated by about 151% and 106% for 31 and 39 °C saturation temperature, respectively. According to Al-Gaheeshi et al. (2016), the enhancement of the average heat transfer coefficient of R134a may result from the higher vapour-liquid density ratio of R134a compared to that of R245fa. That is, a higher vapour-liquid density ratio decreases the void fraction at the same saturation temperature and increases the thickness of the liquid film in both, slug and annular flow. These experimental results are consistent with the observed results of Ong and Thome (2011b) study.

6.5 Comparison with previous prediction methods

The flow boiling experiments produce 5424 data points of two-phase heat transfer coefficient in four different tubes, including 932 data points for 1.1 mm, 1348 for 2.01 mm, 1644 for 2.88 mm and 1500 for 4.26 mm tube. The experimental data are compared to the predictions of 10 existing correlations of flow boiling heat transfer coefficient, including one correlation of pool boiling (Cooper, 1984) and nine mini/micro-scale correlations. The selected flow boiling correlations for mini/micro-scale are Kew and Cornwell (1997), Bertsch et al. (2009), Li and Wu (2010b), Mahmoud and Karayiannis (2012), Fang et al. (2015), Turgut et al. (2016), Kanizawa et al. (2016), Fang et al. (2017) and Shah (2017). These correlations were chosen for the comparison based on to be relevant to the present experimental conditions. Full details for these correlations are included in Appendix C. The comparative results of the correlations against all four separate subsets of the experimental data for four tubes (1.1 – 4.26 mm) are listed in Table 6.2where MAE is the mean absolute error, expressed by

$$\mathrm{MAE} = \frac{1}{N}\sum_{i=1}^{N}\left|\frac{\alpha_{pre} - \alpha_{exp}}{\alpha_{exp}}\right| \tag{6.1}$$

where α_{pre} and α_{exp} are the predicted and experimental two-phase heat transfer coefficients and *N* represents the total number of the data points. The MAE is employed as the criterion for assessing the accuracy of the heat transfer correlation, and the β is used to recognize the percentage of data within ±30% error bands for each correlation. The most commonly used two-phase heat transfer correlations of mini/micro-scale are assessed in terms of the influence of tube diameter. The microscale heat transfer correlations are described and discussed in this section.

Table 6.2 Statistical comparison between experimental data and predictions of two-phase heat transfer correlations for the small-scale channel.

Author(s)	D (mm)	1.1	2.01	2.88	4.26	Overall
	Data points	932	1348	1644	1500	5424
Cooper (1984)	MAE (%)	27.67	13.5	20.75	30.94	22.96
	β (%)	61.59	93.25	80.41	38.53	68.79
Kew and Cornwell (1997)	MAE (%)	47.63	30.02	26.73	22.48	29.96
	β (%)	10.73	50.82	65.63	72.27	54.35
Bertsch et al. (2009)	MAE (%)	30.55	18.02	28.58	37.92	28.88
	β (%)	49.36	81.31	55.23	23.07	51.81
Li and Wu (2010b)	MAE (%)	25.65	26.61	24.65	29.2	26.57
	β (%)	58.69	65.36	66.12	64.93	64.33
Mahmoud and Karayiannis (2012)	MAE (%)	21.16	19.8	25.42	30.38	24.66
	β (%)	75.54	78.26	66.3	56.13	68.05
Fang et al. (2015)	MAE (%)	17.4	19.74	20.01	20.75	19.7
	β (%)	83.8	78.34	77.8	76.27	78.54
Turgut et al. (2016)	MAE (%)	36.19	18.62	21.34	19.19	22.62
	β (%)	34.87	88.5	79.26	85.4	75.63
Kanizawa et al. (2016)	MAE (%)	28.76	13.44	12.53	11.15	15.16
	β (%)	56.44	94.81	92.15	95.2	87.52
Fang et al. (2017)	MAE (%)	16.78	19.14	20.27	21.33	19.68
	β (%)	100	100	100	100	100
Shah (2017)	MAE (%)	35.92	25.06	23.42	20.28	25.11
	β (%)	38.09	62.91	68.49	73.6	63.29

6.5.1 Cooper (1984) correlation

The Cooper (1984) correlation was widely utilized in the literature to provide pool boiling predictions. Hence, for flow boiling, it is considered the best correlation to predict two-phase heat transfer coefficient data for nucleate boiling (Bertsch et al., 2009). In general, a very good agreement between its predictions and the experimental data of flow boiling may give an indication of the dominant nucleate boiling in the heat transfer mechanism. The author developed this correlation based on 6000 experimental data points covering water, and refrigerants. It considers the effects of reduced pressure, molecular weight, heat flux and surface roughness, see Appendix C. Figure 6.18 shows that the best performance of correlation is found in the 2.01 mm tube with prediction 93.25% of the experimental data within the ±30% comparing to the other tubes. The correlation shows fair predictions for the 2.88 mm tube date with the β value of 80.41%, following by 61.59% of the 1.1 mm tube data. The worst predictions are presented by the

correlation for the 4.26 mm tube with only 38.53% of experimental data within ±30% error bands, as shown in Figure 6.18d. As it is known, the predictive ability of Cooper (1984) equation should relate to the dominance of nucleation mechanism within the tube. The correlation generally underpredicts most of the data for all tubes, with sometimes significant scatter, especially in the 1.1 and 2.88 mm tubes, evidenced by lower MAE values of 27.67%, 13.5%, 20.75% and 30.94%, for 1.1, 2.01, 2.88 and 4.26 mm tube, respectively. In addition, a larger difference in the predicted results is likely to be due to the presence of changes in the surface roughness values for all tubes, see Subsection 3.2.4.

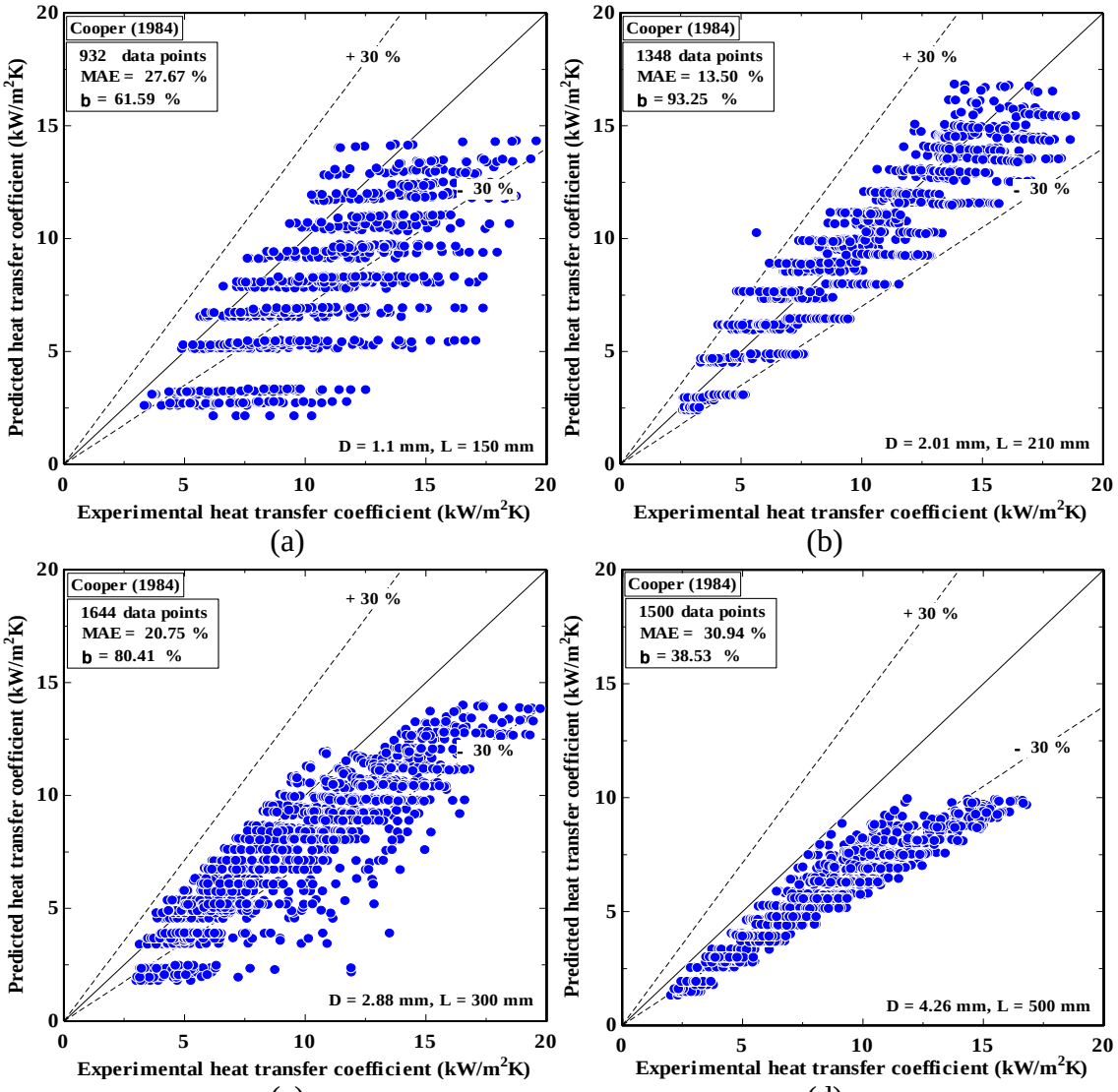

Figure 6.18 Comparison of experimental data with predictions of Cooper (1984) correlation for: (a) D = 1.1 mm, (b) D = 2.01 mm, (c) D = 2.88 mm, and (d) D = 4.26 mm.

6.5.2 Kew and Cornwell (1997) correlation

Kew and Cornwell (1997) performed an experimental study and develop a correlation based on the measurements of saturated boiling heat transfer of R141b flowing in tubes with a diameter range of 1.39 – 3.69 mm. They found the contribution of nucleate boing in the low vapour quality region and convective boiling in the high vapour quality region. This was based on the dependence of heat transfer coefficient on heat flux in the low quality region, while its dependence on vapour quality and its independence from heat flux in the high quality region. Therefore, they decided to modify the Lazarek and Black (1982) model, at which Nusselt number (*Nu*) became a function of liquid Reynolds number (Re_l), Boiling number (*Bo*) and vapour quality (*x*). The expression is given in Appendix C. As shown in Figure 6.19, the flow boiling heat transfer correlation intended for mini/micro-channels shows significant underprediction for all four tubes of the experimental study, and large scatter especially for the data of 1.1 mm and 2.88 mm tubes. The higher MAE value is 47.36% for the 1.1 mm tube, followed by 30.02% for the 2.01 mm tube. With increasing the tube diameter to 2.88 and hence 4.26 mm, the MAE values become lower at 26.73% and 22.48%, respectively. On the contrary, the β value increases with increasing the tube diameter, evidenced by only 10.73%, 50.82%, 65.63% and 72.2% of data within ±30%, for1.1, 2.01, 2.88 and 4.26 mm tube, respectively. Moreover, the worst performance of correlation in the 1.1 mm tube may be attributed to use of a narrow range of experimental data, one working fluid (R141b) and a channel size greater than 1.3 mm.

6.5.3 Bertsch et al. (2009) correlation

Bertsch et al. (2009) presented a heat transfer correlation for saturated flow boiling with considering the effect of channel size. This correlation was modified based on the Chen (1966) model by applying a superposition of nucleate boiling and convection contributions. Further, the enhancement factor (*E*) considered the effect of bubble confinement in small channels, while the suppression factor (*S*) appeared to be independent of the channel size, see Appendix C. The correlation was developed based on 3899 data points from 14 studies in the literature involving 12 different wetting and non-wetting fluids, vertical and horizontal channels with hydraulic diameters ranging from 0.16 to 2.92 mm. In Figure 6.20, the correlation shows significant underprediction

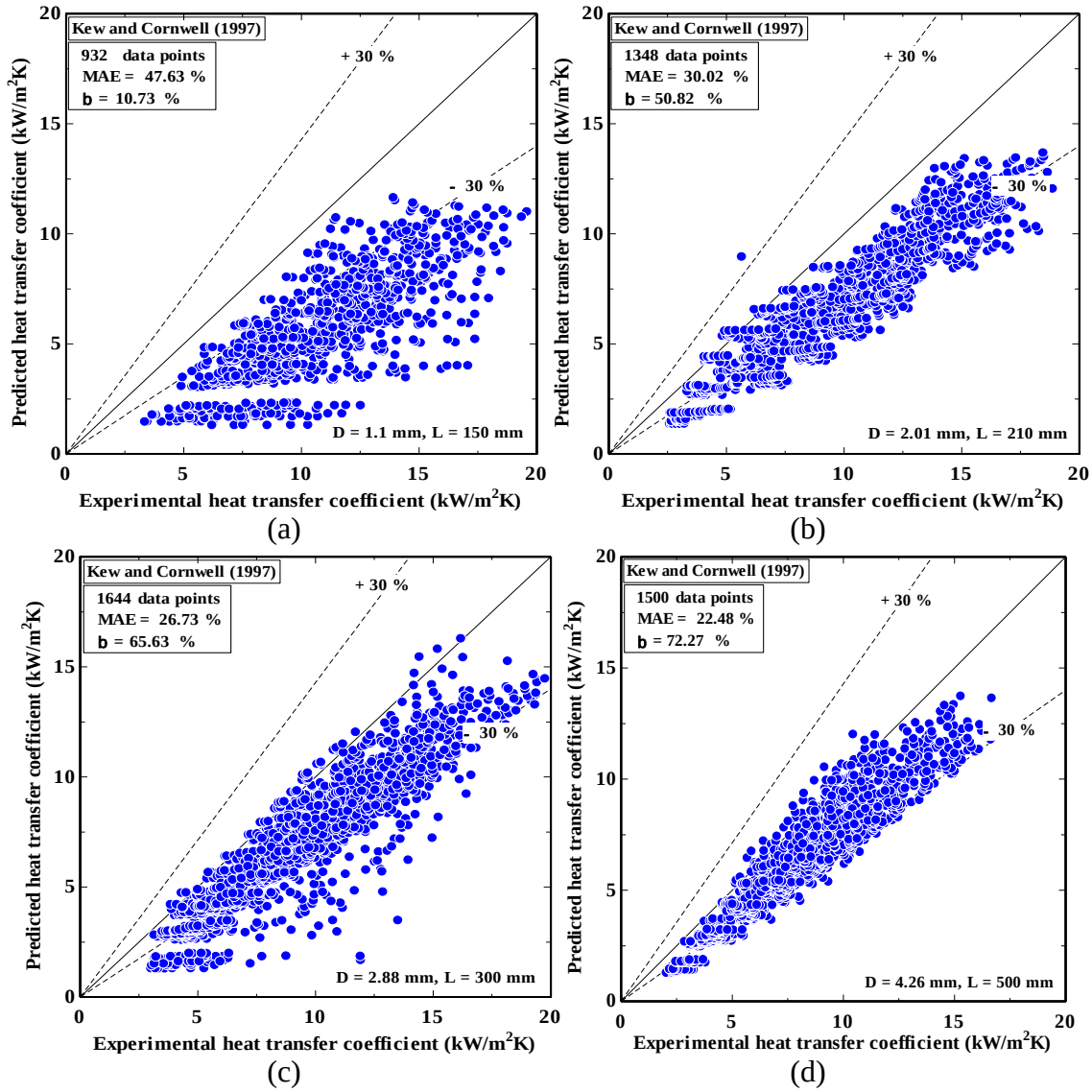

Figure 6.19 Comparison of experimental data with predictions of Kew and Cornwell (1997) correlation for: (a) D = 1.1 mm, (b) D = 2.01 mm, (c) D = 2.88 mm, and (d) D = 4.26 mm.

of most of the data for all tubes, plus some scatter out of the -30% error band. The MAE values are 30.55%, 18.02%, 28.58% and 37.92%, for 1.1, 2.01, 2.88, 4.26 mm tube, respectively. Therefore, the higher β value is for the 2.01 mm tube, following by the 2.88 mm tube, of 81.31% and 55.23% within ±30%, respectively. Its worst performance in the 1.1 mm and 4.26 mm tubes may be ascribed to the surface roughness of inner tube wall which is reflected in the heat transfer predictions of nucleate boiling by the Cooper (1984) equation. The surface roughness value of 4.26 mm tube is much lower than those of other tubes, its surface roughness value of the 1.1 mm tube is much higher than those of other tubes, see Subsection 3.2.4. The correlation predicts 49.36% of the 1.1 mm tube data and only 23.07% of the 4.26 mm tube data. In addition, this limited performance is attributed

to the use of a narrow range of experimental data for R245fa flowing in channel size less than 1 mm.

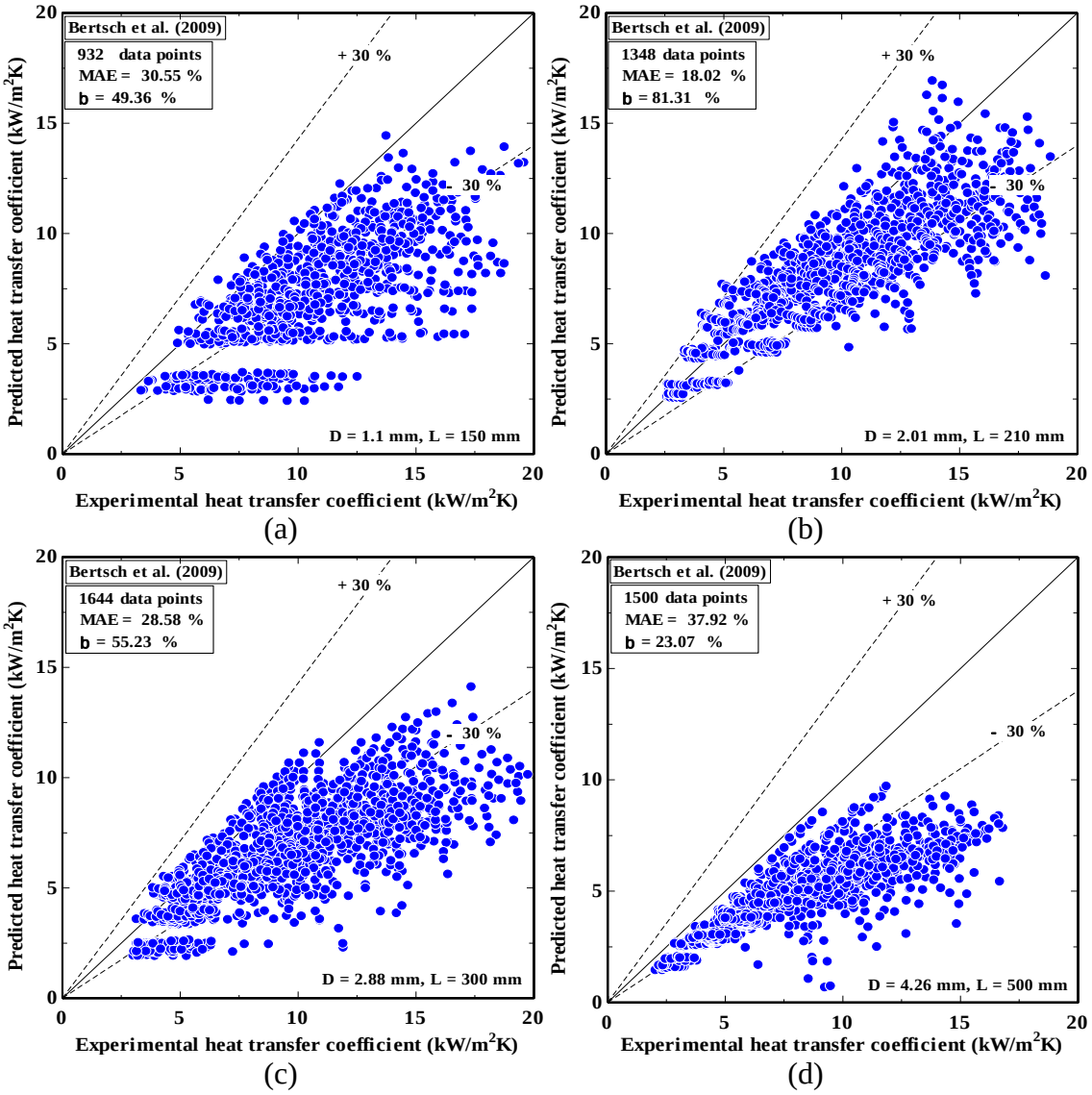

Figure 6.20 Comparison of experimental data with predictions of Bertsch et al. (2009) correlation for: (a) D = 1.1 mm, (b) D = 2.01 mm, (c) D = 2.88 mm, and (d) D = 4.26 mm.

6.5.4 Li and Wu (2010b) correlation

Li and Wu (2010b) proposed a heat transfer correlation for flow boiling in mini and micro channels. The correlation developed from 769 experimental databanks covering 12 fluid types and tubes with a diameter ranging from 0.148 to 3.25 mm. The authors depended on the Lazarek and Black (1982) model to proposed their correlation, see Appendix C. It considered the effect of channel size through the Reynolds number

accounting for inertia and viscous forces and Bond number accounting for gravity force and surface tension. Figure 6.21 reveals that the correlation provides an agreement with all tubes, with the β values of 58.69%, 65.36%, 66.12% and 64.93% within ±30% error bands, for 1.1, 2.01, 2.88, 4.26 mm tube, respectively. Further, the correlation overpredicts the data corresponding to lower vapour quality and underpredicts the data corresponding to higher vapour quality for all tubes, evidenced by the MAE values of 25.65%, 26.61%, 24.65% and 29.2%, for 1.1, 2.01, 2.88, 4.26 mm tube, respectively. The limited performance of this correlation is due to the use of a narrow range of experimental data for R245fa flowing in tube diameter less than 1 mm.

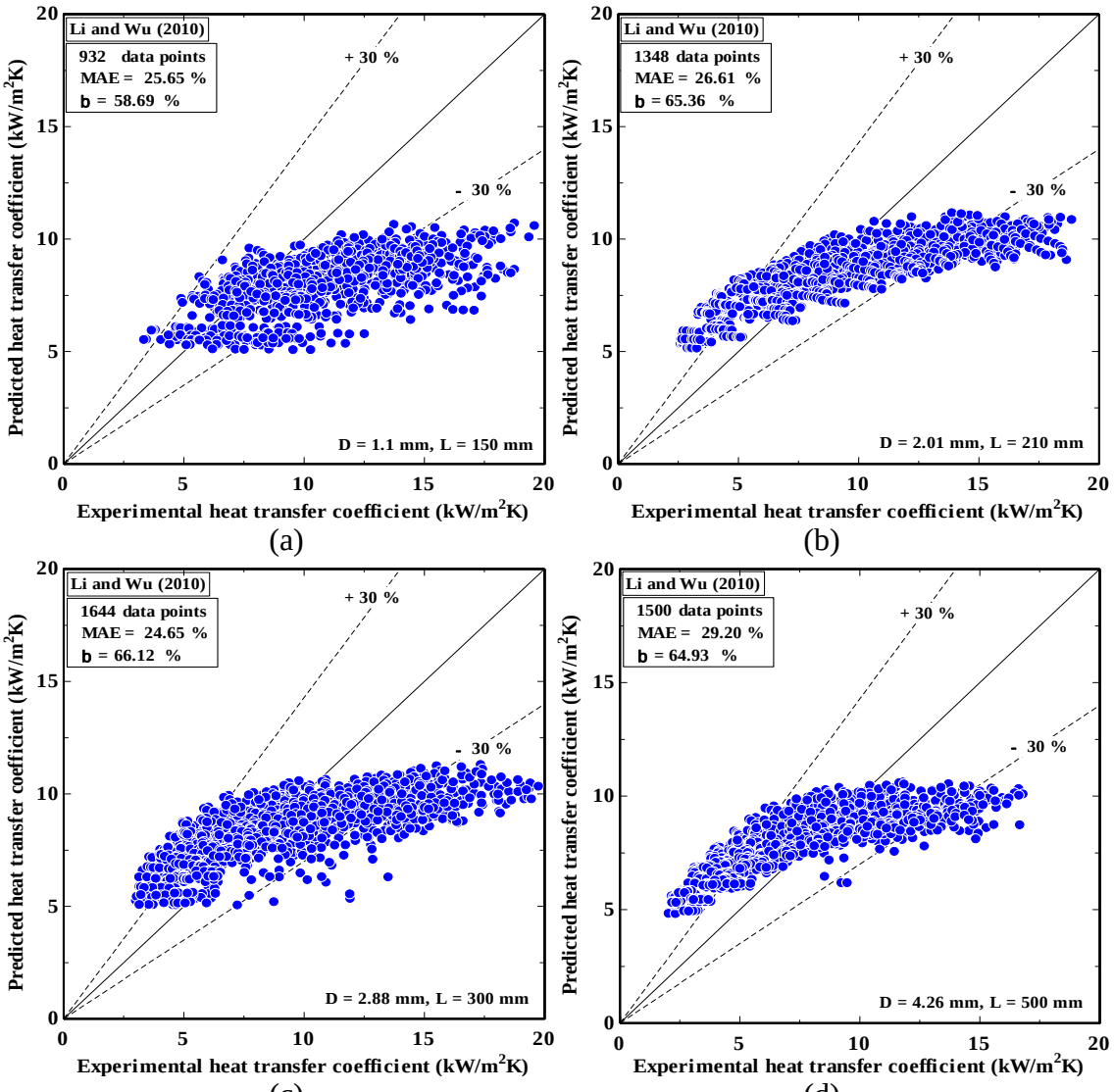

Figure 6.21 Comparison of experimental data with predictions of Li and Wu (2010b) correlation for: (a) *D* = 1.1 mm, (b) *D* = 2.01 mm, (c) *D* = 2.88 mm, and (d) *D* = 4.26 mm.

6.5.5 Mahmoud and Karayiannis (2012) correlation

Mahmoud and Karayiannis (2012) proposed a boiling heat transfer correlation based on their work with R134a. The correlation took into account the influence of channel size within the Confinement number accounting for confined bubble size and channel size. It was formed by using the non-linear least square fitting method to fit a multi-parameter with databank consisting of 5152 experimental data of R134a flowing in vertical tubes with an inner diameter ranging from 1.1 to 4.26 mm. The expression is presented in Appendix C. According to Figure 6.22, the correlation of Mahmoud and Karayiannis (2012) generally presents fair predictions for all tubes, proved by MAE values of 21.16%, 19.8%, 25.42% and 30.38%, for 1.1, 2.01, 2.88 and 4.26 mm tubes, respectively. There is scatter in the prediction of 1.1 and 2.88 mm tubes, see Figure 6.22a and Figure 6.22c. The correlation shows underprediction for the 1.1 mm tube with β of 75.54% within ±30%. For the 2.01 mm tube, it shows overprediction at lower vapour quality, with slight underprediction at higher vapour quality, with β of 78.26% within ±30%. It also presents overprediction for 2.88 mm and 4.26 mm tubes, with β of 66.3% and 56.13% within ±30%, respectively. This correlation gives best prediction, if it is improved for the heat transfer coefficient of R245fa fluid.

6.5.6 Fang et al. (2015) correlation

Fang et al. (2015) proposed a specific expression of the heat transfer correlation for the saturated flow boiling of water in micro and mini-channels. Further, they compiled 1055 experimental data points from nine independent studies in the open literature. The correlation was developed based on collecting dimensionless parameters from the fifteen correlations that have better performances. They also defined a new dimensionless number, $Fa = (\rho_l - \rho_v)\sigma/G^2D$, Fang number ($Fa$) which was associated with the formation and departure of bubbles. Moreover, they presented two factors (S and E), where S factor contained the Boiling number (Bo), liquid-vapour density ratio and molecular weight and the E factor contained vapour quality (x) and liquid-vapour density ratio. The correlation presented Nusselt number (Nu) as a function of the additive model of two factors (S and E), liquid Reynolds number (Re_l), Fang number, and liquid Prandtl number (Pr_l) as well as the ratio of the liquid viscosity at the fluid temperature ($\mu_{l,l}$) to the inside wall temperature ($\mu_{l,w}$). The expression is given in Appendix C. Furthermore,

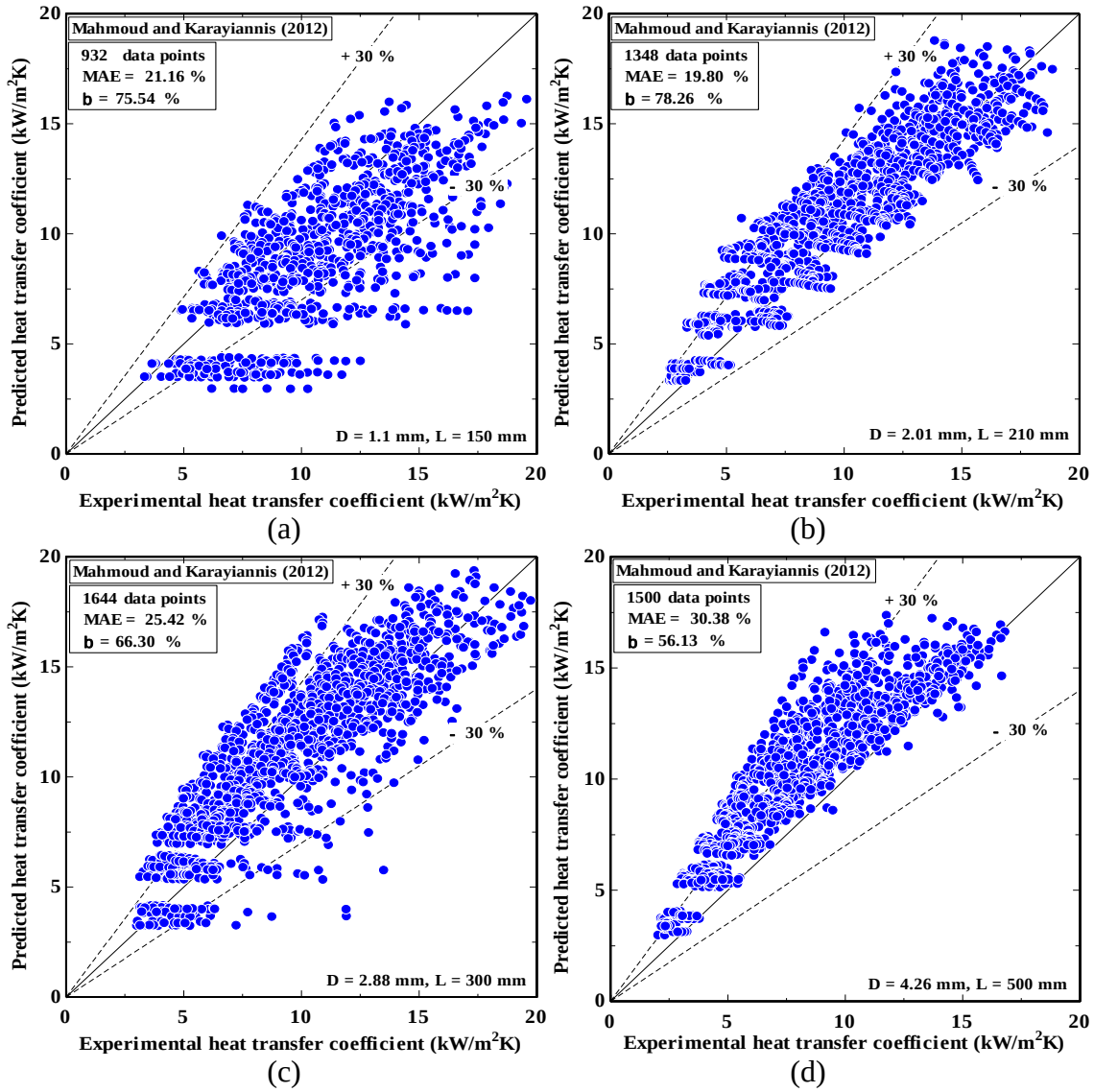

Figure 6.22 Comparison of experimental data with predictions of Mahmoud and Karayiannis (2012) correlation for: (a) D = 1.1 mm, (b) D = 2.01 mm, (c) D = 2.88 mm, and (d) D = 4.26 mm.

this correlation also works well for R22, R134a, R410A and R717. Figure 6.23 exhibits that the correlation provides good agreements with all four tubes (1.1 – 4.26 mm), in addition to the experimental data being scattered, overpredicted at low exit vapour quality and underpredicted at high exit vapour quality. The MAE values decrease from only 20.75% to 17.4% with decreasing tube diameter from 4.26 mm to1.1 mm, while the β values increase from 76.27% to 80.8% with decreasing the tube diameter from 4.26 mm to 1.1 mm. The correlation of Fang et al. (2015) extrapolates fairly well to the larger tube (>1.73 mm), with the best predictions, although this correlation was developed based on

the data being intended for micro channels with a diameter range of 0.207 – 1.73 mm and water as working fluid.

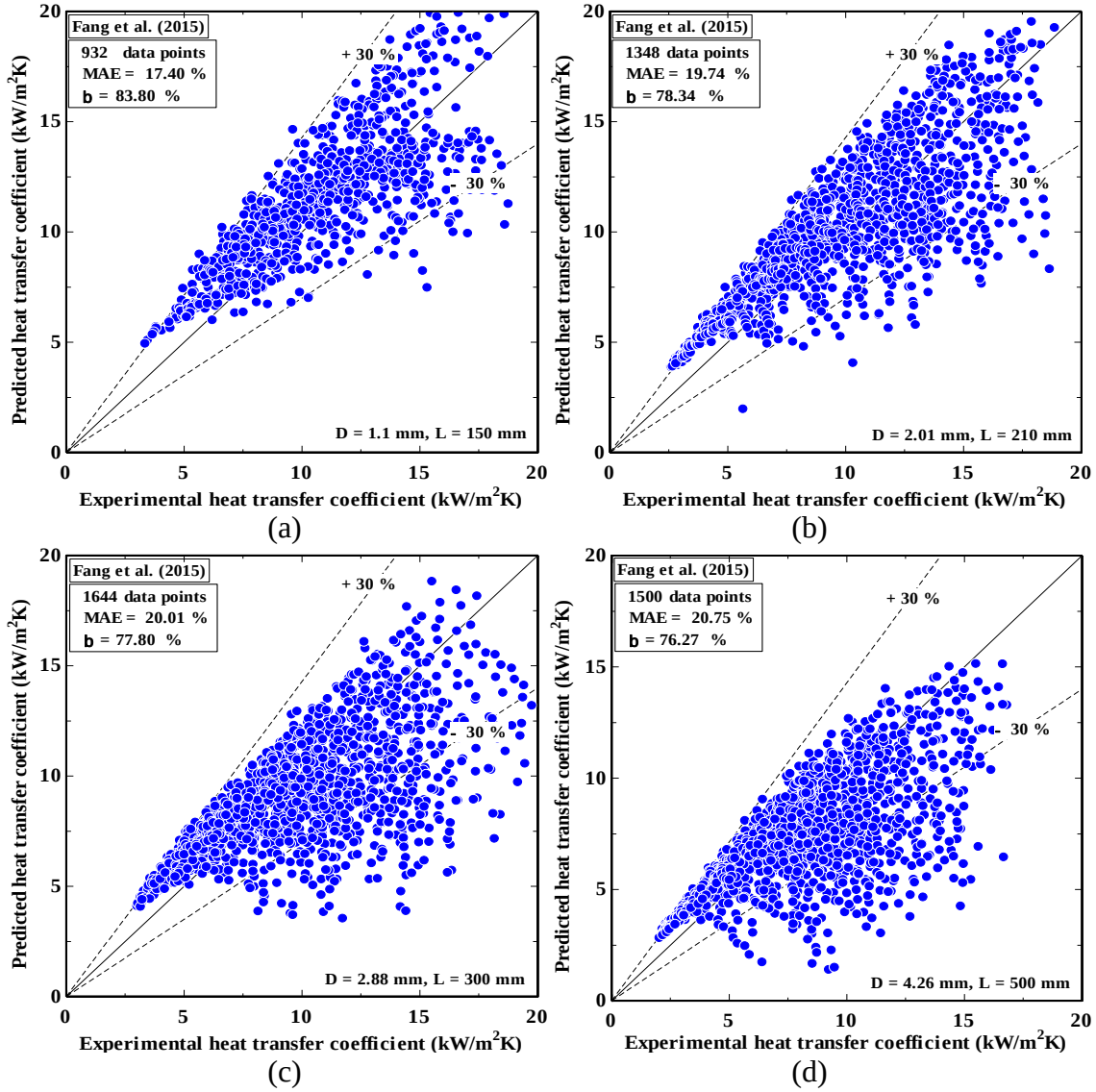

Figure 6.23 Comparison of experimental data with predictions of Fang et al. (2015) correlation for: (a) D = 1.1 mm, (b) D = 2.01 mm, (c) D = 2.88 mm, and (d) D = 4.26 mm.

6.5.7 Turgut et al. (2016) correlation

Turgut et al. (2016) developed an asymptotic model (with n = 2) of the correlation for saturated boiling heat transfer coefficient in micro- and macro-tubes based on the consolidated database consisting of 3594 data points of R134a compiled from 19 sources. Ranges of the database cover a hydraulic diameter between 0.5 and 13.84 mm and

saturation temperatures between −8.8 and 52.4 °C. They took into account the effects of channel size and surface roughness of channel wall. Further, they suggested the use of the fluid-specific reduced pressure correlation proposed by Gorenflo (1993) and Dittus and Boelter (1930) correlations to predict the nucleate boiling and convective mechanisms, respectively. They correlated the enhancement factor (E) as a function of the reciprocal of the Lockhart-Martinelli parameter (X_{tt}) which was proposed by Lockhart and Martinelli (1949) for turbulent-turbulent mixture flow. Also, they correlated the suppression factor (S) as a function of the vapour quality and the reduced pressure (P_r). The details of correlation summarized in Appendix C. According to Figure 6.24, the performance of correlation in the 1.1 mm tube is lower with a prediction of 34.87% inside the lines of ±30%, but its performance improves to predict 88.5%, 79.25% and 85.4% of the experimental data for 2.01, 2.88 and 4.26 mm tubes, respectively. In general, the correlation exhibits underprediction for all data of four tubes (1.1 – 4.26 mm), evidenced by the MAE values of 36.19%, 18.62%, 21.34% and 19.19%, respectively. There is also the presence of scatters in the predictions of 1.1 mm and 2.88 mm tubes falling outside -30%, as shown in Figure 6.24a and Figure 6.24c. In addition, this worst performance in the 1.1 mm tube may be ascribed to the use of a narrow range of experimental data, one working fluid (R134a). Further, this fluid R134a considers from fluids which have higher reduced pressure (i.e. lower critical pressure), higher vapour to liquid density ratio and lower surface tension compared to those of R245fa. The properties of R134a result in a relatively low void fraction. This also affects confinement in narrow passages, which plays an important role in changes of the flow pattern and hence the two-phase heat transfer coefficient.

6.5.8 Kanizawa et al. (2016) correlation

The experimental results for the heat transfer coefficient during the flow boiling of R134a, R245fa and R600a in small diameter tubes in addition to a boiling heat transfer correlation were presented by Kanizawa et al. (2016). The experimental database involved 2047 data points covering the tube diameter range of 0.38 – 2.6 mm. Based on this database, the authors developed a superposition model with the contributions of nucleate boiling and convective boiling, see Appendix C. The nucleate boiling effects were estimated by the correlation of Stephan and Abdelsalam (1980) for pool boiling of organic refrigerants, while the convective effects were estimated by the correlation of Dittus and Boelter (1930) assuming only the liquid phase flowing in the tube. Further, the

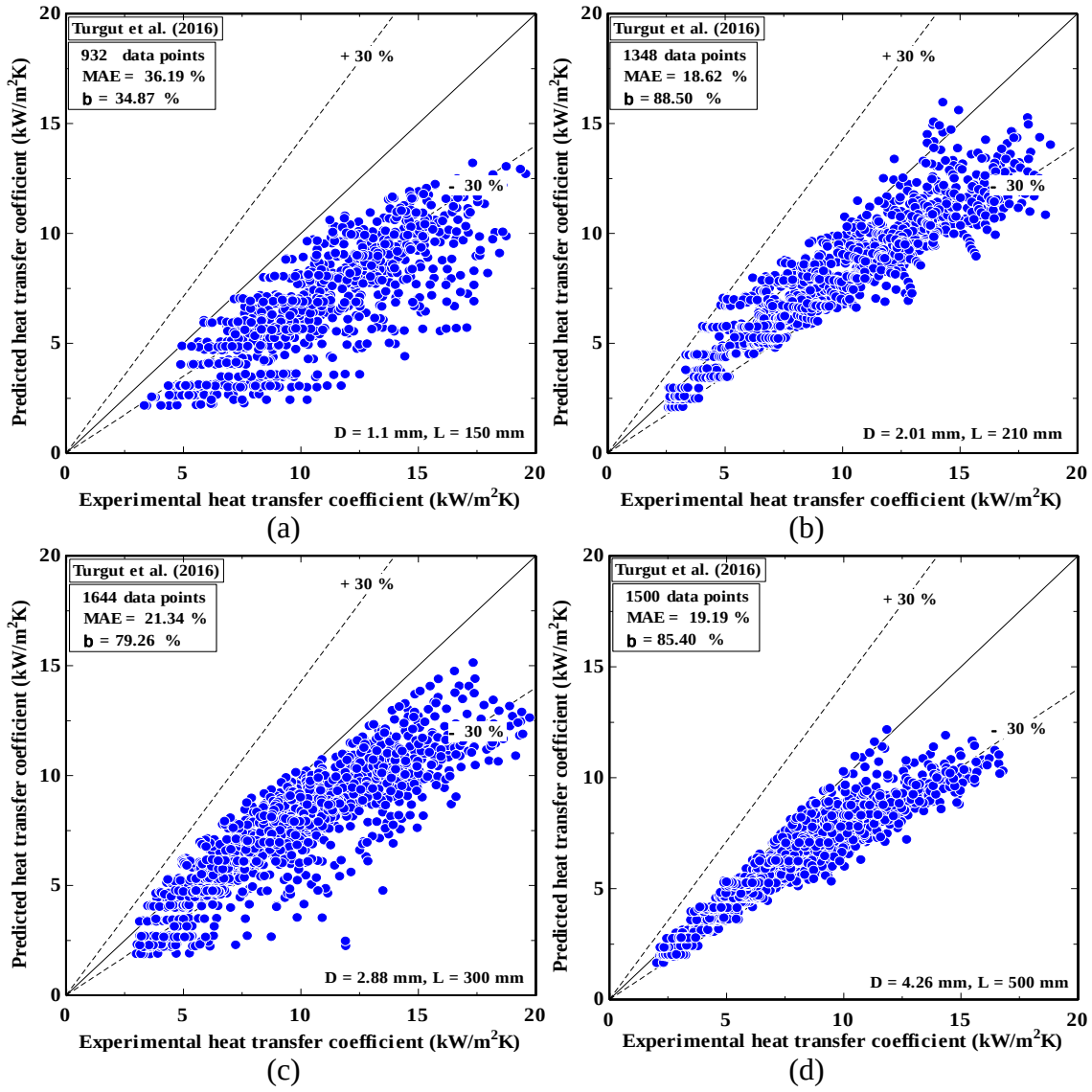

Figure 6.24 Comparison of experimental data with predictions of Turgut et al. (2016) correlation for: (a) D = 1.1 mm, (b) D = 2.01 mm, (c) D = 2.88 mm, and (d) D = 4.26 mm.

enhancement factor (E) was a function of the multiplicative constant, the reciprocal of the Lockhart-Martinelli parameter, and the Weber number based on the gas in situ velocity, while the suppression factor (S) appeared to be dependent on Bond number (Bd) and two-phase modified Reynolds number (Re_{tp}). The enhancement factor took into account the cross-sectional velocities distribution of both phases. The suppression factor (S) accounted for capturing the effects of confined bubble growth on the suppression of nucleate boiling. Figure 6.25a show that most of the 1.1 mm tube data are underpredicted by the Kanizawa et al. (2016) correlation with 28.76% MAE and the β value of 56.44% in addition to a scatter in the prediction out -30% error band. This is because the enhancement factor (E) was a function of the reciprocal of the Lockhart-Martinelli

parameter which was calculated assuming turbulent flow for the liquid phase. However, the liquid phase flows inside the 1.1 mm tube under laminar flow conditions. In Figure 6.25(b-d), the experimental data of 2.01, 2.88 and 4.26 mm tubes are best predicted by correlation and predictions 94.81%, 92.15% and 95.2% inside the lines of ±30%, respectively. Also, there is a dispersion of the predictions for 2.88 mm tube outside -30%, see Figure 6.25c. The MAE values are very lower, of 13.44% for 2.01 mm, 12.53% for 2.88 mm, and 11.15% for 4.26 mm tube. Notice that for this correlation, the data of heat transfer coefficient corresponding to its validity range are considered and even extended to contain the data for tube larger than 2.6 mm.

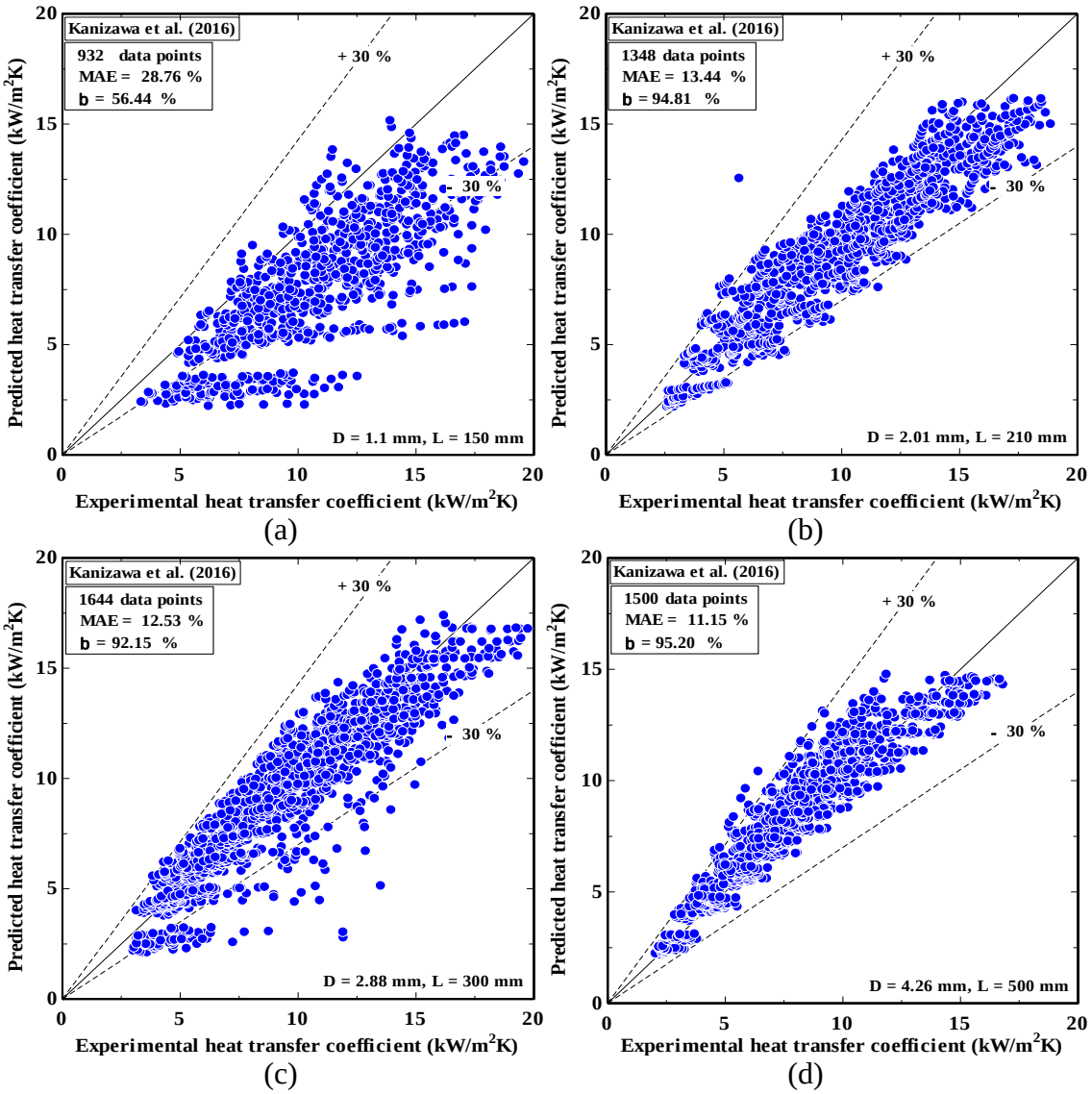

Figure 6.25 Comparison of experimental data with predictions of Kanizawa et al. (2016) correlation for: (a) D = 1.1 mm, (b) D = 2.01 mm, (c) D = 2.88 mm, and (d) D = 4.26 mm.

6.5.9 Fang et al. (2017) correlation

Fang et al. (2017) extended the correlation of Fang et al. (2015) to involve other fluids by evaluating the fluid-dependent parameter (F_{fl}) for each fluid from the experimental data. The new correlation was developed based on the first database consisting of 17778 experimental data points from 101 sources and 13 different fluids. Also, it was validated with the second database containing 6664 experimental data points from 60 sources and 18 different fluids. The validation results showed that the new correlation has a mean absolute deviation (MAD) of 4.4% against the second database. The correlation was Nusselt number (Nu) as function of fluid-dependent parameter (F_{fl}), molecular weight, Boiling number (Bo), liquid only Froude number (Fr_{lo}), Bond number (Bd), liquid-vapour density ratio, and reduced pressure (P_r) as well as the ratio of the liquid viscosity at the fluid temperature ($\mu_{l,l}$) to the inside wall temperature ($\mu_{l,w}$). The expression is presented in Appendix C. Figure 6.26 shows the two-phase heat transfer correlation from Fang et al. (2017) provides excellent predictions for all four separate subsets of the experimental data for four tubes: 1.1, 2.01, 2.88 and 4.26 mm tubes, with the MAE values of 16.78%, 19.14%, 20.27% and 21.33%, respectively. It shows relative underprediction by very higher β values for all tubes, of 100% of all data within ±30% error bands. These best predictions of correlation could be attributed to the fact that the authors used the effect of liquid viscosity ratio on the heat transfer coefficient. Furthermore, they distinguished the effect of fluid on the correlation predictions through utilizing the molecular weight of fluid, the fluid-dependent parameter and, especially, the wide range of experimental data for R245fa flowing in vertical and horizontal small tubes.

6.5.10 Shah (2017) correlation

Shah (2017) also extended his old correlation Shah (1982) to indicate the boundary between conventional and mini/micro channels for flow boiling inside channels as a function of vapour Weber number (We_v) and Boiling number (Bo). He found that the Weber number accounts for surface tension force and inertia force as well as the influences of surface tension become strong at $We_v < 100$. Additionally, an increase in the Boiling number (Bo) renders the effect of Weber number tends to diminish. Therefore, the author suggested the E factor, $E = 2.1 - 0.008We_v - 110Bo$, to multiply by his old correlation and if the E factor is less than 1, use $E = 1$. The details of correlation are

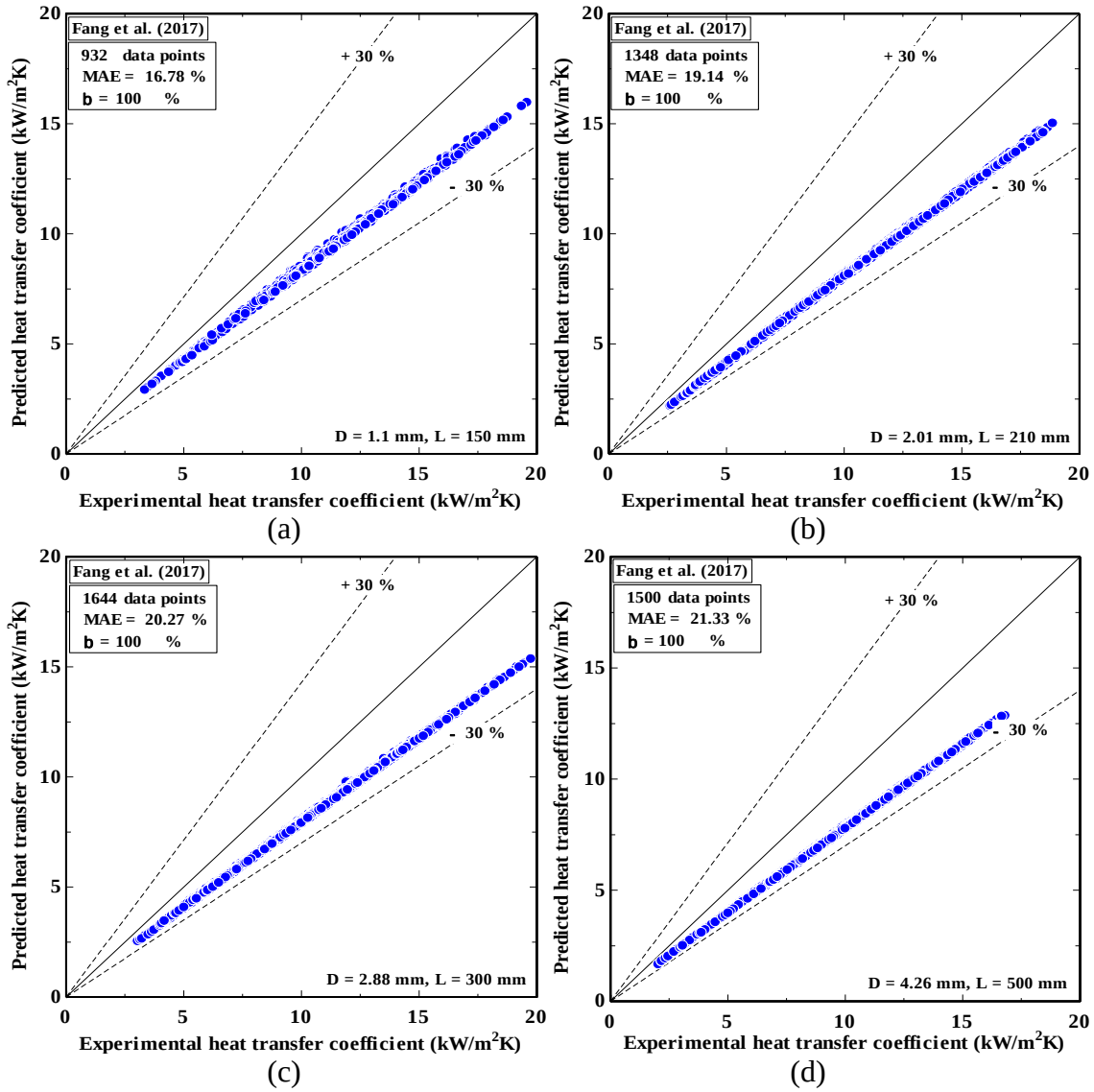

Figure 6.26 Comparison of experimental data with predictions of Fang et al. (2017) correlation for: (a) D = 1.1 mm, (b) D = 2.01 mm, (c) D = 2.88 mm, and (d) D = 4.26 mm.

expressed in Appendix C. The new unified correlation was based 4852 experimental data points from 81 independent sources in the literature including the diameter ranging from 0.38 to 27.1 mm and 30 different fluids. This correlation presents relatively satisfied predictions for 2.01, 2.88 and 4.26 mm tubes with the β values of 62.91%, 68.49% and 73.6% within ±30% error bands, respectively, but its performance become worst for the 1.1 mm tube by 38.09% of experimental data with ±30% error bands and few scatters out -30%, as shown in Figure 6.27. The correlation of Shah (2017) generally underpredicts most of the heat transfer coefficient data for all four tubes (1.1 – 4.26 mm), evidenced by MAE values of 35.78%, 23.04%, 22.48% and 18.8%, respectively. Moreover, the limited

performance of correlation is due to the use of a narrow range of experimental data for R245fa which was determined by about 7% of all consolidated database.

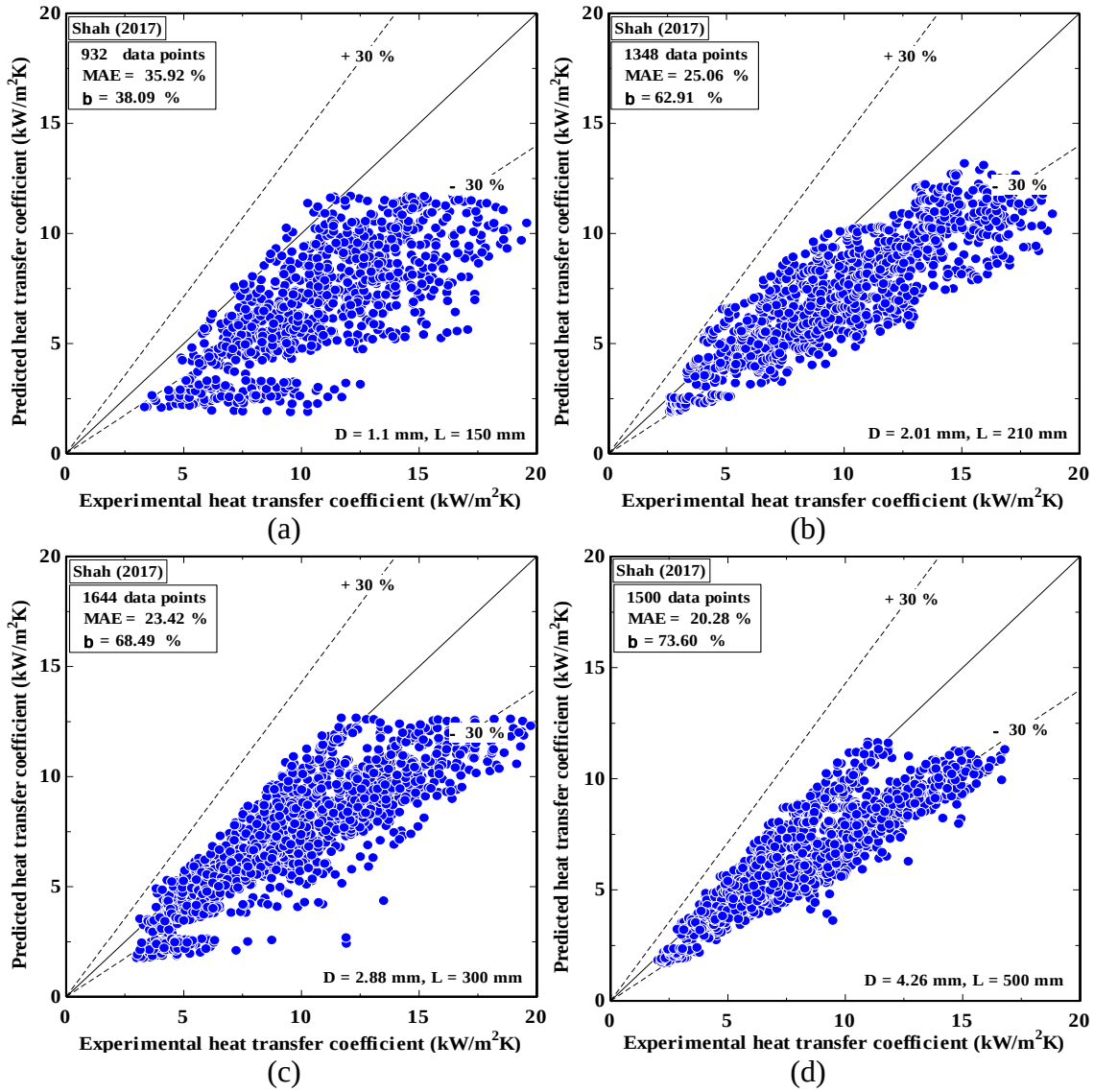

Figure 6.27 Comparison of experimental data with predictions of Shah (2017) correlation for: (a) D = 1.1 mm, (b) D = 2.01 mm, (c) D = 2.88 mm, and (d) D = 4.26 mm.

The saturated flow boiling heat transfer coefficient in vertical flow was compared to some well-known correlations. Among the 10 existing heat transfer correlations, the Fang et al. (2015) correlation was not developed for R245fa. It is included here for the reason that the aim of the comparison is to provide a guide for selecting an apposite correlation which has the best accuracy of prediction for R245fa. The comparison results with selected correlations presented above demonstrated that Fang et al. (2017) correlation

tends to provide excellent predictions for most of the small tube data (1.1 – 4.26 mm) with β values of 100% within ±30% error bands. It shows underprediction for all tube. The MAE value decreases as the tube diameter decreases. The Kanizawa et al. (2016) correlation shows the best predictions for most of the experimental data for 2.01, 2.88 and 4.26 mm tubes. Further, the data of 2.01 mm and 2.88 mm tubes are overpredicted by the Kanizawa et al. (2016) correlation in low vapour quality, while for high vapour quality, the data are underpredicted. This correlation also overpredicts the data of 4.26 mm tube. Moreover, the Cooper (1984) correlation provides underprediction for the data of 2.01 and 2.88 mm tubes with the higher β value. The Turgut et al. (2016) correlation underpredicts 88.5% and 85.4% of the experimental data of 2.01 and 4.26 mm tube, respectively. The 2.01 mm tube data are underpredicted by the Bertsch et al. (2009) correlation with 81.31% of data within ±30%. The Fang et al. (2015) correlation gives a good agreement with the data of 1.1 mm, evidenced by the β value of 83.8% within ±30%. It provides underprediction for the data at low vapour quality and overprediction for the data at high vapour quality.

6.6 Summary

The experimental results of R245fa flow boiling heat transfer inside five small tubes with a diameter ranging from 1.1 to 4.26 mm are presented and discussed in this chapter. The experimental tests are conducted under the operating conditions including mass flux ranging from 200 to 500 kg/m^{2}s, heat flux ranging from 3.4 to 188.5 kW/m^2, system pressure ranging from 185 to 310 kPa, vapour quality up to the dryout incipience. In this work, the verification of heat transfer mechanism (nucleate boiling and convective boiling) for R245fa fluid, the effect of diameter tube in vertical orientation, the effect of copper coating and the effect of thermophysical fluid properties on heat transfer rate consider new contributions. The following conclusions are drawn from the discussion of the experimental results of saturated flow boiling heat transfer coefficient for R245fa and the influence of main parameters on two-phase heat transfer coefficient.

- The boiling curve reveals that the onset of nucleate boiling appreciably occurs at lower heat fluxes in all tubes and the wall superheat of boiling incipience in the 1.1

mm tube is significantly lower than those in the rest of tubes. The heat flux after the onset of nucleate boiling increases linearly with wall superheat. The slope of boiling curve changes at higher heat fluxes because of the occurrence of local dryout, especially in the 1.1 mm and 2.01 mm tubes. Hysteresis occurs evidently at all axial locations of all tubes. Additionally, the coating has a strong influence on the onset of nucleate boiling.

- The local heat transfer coefficient of 1.1 and 2.88 mm tubes increases with increasing heat flux for vapour quality up to about 0.4. After this vapour quality value, the heat flux effect diminishes. Then, the local heat transfer coefficient increased slightly with vapour quality. However, the dryout inception in the 1.1 mm tube occurs after the vapour quality value of 0.4 and expands along the high vapour quality region. For 2.01 and 4.26 mm tubes, the local heat transfer coefficient increases with increasing heat flux for all vapour qualities and also it increases slightly with vapour quality for higher heat fluxes near the outlet of the tube.
- The behaviour of the local heat transfer coefficients of 1.1 and 2.88 mm tube is slightly dependent on the mass flux and vapour quality. This gives an indication of the contribution of nucleate boiling and convective mechanisms in the heat transfer process. On the contrary, there is insignificant effect of mass flux along 2.01 and 4.26 mm tube at low heat fluxes. It can be concluded that the nucleate boiling effects seem to dominate in all vapour qualities along tubes. For higher heat fluxes, the nucleate boiling predominates in the flow boiling heat transfer in slug flow and churn flow regions. Additionally, the nucleate boiling and the convective boiling contribute to the heat transfer in the annular flow region. In particular, the convection mechanism dominates prominently near the tube outlet.
- The local heat transfer coefficient increases as the system pressure increases. The effect of pressure on the heat transfer coefficient for all tested tubes is similar.
- The channel size has a strong influence on the enhancement of local heat transfer coefficient. The enhancement in average heat transfer coefficient is determined by 83% when the tube diameter is reduced from 4.26 to 1.1 mm. Thus, this enhancement in the use of small-sized channel is considered a further improvement in the performance and size of the heat exchanger.

- The trend of the local heat transfer coefficient of the coated tube was almost similar to that of the uncoated tube. Also, the average heat transfer coefficient was enhanced by 33% when the inner tube surface is copper coating.
- The trend of the local heat transfer coefficient of R134a was almost similar to that of R245fa with the exception of local dryout. The average heat transfer coefficient of R134a is about 106 – 151% larger than that of R245fa for the operational range studied. The dominant heat transfer mechanism is also represented by nucleate boiling for both fluids, particularly for 4.26 mm tube tested in this study.
- The comparison results between the experimental data and the selected correlations presented above demonstrated that among the selected correlations, just correlation of Fang et al. (2017) predicted all four separate subsets of the experimental data for four tubes with fair and similar accuracy.

Chapter 7

Conclusions and Future Work

The focus of this study has been on the knowledge of the fundamental principles of two-phase flow patterns, two-phase pressure drop and saturated flow boiling heat transfer coefficient in vertical small-diameter tubes under the range of operating conditions. This was accompanied with an assessment of predictive models and existing correlations were intended for flow boiling characteristics, namely flow patterns and their transition criteria, pressure drop and heat transfer coefficient. Main contributions include: (a) the verification of heat transfer mechanism (nucleate boiling and convective boiling) for R245fa as working fluid, (b) the effect of tube diameter on flow pattern regimes, two-phase pressure drop and flow boiling heat transfer coefficient in the vertical orientation, (c) the effect of surface microstructure (copper coating) on two-phase pressure drop and flow boiling heat transfer coefficient, (d) the effects of chosen working fluid and thermophysical fluid properties on flow regimes, two-phase pressure drop and flow boiling heat transfer rate in the vertical orientation and (e) notice that for this study, the saturation temperature ranged from 31.22 to 46.73 °C which has not been tested before for the R245fa as a working fluid in the small diameter tubes, such as 1.1, 2.01, 2.88 and 4.26 mm with heated length of 150, 210, 300 and 500 mm, respectively. This chapter is designed to draw conclusions of the present study and provide a few recommendations for future work in this field.

7.1 Conclusions

The conclusions of the experimental results of R245fa flow boiling heat transfer inside five small tubes with a diameter ranging from 1.1 to 4.26 mm are presented in this section. The experimental tests are conducted under the operating conditions including mass flux ranging from 200 to 500 kg/m^{2}s, heat flux ranging from 3.4 to 188.5 kw/m^2, system pressure ranging from 185 to 310 kPa, vapour quality up to the dryout incipience. The main conclusions are drawn from the findings and summarized as follows:

7.1.1 Flow pattern characteristics

The following conclusions are drawn from the discussion of the results of flow patterns and their transition boundaries:

- The flow patterns in flow boiling of R245fa, inside four vertical stainless-steel tubes with different inner diameters, were investigated under a wide range of conditions. The four observed flow regimes are identified as bubbly flow, slug flow, churn flow and annular flow. The flow boiling visualisation was recorded by a high-speed camera (frame rates of 1000 f/s and 512 × 512 pixels) with experiments of increasing and decreasing heat flux. In increasing heat flux experiments, the churn and annular flows were the only dominant patterns in all four tubes. The slug flow was often discerned at lower mass flux except for the tube of 1.1 mm, it was not observed at all. This is contrary to decreasing heat flux experiments where all flow patterns including the bubble flow were observed in all the tubes. This shows a strong impact of hysteresis.
- The flow patterns and transition boundaries for R245fa are affected by mass flux, system pressure, and tube diameter. The vapour quality corresponding to flow pattern transition boundary tends to decrease with increasing mass flux for all tubes. The system pressure corresponding to higher saturation temperature contributes to the flow pattern transitions shifting to lower superficial vapour velocities consequently higher initial vapour quality of flow regime transition. This situation is attributed to pressure influence on thermophysical properties of refrigerant. With decreasing tube diameter, the bubbly-slug transition moves to low superficial vapour velocities, while the slug-churn and churn-annular transitions shift towards high superficial vapour velocities (higher vapour qualities).
- The experimental flow pattern maps of R245fa were compared with seven predictive models developed for mini- and micro-channels in two-phase flow. The comparison results show that the qualitative agreement was found with bubbly-slug transition lines of Mahmoud and Karayiannis (2016) and Tibiriçá et al. (2017). However, the agreement between data of slug and churn flow with flow maps of Karayiannis et al. (2014) and in their applicability ranges appeared to be not satisfactory. Contrarily, the transition criterion given by Tibiriçá et al. (2017) can reproduce slug-churn transition well for all produced experimental flow maps.

What is more, the predictive churn-annular transition curve of Ong and Thome (2011a) had a similar tend to experimental transition. Also, the trend of Tibiriçá et al. (2017) transition curve was in best consistent with the churn to annular flow transition. However, this predictive transition criterion had deviation slightly towards low vapour quality with decreasing tube diameter. Generally, there is no specific flow pattern map satisfactory or able to accurately predict all the transition boundaries.

7.1.2 Pressure drop characteristics

The following conclusions are drawn from the discussion of the experimental results of measured flow boiling pressure drop for R245fa flowing in four tubes (1.1 – 4.26 mm) and the effect of key parameters on flow boiling pressure drop:

- The mass flux has a slight effect on the two-phase pressure drop in low exit vapour quality ($x_e < 0.1$) in all tube diameters. For higher exit vapour quality ($x_e > 0.1$), the influence of the mass flux on two-phase pressure drop becomes significant. Also, the measured two-phase pressure drop increases with exit vapour quality. This is due to the change in two-phase flow patterns during flow channel leading to higher flow velocity which depends on vapour quality and mass flux. The increase in mass flux results in increased frictional forces between fluid and tube wall and consequently increasing the two-phase pressure drop.
- The two-phase pressure drop increases with heat flux. This is attributed to higher vaporization in the flow channel resulting from increasing heat flux which causes an increase in the vapour quality and vapour phase velocity and thus the pressure drop.
- The two-phase pressure drop decreases significantly as the system pressure increases. This behaviour is attributed to the pressure influence on the thermodynamic properties of the fluid namely as vapour density and liquid viscosity.
- The two-phase pressure gradient increases substantially with the decrease in tube diameter. This could be because of the presence of the large velocity gradient in the thin liquid film close to channel wall and consequently high wall shear stress and high interfacial shear stress, leading to the higher two-phase pressure gradient.

- The two-phase pressure drop of the coated tube is higher than that of the uncoated tube for all mass fluxes. This is a result of the surface roughness of coated tube is about three times higher than that of the uncoated tube.
- The comparison of two different fluids shows that the measured two-phase pressure drop of R245fa is obviously higher than that of R134a. This phenomenon arises from the difference in physical properties of the two refrigerants, where the fluid has high reduced pressure causing a lower pressure drop in two-phase flow.
- The experimental data of two-phase pressure drop are compared with fifteen predictive models developed for the conventional to microchannels in two-phase flow. The comparison results show that the homogeneous flow model slightly under-predicts the data of 4.26 mm tube. However, the performance of the homogeneous flow model becomes worse with decreasing the tube diameter from 4.26 mm to 1.1 mm. For the separated flow models, the correlations of Grönnerud (1979), Friedel (1979), Müller-Steinhagen and Heck (1986), and Mishima and Hibiki (1996) show best predictions for most data of 4.26 mm tube. Further, the data of 2.01 mm and 2.88 mm tubes are underpredicted by Chisholm (1973a), Hwang and Kim (2006) and Kim and Mudawar (2013) but with higher MAE and β values for 2.01 mm tube. The data of 1.1 mm tube are not well predicted by any of the selected predictive methods. Generally, there is a deviation with decreasing tube diameter for most of the predictive methods.

7.1.3 Heat transfer characteristics

The following conclusions are drawn from the discussion of the experimental results of saturated flow boiling heat transfer coefficient for R245fa and the influence of main parameters on two-phase heat transfer coefficient:

- The boiling curve reveals that the onset of nucleate boiling appreciably occurs at lower heat fluxes in all tubes and the wall superheat of boiling incipience in the 1.1 mm tube is significantly lower than those in the rest of tubes. The heat flux after the onset of nucleate boiling increases linearly with wall superheat. The slope of boiling curve changes at higher heat fluxes because of the occurrence of local dryout, especially in the 1.1 mm and 2.01 mm tubes. Hysteresis occurs evidently at all axial locations of all tubes. Additionally, the coating has a strong influence on the onset of nucleate boiling.

- The local heat transfer coefficient of 1.1 and 2.88 mm tubes increases with increasing heat flux for vapour quality up to about 0.4. After this vapour quality value, the heat flux effect diminishes. Then, the local heat transfer coefficient increased slightly with vapour quality. However, the dryout inception in the 1.1 mm tube occurs after the vapour quality value of 0.4 and expands along the high vapour quality region. For 2.01 and 4.26 mm tubes, the local heat transfer coefficient increases with increasing heat flux for all vapour qualities and also it increases slightly with vapour quality for higher heat fluxes near the outlet of the tube.
- The behaviour of the local heat transfer coefficients of 1.1 and 2.88 mm tube is slightly dependent on the mass flux and vapour quality. This gives an indication of the contribution of nucleate boiling and convective mechanisms in the heat transfer process. On the contrary, there is insignificant effect of mass flux along 2.01 and 4.26 mm tube at low heat fluxes. It can be concluded that the nucleate boiling effects seem to dominate in all vapour qualities along tubes. For higher heat fluxes, the nucleate boiling predominates in the flow boiling heat transfer in slug flow and churn flow regions. Additionally, the nucleate boiling and the convective boiling contribute in the annular flow region. In particular, the convection mechanism dominates prominently near the tube outlet.
- The local heat transfer coefficient increases as the system pressure increases. The effect of pressure on the heat transfer coefficient for all tested tubes is similar.
- The channel size has a strong influence on the enhancement of local heat transfer coefficient. The enhancement in average heat transfer coefficient is determined by 83% when the tube diameter is reduced from 4.26 to 1.1 mm due to an increase in the confinement effect (this is enhanced the heat transfer cross liquid film to liquid-vapour interface). Thus, this enhancement during the use of small-sized channel is considered a further improvement in the performance and size of the heat exchanger. However, there is a disadvantage to the use of small-scale tubes. That is, a decrease in tube size causes an increase in the pressure drop within the cooling system. This, in turn, requires a higher pumping power, which increases cost consumption. For example, if the cooling load is equal to 50 W with using the R245fa as a working fluid at 300 kg/m^{2}s mass flux and 185 kPa system pressure. It can be seen that the 1.1 mm tube yields a higher pressure drop (34.42

kPa) while the 4.26 mm tube yields a lower pressure drop (0.227 kPa). The pumping power is a function of the fluid flow rate and the pressure drop (i.e. Power = fluid flow rate x pressure drop). The pumping power consumed for the 1.1 mm and 4.26 mm tubes is determined by 7400 µW and 742 µW, respectively. Thus, the pumping power consumed for a cooling system using the 1.1 mm tube is about ten times higher than that of a cooling system using the 4.26 mm tube. In other words, the increase in power consumption of the pump is determined by 897.3% when the tube diameter is reduced from 4.26 to 1.1 mm.

- The trend of the local heat transfer coefficient of the coated tube was almost similar to that of the uncoated tube. Also, the average heat transfer coefficient was enhanced by 33% when the inner tube surface coated with a copper coating.
- The trend of the local heat transfer coefficient of R134a was almost similar to that of R245fa with the exception of local dryout. The average heat transfer coefficient of R134a is about 106 – 151% larger than that of R245fa for the operational range studied. The dominant heat transfer mechanism is also represented by nucleate boiling for both fluids, particularly for 4.26 mm tube tested in this study.
- The comparison results between the experimental data and the selected correlations presented above demonstrated that among the selected correlations, just correlation of Fang et al. (2017) predicted all four separate subsets of the experimental data for four tubes with fair and similar accuracy.

7.2 Recommendations

According to the experimental findings in this present work, few recommendations for future work are summarized as follows:

- Due to the difference in properties of the new synthetic fluids and to attain an accurate map of two-phase flow patterns in mini/micro channels, it is recommended to extend the operational range of the experiments to include different fluids and a broad range of mass flux as well as focus on tube diameters less than 1 mm.
- Because of all pressure drop correlations in the literature are incapable to predict the two-phase pressure drop for R245fa across 1.1 mm tube, it is recommended to emphasize on a wider study of flow boiling pressure drop in mini/micro

channels, especially tube diameter less than 2 mm with different fluids to develop a new comprehensive prediction method.

- The influences of coating on flow boiling are not clear. There are many parameters in the coating enhanced heat transfer process in a microchannel, such as coating method, coating type, coated surface structure and coated surface roughness. Two-phase pressure drop and heat transfer coefficient are all seen to be different for the coated channel. Thus, a parametric study is necessary to better understand the flow boiling in the coated channel.
- Due to the difficulty of imagining the boiling flow phenomenon in metallic small-scale tubes, a transparent tube surrounded by a substance being capable of heating such as fused silica tube is recommended in order to better understand bubble nucleation, bubble growth, interface tracking and variation of liquid film thickness, as well as to prove bubble nucleation inside liquid film at annular flow region as underlying case.
- Because of the difference in properties of the new synthetic fluids and to obtain a reliable heat transfer correlation for flow boiling in mini/micro channels which involves the predictions of nucleate boiling and convective mechanisms, it is recommended to extend the operational range of the experiments to include different fluids and a broad range of the operating conditions as well as focus on tube diameters less than 1 mm. However, heat transfer correlation of flow boiling is very challenging.
- Investigation of critical heat flux in a microchannel with different fluids as a baseline case is recommended due to the difference in properties of the new synthetic fluids. This can assist to understand effects of thermophysical properties of fluid on critical heat flux.
- Investigation of experimental data reproducibility in a microchannel at different operational intervals is recommended. The repeatability of experimental data under the same conditions with different operational intervals becomes difficult to attain. This is due to the high heat fluxes affecting the surface conditions of the inner tube wall. This can contribute to realise the effect of operational intervals on the performance of cooling system with high heat fluxes.

References

Abadi, G. B., Moon, C. and Kim, K. C. (2016). Effect of Gravity Vector on Flow Boiling Heat Transfer, Flow Pattern Map, and Pressure Drop of R245fa Refrigerant in Mini Tubes. *International Journal of Multiphase Flow*, 83, Elsevier, p.202–216.

Akbar, M., Plummer, D. and Ghiaasiaan, S. (2003). Brief communication on gas-liquid two-phase flow regimes in microchannels. *International journal of multiphase flow*, 29 (5), Elsevier, p.855–865.

Akers, W., Deans, H. and Crosser, O. (1958). Condensing heat transfer within horizontal tubes. *Chem. Eng. Progr.*, 54 (10), Rice Inst., Houston, Texas; Princeton Univ. of Oklahoma, Norman, p.87–90.

Alexeyev, A., Filippov, Y. P. and Mamedov, I. (1991). Flow patterns of two-phase helium in horizontal channels. *Cryogenics*, 31 (5), Elsevier, p.330–337.

Ali, R., Palm, B. and Maqbool, M. H. (2011). Experimental investigation of two-phase pressure drop in a microchannel. *Heat Transfer Engineering*, 32 (13-14), Taylor & Francis, p.1126–1138.

Ali, R., Palm, B., Martín-Callizo, C. and Maqbool, M. H. (2013). Study of Flow Boiling Characteristics of a Microchannel Using High Speed Visualization. *Journal of heat transfer*, 135 (8), American Society of Mechanical Engineers, p.081501.

Anwar, Z., Palm, B. and Khodabandeh, R. (2015a). Flow Boiling Heat Transfer and Dryout Characteristics of R600a in a Vertical Minichannel. *Heat Transfer Engineering*, 36 (14-15), Taylor & Francis, p.1230–1240.

Anwar, Z., Palm, B. and Khodabandeh, R. (2015b). Flow boiling heat transfer, pressure drop and dryout characteristics of R1234yf: experimental results and predictions. *Experimental Thermal and fluid Science*, 66, Elsevier, p.137–149.

Arcanjo, A. A., Tibiriçá, C. B. and Ribatski, G. (2010). Evaluation of flow patterns and elongated bubble characteristics during the flow boiling of halocarbon refrigerants in a micro-scale channel. *Experimental Thermal and Fluid Science*, 34 (6), Elsevier, p.766–775.

Barnea, D., Luninski, Y. and Taitel, Y. (1983). Flow pattern in horizontal and vertical two phase flow in small diameter pipes. *The Canadian Journal of Chemical Engineering*, 61 (5), Wiley Online Library, p.617–620.

Beattie, D. and Whalley, P. (1982). A simple two-phase frictional pressure drop calculation method. *International Journal of Multiphase Flow*, 8 (1), Elsevier, p.83–87.

Bergman, T. L., Lavine, A. S., Incropera, F. P. and DeWitt, D. P. (2011). *Fundamentals of heat and mass transfer*. John Wiley & Sons.

Bertsch, S. S., Groll, E. A. and Garimella, S. V. (2009). A composite heat transfer correlation for saturated flow boiling in small channels. *International Journal of Heat and Mass Transfer*, 52 (7), Elsevier, p.2110–2118.

Blasius, H. (1913). Das Ähnlichkeitsgesetz bei Reibungsvorgängen in Flüssigkeiten. *Mitteilungen über Forschungsarbeiten auf dem Gebiete des Ingenieurwesens*, Springer Berlin Heidelberg, p.131.

Boucher, O. (2010). Stratospheric ozone, ultraviolet radiation and climate change. *Weather*, 65 (4), Wiley Online Library, p.105–110.

Brauner, N. and Maron, D. M. (1992). Identification of the range of "small diameters" conduits, regarding two-phase flow pattern transitions. *International Communications in Heat and Mass Transfer*, 19 (1), Elsevier, p.29–39.

Charnay, R., Bonjour, J. and Revellin, R. (2014a). Experimental investigation of R-245fa flow boiling in minichannels at high saturation temperatures: flow patterns and flow pattern maps. *International Journal of Heat and Fluid Flow*, 46, Elsevier, p.1–16.

Charnay, R., Revellin, R. and Bonjour, J. (2013). Flow pattern characterization for R-245fa in minichannels: optical measurement technique and experimental results. *International Journal of Multiphase Flow*, 57, Elsevier, p.169–181.

Charnay, R., Revellin, R. and Bonjour, J. (2014b). Flow boiling characteristics of R-245fa in a minichannel at medium saturation temperatures. *Experimental Thermal and Fluid Science*, 59, Elsevier, p.184–194.

Charnay, R., Revellin, R. and Bonjour, J. (2015a). Discussion on the validity of prediction tools for two-phase flow pressure drops from experimental data obtained at high saturation temperatures. *International Journal of Refrigeration*, 54, Elsevier, p.98–125.

Charnay, R., Revellin, R. and Bonjour, J. (2015b). Flow boiling heat transfer in minichannels at high saturation temperatures: Part I-Experimental investigation and analysis of the heat transfer mechanisms. *International Journal of Heat and Mass Transfer*, 87, Elsevier, p.636–652.

Chen, J. C. (1966). Correlation for boiling heat transfer to saturated fluids in convective flow. *Industrial & engineering chemistry process design and development*, 5 (3), ACS Publications, p.322–329.

Chen, L. (2006). *Flow patterns in upward two-phase flow in small diameter tubes, PhD thesis, Brunel University London, UK*.

Chen, L., Tian, Y. S. and Karayiannis, T. G. (2005). R134a flow patterns in small-diameter tubes. *Proceedings of the Institution of Mechanical Engineers, Part E: Journal of Process Mechanical Engineering*, 219 (2), SAGE Publications, p.167–181.

Chen, L., Tian, Y. S. and Karayiannis, T. G. (2006). The effect of tube diameter on vertical two-phase flow regimes in small tubes. *International Journal of Heat and Mass*

Transfer, 49 (21), Elsevier, p.4220–4230.

Chen, W., Twu, M. and Pan, C. (2002). Gas-liquid two-phase flow in micro-channels. *International Journal of Multiphase Flow*, 28 (7), Pergamon, p.1235–1247.

Chen, X., Chen, S., Chen, J., Li, J., Liu, X., Chen, L. and Hou, Y. (2017). Two-phase flow boiling frictional pressure drop of liquid nitrogen in horizontal circular mini-tubes: Experimental investigation and comparison with correlations. *Cryogenics*, 83, Elsevier, p.85–94.

Cheng, L., Ribatski, G., Quibén, J. M. and Thome, J. R. (2008a). New prediction methods for CO 2 evaporation inside tubes: Part I-A two-phase flow pattern map and a flow pattern based phenomenological model for two-phase flow frictional pressure drops. *International Journal of Heat and Mass Transfer*, 51 (1), Elsevier, p.111–124.

Cheng, L., Ribatski, G. and Thome, J. R. (2008b). Two-phase flow patterns and flow-pattern maps: fundamentals and applications. *Applied Mechanics Reviews*, 61 (5), American Society of Mechanical Engineers, p.050802.

Cheng, L., Ribatski, G., Wojtan, L. and Thome, J. R. (2006). New flow boiling heat transfer model and flow pattern map for carbon dioxide evaporating inside horizontal tubes. *International journal of heat and mass transfer*, 49 (21), Elsevier, p.4082–4094.

Cheng, P. and Wu, H. (2006). Mesoscale and microscale phase-change heat transfer. *Advances in heat transfer*, 39, Elsevier, p.461–563.

Chisholm, D. (1967). A theoretical basis for the Lockhart-Martinelli correlation for two-phase flow. *International Journal of Heat and Mass Transfer*, 10 (12), Elsevier, p.1767–1778.

Chisholm, D. (1973a). Pressure gradients due to friction during the flow of evaporating two-phase mixtures in smooth tubes and channels. *International Journal of Heat and Mass Transfer*, 16 (2), Elsevier, p.347–358.

Chisholm, D. (1973b). Void fraction during two-phase flow. *Journal of Mechanical Engineering Science*, 15 (3), SAGE Publications Sage UK: London, England, p.235–236.

Choi, K. I., Chien, N. B. and Oh, J. T. (2013). Heat Transfer Coefficient during Evaporation of R-1234yf, R-134a, and R-22 in Horizontal Circular Small Tubes. *Advances in Mechanical Engineering*, SAGE PublicationsSage UK: London, England.

Choi, K. I., Pamitran, A. S., Oh, J. T. and Saito, K. (2009). Pressure drop and heat transfer during two-phase flow vaporization of propane in horizontal smooth minichannels. *International Journal of Refrigeration*, 32 (5), Elsevier, p.837–845.

Choi, K.-I., Oh, J.-T., Saito, K. and Jeong, J. S. (2014). Comparison of heat transfer coefficient during evaporation of natural refrigerants and R-1234yf in horizontal small tube. *International Journal of Refrigeration*, 41, Elsevier, p.210–218.

Choi, K.-I., Pamitran, A., Oh, C.-Y. and Oh, J.-T. (2007). Boiling heat transfer of R-22, R-134a, and CO 2 in horizontal smooth minichannels. *International Journal of Refrigeration*, 30 (8), Elsevier, p.1336–1346.

Choi, S. B., Barron, R. F. and Warrington, R. O. (1991). Fluid flow and heat transfer in microtubes. In: *ASME DSC*, 32, 1991, p.123–134.

Chung, P.-Y. and Kawaji, M. (2004). The effect of channel diameter on adiabatic two-phase flow characteristics in microchannels. *International Journal of Multiphase Flow*, 30 (7), Elsevier, p.735–761.

Cicchitti, A., Lombardi, C., Silvestri, M., Soldaini, G. and Zavattarelli, R. (1960). Two-phase cooling experiments: pressure drop, heat transfer and burnout measurements. *Energia Nucleare*, 7 (6), p.407–425.

Del Col, D., Bisetto, A., Bortolato, M., Torresin, D. and Rossetto, L. (2013a). Experiments and updated model for two phase frictional pressure drop inside minichannels. *International journal of heat and mass transfer*, 67, Elsevier, p.326–337.

Del Col, D., Bortolin, S., Torresin, D. and Cavallini, A. (2013b). Flow boiling of R1234yf in a 1 mm diameter channel. *International journal of refrigeration*, 36 (2), Elsevier, p.353–362.

Coleman, H. W. and Steele, W. G. (2009). *Experimentation, validation, and uncertainty analysis for engineers*. third. John Wiley & Sons.

Coleman, J. W. and Garimella, S. (1999). Characterization of two-phase flow patterns in small diameter round and rectangular tubes. *International Journal of Heat and Mass Transfer*, 42 (15), Elsevier, p.2869–2881.

Collier, J. G. and Thome, J. R. (1994). *Convective boiling and condensation*. third. Clarendon Press, Oxford.

Consolini, L. and Thome, J. R. (2009). Micro-channel flow boiling heat transfer of R-134a, R-236fa, and R-245fa. *Microfluidics and nanofluidics*, 6 (6), Springer, p.731–746.

Cooper, M. (1984). Saturation nucleate pool boiling – a simple correlation. In: *Inst. Chem. Eng. Symp. Ser*, 86 (2), 1984, p.785–793.

Copetti, J. B., Macagnan, M. H. and Zinani, F. (2013). Experimental study on R-600a boiling in 2.6 mm tube. *international journal of refrigeration*, 36 (2), Elsevier, p.325–334.

Cornwell, K. and Brown, R. (1978). Boiling surface topography. In: *Proceedings of 6th international heat transfer conference*, 1, 1978, p.157–161.

Costa-Patry, E., Olivier, J., Michel, B. and Thome, J. R. (2011). Two-phase flow of refrigerants in 85 μm-wide multi-microchannels: Part II-Heat transfer with 35 local heaters. *International Journal of Heat and Fluid Flow*, 32 (2), Elsevier, p.464–476.

Costa-Patry, E., Olivier, J. and Thome, J. (2012). Heat transfer characteristics in a copper micro-evaporator and flow pattern-based prediction method for flow boiling in microchannels. *Frontiers in Heat and Mass Transfer (FHMT)*, 3 (1), p.3002.

Costa-Patry, E. and Thome, J. R. (2013). Flow pattern-based flow boiling heat transfer model for microchannels. *International Journal of Refrigeration*, 36 (2), Elsevier, p.414–420.

Ding, Y., Kakac, S. and Chen, X. (1995). Dynamic instabilities of boiling two-phase flow in a single horizontal channel. *Experimental Thermal and Fluid Science*, 11 (4), Elsevier, p.327–342.

Dittus, F. W. and Boelter, L. M. K. (1930). Heat transfer in automobile radiators of the tubular type. *the University of California Publications in Engineering*, 2 (13), p.443–461.

Dukler, A., Wicks, M. and Cleveland, R. (1964). Frictional pressure drop in two-phase flow: B. An approach through similarity analysis. *AIChE Journal*, 10 (1), Wiley Online Library, p.44–51.

English, N. J. and Kandlikar, S. G. (2006). An experimental investigation into the effect of surfactants on air-water two-phase flow in minichannels. *Heat transfer engineering*, 27 (4), Taylor & Francis, p.99–109.

Fan, Y. and Hassan, I. (2012). Experimental investigation of flow boiling instability in a single horizontal microtube with and without inlet restriction. *Journal of Heat Transfer*, 134 (8), American Society of Mechanical Engineers, p.081501.

Fang, X., Wu, Q. and Yuan, Y. (2017). A general correlation for saturated flow boiling heat transfer in channels of various sizes and flow directions. *International Journal of Heat and Mass Transfer*, 107, Elsevier, p.972–981.

Fang, X., Zhou, Z. and Wang, H. (2015). Heat transfer correlation for saturated flow boiling of water. *Applied Thermal Engineering*, 76, Elsevier, p.147–156.

Faulkner, D., Khotan, M. and Shekarriz, R. (2003). Practical design of a 1000 W/cm^2 cooling system. In: *Semiconductor Thermal Measurement and Management Symposium, 2003. Nineteenth Annual IEEE*, 2003, p.223–230.

Forster, H. K. and Zuber, N. (1955). Dynamics of vapor bubbles and boiling heat transfer. *AIChE Journal*, 1 (4), Wiley Online Library, p.531–535.

Fourar, M. and Bories, S. (1995). Experimental study of air-water two-phase flow through a fracture (narrow channel). *International journal of multiphase flow*, 21 (4), Elsevier, p.621–637.

Friedel, L. (1979). Improved friction pressure drop correlations for horizontal and vertical two-phase pipe flow. In: *European two-phase flow group meeting, Paper E*, 2, 1979, p.1979.

Fukano, T. and Kariyasaki, A. (1993). Characteristics of gas-liquid two-phase flow in a capillary tube. *Nuclear Engineering and Design*, 141 (1-2), Elsevier, p.59–68.

Furukawa, T. and Fukano, T. (2001). Effects of liquid viscosity on flow patterns in vertical upward gas-liquid two-phase flow. *International journal of multiphase flow*, 27 (6), Elsevier, p.1109–1126.

Gaertner, R. F. and Westwater, J. (1960). Population of active sites in nucleate boiling heat transfer. *Chemical Engineering Progress*, 56, General Electric Co., Schenectady, NY.

Al-Gaheeshi, A., Mahmoud, M. M. M. and Karayiannis, T. G. (2016). *Flow boiling heat transfer in a vertical small-diameter tube: effect of different fluids and surface characteristics*. Sendai, Japan: Proceedings of the 4th International Forum on Heat Transfer, IFHT2016.

Garimella, S., Killion, J. and Coleman, J. (2002). An experimentally validated model for two-phase pressure drop in the intermittent flow regime for circular microchannels. *Journal of Fluids Engineering*, 124 (1), American Society of Mechanical Engineers, p.205–214.

Gorenflo, D. (1993). Pool Boiling. In: *VDI-Heat Atlas*, VDI-Verlag, Dusseldorf.

Grauso, S., Mastrullo, R., Mauro, A. W., Thome, J. R. and Vanoli, G. P. (2013). Flow pattern map, heat transfer and pressure drops during evaporation of R-1234ze (E) and R134a in a horizontal, circular smooth tube: Experiments and assessment of predictive methods. *international journal of refrigeration*, 36 (2), Elsevier, p.478–491.

Grönnerud, R. (1979). Investigation of liquid hold-up, flow-resistance and heat transfer in circulation type of evaporators, part IV: two-phase flow resistance in boiling refrigerants. *Annexe 1-1972, Bulletin, de l'Institut du Froid*, p.248.

Gungor, K. and Winterton, R. (1986). A general correlation for flow boiling in tubes and annuli. *International Journal of Heat and Mass Transfer*, 29 (3), Elsevier, p.351–358.

Haaland, S. E. (1983). Simple and explicit formulas for the friction factor in turbulent pipe flow. *Journal of Fluids Engineering*, 105 (1), American Society of Mechanical Engineers, p.89–90.

Hand, E. (2015). Ozone pollution becoming a global, rather than local, problem. *Science, doi:10.1126/science.aad1598*. [Online]. Available at: doi:doi:10.1126/science.aad1598.

Hardik, B. K. and Prabhu, S. V. (2016). Boiling pressure drop and local heat transfer distribution of water in horizontal straight tubes at low pressure. *International Journal of Thermal Sciences*, 110, Elsevier, p.65–82.

Harirchian, T. and Garimella, S. V. (2010). A comprehensive flow regime map for microchannel flow boiling with quantitative transition criteria. *International Journal of*

Heat and Mass Transfer, 53 (13), Elsevier, p.2694–2702.

Hassan, I., Vaillancourt, M. and Pehlivan, K. (2005). Two-phase flow regime transitions in microchannels: a comparative experimental study. *Microscale Thermophysical Engineering*, 9 (2), Taylor & Francis, p.165–182.

Hewitt, G. F. and Hall-Taylor, N. S. (1970). *Annular two-phase flow*. Pergamon press.

Hewitt, G. F. and Roberts, D. (1969). *Studies of two-phase flow patterns by simultaneous X-ray and flash photography, Atomic Energy Research Establishment Harwell (United Kingdom)*.

Huang, H. and Thome, J. R. (2017). An experimental study on flow boiling pressure drop in multi-microchannel evaporators with different refrigerants. *Experimental Thermal and Fluid Science*, 80, Elsevier, p.391–407.

Huo, X. (2005). *Experimental study of flow boiling heat transfer in small diameter tubes, PhD thesis, London South Bank University, UK*.

Huo, X., Chen, L., Tian, Y. and Karayiannis, T. (2004). Flow boiling and flow regimes in small diameter tubes. *Applied Thermal Engineering*, 24 (8), Elsevier, p.1225–1239.

Huo, X., Shiferaw, D., Karayiannis, T., Tian, Y. S. and Kenning, D. B. R. (2007). Boiling two-phase pressure drop in small diameter tubes. In: *Sixth International Conference on: Enhanced, Compact and Ultra-Compact Heat Exchangers: Science, Engineering and Technology*, 2007.

Hwang, Y. W. and Kim, M. S. (2006). The pressure drop in microtubes and the correlation development. *International Journal of Heat and Mass Transfer*, 49 (11), Elsevier, p.1804–1812.

Ide, H., Kariyasaki, A. and Fukano, T. (2007). Fundamental data on the gas-liquid two-phase flow in minichannels. *International Journal of Thermal Sciences*, 46 (6), Elsevier, p.519–530.

Ishii, M. (1977). *One-dimensional drift-flux model and constitutive equations for relative motion between phases in various two-phase flow regimes, ANL-77-47, USA*.

Jacobi, A. M. and Thome, J. R. (2002). Heat transfer model for evaporation of elongated bubble flows in microchannels. *Journal of Heat Transfer*, 124 (6), American society mechanical engineers, p.1131–1136.

Jang, Y., Park, C., Lee, Y. and Kim, Y. (2008). Flow boiling heat transfer coefficients and pressure drops of FC-72 in small channel heat sinks. *international journal of refrigeration*, 31 (6), Elsevier, p.1033–1041.

Kalani, A. (2016). *Flow Boiling Heat Transfer over Open Microchannels with Tapered Manifold, Rochester Institute of Technology, Rochester, New York*.

Kandlikar, S. G. (1990). A general correlation for saturated two-phase flow boiling heat transfer inside horizontal and vertical tubes. *Journal of heat transfer*, 112 (1), American Society of Mechanical Engineers, p.219–228.

Kandlikar, S. G. (2002). Fundamental issues related to flow boiling in minichannels and microchannels. *Experimental Thermal and Fluid Science*, 26 (2), Elsevier, p.389–407.

Kandlikar, S. G. (2010). Scale effects on flow boiling heat transfer in microchannels: a fundamental perspective. *International Journal of Thermal Sciences*, 49 (7), Elsevier, p.1073–1085.

Kandlikar, S. G. and Balasubramanian, P. (2004). Effect of Gravitational Orientation on Flow Boiling of Water in 1054 x 197 µm Parallel Minichannels. In: *ASME 2004 2nd International Conference on Microchannels and Minichannels*, 2004, p.539–550.

Kandlikar, S. G. and Grande, W. J. (2003). Evolution of Microchannel Flow Passages-Thermohydraulic Performance and Fabrication Technology. *Heat transfer engineering*, 24 (1), Taylor & Francis, p.3–17.

Kandlikar, S. and Thakur, B. (1982). A new correlation for heat transfer during flow boiling. In: *Proceedings, 16th Southeastern Seminar on Thermal Sciences*, 1982.

Kanizawa, F. T., Tibiriçá, C. B. and Ribatski, G. (2016). Heat transfer during convective boiling inside microchannels. *International Journal of Heat and Mass Transfer*, 93, Elsevier, p.566–583.

Karayiannis, T. G. and Mahmoud, M. M. (2017). Flow boiling in microchannels: Fundamentals and applications. *Applied Thermal Engineering*, 115, Elsevier, p.1372–1397.

Karayiannis, T. G., Pike-Wilson, E. A., Chen, L., Mahmoud, M. M. and Tian, Y. (2014). Flow Patterns and Comparison with Correlations for Vertical Flow Boiling of R245fa in Small to Micro Tubes. In: *4th Micro and Nano Flows Conference UCL, London, UK, 7-10 September 2014*, 2014, Brunel University London.

Kattan, N., Thome, J. and Favrat, D. (1998). Flow boiling in horizontal tubes: Part 1 – Development of a diabatic two-phase flow pattern map. *Journal of Heat Transfer*, 120 (1), American Society of Mechanical Engineers, p.140–147.

Kays, W. M. and Crawford, M. E. (1993). *Convective Heat and Mass Transfert*. third. McGraw-Hill.

Kew, P. A. and Cornwell, K. (1997). Correlations for the prediction of boiling heat transfer in small-diameter channels. *Applied Thermal Engineering*, 17 (8-10), Elsevier, p.705–715.

Kim, S. M. and Mudawar, I. (2013). Universal approach to predicting two-phase frictional pressure drop for mini/micro-channel saturated flow boiling. *International Journal of Heat and Mass Transfer*, 58 (1), Elsevier, p.718–734.

Kim, S.-M. and Mudawar, I. (2012). Universal approach to predicting two-phase frictional pressure drop for adiabatic and condensing mini/micro-channel flows. *International Journal of Heat and Mass Transfer*, 55 (11), Elsevier, p.3246–3261.

Kutateladze, S. S. (1961). Boiling heat transfer. *International Journal of Heat and Mass Transfer*, 4, Elsevier, p.31–45.

Langhaar, H. L. (1942). Steady flow in the transition length of a straight tube. *J. appl. Mech*, 9 (2), p.55–58.

Lazarek, G. and Black, S. (1982). Evaporative heat transfer, pressure drop and critical heat flux in a small vertical tube with R-113. *International Journal of Heat and Mass Transfer*, 25 (7), Elsevier, p.945–960.

Lee, H. J., Liu, D. Y., Alyousef, Y. and Yao, S. (2010). Generalized two-phase pressure drop and heat transfer correlations in evaporative micro/minichannels. *Journal of Heat Transfer*, 132 (4), American Society of Mechanical Engineers, p.041004.

Li, W. and Wu, Z. (2010a). A general correlation for adiabatic two-phase pressure drop in micro/mini-channels. *International Journal of Heat and Mass Transfer*, 53 (13), Elsevier, p.2732–2739.

Li, W. and Wu, Z. (2010b). A general correlation for evaporative heat transfer in micro/mini-channels. *International Journal of Heat and Mass Transfer*, 53 (9), Elsevier, p.1778–1787.

Lim, T.-W., You, S.-S., Choi, J.-H. and Kim, H.-S. (2015). Experimental Investigation of Heat Transfer in Two-phase Flow Boiling. *Experimental Heat Transfer*, 28 (1), Taylor & Francis, p.23–36.

Lin, S., Kwok, C., Li, R.-Y., Chen, Z.-H. and Chen, Z.-Y. (1991). Local frictional pressure drop during vaporization of R-12 through capillary tubes. *International Journal of Multiphase Flow*, 17 (1), Elsevier, p.95–102.

Linlin, J., Jianhua, L., Liang, Z., Qi, L. and Xiaojin, X. (2017). Characteristics of heat transfer for CO2 flow boiling at low temperature in mini-channel. *International Journal of Heat and Mass Transfer*, 108, Elsevier, p.2120–2129.

Liu, D. and Wang, S. (2008). Flow pattern and pressure drop of upward two-phase flow in vertical capillaries. *Industrial & Engineering Chemistry Research*, 47 (1), ACS Publications, p.243–255.

Lockhart, R. and Martinelli, R. (1949). Proposed correlation of data for isothermal two-phase, two-component flow in pipes. *Chemical Engineering Progress*, 45 (1), p.39–48.

Longo, G. A., Mancin, S., Righetti, G. and Zilio, C. (2016a). HFC32 and HFC410A flow boiling inside a 4 mm horizontal smooth tube. *International Journal of Refrigeration*, 61, Elsevier, p.12–22.

Longo, G. A., Mancin, S., Righetti, G. and Zilio, C. (2016b). Saturated flow boiling of HFC134a and its low GWP substitute HFO1234ze(E) inside a 4mm horizontal smooth tube. *International Journal of Refrigeration*, 64, Elsevier, p.32–39.

Mahmoud, M. and Karayiannis, T. (2012). A statistical correlation for flow boiling heat transfer in micro tubes. In: *Proceedings of the 3rd European Conference on Microfluidics-Microfluidics*, 2012, Heidelberg, Germany, .

Mahmoud, M. M. and Karayiannis, T. G. (2013). Heat transfer correlation for flow boiling in small to micro tubes. *International Journal of Heat and Mass Transfer*, 66, Elsevier, p.553–574.

Mahmoud, M. M. and Karayiannis, T. G. (2016). Flow pattern transition models and correlations for flow boiling in mini-tubes. *Experimental Thermal and Fluid Science*, 70, Elsevier, p.270–282.

Mahmoud, M. M., Karayiannis, T. G. and Kenning, D. B. (2014a). Flow Boiling Pressure Drop of R134a in Microdiameter Tubes: Experimental Results and Assessment of Correlations. *Heat Transfer Engineering*, 35 (2), Taylor & Francis, p.178–192.

Mahmoud, M. M., Karayiannis, T. G. and Kenning, D. B. R. (2014b). Flow Boiling in Small to Microdiameter Tubes. In: *Emerging Topics in Heat Transfer: Enhancement and Heat Exchangers*, 24, WIT Press, p.321.

Mahmoud, M. M. M. (2011). *Flow boiling of R134a in vertical mini-diameter tubes, PhD thesis, Brunel University London, UK*.

Maqbool, M. H., Palm, B. and Khodabandeh, R. (2012a). Boiling heat transfer of ammonia in vertical smooth mini channels: Experimental results and predictions. *International Journal of thermal sciences*, 54, Elsevier, p.13–21.

Maqbool, M. H., Palm, B. and Khodabandeh, R. (2012b). Flow boiling of ammonia in vertical small diameter tubes: two phase frictional pressure drop results and assessment of prediction methods. *International journal of thermal sciences*, 54, Elsevier, p.1–12.

Maqbool, M. H., Palm, B. and Khodabandeh, R. (2013). Investigation of two phase heat transfer and pressure drop of propane in a vertical circular minichannel. *Experimental Thermal and Fluid Science*, 46, Elsevier, p.120–130.

Martín-Callizo, C., Palm, B., Owhaib, W. and Ali, R. (2010). Flow boiling visualization of R-134a in a vertical channel of small diameter. *Journal of Heat Transfer*, 132 (3), American Society of Mechanical Engineers, p.031503.

Mauro, A., Thome, J., Toto, D. and Vanoli, G. (2010). Saturated critical heat flux in a multi-microchannel heat sink fed by a split flow system. *Experimental Thermal and Fluid Science*, 34 (1), Elsevier, p.81–92.

McAdams, W. H., W.K., W. and L.C., H. (1942). Vaporization inside horizontal tubes-II Benzene-oil mixtures. *ASME Transaction*, 64, p.193–200.

McQuillan, K. and Whalley, P. (1985). Flow patterns in vertical two-phase flow. *International Journal of Multiphase Flow*, 11 (2), Elsevier, p.161–175.

McWilliams, A. (2016). The market for thermal management technologies. *Business Communications Company, GB-SMC024K*.

Mehendale, S., Jacobi, A. and Shah, R. (2000). Fluid flow and heat transfer at micro- and meso-scales with application to heat exchanger design. *Applied Mechanics Reviews*, 53 (7), American Society of Mechanical Engineers, p.175–193.

Mehta, H. B. and Banerjee, J. (2014). An investigation of flow orientation on air-water two-phase flow in circular minichannel. *Heat and Mass Transfer*, 50 (10), Springer, p.1353–1364.

Mishima, K. and Hibiki, T. (1996). Some characteristics of air-water two-phase flow in small diameter vertical tubes. *International Journal of Multiphase Flow*, 22 (4), Elsevier, p.703–712.

Mishima, K. and Ishii, M. (1984). Flow regime transition criteria for upward two-phase flow in vertical tubes. *International Journal of Heat and Mass Transfer*, 27 (5), Elsevier, p.723–737.

Moffat, R. J. (1988). Describing the uncertainties in experimental results. *Experimental thermal and fluid science*, 1 (1), Elsevier, p.3–17.

Mohseni, S. and Akhavan-Behabadi, M. (2014). Flow pattern visualization and heat transfer characteristics of R-134a during evaporation inside a smooth tube with different tube inclinations. *International Communications in Heat and Mass Transfer*, 59, Elsevier, p.39–45.

Müller-Steinhagen, H. and Heck, K. (1986). A simple friction pressure drop correlation for two-phase flow in pipes. *Chemical Engineering and Processing*, 20 (6), Elsevier, p.297–308.

De Oliveira, J. D., Copetti, J. B. and Passos, J. C. (2016). An experimental investigation on flow boiling heat transfer of R-600a in a horizontal small tube. *International Journal of Refrigeration*, 72, Elsevier, p.97–110.

Ong, C. L. and Thome, J. R. (2009). Flow boiling heat transfer of R134a, R236fa and R245fa in a horizontal 1.030 mm circular channel. *Experimental Thermal and Fluid Science*, 33 (4), Elsevier, p.651–663.

Ong, C. L. and Thome, J. R. (2011a). Macro-to-microchannel transition in two-phase flow: Part 1-Two-phase flow patterns and film thickness measurements. *Experimental Thermal and Fluid Science*, 1 (35), p.37–47.

Ong, C. L. and Thome, J. R. (2011b). Macro-to-microchannel transition in two-phase flow: Part 2-Flow boiling heat transfer and critical heat flux. *Experimental thermal and fluid science*, 35 (6), Elsevier, p.873–886.

Owhaib, W., Martín-Callizo, C. and Palm, B. (2008). Two-phase flow pressure drop of R-134A in a vertical circular mini/micro channel. In: *ASME 2008 6th International Conference on Nanochannels, Microchannels, and Minichannels*, 2008, p.343–353.

Owhaib, W., Palm, B. and Martín-Callizo, C. (2007). A visualization study of bubble behavior in saturated flow boiling through a vertical mini-tube. *Heat Transfer Engineering*, 28 (10), Taylor & Francis, p.852–860.

Pamitran, A., Choi, K.-I., Oh, J.-T. and Hrnjak, P. (2010). Characteristics of two-phase flow pattern transitions and pressure drop of five refrigerants in horizontal circular small tubes. *International Journal of Refrigeration*, 33 (3), Elsevier, p.578–588.

Pehlivan, K., Hassan, I. and Vaillancourt, M. (2006). Experimental study on two-phase flow and pressure drop in millimeter-size channels. *Applied Thermal Engineering*, 26 (14), Elsevier, p.1506–1514.

Petukhov, B. S. (1970). Heat transfer and friction in turbulent pipe flow with variable physical properties. *Advances in heat transfer*, 6, Academic Press New York, p.503–565.

Pike-Wilson, E. A. (2014). *Flow boiling of R245fa in vertical small metallic tubes, PhD thesis, Brunel University London, UK*.

Pike-Wilson, E. A. and Karayiannis, T. G. (2014). Flow boiling of R245fa in 1.1 mm diameter stainless steel, brass and copper tubes. *Experimental Thermal and Fluid Science*, 59, Elsevier, p.166–183.

Qu, W. and Mudawar, I. (2003). Measurement and prediction of pressure drop in two-phase micro-channel heat sinks. *International Journal of Heat and Mass Transfer*, 46 (15), Elsevier, p.2737–2753.

Quibén, J. M., Cheng, L., da Silva Lima, R. J. and Thome, J. R. (2009). Flow boiling in horizontal flattened tubes: Part I-Two-phase frictional pressure drop results and model. *International Journal of Heat and Mass Transfer*, 52 (15-16), Elsevier, p.3634–3644.

Quibén, J. M. and Thome, J. R. (2007). Flow pattern based two-phase frictional pressure drop model for horizontal tubes. Part I: Diabatic and adiabatic experimental study. *International Journal of Heat and Fluid Flow*, 28 (5), Elsevier, p.1049–1059.

Revellin, R. and Thome, J. R. (2007a). A new type of diabatic flow pattern map for boiling heat transfer in microchannels. *Journal of Micromechanics and Microengineering*, 17 (4), IOP Publishing, p.788–796.

Revellin, R. and Thome, J. R. (2007b). Adiabatic two-phase frictional pressure drops in microchannels. *Experimental Thermal and Fluid Science*, 31 (7), Elsevier, p.673–685.

Rosa, P., Karayiannis, T. and Collins, M. (2009). Single-phase heat transfer in microchannels: the importance of scaling effects. *Applied Thermal Engineering*, 29 (17), Elsevier, p.3447–3468.

Rouhani, S. Z. and Axelsson, E. (1970). Calculation of void volume fraction in the subcooled and quality boiling regions. *International Journal of Heat and Mass Transfer*, 13 (2), Elsevier, p.383–393.

Ruspini, L. C., Marcel, C. P. and Clausse, A. (2014). Two-phase flow instabilities: A review. *International Journal of Heat and Mass Transfer*, 71, Elsevier, p.521–548.

Saisorn, S., Kaew-On, J. and Wongwises, S. (2013). An experimental investigation of flow boiling heat transfer of R-134a in horizontal and vertical mini-channels. *Experimental Thermal and Fluid Science*, 46, Elsevier, p.232–244.

Saisorn, S., Wongpromma, P. and Wongwises, S. (2018). The difference in flow pattern, heat transfer and pressure drop characteristics of mini-channel flow boiling in horizontal and vertical orientations. *International Journal of Multiphase Flow*, Elsevier.

Saitoh, S., Daiguji, H. and Hihara, E. (2007). Correlation for boiling heat transfer of R-134a in horizontal tubes including effect of tube diameter. *International Journal of Heat and Mass Transfer*, 50 (25), Elsevier, p.5215–5225.

Saitoh, S., Dang, C., Nakamura, Y. and Hihara, E. (2011). Boiling heat transfer of HFO-1234yf flowing in a smooth small-diameter horizontal tube. *International Journal of Refrigeration*, 34 (8), Elsevier, p.1846–1853.

Saljoshi, P. and Autee, A. (2017). Experimental investigation of two-phase flow patterns in minichannels at horizontal orientation. *Heat and Mass Transfer*, Springer, p.1–13.

Sempértegui-Tapia, D. F. and Ribatski, G. (2017a). Flow boiling heat transfer of R134a and low GWP refrigerants in a horizontal micro-scale channel. *International Journal of Heat and Mass Transfer*, 108, p.2417–2432.

Sempértegui-Tapia, D. F. and Ribatski, G. (2017b). Two-phase frictional pressure drop in horizontal micro-scale channels: experimental data analysis and prediction method development. *International Journal of Refrigeration*, 79, Elsevier, p.143–163.

Sempértegui-Tapia, D., De Oliveira Alves, J. and Ribatski, G. (2013). Two-phase flow characteristics during convective boiling of halocarbon refrigerants inside horizontal small-diameter tubes. *Heat Transfer Engineering*, 34 (13), Taylor & Francis, p.1073–1087.

Shah, M. (1982). Chart correlation for saturated boiling heat transfer: equations and further study. *ASHRAE Translations*, 88 (1), p.185–196.

Shah, M. M. (2017). Unified correlation for heat transfer during boiling in plain mini/micro and conventional channels. *International Journal of Refrigeration*, 74, Elsevier, p.604–624.

Shah, R. K. (1986). Classification of heat exchangers. In: Kakac, S. and Bergles, A. E. and Mayinger, F. (ed.), *Heat Exchangers: Thermal Hydraulic Fundamentals and*

Design, Hemisphere Publishing Corp., Washington, DC, p.9–46.

Shah, R. K. and London, A. L. (1978). *Laminar flow forced convection in ducts: a source book for compact heat exchanger analytical data*. Irvine Jr, TF and Hartnett, JP (ed.). Academic press.

Shiferaw, D. (2008). *Two-phase flow boiling in small to micro-diameter tubes, PhD thesis, Brunel University London, UK*.

Shiferaw, D., Mahmoud, M., Karayiannis, T. G. and Kenning, D. B. (2011). One-dimensional semimechanistic model for flow boiling pressure drop in small to micro passages. *Heat Transfer Engineering*, 32 (13-14), Taylor & Francis, p.1150–1159.

Shin, J. Y., Kim, M. S. and Ro, S. T. (1997). Experimental study on forced convective boiling heat transfer of pure refrigerants and refrigerant mixtures in a horizontal tube. *International Journal of Refrigeration*, 20 (4), Elsevier, p.267–275.

Stephan, K. and Abdelsalam, M. (1980). Heat-transfer correlations for natural convection boiling. *International Journal of Heat and Mass Transfer*, 23 (1), Elsevier, p.73–87.

Sun, L. and Mishima, K. (2009). Evaluation analysis of prediction methods for two-phase flow pressure drop in mini-channels. *International Journal of Multiphase Flow*, 35 (1), Elsevier, p.47–54.

Suo, M. and Griffith, P. (1964). Two-phase flow in capillary tubes. *Journal of Basic Engineering*, 86 (3), American Society of Mechanical Engineers, p.576–582.

Taitel, Y., Bornea, D. and Dukler, A. (1980). Modelling flow pattern transitions for steady upward gas-liquid flow in vertical tubes. *AIChE Journal*, 26 (3), Wiley Online Library, p.345–354.

Taitel, Y. and Dukler, A. (1976). A model for predicting flow regime transitions in horizontal and near horizontal gas-liquid flow. *AIChE Journal*, 22 (1), Wiley Online Library, p.47–55.

Thome, J., Dupont, V. and Jacobi, A. (2004). Heat transfer model for evaporation in microchannels. Part I: presentation of the model. *International Journal of Heat and Mass Transfer*, 47 (14), Elsevier, p.3375–3385.

Thome, J. R. (2007). *Engineering data book III*. Wolverine Tube Inc.

Thome, J. R. and Consolini, L. (2010). Mechanisms of boiling in micro-channels: critical assessment. *Heat Transfer Engineering*, 31 (4), Taylor & Francis, p.288–297.

Thome, J. R. and El Hajal, J. (2003). Two-phase flow pattern map for evaporation in horizontal tubes: latest version. *Heat Transfer Engineering*, 24 (6), Taylor & Francis, p.3–10.

Tibiriçá, C. B. and Ribatski, G. (2010). Flow Boiling Heat Transfer of R134a and R245fa in a 2.3 mm Tube. *International Journal of Heat and Mass Transfer*, 53 (11), Elsevier, p.2459–2468.

Tibiriçá, C. B. and Ribatski, G. (2011). Two-phase frictional pressure drop and flow boiling heat transfer for R245fa in a 2.32-mm tube. *Heat Transfer Engineering*, 32 (13-14), Taylor & Francis, p.1139–1149.

Tibiriçá, C. B. and Ribatski, G. (2014). Flow patterns and bubble departure fundamental characteristics during flow boiling in microscale channels. *Experimental Thermal and Fluid Science*, 59, Elsevier, p.152–165.

Tibiriçá, C. B. and Ribatski, G. (2015). Flow boiling phenomenological differences between micro-and macroscale channels. *Heat Transfer Engineering*, 36 (11), Taylor & Francis, p.937–942.

Tibiriçá, C. B., Ribatski, G. and Thome, J. R. (2012). Flow boiling characteristics for R1234ze (E) in 1.0 and 2.2 mm circular channels. *Journal of Heat Transfer*, 134 (2), American Society of Mechanical Engineers, p.020906.

Tibiriçá, C. B., Rocha, D. M., Sueth Jr, I. L. S., Bochio, G., Shimizu, G. K. K., Barbosa, M. C. and dos Santos Ferreira, S. (2017). A complete set of simple and optimized correlations for microchannel flow boiling and two-phase flow applications. *Applied Thermal Engineering*, 126, Elsevier, p.774–795.

Tibiriçá, C. B., da Silva, J. D. and Ribatski, G. (2011). Experimental investigation of flow boiling pressure drop of R134a in a microscale horizontal smooth tube. *Journal of Thermal Science and Engineering Applications*, 3 (1), American Society of Mechanical Engineers, p.011006.

Tong, W., Bergles, A. E. and Jensen, M. K. (1997). Pressure drop with highly subcooled flow boiling in small-diameter tubes. *Experimental Thermal and Fluid Science*, 15 (3), Elsevier, p.202–212.

Tran, T., Chyu, M.-C., Wambsganss, M. and France, D. (2000). Two-phase pressure drop of refrigerants during flow boiling in small channels: an experimental investigation and correlation development. *International Journal of Multiphase Flow*, 26 (11), Elsevier, p.1739–1754.

Triplett, K., Ghiaasiaan, S., Abdel-Khalik, S. and Sadowski, D. (1999). Gas-liquid two-phase flow in microchannels Part I: two-phase flow patterns. *International Journal of Multiphase Flow*, 25 (3), Elsevier, p.377–394.

Tullius, J. F., Vajtai, R. and Bayazitoglu, Y. (2011). A review of cooling in microchannels. *Heat Transfer Engineering*, 32 (7-8), Taylor & Francis, p.527–541.

Turgut, O. E., Asker, M. and Çoban, M. T. (2016). Saturated Flow Boiling Heat Transfer Correlation for Small Channels Based on R134a Experimental Data. *Arabian Journal for Science and Engineering*, Springer, p.1–19.

Ullmann, A. and Brauner, N. (2007). The prediction of flow pattern maps in minichannels. *Multiphase Science and Technology*, 19 (1), Begel House Inc.

Venkatesan, M., Das, S. K. and Balakrishnan, A. (2010). Effect of tube diameter on two-phase flow patterns in mini tubes. *The Canadian Journal of Chemical Engineering*, 88 (6), Wiley Online Library, p.936–944.

Wang, E., Zhang, H., Fan, B., Ouyang, M., Zhao, Y. and Mu, Q. (2011). Study of working fluid selection of organic Rankine cycle (ORC) for engine waste heat recovery. *Energy*, 36 (5), Elsevier, p.3406–3418.

Webb, R. L. and Gupte, N. S. (1992). A critical review of correlations for convective vaporization in tubes and tube banks. *Heat Transfer Engineering*, 13 (3), Taylor & Francis, p.58–81.

Wei, L., Pan, L.-M., Zhao, Y.-M., Ren, Q.-Y. and Zhang, W.-Z. (2017). Numerical study of adiabatic two-phase flow patterns in vertical rectangular narrow channels. *Applied Thermal Engineering*, 110, Elsevier, p.1101–1110.

Wojtan, L., Ursenbacher, T. and Thome, J. R. (2005). Investigation of flow boiling in horizontal tubes: Part I – A new diabatic two-phase flow pattern map. *International Journal of Heat and Mass Transfer*, 48 (14), Elsevier, p.2955–2969.

Wu, Z. and Sundén, B. (2014). On further enhancement of single-phase and flow boiling heat transfer in micro/minichannels. *Renewable and Sustainable Energy Reviews*, 40, Elsevier, p.11–27.

Xu, Y. and Fang, X. (2012). A new correlation of two-phase frictional pressure drop for evaporating flow in pipes. *international journal of refrigeration*, 35 (7), Elsevier, p.2039–2050.

Xu, Y., Fang, X., Li, D., Li, G., Yuan, Y. and Xu, A. (2016a). An experimental study of flow boiling frictional pressure drop of R134a and evaluation of existing correlations. *International Journal of Heat and Mass Transfer*, 98, Elsevier, p.150–163.

Xu, Y., Fang, X., Li, G., Li, D. and Yuan, Y. (2016b). An experimental study of flow boiling heat transfer of R134a and evaluation of existing correlations. *International Journal of Heat and Mass Transfer*, 92, Elsevier, p.1143–1157.

Xu, Y., Fang, X., Su, X., Zhou, Z. and Chen, W. (2012). Evaluation of frictional pressure drop correlations for two-phase flow in pipes. *Nuclear engineering and design*, 253, Elsevier, p.86–97.

Yan, Y.-Y. and Lin, T.-F. (1998). Evaporation heat transfer and pressure drop of refrigerant R-134a in a small pipe. *International Journal of Heat and Mass Transfer*, 41 (24), Elsevier, p.4183–4194.

Yang, C.-Y. and Shieh, C.-C. (2001). Flow pattern of air-water and two-phase R-134a in small circular tubes. *International Journal of Multiphase Flow*, 27 (7), Elsevier,

p.1163–1177.

Yang, Z., Gong, M., Chen, G., Zou, X. and Shen, J. (2017). Two-phase flow patterns, heat transfer and pressure drop characteristics of R600a during flow boiling inside a horizontal tube. *Applied Thermal Engineering*, 120, Elsevier, p.654–671.

Yang, Z. Q., Chen, G. F., Zhuang, X. R., Song, Q. L., Deng, Z., Shen, J. and Gong, M. Q. (2018a). A new flow pattern map for flow boiling of R1234ze (E) in a horizontal tube. *International Journal of Multiphase Flow*, 98, Elsevier, p.24–35.

Yang, Z.-Q., Chen, G.-F., Yao, Y., Song, Q.-L., Shen, J. and Gong, M.-Q. (2018b). Experimental study on flow boiling heat transfer and pressure drop in a horizontal tube for R1234ze (E) versus R600a. *International Journal of Refrigeration*, 85, Elsevier, p.334–352.

Zhang, P. and Fu, X. (2009). Two-phase flow characteristics of liquid nitrogen in vertically upward 0.5 and 1.0 mm micro-tubes: visualization studies. *Cryogenics*, 49 (10), Elsevier, p.565–575.

Zhang, S., Huaixin, W. and Tao, G. (2011a). Performance comparison and parametric optimization of subcritical Organic Rankine Cycle (ORC) and transcritical power cycle system for low-temperature geothermal power generation. *Applied energy*, 88 (8), Elsevier, p.2740–2754.

Zhang, T., Cao, B., Fan, Y., Gonthier, Y., Luo, L. and Wang, S. (2011b). Gas-liquid flow in circular microchannel. Part I: Influence of liquid physical properties and channel diameter on flow patterns. *Chemical engineering science*, 66 (23), Elsevier, p.5791–5803.

Zhang, W., Hibiki, T. and Mishima, K. (2010). Correlations of two-phase frictional pressure drop and void fraction in mini-channel. *International Journal of Heat and Mass Transfer*, 53 (1), Elsevier, p.453–465.

Zhao, T. and Bi, Q. (2001). Co-current air-water two-phase flow patterns in vertical triangular microchannels. *International Journal of Multiphase Flow*, 27 (5), Elsevier, p.765–782.

Zhu, Y., Wu, X. and Zhao, R. (2017a). R32 flow boiling in horizontal mini channels: Part I. Two-phase flow patterns. *International Journal of Heat and Mass Transfer*, 115, Elsevier, p.1223–1232.

Zhu, Y., Wu, X. and Zhao, R. (2017b). R32 flow boiling in horizontal mini channels: Part II Flow-pattern based prediction methods for heat transfer and pressure drop. *International Journal of Heat and Mass Transfer*, 115, Elsevier, p.1233–1244.

Zivi, S. (1964). Estimation of steady-state steam void-fraction by means of the principle of minimum entropy production. *Journal of Heat Transfer*, 86 (2), American Society of Mechanical Engineers, p.247–251.

Appendix A

Flow Pattern Models and Correlations

Table A.1 The existing flow regime maps used for comparison with observed flow pattern data.

Author	Models	Conditions
Revellin and Thome (2007a)	Isolated bubble-Coalescing bubble transition $x_{IB/CB} = 0.763(Re_l Bo/We_v)^{0.41}$ Coalescing bubble-Annular transition $x_{CB/A} = 0.00014 Re_l^{1.47} We_l^{-1.23}$	*Diabatic two-phase flow in horizontal tubes.* *D: 0.509 – 0.79 mm* *T_{sat}: 26, 30, and 35 °C* *x: 0 – 0.95* *q: 3.1 – 597 kW/m^2* *G: 200 – 2000 kg/m^{2}s* *Fluid: R134a and R245fa*
Ong and Thome (2011a)	Isolated bubble-Coalescing bubble transition $x_{IB/CB} = 0.36 Co^{0.2} \left(\frac{\mu_v}{\mu_l}\right)^{0.65} \left(\frac{\rho_v}{\rho_l}\right)^{0.9} \frac{Re_v^{0.75} Bo^{0.25}}{We_l^{0.91}}$ Coalescing bubble-Annular transition $x_{CB/A} = 0.047 Co^{0.05} \left(\frac{\mu_v}{\mu_l}\right)^{0.7} \left(\frac{\rho_v}{\rho_l}\right)^{0.6} \frac{Re_v^{0.8}}{We_l^{0.91}}$	*Diabatic two-phase flow in horizontal tubes.* *D: 1.03 – 3.04 mm* *T_{sat}: 31°C* *x: 0 – 1* *q: 8.4 – 221.6 kW/m^2* *G: 200 – 1500 kg/m^{2}s* *Fluid: R134a, R236fa and R245fa*
Costa-Patry and Thome (2013)	Coalescing bubble-Annular transition $x = 425 \left(\frac{\rho_v}{\rho_l}\right)^{0.1} \frac{Bo^{1.1}}{Co^{0.5}}$	*Diabatic two-phase flow in horizontal tubes.* *D: 0.146 – 3.04 mm* *T_{sat}: 10 – 30.5°C* *x: 0 – 1* *q: 8 – 1400 kW/m^2* *G: 100 – 1100 kg/m^{2}s* *Fluid: R134a, R1234ze(E), R236fa and R245fa*
Karayiannis et al. (2014)	Bubbly-Slug transition $J_l = \left(\frac{1}{\epsilon C_o} - 1\right) J_v - \frac{0.35}{C_o} \left(\frac{gD\Delta\rho}{\rho_l}\right)^{0.5}$ $\epsilon = 0.138(J_v + J_l)^{0.344}$ $C_o = 1.2 - 0.2(\rho_v/\rho_l)^{0.5}$ Slug-Churn transition $J_l = 81.08 \left(\frac{\mu_l}{D\rho_l}\right) \left(\frac{\rho_v J_v^2 D}{\sigma}\right)^{1.626} \left(J_v \sqrt{\frac{\rho_v}{gD\Delta\rho}}\right)^{-0.267}$	*Diabatic two-phase flow in vertical tubes.* *2392 data points.* *D: 1.1 – 4.26 mm* *P: 600 – 14000 kPa* *x: 0.05 – 0.95* *G: 50 – 6400 kg/m^{2}s* *Fluid: R134a*

	$J_v = 587.1\left(\frac{\mu_l}{D\rho_v}\right)^{1.447}\left(\frac{\rho_l D}{\sigma}\right)^{0.937}$ $J_l = 2.75\,(\sigma/(f_l\rho_l D)^{0.5}) - J_v$ $f_l = 0.046Re^{-0.2},\ Re = \rho_l\,(J_v - J_l)/\mu_l$ <u>Churn-Annular transition</u> $J_l = \left(1.567\times10^{-17}\frac{\sigma}{\rho_l D}\left(\frac{J_v^2\rho_v D}{\mu_v\sqrt{gD}}\right)^{3.41}\right)^{0.5}$ $J_v = \left(3.119\times10^{5}\frac{\mu_v\sqrt{gD}}{\rho_v D}\right)^{0.5}$	
Mahmoud and Karayiannis (2016)	<u>Bubbly-Slug transition</u> $J_l = 0.33\left[\frac{J_v}{0.67} + \sqrt{\frac{4\sigma}{\rho_l D}}\right]$	*Diabatic two-phase flow in vertical tubes.* *D: 1.1 mm* *P: 1.85 kPa* *x: 0.008 – 0.95* *q: 3 – 25 kW/m^2* *G: 100 – 400 kg/m^{2}s* *Fluid: R245fa*
Zhu et al. (2017a)	<u>Slug-Churn transition</u> $x_{SC} = 14.17\left(\frac{\rho_v}{\rho_l}\right)^{0.3747}\frac{Bo^{0.3614}}{Co^{0.1044}}$ <u>Churn-Annular transition</u> $x_{CA} = 0.03388\left(\frac{\rho_v}{\rho_l}\right)^{0.6786}\left(\frac{\mu_v}{\mu_l}\right)^{0.5371}\cdot\frac{Re_v^{0.8094}Bo^{0.1984}}{Co^{-0.2829}We_l^{0.4297}}$	*Diabatic two-phase flow in horizontal tubes.* *D: 1 – 2 mm* *T_{sat}: 10 – 20°C* *x: 0 – 1* *q: 10 – 30 kW/m^2* *G: 50 – 600 kg/m^{2}s* *Fluid: R32*
Tibiriçá et al. (2017)	<u>Bubble-Slug transition</u> $x_{BS} = \left[1 + 1.268\left(\frac{\rho_l}{\rho_v}\right)^{2.793}Re_l^{0.3283}\left(\frac{\mu_l}{\mu_v}\right)^{-3.383}\right]^{-1}$ <u>Slug-Churn transition</u> $x_{SC} = \left[1 + 0.0721\left(\frac{\rho_l}{\rho_v}\right)^{0.7215}Re_l^{0.7864}Su_l^{-0.3003}\right]^{-1}$ <u>Churn-Annular transition</u> $x_{CA} = \left[1+10^{-2.1765}\left(\frac{\rho_l}{\rho_v}\right)^{0.6534}Re_l^{0.4444}Fr_l^{0.2416}\right]^{-1}$	*Diabatic two-phase flow in horizontal tubes.* *395 data points.* *D: 0.25 – 5.5 mm* *Fluid: R134a, R1234ze(E), R236fa, R245fa and air-water.*

Appendix B

Two-Phase Pressure Drop Correlations

Table B.1 Separated flow models for the two-phase pressure drop in conventional tubes.

Author(s)	Correlation	Void fraction	Conditions
Lockhart and Martinelli (1949)	$-\left(\frac{dP}{dz}\right)_{fr} = \frac{2 f_l G^2 (1-x)^2 v_l}{D_h} \phi_l^2$, $\phi_l^2 = 1 + \frac{C}{X} + \frac{1}{X^2}$ $X = \sqrt{\frac{(dP/dz)_l}{(dP/dz)_v}} = \left(\frac{1-x}{x}\right)\left(\frac{\rho_v}{\rho_l}\right)^{0.5}\left(\frac{f_l}{f_v}\right)^{0.5}$ $-\left(\frac{dP}{dz}\right)_l = f_l \frac{2G^2(1-x)^2}{D_h \rho_l}$ $-\left(\frac{dP}{dz}\right)_v = f_v \frac{2G^2 x^2}{D_h \rho_v}$ $C = 5(vv), 10\ (tv), 12\ (vt), 20\ (tt)$	Lockhart and Martinelli (1949)	*Horizontal flow in tubes* *D: 1.49–25.83 mm* *P: 110.3–358.5 kPa* *Re_l: 1.1–124000* *Re_v: 7–86000* *Fluid: Air-Benzene, Air-Kerosene, Air-Water, and Air-various oils*
Chisholm (1973a)	$-\left(\frac{dP}{dz}\right)_{fr} = \frac{2 f_{lo} G^2 v_l}{D_h} \phi_{lo}^2$ $\phi_{lo}^2 = 1 + (\Gamma^2 - 1)\left[B x^{\frac{(2-n)}{2}}(1-x)^{\frac{(2-n)}{2}} + x^{2-n}\right]$ $\Gamma^2 = \frac{(dP/dz)_{vo}}{(dP/dz)_{lo}} = \left(\frac{\rho_l}{\rho_v}\right)^{0.5}\left(\frac{\mu_v}{\mu_l}\right)^{n/2}$ For smooth tubes $n = 0.25$, and for rough tube $n = 0$ $when\ 0 < \Gamma \leq 9.5$: $B = 4.8\ for\ G \leq 500\ kg/m^2 s$; $B = 2400/G\ \ for\ 500 < G < 1900\ kg/m^2 s$; $B = 55/\sqrt{G}\ \ for\ G \geq 1900\ kg/m^2 s$; $when\ 9.5 < \Gamma < 28$: $B = 520/(\Gamma\sqrt{G})\ \ for\ G \leq 600\ kg/m^2 s$; $B = 21/\Gamma\ \ for\ G > 600\ kg/m^2 s$; $when\ \Gamma \geq 28$: $B = 15000/(\Gamma^2\sqrt{G})$	Chisholm (1973b)	*Vertical and horizontal turbulent flow in smooth tubes* *P: 600–4130 kPa* *G: 339–4068 kg/m^{2}s* *x: 0–1* *Fluid: Water.*
Grönnerud (1979)	$-\left(\frac{dP}{dz}\right)_{fr} = \frac{2 f_{lo} G^2 v_l}{D_h} \phi_{lo}^2$ $\phi_{lo}^2 = 1 + \left(\frac{dP}{dz}\right)_{FR}\left[\frac{\left(\frac{v_v}{v_l}\right)}{\left(\frac{\mu_l}{\mu_v}\right)^{0.25}} - 1\right]$ $\left(\frac{dP}{dz}\right)_{FR} = f_{FR}[x + 4(x^{1.8} - x^{10} f_{FR}^{0.5})]$ $f_{FR} = \begin{cases} 1 & , Fr_l \geq 1 \\ Fr_l^{0.3} + 0.0055\left(\ln\frac{1}{Fr_l}\right)^2 & , Fr_l < 1 \end{cases}$	Lockhart and Martinelli (1949)	*Horizontal flow in tubes 1000 data points* *D: 26.2 mm* *x: 0–1* *Fluid: R12 and R717*
Friedel (1979)	$-\left(\frac{dP}{dz}\right)_{fr} = \frac{2 f_{lo} G^2 v_l}{D_h} \phi_{lo}^2$ $\phi_{lo}^2 = E + \frac{3.24FH}{Fr_H^{0.045} We_H^{0.035}}$	Lockhart and Martinelli (1949)	*25000 data points* *D ≥ 4 mm*

	$Fr_H = \frac{G^2}{gD_h\rho_H^2}, We_H = \frac{G^2 D_h}{\sigma\rho_H}$ $\rho_H = \frac{1}{xv_v + (1-x)v_l}$ $E = (1-x)^2 + x^2\frac{\rho_l f_{vo}}{\rho_v f_{lo}}$ $F = x^{0.78}(1-x)^{0.224}$ $H = \left(\frac{\rho_l}{\rho_v}\right)^{0.91}\left(\frac{\mu_v}{\mu_l}\right)^{0.19}\left(1-\frac{\mu_v}{\mu_l}\right)^{0.7}$		$\left(\frac{\mu_l}{\mu_v}\right) < 1000$ *Fluid: Air-Water, and refrigerants.*
Müller-Steinhagen and Heck (1986)	$-\left(\frac{dP}{dz}\right)_{fr} = C(1-x)^{\frac{1}{3}} + \left(-\left(\frac{dP}{dz}\right)_{vo}\right)x^3$ $C = -\left(\frac{dP}{dz}\right)_{lo} + 2\left(-\left(\frac{dP}{dz}\right)_{vo} - \left(-\left(\frac{dP}{dz}\right)_{lo}\right)\right)x$ $-\left(\frac{dP}{dz}\right)_{lo} = \frac{2f_{lo}G^2 v_l}{D_h}$ $-\left(\frac{dP}{dz}\right)_{vo} = \frac{2f_{vo}G^2 v_v}{D_h}$	Lockhart and Martinelli (1949)	*9300 data points* *D: 4–392 mm* *x: 0.01–0.97* *Re_{lo} > 100* $\left(\frac{dP}{dz}\right)_{vo} > \left(\frac{dP}{dz}\right)_{lo}$ *Fluid: Air-Water, Air-Oil, Argon, N_2, R11, and R12*

Table B.2 Separated flow models for the two-phase pressure drop in mini/micro tubes.

Author(s)	**Correlation**	**Void fraction**	**Conditions**
Mishima and Hibiki (1996)	$-\left(\frac{dP}{dz}\right)_{fr} = \frac{2f_l G^2(1-x)^2 v_l}{D_h}\phi_l^2$ $\phi_l^2 = 1 + \frac{C}{X} + \frac{1}{X^2}$ $X = \sqrt{\frac{(dP/dz)_l}{(dP/dz)_v}} = \left(\frac{1-x}{x}\right)\left(\frac{\rho_v}{\rho_l}\right)^{0.5}\left(\frac{f_l}{f_v}\right)^{0.5}$ $C = 21(1-e^{-319D}), D \quad (mm)$	Lockhart and Martinelli (1949)	*Vertical and horizontal flow in tubes and channels* *D: 1.05–4.08 mm* *J_g: 0.02–50 m/s* *J_l: 0.002–8 m/s* *Fluid: Air-water, Ammonia, and N_2-R113*
Qu and Mudawar (2003)	$-\left(\frac{dP}{dz}\right)_{fr} = \frac{2f_l G^2(1-x)^2 v_l}{D_h}\phi_l^2$ $\phi_l^2 = 1 + \frac{C}{X} + \frac{1}{X^2}$ $X = \sqrt{\frac{(dP/dz)_l}{(dP/dz)_v}} = \left(\frac{1-x}{x}\right)\left(\frac{\rho_v}{\rho_l}\right)^{0.5}\left(\frac{f_l}{f_v}\right)^{0.5}$ $X_{vv} = \left(\frac{\mu_l}{\mu_v}\right)^{0.5}\left(\frac{1-x}{x}\right)^{0.5}\left(\frac{v_l}{v_v}\right)^{0.5}$ $C = 21(1-e^{-319D_h})(0.00418G + 0.0613)$	Zivi (1964)	*Horizontal flow in channels* *D: 0.35 mm* *G: 134.9–400.1kg/m^{2}s* *T_{in}: 30 and 60 ^{o}C* *P_{out}: 117 kPa* *Fluid: Water*
Hwang and Kim (2006)	$-\left(\frac{dP}{dz}\right)_{fr} = \frac{2f_l G^2(1-x)^2 v_l}{D_h}\phi_l^2$ $\phi_l^2 = 1 + \frac{C}{X} + \frac{1}{X^2}$ $X = \sqrt{\frac{(dP/dz)_l}{(dP/dz)_v}} = \left(\frac{1-x}{x}\right)\left(\frac{\rho_v}{\rho_l}\right)^{0.5}\left(\frac{f_l}{f_v}\right)^{0.5}$ $C = 0.227Re_{lo}^{0.452}X^{-0.32}Co^{-0.82}$	Lockhart and Martinelli (1949)	*D: 0.244, 0.43, and 0.792 mm* *P: 144–660 kPa* *G: 140–950 kg/m^{2}s* *x: 0.08–0.95* *Fluid: R134a*
Sun and Mishima (2009)	$-\left(\frac{dP}{dz}\right)_{fr} = \frac{2f_l G^2(1-x)^2 v_l}{D_h}\phi_l^2$ For laminar flow (Re_l < 2000 and Re_v < 2000): $\phi_l^2 = 1 + \frac{C}{X} + \frac{1}{X^2}$ $X = \sqrt{\frac{(dP/dz)_l}{(dP/dz)_v}} = \left(\frac{1-x}{x}\right)\left(\frac{\rho_v}{\rho_l}\right)^{0.5}\left(\frac{f_l}{f_v}\right)^{0.5}$ $C = 26\left(1 + \frac{Re_l}{1000}\right)\left[1 - \exp\left(\frac{-0.153}{0.8 + 0.27Co}\right)\right]$	Lockhart and Martinelli (1949)	*Vertical and horizontal flow in tubes and channels* *2092 data points* *D: 0.506–12 mm* *G: 50–2000 kg/m^{2}s* *Re_l: 10–37000* *Re_v: 3–400000* *Fluid: R123, R134a, R22,*

	For turbulent flow (Re_l > 2000 and Re_v > 2000): $\phi_l^2 = 1 + \frac{C}{X^{1.19}} + \frac{1}{X^2}$ $X = \sqrt{\frac{(dP/dz)_l}{(dP/dz)_v}} = \left(\frac{1-x}{x}\right)\left(\frac{\rho_v}{\rho_l}\right)^{0.5}\left(\frac{f_l}{f_v}\right)^{0.5}$ $C = 1.79\left(\frac{Re_v}{Re_l}\right)^{0.4}\left(\frac{1-x}{x}\right)^{0.5}$		*R236ea, R245fa, R404a, R407C, R410a, R507, CO_2, Water and air.*
Li and Wu (2010a)	$-\left(\frac{dP}{dz}\right)_{fr} = \frac{2 f_l G^2 (1-x)^2 v_l}{D_h}\phi_l^2$ $\phi_l^2 = 1 + \frac{C}{X} + \frac{1}{X^2},\ X = \sqrt{\frac{(dP/dz)_l}{(dP/dz)_v}} = \left(\frac{1-x}{x}\right)\left(\frac{\rho_v}{\rho_l}\right)^{0.5}\left(\frac{f_l}{f_v}\right)^{0.5}$ $C = \begin{cases} 11.9Bd^{0.45} & , \quad Bd \le 1.5 \\ 109.4(BdRe_l^{0.5})^{-0.56}, & 1.5 < Bd \le 11 \end{cases}$	Lockhart and Martinelli (1949)	*Vertical and horizontal flow in tubes and channels* *769 data points* *D: 0.148–3.25 mm* *G: 198–2000 kg/m²s* *T_{sat}: -8.5–65 °C* *x: 0–1* *Fluid: R134a, R245fa, R236ea, R410a, Ammonia, Propane, R22, R12, R404a, N_2, R422d, and R32*
Lee et al. (2010)	$-\left(\frac{dP}{dz}\right)_{fr} = \frac{2 f_l G^2 (1-x)^2 v_l}{D_h}\phi_l^2$ $\phi_l^2 = 1 + \frac{C}{X} + \frac{1}{X^2}$ $X = \sqrt{\frac{(dP/dz)_l}{(dP/dz)_v}} = \left(\frac{1-x}{x}\right)\left(\frac{\rho_v}{\rho_l}\right)^{0.5}\left(\frac{f_l}{f_v}\right)^{0.5}$ $C = 121.6(1 - e^{-22.7Bd})x^{1.85}$	Zivi (1964)	*Horizontal flow in tubes and channels* *484 data points* *D: 0.35–2.46 mm* *G: 20.3–2267 kg/m²s* *x: 0–0.98* *Re_{lo}: 50–10100* *Re_{vo}: 1200–155000* *Fluid: Water, N-pentane, Ammonia, CO_2, R410a, R134a, and R12*
Xu and Fang (2012)	$-\left(\frac{dP}{dz}\right)_{fr} = \left(\Gamma x^3 + (1-x)^{\frac{1}{3}}\left(1 + 2\text{x}(\Gamma^2 - 1)\right)\right)(1 + 1.54(1-x)^{0.5}La^{1.47})$ $\Gamma^2 = \frac{(dP/dz)_{vo}}{(dP/dz)_{lo}} = \left(\frac{\rho_l}{\rho_v}\right)\ \left(\frac{f_{vo}}{f_{lo}}\right)$ $-\left(\frac{dP}{dz}\right)_{lo} = \frac{2 f_{lo} G^2 v_l}{D_h}$ $-\left(\frac{dP}{dz}\right)_{vo} = \frac{2 f_{vo} G^2 v_v}{D_h}$	Lockhart and Martinelli (1949)	*Vertical and horizontal flow in tubes* *2622 data points* *D: 0.81–19.1 mm* *q: 0.6–150 kw/m²* *G: 25.4–1150 kg/m²s* *x: 0–1* *Fluid: R12, R134a, R22, R32, R125, R123, CO_2, R407C, R507, R410a, R404a, R507a, Ammonia and R11.*
Kim and Mudawar (2012)	$-\left(\frac{dP}{dz}\right)_{fr} = \frac{2 f_l G^2 (1-x)^2 v_l}{D_h}\phi_l^2$ $\phi_l^2 = 1 + \frac{C}{X} + \frac{1}{X^2}$ $X = \sqrt{\frac{(dP/dz)_l}{(dP/dz)_v}} = \left(\frac{1-x}{x}\right)\left(\frac{\rho_v}{\rho_l}\right)^{0.5}\left(\frac{f_l}{f_v}\right)^{0.5}$ $-\left(\frac{dP}{dz}\right)_l = f_l \frac{2G^2(1-x)^2}{D_h \rho_l}$	Zivi (1964)	*Vertical and horizontal flow in tubes and channels* *7115 data points* *D: 0.0695–6.22 mm* *P_r: 0.0052–0.91* *G: 4–8528 kg/m²s* *x: 0–1* *Re_{lo}: 3.9–89798*

	$-\left(\frac{dP}{dz}\right)_v = f_v \frac{2G^2x^2}{D_h\rho_v}$ $C = \begin{cases} 3.5\times10^{-5}Re_{lo}^{0.44}Su_{vo}^{0.5}\left(\frac{\rho_l}{\rho_v}\right)^{0.48}, & (vv) \\ 0.0015Re_{lo}^{0.59}Su_{vo}^{0.19}\left(\frac{\rho_l}{\rho_v}\right)^{0.36}, & (vt) \\ 8.7\times10^{-4}Re_{lo}^{0.17}Su_{vo}^{0.5}\left(\frac{\rho_l}{\rho_v}\right)^{0.14}, & (tv) \\ 0.39Re_{lo}^{0.03}Su_{vo}^{0.1}\left(\frac{\rho_l}{\rho_v}\right)^{0.35}, & (tt) \end{cases}$		*Re_l: 0–79202* *Re_v: 0–253810* *Fluid: R134a, R12, N_2-water, N_2-ethanol, R410a, R407a, R22, R404a, CO_2, Ammonia, R245fa, R236ea, Propane, Methane, CO_2-water and Air-water*
Kim and Mudawar (2013)	$-\left(\frac{dP}{dz}\right)_{fr} = \frac{2f_lG^2(1-x)^2v_l}{D_h}\phi_l^2$ $\phi_l^2 = 1+\frac{C}{X}+\frac{1}{X^2}$ $X = \sqrt{\frac{(dP/dz)_l}{(dP/dz)_v}} = \left(\frac{1-x}{x}\right)\left(\frac{\rho_v}{\rho_l}\right)^{0.5}\left(\frac{f_l}{f_v}\right)^{0.5}$ $-\left(\frac{dP}{dz}\right)_l = f_l\frac{2G^2(1-x)^2}{D_h\rho_l}$ $-\left(\frac{dP}{dz}\right)_v = f_v\frac{2G^2x^2}{D_h\rho_v}$ $C = \begin{cases} C^*\left[1+60We_{lo}^{0.32}\left(Bo\frac{P_h}{P_F}\right)^{0.78}\right], & Re_l \geq 2000 \\ C^*\left[1+530We_{lo}^{0.52}\left(Bo\frac{P_h}{P_F}\right)^{1.09}\right], & Re_l < 2000 \end{cases}$ $C^* = \begin{cases} 3.5\times10^{-5}Re_{lo}^{0.44}Su_{vo}^{0.5}\left(\frac{\rho_l}{\rho_v}\right)^{0.48}, & (vv) \\ 0.0015Re_{lo}^{0.59}Su_{vo}^{0.19}\left(\frac{\rho_l}{\rho_v}\right)^{0.36}, & (vt) \\ 8.7\times10^{-4}Re_{lo}^{0.17}Su_{vo}^{0.5}\left(\frac{\rho_l}{\rho_v}\right)^{0.14}, & (tv) \\ 0.39Re_{lo}^{0.03}Su_{vo}^{0.1}\left(\frac{\rho_l}{\rho_v}\right)^{0.35}, & (tt) \end{cases}$	Zivi (1964)	*Vertical and horizontal flow in tubes and channels* *2378 data points* *D: 0.349–5.35 mm* *P_r: 0.005–0.78* *G: 33–2738 kg/m^{2}s* *x_{ex}: 0–1* *Re_{lo}: 156–82010* *Re_l: 0–16020* *Re_v: 0–199500* *Fluid: R134a, R12, R410a, R22, CO_2, Ammonia, R245fa, FC72, and Water*

Appendix C

Flow Boiling Heat Transfer correlations

Table C.1 Existing flow boiling heat transfer correlations for micro-channels.

Author(s)	Correlation	Application condition
Cooper (1984)	$\alpha_{tp} = 55\, P_r^{0.12-0.2\, logR_P}(-log\, P_r)^{-0.55} MW^{-0.5} q^{0.67}$	*Vertical up and down flow in tubes.* *6000 data points.* *For nucleate pool boiling* *Fluid: Water, R12, R13b1, R114, R21, R22, R13, R11, R115, R226, RC318, R113 and others.*
Kew and Cornwell (1997)	$\alpha_{tp} = 30\, Re_{lo}^{0.857} Bo^{0.714}(1-x)^{-0.143}\frac{k_l}{D}$	*Vertical flow in tubes.* *D: 1.39 – 3.69 mm* *P: 250 kPa* *q: 9.7 – 90 kW/m²* *G: 188 – 1480 kg/m²s* *Fluid: R141b.*
Bertsch et al. (2009)	$\alpha_{tp} = E\alpha_{cb} + S\alpha_{nb}$ $\alpha_{cb} = \alpha_{cb,l}(1-x) + \alpha_{cb,v}x$ $\alpha_{cb,l} = \left(3.66 + \frac{0.0668\frac{D}{L}Re_{lo}Pr_l}{1+0.04\left(\frac{D}{L}Re_{lo}Pr_l\right)^{2/3}}\right)\frac{k_l}{D}$ $\alpha_{cb,v} = \left(3.66 + \frac{0.0668\frac{D}{L}Re_{vo}Pr_v}{1+0.04\left(\frac{D}{L}Re_{vo}Pr_v\right)^{2/3}}\right)\frac{k_v}{D}$ $\alpha_{nb} = 55\, P_r^{0.12-0.2\, logR_P}(-log\, P_r)^{-0.55} MW^{-0.5} q^{0.67}$ $E = 1-x$ $S = 1 + 80(x^2 - x^6)e^{-0.6Co}$	*Vertical and horizontal flow in tubes and multichannel.* *3899 data points* *D: 0.16 – 2.92 mm.* *T_{sat}: -194 – 97 °C* *x: 0 – 1* *q: 4 – 1150 kW/m²* *G: 20 – 3000 kg/m²s* *Fluid: Water, R134a, R236fa, R245fa, R11, R123, FC77, R113, R141b, R12, R410a and Nitrogen.*
Li and Wu (2010b)	$\alpha_{tp} = 334 Bo^{0.3}(Bd\, Re_l^{0.36})^{0.4}\, \frac{k_l}{D}$	*Vertical and horizontal flow in tubes and multichannel.* *3700 data points.* *D: 0.16 – 3.1 mm.* *P: 100 – 1200 kPa* *x: 0 – 1* *q: 0 – 1150 kW/m²* *G: 20.3 – 3570 kg/m²s* *Fluid: R12, R134a, R11, R123, Water, CO_2, R410a, FC77, R22, Ethanol, R236fa, R245fa and Propane.*

Mahmoud and Karayiannis (2012)	$\alpha_{tp} = 3320 \frac{Bo^{0.63} We_l^{0.2} Re_l^{0.11}}{Co^{0.6}} \frac{k_l}{D}$	*Vertical up flow in tubes.* *5152 data points.* *D: 1.1 – 4.26 mm* *P: 600 – 1400 kPa* *q: 2.4 – 175.4 kW/m²* *G: 100 – 500 kg/m²s* *Fluid: R134a.*
Fang et al. (2015)	$\alpha_{tp} = 0.00061(S+E) Re_l \ Pr_l^{0.4} \ Fa^{0.11} \frac{k_l}{D} \left[ln\left(1.02 \frac{\mu_l}{\mu_{l,W}}\right)\right]^{-1}$ $S = 142.5 Bo^{0.9} MW^{0.55} \left(\frac{\rho_l}{\rho_v}\right)^{0.33}$ $E = x \left(\frac{x}{1-x}\right)^{0.9} \left(\frac{\rho_l}{\rho_v}\right)^{0.35}$	*Vertical and horizontal flow in tubes and multichannel.* *1055 data points* *D: 0.207 – 1.73 mm.* *T_{sat}: 99.6 – 201.31 °C* *P: 101 – 1600 kPa* *x: 0 – 0.96* *q: 27.7 – 4788 kW/m²* *G: 17 – 1782 kg/m²s* *Fluid: Water.*
Turgut et al. (2016)	$\alpha_{tp} = \sqrt{(\alpha_{nb}^2 + \alpha_l^2)}$ $\alpha_l = \left(0.023 Re_l^{0.8} Pr_l^{0.4} \frac{k_l}{D}\right)\left(1.63366 \left(\frac{1}{X_{tt}}\right)^{0.94494}\right)$ $\alpha_{nb} = 9.86075 \alpha_{Goren}^{0.80244} \ P_r^{0.28773} (1-x)^{0.40314}$ $\alpha_{Goren} = \alpha_0 F_{PF} \left(\frac{q}{q_o}\right)^{nf} \left(\frac{R_p}{R_{p0}}\right)^{0.133}$ $\alpha_0 = 3641 \frac{W}{m^2 K}$ (for R245fa) $q_0 = 20000 \ W/m^2$ $P_{r0} = 0.1$ $R_{p0} = 0.4 \ \mu m$ Note $R_a = 0.4 \ R_P$ $F_{PF} = 1.2 \ P_r^{0.27} + \left(2.5 + \frac{1}{1-P_r}\right) P_r$ $nf = 0.9 - 0.3 P_r^{0.3}$ $R_P = 0.4$ when it is not specified. $X_{tt} = \left(\frac{1-x}{x}\right)^{0.9} \left(\frac{\rho_v}{\rho_l}\right)^{0.5} \left(\frac{\mu_l}{\mu_v}\right)^{0.1}$	*Vertical and horizontal flow in tubes.* *3594 data points.* *D: 0.5 – 13.84 mm* *P: 263.4 – 1400 kPa* *T_{sat}: -8.8 – 52.4 °C* *x: 0 – 1* *q: 3 – 150 kW/m²* *G: 50 – 1500 kg/m²s* *Fluid: R134a.*
Kanizawa et al. (2016)	$\alpha_{tp} = E\alpha_l + S\alpha_{nb}$ $\alpha_l = 0.023 Re_l^{0.8} Pr_l^{0.4} \frac{k_l}{D}$ $\alpha_{nb} = 207 \frac{k_l}{d_b} \left(\frac{q d_b}{k_l T_{sat}}\right)^{0.745} \left(\frac{\rho_v}{\rho_l}\right)^{0.581} Pr_l^{0.533}$ $E = 1 + \frac{2.5 X^{-1.32}}{1 + We_{u_v}^{0.24}}$ $S = \frac{1.06 Bd^{-8.1^{-3}}}{1 + 0.12\left(Re_{tp} \times 10^{-4}\right)^{0.86}}$ $Re_{tp} = Re_{lo} E^{1.25}$, $d_b = 0.51 \left(\frac{2\sigma}{g(\rho_l - \rho_v)}\right)^{0.5}$ $X = \begin{cases} \left(\frac{1-x}{x}\right)^{0.9} \left(\frac{\rho_v}{\rho_l}\right)^{0.5} \left(\frac{\mu_l}{\mu_v}\right)^{0.1} & , \ Re_v > 1000 \\ \frac{Re_v^{0.4}}{18.7} \left(\frac{1-x}{x}\right)^{0.9} \left(\frac{\rho_v}{\rho_l}\right)^{0.5} \left(\frac{\mu_l}{\mu_v}\right)^{0.1} & , \ Re_l \leq 1000 \end{cases}$ $We_{u_v} = \frac{(Gx)^2 D_i}{\sigma \rho_v \epsilon^2}$, $Fr_m = \frac{G^2}{(\rho_l - \rho_v)^2 g \ D}$	*Horizontal flow in tubes.* *2047 data points.* *D: 0.38 – 2.6 mm* *T_{sat}: 21.5 – 58.3 °C* *x: 0.01 – 0.93* *q: 5 – 185 kW/m²* *G: 49 – 2200 kg/m²s* *Fluid: R134a, R245fa and R600a.*

	$\epsilon = \left[1 + 1.021 Fr_m^{-0.092} \left(\frac{\mu_l}{\mu_v}\right)^{-0.368} \left(\frac{\rho_v}{\rho_l}\right)^{1/3} \left(\frac{1-x}{x}\right)^{2/3}\right]^{-1}$	
Fang et al. (2017)	$\alpha_{tp} = F_{fl} MW^{-0.18} Bo^{0.98} Fr_{lo}^{0.48} Bd^{0.72} \left(\frac{\rho_l}{\rho_v}\right)^{0.29} \frac{k_l}{D} \left[ln\left(\frac{\mu_l}{\mu_{l,W}}\right)\right]^{-1} F$ For R245fa, F_{fl} = 1890 $F = \begin{cases} 1 & , \ P_r \le 0.43 \\ 1.38 - P_r^{1.15} & , \ P_r > 0.43 \end{cases}$	*Vertical and horizontal flow in tubes and multichannel.* *17778 data points* *D: 0.207 – 32 mm.* *P_r: 0.0045 – 0.93* *x: 0.0001 – 0.998* *q: 0.2 – 4788 kW/m^2* *G: 10 – 1782 kg/m^{2}s* *Fluid: R134a, R22, R410A, R407C, R1234yf, R236fa, R245fa, R32, Ammonia, Water, Nitrogen, R290, and CO_2.*
Shah (2017)	$\alpha_{tp} = \max(\psi_{nb}, \psi_{cb})\, \alpha_l E$ $E = \max(1, 2.1 - 0.008 We_v - 110 Bo)$ $\alpha_l = 0.023 Re_l^{0.8} Pr_l^{0.4} \frac{k_l}{D}$ $\psi_{nb} = \begin{cases} 230 Bo^{0.5} & , \ Bo > 0.3\times10^{-4}, \ Cov > 1 \\ 1 + 46\, Bo^{0.5} & , \ Bo < 0.3\times10^{-4}, \\ F\, Bo^{0.5} e^{(2.74\, Cov^{-0.1})}, & 1 \ge Cov > 0.1 \\ F\, Bo^{0.5} e^{(2.47\, Cov^{-0.15})}, & Cov \le 0.1 \end{cases}$ $F = \begin{cases} 14.7 \ , & Bo \ge 11\times10^{-4} \\ 15.43, & Bo < 11\times10^{-4} \end{cases}$ $\psi_{cb} = \frac{1.8}{Cov^{0.8}}$	*Vertical, horizontal, up flow in tubes and multichannel.* *4852 data points.* *D: 0.38 – 27.1 mm* *P_r: 0.0046 – 0.787* *Bo: 0.15 – 527* *G:1 –2437 kg/m^{2}s* *Fluid: Water, CO_2, R11, R12, R22, R32, R113, R123, R114, R123, R134a, R152a, R1234yf, R236fa, R245fa, Ammonia, Propane, Isobutane, Carbon Tetrachloride, Isopropyl Alcohol, Ethanol, Methanol, N-Butanol, Cyclohexane, Benzene, Heptane, Pentane, Argon, Hydrogen, Nitrogen, and Helium.*

Publications

- Al-Gaheeshi, A., Mahmoud, M. M. M. and Karayiannis, T. G. (2016). Flow boiling heat transfer in a vertical small-diameter tube: effect of different fluids and surface characteristics. Sendai, Japan: Proceedings of the 4th International Forum on Heat Transfer, IFHT2016.
- Al-Gaheeshi, A., Mahmoud, M. M. M. and Karayiannis, T. G. (2017). Flow Boiling Heat Transfer of R245fa in Vertical Small-Micro Diameter Tubes. Brunel University London: 15th UK Heat Transfer Conference, UKHTC2017.